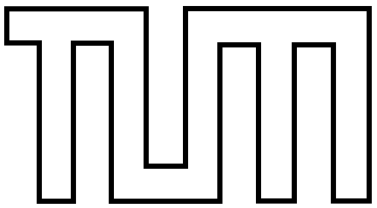

TECHNISCHE
UNIVERSITÄT
MÜNCHEN

TUM School of Engineering and Design

Monitoring Water Quality of Inland Waters by Remote Sensing and Machine Learning: From Local to Global Applications

Leonardo Francisco Arias Rodríguez, M.Sc.

Vollständiger Abdruck der von der TUM School of Engineering and Design der Technischen Universität München zur Erlangung des akademischen Grades eines

Doktors der Ingenieurwissenschaften (Dr.-Ing.)

genehmigten Dissertation.

Vorsitzende:
Dr. rer. nat. habil. Gabriele Chiogna

Prüfer*innen der Dissertation:
1. Prof. Dr.-Ing. Markus Disse
2. Prof. Dr. Zheng Duan
3. apl. Prof. Dr. rer. nat. habil. Brigitte Helmreich

Die Dissertation wurde am 04.07.2022 bei der Technischen Universität München eingereicht und durch die TUM School of Engineering and Design am 22.09.2022 angenommen.

"Conocí a un viajero
de una tierra antigua,
quien dijo:

"Dos enormes piernas pétreas,
sin su tronco, se yerguen en el desierto.
A su lado, en la arena, semihundido
yace un rostro hecho pedazos, cuyo ceño,
y mueca en la boca, y desdén de frío dominio,
cuentan que su escultor comprendió bien esas pasiones
las cuales aún sobreviven,
grabadas en estos inertes objetos,
a las manos que las tallaron
y al corazón que las alimentó.

Y en el pedestal se leen estas palabras:
"Mi nombre es Ozymandias, Rey de Reyes:
¡Contemplad mis obras, poderosos, y desesperad!"
Nada queda a su lado.
Alrededor de la decadencia de estas colosales ruinas,
infinitas y desnudas, se extienden, a lo lejos,
las solitarias y llanas arenas"

—Percy Shelley, "Ozymandias", 1819.

Abstract

Inland waters such as lakes, reservoirs and rivers are crucial for the Earth's environment. They supply habitat for vegetation and wildlife and provide humankind with several ecosystem services crucial for human development. Anthropogenic activity exposes these ecosystems to several stressors that threaten their ecological status and resources causing eutrophication, organic and inorganic contamination that affects considerable the water quality of its waters. Therefore, continuous monitoring of their status is crucial to detect disruption events and prevent environmental disasters. Conventional monitoring of inland waters by sample collection in field is laborious and timely consuming and lacks applicability at higher spatial and temporal scales to assess properly water quality in inland waters. To contribute to the comprehensive assessment and management of inland waters by the improvement of inland waters monitoring, this dissertation develops several methodologies that combine remote sensing techniques and machine learning approaches at different levels of applicability.

First, a study case based in central Mexico supports water quality monitoring of individual lakes and reservoirs at local scale. The approach develops remote-sensing-based machine learning models for water quality parameters estimation and it combines in-situ collected measurements across the reservoir and remote sensing reflectance data from the Medium Resolution Imaging Spectrometer (MERIS). The predicting models are applied to multitemporal imagery to analyze spatial and temporal water quality variations in the reservoir from 2002 to 2012 and detects yearly patterns caused by dry and rainy seasons where several disruptive causes are identified. When successfully applied at this scale, the methodology is then upscaled with the aim to combine data measurements at national level and support water management in the region. Remote sensing data from the remote sensors Landsat-8 OLI, Sentinel-3 OLCI, and Sentinel-2 MSI is combined with time series (2013 - 2019) of field data measurements from the whole country and modelled using an extreme learning machine approach (ELM). Additionally, ready-to-use water products from remote sensing sensors are evaluated against in-situ measurements. This work identifies that remote sensing requires integration with monitoring water quality programs tasks particularly in developing countries, the need to assess the reliability of available remote sensors to complement the limited water monitoring tasks and the usefulness of atmospherically corrected data to develop predictive water quality models. River water quality is later evaluated within the Danube River. Floodplain restoration and its effects on water quality are investigated using time series analysis of nutrients' concentrations and Water Quality Indices (WQI) are obtained based on different physicochemical parameters. Sentinel-2 based models are developed to model water quality in the river and assess the effects of river restoration. The water quality upstream and downstream the floodplains is modeled and the spatial distribution in the surface is evaluated. The findings support the assessment of nature-based solutions on the river and provide insights about the benefits of river restoration.

The major challenge when monitoring inland waters are the transferability of the models to diverse regions around the world and the retrieval non-optically active parameters (nOAC). This is assessed in this dissertation with the incorporation of water quality data from monitoring systems across the world and remote sensing data from operational satellites for a synergistic analysis. Harmonized remote sensing data of Landsat-8 and Sentinel-2 are used to increase data availability and create a dataset with worldwide lake characteristics' to be processed with machine learning approaches. The results suggest that remote sensing and machine learning are capable to develop predictive models to model water quality at global scale and contribute to overcome current limitations in the field of remote sensing of inland waters.

This dissertation contributes to improve monitoring of inland waters from local to worldwide applications and points the major needs to be investigated with further research in the field: field data accessibility at global scale, remote sensing data fusion and atmospheric correction, and spectral characterization of non-optically active constituents.

Zusammenfassung

Binnengewässern wie Seen, Stauseen und Flüsse sind für die Umwelt der Erde von entscheidender Bedeutung. Sie bieten Lebensraum für Pflanzen und Tiere sowie verschiedene Ökosystemdienstleistungen, die für die menschliche Entwicklung entscheidend sind. Durch anthropogene Aktivitäten sind diese Ökosysteme verschiedenen Stressfaktoren ausgesetzt, die ihren ökologischen Zustand und ihre Ressourcen bedrohen und zu Eutrophierung und organischer und anorganischer Verschmutzung führen, was die Wasserqualität der Gewässer erheblich beeinträchtigt. Daher ist eine kontinuierliche Überwachung ihres Zustands von entscheidender Bedeutung, um Störungen zu erkennen und Umweltkatastrophen zu verhindern. Die herkömmliche Überwachung von Innengewässern durch die Entnahme von Feldproben ist arbeits- und zeitaufwändig und eignet sich nicht für eine angemessene Bewertung der Wasserqualität in Binnengewässern auf einer grösseren räumlichen und zeitlichen Ebene. Um durch die Verbesserung der Überwachung von Innengewässern einen Beitrag zur umfassenden Bewertung und Bewirtschaftung von Binnengewässern zu leisten, werden in dieser Dissertation mehrere Methoden entwickelt, die Fernerkundungstechniken und Ansätze des maschinellen Lernens auf verschiedenen Ebenen der Anwendbarkeit kombinieren.

Zunächst unterstützt eine Fallstudie in Zentralmexiko die Überwachung der Wasserqualität von einzelnen Seen und Stauseen auf lokaler Ebene. Der Ansatz entwickelt fernerkundungsbasierte maschinelle Lernmodelle für die Schätzung von Wasserqualitätsparametern und kombiniert in-situ gesammelte Messungen im gesamten Stausee mit Fernerkundungs-Reflexionsdaten des Medium Resolution Imaging Spectrometer (MERIS). Die Vorhersagemodelle werden auf multitemporale Bilder angewandt, um die räumlichen und zeitlichen Schwankungen der Wasserqualität im Stausee von 2002 bis 2012 zu analysieren und jährliche Muster zu erkennen, die durch Trocken- und Regenzeiten verursacht werden, wobei mehrere störende Ursachen identifiziert werden. Nach erfolgreicher Anwendung in diesem Massstab wird die Methodik dann mit dem Ziel hochskaliert, Datenmessungen auf nationaler Ebene zu kombinieren und die Wasserwirtschaft in der Region zu unterstützen. Fernerkundungsdaten von den Fernerkundungssensoren Landsat-8 OLI, Sentinel-3 OLCI und Sentinel-2 MSI werden mit Zeitreihen (2013-2019) von Felddatenmessungen aus dem ganzen Land kombiniert und mithilfe eines maschinellen Ansatzes mit extreme learning maschine (ELM) modelliert. Außerdem werden gebrauchsfertige Wasserprodukte von Fernerkundungssensoren mit In-situ-Messungen verglichen. Diese Arbeit zeigt auf, dass die Fernerkundung in Überwachungsprogramme für die Wasserqualität integriert werden muss (insbesondere in Entwicklungsländern), dass die Zuverlässigkeit der verfügbaren Fernsensoren bewertet werden muss, um die begrenzten Wasserüberwachungstätigkeiten zu ergänzen, und dass atmosphärisch korrigierte Daten für die Entwicklung von prädiktiven Wasserqualitätsmodellen nützlich sind. Die Wasserqualität der Flüsse wird später an der Donau bewertet. Die Auenrenaturierung und ihre Auswirkungen auf die Wasserqualität werden anhand von Zeitreihenanalysen der Nährstoffkonzentrationen untersucht, und es werden Wasserqualitätsindizes (WQI) auf Grundlage verschiedener physikalisch-chemischer Parameter ermittelt. Sentinel-2-basierte Modelle werden entwickelt, um die Wasserqualität im Fluss zu modellieren und die Auswirkungen der Flussrenaturierung zu bewerten. Die Wasserqualität flussaufwärts und flussabwärts der Auen wird modelliert und die räumliche Verteilung in der Fläche wird bewertet. Die Ergebnisse unterstützen die Bewertung naturnaher Lösungen am Fluss und geben Aufschluss über den Nutzen der Flussrenaturierung.

Die wichtigsten Aspekte bei der Überwachung von Binnengewässern sind die Übertragbarkeit der Modelle auf verschiedene Regionen der Welt und die Ermittlung von nicht-optisch aktiven Parametern (nOAC). Dies wird in dieser Arbeit durch die Einbeziehung von Wasserqualitätsdaten aus Überwachungssystemen auf der ganzen Welt und Fernerkundungsdaten von operationellen Satelliten für eine synergistische Analyse bewertet. Harmonisierte Fernerkundungsdaten von Landsat-8 und Sentinel-2 werden verwendet, um die Datenverfügbarkeit zu erhöhen und einen Datensatz mit weltweiten Seemerkmalen zu erstellen, der mit Ansätzen des maschinellen Lernens verarbeitet werden kann. Die Ergebnisse deuten darauf hin, dass Fernerkundung und maschinelles Lernen in der Lage sind, Vorhersagemodelle zu entwickeln, um die Wasserqualität auf globaler Ebene zu modellieren und dazu beizutragen, die derzeitigen Einschränkungen

im Bereich der Fernerkundung von Binnengewässern zu überwinden.

Diese Dissertation trägt dazu bei, die Überwachung von Inlandsgewässern von lokalen bis hin zu weltweiten Anwendungen zu verbessern, und weist auf die wichtigsten Erfordernisse hin, die in der weiteren Forschung auf diesem Gebiet untersucht werden müssen: die Zugänglichkeit von Felddaten auf globaler Ebene, die Fusion von Fernerkundungsdaten und die atmosphärische Korrektur sowie die spektrale Charakterisierung von nicht-optisch aktiven Bestandteilen.

Affidavit

I hereby affirm that I wrote this dissertation independently and on my own without illegal assistance of third parties. To the best of my knowledge, all sources that I used to prepare that thesis are labeled as such. This thesis has not been received by any examination board, neither in this nor in a similar form.

Hiermit erkläre ich an Eides statt, dass ich die vorliegende Dissertation, abgesehen von der Beratung durch meine Betreuer/innen, nach Inhalt und Form selbstÃ¤ndig verfasst habe und keine weiteren Quellen und Hilfsmittel als die hier angegebenen verwendet habe. Diese Arbeit hat weder ganz noch in Teilen bereits an anderer Stelle im Rahmen eines Prüfungsverfahrens vorgelegen. Als kumulative Dissertation sind Kapitel 3 bis 6 wie zu Beginn der Kapitel vermerkt in den genannten Zeitschriften veröffentlicht. Ich erkläre, dass die vorliegende Arbeit unter Einhaltung der Regeln guter wissenschaftlicher Praxis der TUM entstanden ist.

Leonardo Francisco Arias Rodriguez
Munich,
Juli 4, 2022

Acknowledgements

I would like to deeply thank Prof. Dr. Markus Disse and Prof. Dr. Zheng Duan for the generous opportunity they offered me to carry out this research at the Chair oh Hydrology at Technical University of Munich. I am particularly grateful for their great confidence and the considerable advice, which I received during the development of this doctoral project. But I am even more thankful for their unvaluable and sincere understanding, patience, and support during the most difficult moments, which helped me to grow as a researcher but also as a person. On the other side, this doctoral project could have not been possible without the support and trust of the Mexican Science Council (CONACYT). The opportunity to be beneficiary from one of their scholarships opened the door to improve my skills in academia and it allowed me to develop a small contribution for the improvement of water managing in the country (and globally) through my research. Thank you very much to all Mexicans for the opportunity you gave me, I continue working to not disappoint you. I also want to deeply thank to all the professors and teachers that had have any influence in my formation and in my way of thinking. I believe we are a sum of all the teachings we receive, and I want to deeply thank you because with your work, you have made a big impact on me which today is culminated with the end of my doctoral project. I want to thank particularly to Dr. Sergio Ignacio Martinez Martinez, M.Sc. Rodrigo Sepulveda, Dr. Enrique Cesar Valdez and M.Sc. Alba Beatriz Vazquez Gonzalez from the UAA and the UNAM, for their great teachings in Hydrology, Water Quality and Remote Sensing, which were the base to develop this dissertation.

I want to thank my friends who have supported here in Munich. They provided me with the strong pillar of friendship which gave support and strength to go further and to overcome the challenges that appeared during this time in Munich, Mexico City, Barcelona and Aguascalientes. I would not be here without the friendship and love of Eduardo, Aida, Carlos, Abdias, Natanael, Neftali, Flor, Monica, Humberto, all my UAA friends and colleagues, Abraham and Carlos, Javier and Jaime, Pedro, Ricardo, Pablo, Marco, Francesca, Anna, Bea, Nathalie, Monica, Michael, Pablo, Mounia, Christina and Maria. Additionally, thank you very much to Andres because of the long time you had to deal with me and for the immense support you gave in so many different situations, and to Jaime for being the better person I know, I debt you so much. I feel lucky to have shared an office and a wonderful scientific environment with all my colleagues at TUM and at the Chair of Hydrology and River Basin. I believe I could have not chosen a better place to spend the last four years. I am especially grateful with Michael Tarantik for his always friendly and kind nature and to Francesca Perosa who shared with me so much time together as desk-neighbor but more as a friend that make me happy every day I was in my office. Many thanks to Christiane Zach-Cretaine for her support regarding all the administrative procedures at TUM. Also, I am very grateful to the students I supervised during their master's degree studies and who greatly contributed to my research, thank you very much specially to Leo Mertinat, Bapitha Kumar, Alain Hoyek and Ulas Tuzun.

I would also like to thank my committee member Prof. Dr. Brigitte Helmreich who accepted to examine my dissertation and to Prof. Dr. Gabriele Chiogna to act as Chairman but more as a reference and guide in our office in Augustenstraße. I would like to show my appreciation to the TUM Library for their financial support for open-source publishing on research journals. It is a great pleasure to thank my co-authors Jose de Jesus Diaz Torres, Jingshui Huang and Ye Tuo, for their valuable support and contributions to my research articles.

Finally, I want to deeply thank my family, to my mother Esperanza, to my father Teodoro and to my brother Luis Daniel, for believe in me and in my potential, and to give me the opportunity to be far away with the immense sacrifice that implies.

Research Articles

This cumulative doctoral thesis is based on the following peer-reviewed research papers. Most of the contents of this work have been presented and discussed in the following publications:

- **Arias-Rodriguez, L.F.**; Tuzun, U.F.; Duan, Z.; Huang, J.; Tuo, Y.; Disse, M., **(2022)** Global Water Quality of Inland Waters with Harmonized Landsat-8 and Sentinel-2 using Cloud-Computed Machine Learning (For peer review)

- Hoyek, A.; **Arias-Rodriguez, L.F.**; Perosa, F. **(2022)** Holistic Approach for Estimating Water Quality Ecosystem Services of Danube Floodplains: Field Measures, Remote Sensing, and Machine Learning. Hydrobiology, 1, 211-231. https://doi.org/10.3390/hydrobiology1020016

- **Arias-Rodriguez, L.F.**; Duan, Z.; Diaz-Torres, J.d.J.; Basilio Hazas, M.; Huang, J.; Kumar, B.U.; Tuo, Y.; Disse, M. **(2021)** Integration of Remote Sensing and Mexican Water Quality Monitoring System Using an Extreme Learning Machine. Sensors, 21, 4118. https://doi.org/10.3390/s21124118

- **Arias-Rodriguez, L.F.**; Duan, Z.; Sepulveda, R.; Martinez-Martinez, S.I.; Disse, M. **(2020)** Monitoring Water Quality of Valle de Bravo Reservoir, Mexico, Using Entire Lifespan of MERIS Data and Machine Learning Approaches. Remote Sens.12, 1586. https://doi.org/10.3390/rs12101586

Topic-related peer-reviewed journal articles:

- Tran, B. Y., **Arias-Rodriguez, L.F.**; Huang, J., **(2022)**: Predicting high-frequency nutrient dynamics in the Danube River with surrogate models using sensors and Random Forest, Front. Water 4:894548, https://doi.org/10.3389/frwa.2022.894548

- F. Hofmeister, **Arias-Rodriguez, L.F.**, V. Premier, C. Marin, C. Notarnicola, M. Disse, G. Chiogna, **(2022)**, Intercomparison of Sentinel-2 and modelled snow cover maps in a high-elevation Alpine catchment, Journal of Hydrology X, doi: https://doi.org/10.1016/j.hydroa.2022.100123

- Perosa, F.; Gelhaus, M.; Zwirglmaier, V.; **Arias-Rodriguez, L.F.**; Zingraff-Hamed, A.; Cyffka, B.; Disse, M. **(2021)** Integrated Valuation of Nature-Based Solutions Using TESSA: Three Floodplain Restoration Studies in the Danube Catchment. Sustainability, 13, 1482. https://doi.org/10.3390/su13031482

Topic-related journal articles under review:

- Adla, S., Bruckmaier, F., **Arias-Rodriguez, L.F.**, Tripathi, S., Disse, M., and Pande, S., **(2022)**: Impact of calibrating a low-cost capacitance-based soil moisture sensor on FAO AquaCrop model performance, (For peer review)

Contents

List of Figures

List of Tables

Acronyms

AC: Atmospheric correction

BRDF: Bidirectional reflectance distribution functions

BOA: Bottom of the atmosphere

BOD: Biochemical oxygen demand

C2RCC: Case 2 regional coast colour atmospheric correction

CDOM: Colored dissolved organic matter

Chl-a: Chlorophyll-a

COD: Chemical oxygen demand

CONACYT: Consejo nacional de ciencia y tecnologia

CONAGUA: Comision nacional el agua

CV: Cross validation

DO: Dissolved oxygen

DS: Dataset

ELM: Extreme learning machine

ENVISAT: Environmental satellite

ESA: European space agency

ETM+: Enhanced thematic mapper

EUMETSAT: European organization for the exploitation of meteorological satellites

FP: Floodplain

GIS: Geographycal information systems

GLWD: Global lakes and wetlands database

GEE: Google earth engine

GPR: Gaussian processes regressor

HAB: Harmful algae bloom

HLS: Harmonized Landsat-8 and Sentinel-2

HRG: High-resolution geometric sensor

ICOR: Image correction for atmospheric effects

IOP: Inherent optical properties

L8: Landsat-8

LaRSC: Land surface reflectance code

LOOCV: Leave one out cross validation

LR: Linear regression

MERIS: Medium resolution imaging spectrometer

ML: Machine learning

MODIS: Moderate resolution imaging spectroradiometer

MSI: Multi spectral instrument

MSS: Multi-spectral scanner

NASA: National aeronautics and space administration

NbS: Nature based solutions

NDVI: Normalized difference vegetation index

NIR: Near infrared region of the electromagnetic spectrum

NN: Neural networks

nOAC: non-optically active constituents

NDSI: normalized difference snow index

NTU: Nephelometric turbidity units

OAC: Optically active components

OECD: Organisation for economic co-operation and development

OLCI: Ocean and land colour instrument

OLI: Operational land manager

PS: Power set

RTM: Radiative transfer model

RFR: Random forest regressor

RNMCA: Red nacional de monitoreo de la calidad del agua

Rrs: Remote sensing reflectance

RS: Remote sensing

S2: Senitnel-2

S3: Sentinel-3

SDD: Secchi disk depth

6S: Second Simulation of the Satellite Signal in the Solar Spectrum

SINA: Sistema nacional del agua

SNAP: Sentinel application platform

SPOT: Satellite pour l'observation de la terre

SVC: Support vector classification

SVM: Support vector machine

SVR: Support vector regression

SWIR: Shortwave infrared

TM: Thematic mapper

TOA: Top of the atmosphere

TSM: Total suspended matter

TSS: Total suspended solids

UNEP: United nations environment programme

USGS: United states geological survey

VIS: Visible region of the electromagnetic spectrum

WFD: Water framework directive

WFR: Water full resolution product

WQ: Water Quality

1 Motivation and Focus of the Dissertation

We can see our world from the space. It is possible now to interpret local events with a higher perspective because our scope and sight are enhanced by the technical resources we have developed. For example, we now understand isolated events as a 5-day-rain in dry central Mexico because we see the presence of a hurricane in the Caribbean Sea, which sends rain clouds inside the continent.

With this idea in consideration, it is important to realize the potential that this technology enables in terms of monitoring. When used intensively, it allows us a permanent observation of the events we are interested in the surface. With this constant attention, we can detect the occurrence of disruptive events and act timely to take countermeasures or even prevent further consequences. In this way, it is possible to avoid great damages to the goods of importance for our society, which can directly affect our health, our infrastructure, the weather or the natural resources of the planet.

Water plays a crucial role as driver of the health and development of humankind, and in greater instance it is the one of the main drivers of the Earth's life. The waters inside the continents, called inland waters provide an environment for several life species and they are a key driver for the hydrological, nutrient and carbon cycles. Human society uses inland waters as a source for water extraction to supply drinking water and irrigation in agriculture, but water is also crucial for industry as power production and transportation. Unfortunately, anthropogenic activities pose great hazard for water environments and threat natural ecosystems and human health itself. Agricultural, commercial, industrial and residential activities contribute to the deterioration of waters by the exposure of water to a variety of harmful pollutants and pathogens. Supply of fresh water becomes challenging when increasing population and contamination. As human activities continue to progress, it is important to protect water resources and ensures the sustainable development of human activities to maintain an adequate natural balance between development, resources consumption and waste disposal. It is therefore human responsibility to keep and maintain the adequate status the water we have enjoyed for many generations (Figure 1.1). To keep the water in adequate conditions for its usage for natural and human purposes, it is necessary to be aware of the evolution of its status. The detection of sudden changes in water quality could allow to control hazardous events and a timely response with restoration measures. Therefore, there is an urgent need to establish capable monitoring systems to manage water quality from local to global scale. Efforts have been made in this direction by several nation institutions in their respective territories to manage their water resources. For example, the US Clean Water Act, US Clean Water Act (Senate, 2002), the Canada Water Act (Gall, 1974), the Water Framework Directive in Europe (Todo & Sato, 2002), the South African National Water Act (Africa, 1998), the Chilean General Water Direction (RFMA, 2014) and the Mexican water Quality Monitoring System (CONAGUA, 2018). But a common limitation in current monitoring programs is that conventional monitoring approaches are inadequate for permanent and large-scale monitoring.

This thesis focuses on developing managing tools that contribute to the responsibility of human society with the water environment and the dedication of human efforts to overseen water resources. With the usage of human technology and technique, this thesis seeks to contribute to better understanding of the events surrounding the dynamics of water quality in inland waters and the adequate methodologies to a sustainable monitor process that contributes to the protection of water resources. When recognizing the significance and implication of this matter, it is necessary to expose the advantages and current challenges of monitoring water resources. Additionally it informs about the risks faced by water resources, particularly inland waters as lakes, rivers and reservoirs exposed continuously to anthropogenic activities, and it reveals how conventional monitoring techniques are no longer adequate to face them. Also, it contributes to establish methodologies that foster automated monitoring of inland waters as a resource

to answer climate change and anthropogenic stressors. The focus of this research is therefore to develop and apply remote sensing and machine learning approaches to support monitoring tasks, as current water monitoring programs around the world lack the capacity to detect quickly and accurately harmful events.

Figure 1.1: Dettifoss waterfall, Iceland (jrmelot at flickr).

1.1 General goal

The general goal of the thesis is:

"The optimum utilization of remote sensing data and machine learning algorithms to develop predictive models that enhance temporal and spatial monitoring water quality in inland waters worldwide"

This is addressed by the combination of diverse methodologies. Initially, image processing is necessary to apply with the necessary corrections of remote sensing data and extraction of pixel value of radiometric parameters that measure electromagnetic radiation from water surface. Additionally, statistical and data analysis is necessary to understand both field and radiometric data and evaluate the feasibility of a combined synergistic approach that relates both datasets.

A modeling approach is then conducted using machine learning algorithms that ensures state-of-the-art techniques to handle with complex non-linear relationships between remote sensing data and water quality parameters which commonly does not show normality in distribution. This allows developing and applying predictive models for monitoring water quality which are evaluated at studies in local, national, continental and global scales, contributing to consolidate global water quality monitoring.

1.2 Research objectives

Compared to conventional water quality monitoring methods, remote sensing-based monitoring has increasingly enabled an exponential analysis both in temporal and spatial scales because the spatial and temporal scales that can be covered. However, there are still current challenges under investigation in research to consolidate this methodology. For remote sensing of inland waters, the following requirements must be met in order to develop an evaluation methodology:

- Availability of field samples should be in adequate quantity for machine learning calibration
- Existence of temporal overlapping between remote sensing image acquisitions and field sampling dates to ensure homogeneity in spectral characteristics
- Atmospheric correction of remote sensing images is required to derive remote sensing reflectance from water surface

Aiming at the development of field sampling campaigns, remote sensing approaches and machine learning algorithms fulfilling the above mentioned requirements, three following objectives are to be achieved:

Objective 1: Archived remote sensing imagery applied to the detection of hazard events using machine learning

The goal is to use archived remote sensing MERIS imagery from 2002 - 2012 and machine learning approaches for a single reservoir as study area, the Valle de Bravo Reservoir in central Mexico.

The intention is to detect distuptive events during the monitoring period and demonstrate the usefulness of non-operational sensors to understand hazard events for water quality in previous years. The study case, Valle de Bravo, represents the major source of drinking water for Mexico City metropolitan area. This objective introduces the methodology in a developing country with typical water quality monitoring routine tasks.

Objective 2: Improve water quality monitoring systems by the integration of remote sensing and machine learning using the RNMCA data

This objective seeks to analyze the data from the water quality monitoring system in Mexico (RNMCA) at a higher level with several study cases. Existing remote sensing products for water quality should be compared with time series data from the national water authority in the country to evaluate its usefulness as supporter for water quality monitoring. Additionally, locally calibrated models should be trained to consider this approach an integrated system based on water quality and remote sensing data. The most adequate sensors to support monitoring tasks are considered and evaluated.

Objective 3: Estimation of changes in water quality along the Danube River using Sentinel-2 data

The water quality and the effects of several floodplains are evaluated in the Danube River as a study case. The application is therefore at a continental level and uses the water quality data measured at transnational locations as well as high-resolution remote sensing imagery to develop machine learning models and evaluate changes in water quality alongside the river at yearly scale along the river.

Objective 4: Development of a global water quality and remote sensing dataset applied to worldwide water quality monitoring

The ultimate goal aims to unify water quality data of world-wide-monitoring-programs water quality measurements and combine them with homogenized remote sensing data from several sensors. This will allow to develop machine learning models that learn from a rich and comprehensive dataset with a great variety of different characteristics and patterns inside the water parameters behavior. This is expected to improve model performance in terms of error metrics and overcome the traditional limitation of regional transferability, which is present in remote sensing of inland waters. Additionally, modeling of more complex parameters which are not optically active in waters is also investigated to create models capable to predict variations in water quality parameters that does not modify spectral behavior of radiation in water..

1.3 Structure

The presentation and discussion of the methodology and results found is made via publication in international research journals. At the time of writing this dissertation, three peer-reviewed research articles are published, and one additional manuscript is submitted and currently under review. The corresponding citation, research journals and weblinks for further consultation and indicated at the beginning of each section.

The structure of this thesis is divided in several sections and it is organized as follows: The section 2 gives an overview of the background of conventional water sampling, remote sensing, machine learning and water quality. Additionally, this chapters also mention the main contributions of remote sensing when retrieving water parameters in inland waters. The section 3, section 4, section 5 and section 6 present the four main contributions from the author focused on the fulfillment of the research objectives which are listed as follows:

- Section 3: Monitoring Water Quality of Valle de Bravo Reservoir, Mexico, Using Entire Lifespan of MERIS Data and Machine Learning Approaches
- Section 4: Integration of Remote Sensing and Mexican Water Quality Monitoring System Using an Extreme Learning Machine
- Section 5: Holistic Approach for Estimating Water Quality Ecosystem Services of Danube Floodplains: Field Measures, Remote Sensing, and Machine Learning
- Section 6: Global Water Quality of Inland Waters with Harmonized Landsat-8 and Sentinel-2 Data using Cloud-Computed Machine Learning

The results of this thesis and an outlook on further research are discussed in section 7. A summary structure of the dissertation with corresponding objectives, methods, data, scale and publications is shown in Table 1.1.

Table 1.1: Structure of the cumulative dissertation.

Objective	Methodology	Data	Scale	Publication
1. Archived remote sensing imagery applied to the detection of hazard events using machine learning	WQ + RS data modeling Algorithm: GPR Validation: LOOCV	2010 Field campaigns MERIS archive	Local	**Arias-Rodriguez, L.F.** et al. (2020) Monitoring Water Quality of Valle de Bravo Reservoir Mexico, Using MERIS, Data and Machine Learning Approaches. Remote Sens. https://doi.org/10.3390/rs12101586
2. Improve water quality monitoring systems by the integration of remote sensing and machine learning using the RNMCA[a] data	S3 OLCI Products validation (Chl-a, TSM) WQ + RS data modeling Algorithm: ELM Validation: k = 10 CV	2012 - 2018 WQ RNMCA Landsat-8 L1T Sentinel-3 C2RCC Sentinel-2 C2RCC	National	**Arias-Rodriguez, L.F.** et al. (2021) Integration of Remote Sensing and Mexican Water Quality Monitoring System Using an Extreme Learning Machine. Sensors, https://doi.org/10.3390/s21124118
3. Estimation of changes in water quality along the Danube River using Sentinel-2 data	C2RCC Products validation (Chl-a, TSM) WQ + RS data modeling Algorithm: RFR Validation: k = 10 CV	2015 - 2018 WQ WQ Danube Data Sentinel-2 C2RCC	Continental	Hoyek, A.; **Arias-Rodriguez, L.F.**, et al. (2022) Holistic Approach for Estimating Water Quality Ecosystem Services of Danube Floodplains: Field Measures, Remote Sensing, and Machine Learning. Hydrobiology, https://doi.org/10.3390/hydrobiology1020016
4. Development of a global water quality and remote sensing dataset applied to worldwide water quality monitoring	L8 and S2 RS data harmonization WQ + RS data modeling Algorithm: ELM Validation: k = 10 CV	2013 - 2021 WQ Global data Harmonized Landsat, Sentinel-2	Global	**Arias-Rodriguez, L.F.**, et al. (2022) Global Water Quality of Inland Waters with Harmonized Landsat-8 and Sentinel-2 using Cloud-Computed Machine Learning. (For peer review)

[*] Abbreviations:

C2RCC: Case 2 regional coast colour atmospheric
CV: Cross validation
ELM: Extreme learning machine
GPR: Gaussian processes regressor
L8: Landsat-8
LOOCV: Leave one out cross validation
MERIS: Medium resolution imaging spectrometer
OLCI: Ocean and land colour instrument
RFR: Random forest regressor
RNMCA: National Monitoring Network System (Mexico)
RS: Remote sensing
S2: Senitnel-2
S3: Sentinel-3
WQ: Water Quality

2 Background and State-of-the-Art

Inland waters including lakes, ponds, streams, rivers and wetlands (marshes, mangroves, floodplains and swamps) are extremely important at global level, both in terms of quantity and the ecosystem services they provide, for example, they are crucial for water supply for drinking water, sanitation, irrigation, industry, transportation and recreation (Hartmann et al., 2013). It is believed that there are more than 117 million waterbodies larger than 0.002 km^2 in the planet, a 3.7% of the non-glaciated land area of the Earth (Verpoorter, Kutser, Seekell, & Tranvik, 2014).

Nevertheless, these water bodies are monitored in a small portion in regular and consistent monitoring programs and the focus is set usually on larger water bodies while most of small inland waters are unattended in despite of its combined importance (Giardino et al., 2019). The lack of adequate monitoring avoids the detection of disrupting events in water bodies as increased eutrophication and pollution, posing an environmental threat on these resources. This is caused mainly by global urbanization, inadequate discharges of sewage, industrial and agricultural run-off water which triggers nutrient concentrations and appearance of toxic algae blooms. The consequences are the loss of most of their ecosystem services and existing biodiversity, recreation and tourism caused (P. Mishra et al., 2015). Conventional monitoring of inland waters is performed by collection of water samples from field (Figure 2.1) and then analyzed in laboratory to determine several water parameters to interpret water quality.

This methodology is highly accurate; however, it has several disadvantages that limit its application to a greater extent. For example, field collection based on sampling boats is labor intensive, time consuming and expensive, even for small waterbodies. A complete coverage of large waterbodies is then even more limited and out of the possibilities of many countries with limited monitoring programs. In terms of application, point sampling methods lack the ability to identify and detect spatial and temporal variations in water quality. Therefore, to provide comprehensive assessment and management of inland waters is limited when using conventional methodologies (W. Duan, Takara, et al., 2013; W. Duan, He, et al., 2013; Gholizadeh, Melesse, & Reddi, 2016).

Figure 2.1: Water quality sampling from bridge, April 20, 1947. A safety conscious (note the flag on the crane) hydrographer collects a water quality sample from a bridge over a river (USGS).

2.1 Remote sensing

Advances in Earth observation allows to use the Remote Sensing technology to support monitoring tasks and overcome its challenges, as done since decades (Figure 2.2). By means of Remote Sensing techniques, the electromagnetic radiation is measured by a sensor on board of a certain carrier device (satellite, airplane, drone) and this information is used to derive certain characteristics of a determined object through several possible methodologies, in this case, a water body (Dörnhöfer & Oppelt, 2016).

Figure 2.2: The US TIROS-1 weather satellite in 1960 (NASA).

The path of the incoming electromagnetic radiation from the sun (Figure 2.3) starts in the atmosphere, where it is affected by absorption and interaction by the constituents of the atmosphere. Then in the water surface, radiation is reflected or absorbed, and it continues its travel through the water column. Water constituents such as chlorophyll-a, suspended solids or colored dissolved organic matter interact with the radiation as well and this interactions conform the inherent optical properties of a water body (Odermatt, Gitelson, Brando, & Schaepman, 2012). Afterwards, the portion of the electromagnetic radiation that is reflected from the water surface moves in the direction of the atmosphere and it is affected once again by scattering and absorption before it is captured by a remote sensor.

It is estimated that between 90 - 98 % of the signal captured by a sensor comes from water surface and atmosphere scattering (Gitelson & Kondratyev, 1991) and the remaining portion is which contains the signal of the water leaving reflectance, which is a vital apparent optical constituent for remote sensing of inland waters. All of this contributors of electromagnetic radiation in the signal detected by the sensor need to be removed to accurately measure the incoming radiation of a waterbody and therefore an atmospheric correction of remote sensing images is crucial for most of the remote sensing techniques (Mouw et al., 2015).

The region of the electromagnetic radiation which is of interest is located mostly in the visible and near-infrared wavelengths (400 - 900 nm) (A. G. Dekker et al., 2002). This is because the higher absorption of water in the near and shortwave infrared wavelengths and therefore, the visible wavelengths are responsible for most of the water leaving radiance (Doxaran, Froidefond, Lavender, & Castaing, 2002; Röttgers, McKee, & Utschig, 2014). This situation occurs differently in optically complex waters, which can show higher levels of turbidity or can be shallow waters, and an additional contribution of reflectance exceeds the absorption of water in the near and shortwave spectrum (Sathyendranath et al., 2000; Doxaran et al., 2002). Available remote sensors can be carried in aircrafts or satellite platforms. In this thesis, the focus in on optical satellite remote sensing since its data availability is more suited

for the purposed later described. Satellite sensors are carried by a spacecraft which orbits outside of the Earth's atmosphere and for water quality estimations, different sensors can be used. Traditionally, satellites dedicated to map ocean color have been used for inland waters, such as the Moderate Resolution Imaging Spectroradiometer (MODIS, since 1999) (Miller & McKee, 2004; Falcini et al., 2012; Adamo et al., 2013; Qin et al., 2015), the Medium Resolution Imaging Spectrometer (MERIS, 2002 - 2012) (Matthews, Bernard, & Winter, 2010; Bresciani, Stroppiana, Odermatt, Morabito, & Giardino, 2011; Bresciani, Vascellari, Giardino, & Matta, 2012; Palmer et al., 2015), and the Sentinel-3 Ocean and Land Cover Instrument (OLCI, since 2015) (Shen et al., 2017).

Land surface optical sensors are also commonly used, mainly the Landsat constellation of the (Multispectral Scanner (MSS, 1984 - 2013) (Ritchie, Cooper, & Schiebe, 1990; Mertes, Smith, & Adams, 1993; Kloiber, Brezonik, & Bauer, 2002); Thematic Mapper (TM, 1994 - 2013) (A. Dekker & Peters, 1993; Yacobi, Gitelson, & Mayo, 1995; Y. Wang, Xia, Fu, & Sheng, 2004)]; Enhanced Thematic Mapper (ETM+, since 1999) (Ouillon, Douillet, & Andréfouët, 2004; Tyler, Svab, Preston, Présing, & Kovács, 2006; H. Duan, Zhang, Zhang, Song, & Wang, 2007); and Operational Land Imager (OLI, since 2013) (Watanabe et al., 2015; Z. Lee, Shang, Qi, Yan, & Lin, 2016) and the Sentinel 2 A/B MultiSpectral Instrument (MSI, since 2015) (Toming et al., 2016; Kutser et al., 2016), and SPOT High-Resolution Geometric Sensor (HRG, 2002 - 2015) (Doxaran et al., 2002). A summary with the characteristics of the most commonly used sensors are shown in Table 2.1.

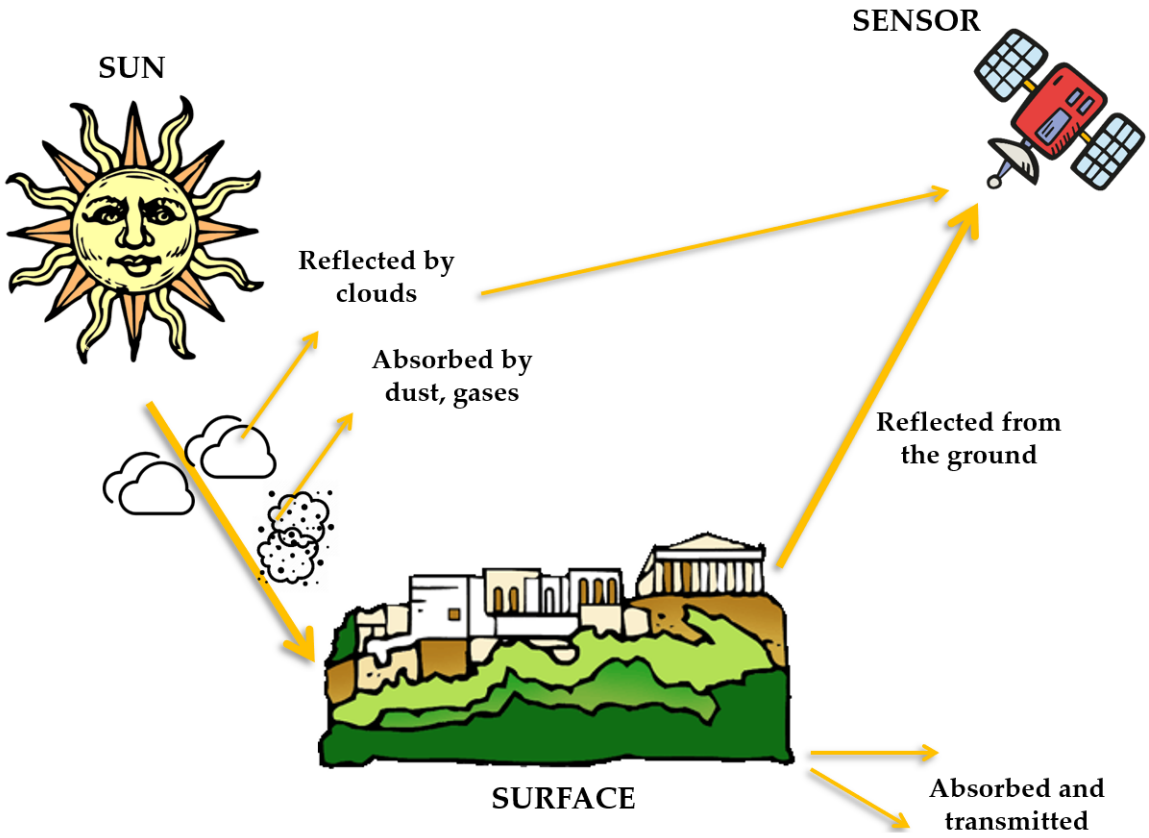

Figure 2.3: Main components associated with remote sensing activities.

The higher absorption of visible radiation in comparison to near and shortwave spectrum causes a weak signal of visible wavelengths and lead to the need to develop sensors with higher radiometric resolution and therefore, the inclusion of several bands of acquired reflectance at different wavelengths (Matthews, 2011). Therefore, sensors have been designed with different characteristics as multispectral sensors with few wide bands (10 nm to 80 nm) or multispectral sensors with hundreds of narrow bands (1 - 10 nm). Depending on the desired application, the study area and the available data, the selection of the sensor is highly important. Details as the spatial, temporal, spectral and radiometric resolution defines the utility of the data from one sensor and a tradeoff between these characteristics usually has to be done to reach an optimal point. The water leaving reflectance is then used to obtain quantitative information on water constituents. These water constituents can be used and interpreted as water quality indicators, based on their levels and concentrations (Gholizadeh et al., 2016). To retrieve such information, several algorithms have been used and many more are in current development. The models that develop a relationships between the specific optically active water constituent and the optical quality of the waterbody are known as bio-optical models (Hutchinson, 1973). These models are classified based on the approach they apply to develop such relationship: empirical, semi-analytical or machine learning based models (Topp, Pavelsky, Jensen, Simard, & Ross, 2020).

Table 2.1: Summary of characteristics of the most commonly used remote sensors for water quality of inland waters.

Purpose	Satellite	Sensor	Operation	Bands (400 - 1000 nm)	Overpass	Resolution (m)
Ocean Color						
	Terra/Aqua	MODIS	Since 1999	2 - 9	Daily	250 - 1000
	ENVISAT	MERIS	2002 - 2012	15	2 - 3 days	300
	Sentinel-3 A/B	OLCI	Since 2015	21	5 days	300
Land Surface						
	Landsat-5	MSS	1984 - 2013	4	16 days	60
	Landsat-6	TM	1993 - 2013	4	16 days	30
	Landsat-7	ETM+	Since 1999	4	16 days	30
	Landsat-8	OLI	Since 2013	5	16 days	30
	Sentinel-2 A/B	MSI	Since 2015	9	5 - 10 days	10 - 30
	SPOT-5	HRG	2002 - 2015	5	26 days	5 - 20

The basic standard linear regression has been applied as an empirical method since decades as the conventional approach to develop a predictive model. The linear relationship is developed based on the water measurements taken on the field and the remote sensing reflectance values acquired by the remote sensors and stored in the different bands of the satellite image. The coincidence between the water sampling and the image acquisition is the first requirement to cover to ensure the relationship is significant. The main constraint of this approach is the limitation to apply the developed model beyond the area of development, which typically consisted of single lakes or reservoirs, because of the large variations of water parameters and spectral features in space and time (Giardino, Oggioni, Bresciani, & Yan, 2010). However, this method has been extensively applied in the literature due its simplicity and well know methodology. The computer requirements are low, ideal to develop models in the pre-computing era. The radiometric features are the input in form of several bands or band ratios to develop the predictive model, which are correlated to observations of the parameter of interest and evaluated through error metrics.

Semi-empirical approaches utilize predictive models that incorporate knowledge of the physical properties of the target parameter and creating indexes specifically developed for a certain parameter, as transparency, chlorophyll-a or suspended solids. These models are the equivalent of the terrestrial indexes for vegetation (NDVI) or snow (NSDI), designed to highlight spectral characteristics of the target parameter. Examples of these are the normalized difference chlorophyll index (S. Mishra & Mishra, 2012), the maximum chlorophyll index (Gower, King, Borstad, & Brown, 2005), the Maximum Peak Chlorophyl (Matthews, 2014) Floating Algal Index (Hu, 2009), and the normalized difference suspended sediment index (Shahzad et al., 2018). These models are limited by the required measurements of specific wavelengths from a sensor where a target parameter may display a particular spectral behavior. Such

measurement is not always acquired by all the sensors due its limitation in spectral resolution.

Analytical algorithms (Seyhan & Dekker, 1986; A. G. Dekker, Malthus, & Seyhan, 1991; Kutser & Arst, 1994; Heege, Kiselev, Wettle, & Hung, 2014) were developed on the basis of the inherent and apparent optical properties of the water and the atmosphere (C. Mobley, 1994; Sathyendranath et al., 2000) to retrieve absorption and backscattering coefficients that can be separated into the elements of interest (optically active constituents) based on an inverse equation (Morel & Gordon, 1980; Sathyendranath et al., 2000; Giardino et al., 2019). Semi-analytical algorithms are the most common in literature because they incorporate in-situ measurements to calibrate the inverse equation (Matthews, 2011). Based on the physics-related nature of this approach, the main advantage is the generalization of the models across spatial and temporal scales. However, the validation of semi-analytical algorithm requires large in-situ measurements and the complexity behind the theoretical development makes the application of this method challenging (Malthus, Hestir, Dekker, & Brando, 2012).

Recently, the introduction of predictive models based on artificial intelligence, and more specifically, the learning branch of it, has demonstrated that machine learning models are capable to construct complex non-linear relationships between remote sensing data and water quality parameters. These approaches are described more in detail in the following section.

2.2 Machine learning

A great variety of algorithms are available for predictions based on machine learning approaches (Camps-Valls, 2009; Lary, Alavi, Gandomi, & Walker, 2016). Recent applications (Figure 2.4) are based on artificial neural networks (Schiller & Doerffer, 1999; Imen, Chang, & Yang, 2015), random forest (Lin, Novitski, Qi, & Stevenson, 2018; Ruescas et al., 2018), support vector machines (D. Sun, Qiu, Li, Shi, & Gong, 2014), or gaussian processes regression (Blix et al., 2017). However, more complex and advanced deep learning models have also been applied in the water quality estimations with success (Peterson, Sagan, Sidike, Cox, & Martinez, 2018; Sagan et al., 2020; Y. Zhang, Wu, Ren, Deng, & Zhang, 2020; Arias-Rodriguez et al., 2021). A summary of commonly used algorithms is provided in Table 2.2.

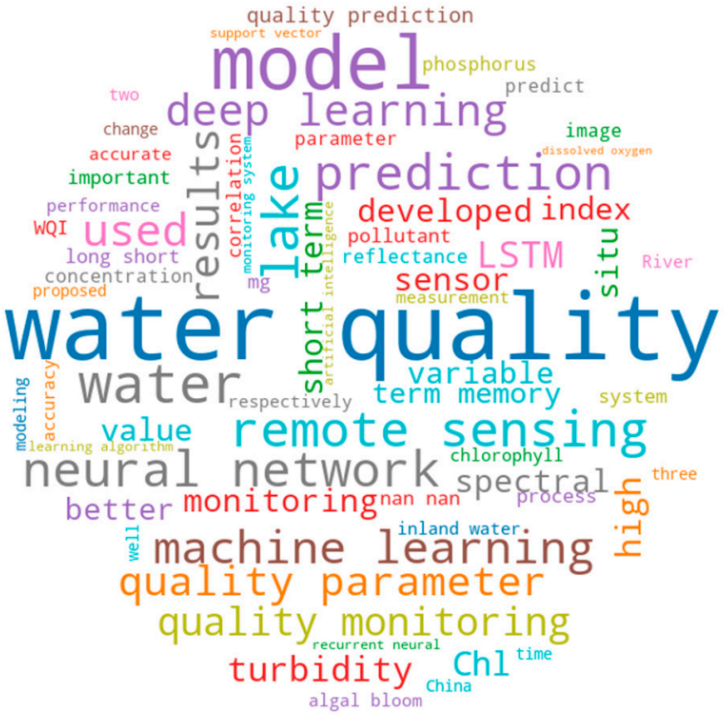

Figure 2.4: Word cloud generated from research articles titles, abstracts, and keywords from research review of remote sensing of water quality of inland waters (taken from Yang et al. 2022).

Machine learning models are characterized for the ability to learn from data. Typically, in a common scenario the outcome is the observed measurement to be predicted. The algorithm uses different variables or features to create and describe the relationship between the two types of data. Usually a training set of data is created from the available data to build the prediction model. In the training dataset, the outcome and features are available for the algorithm to train itself and accurately predict the outcome. The trained model is used then to predict outcomes from features independent from the training dataset (Hastie, Tibshirani, & Friedman, 2009). When used in limited training conditions or in lack of sufficient training data, machine learning models may over-fit the data and the generalization ability can be lost. Therefore, the training and testing datasets are usually evaluation in several random combinations of input data to ensure the representativity of the training process. The main limitation of transferability inherent to empirical models is present in machine learning models because the accuracy of predictions depends greatly on the available training and testing data and the ranges of such observations.

On the other hand, this can be one of the main advantages of machine learning, specially in the digital era where the amount of data produced is abundant. The usefulness of machine learning approaches is particularly increased in the field of remote sensing applications, where geospatial big data leads applications that uses large amounts of spatial data. The potential is enormous since this availability could lead to an automated identification and monitoring of large-scale water bodies and water quality effectively and efficiently (Yang et al., 2022) if effective and efficient processing and analysis is applied (Z. Lee et al., 2018). However, important challenges still limit the full application of machine learning (Yang et al., 2022). Large spatial datasets and long-time archives are complex to deal with, and remote sensing imagery and its processing is also technically demanding. Adequate resources need to be destinated to increase the capacity of stakeholders to work quickly and reliable when monitoring inland waters. Additionally, machine learning models have inherent modeling process challenges. Simpler models are accurate but they often lack scalability. Complex models are computationally extensive and the hyperparameter tuning is time consuming and demanding. Furthermore, machine learning models perform better when feed with abundant training data and, in remote sensing of inland waters, satellite and field samples mismatch is maybe the greater obstacle to increase available data.

Table 2.2: Recent studies using machine learning algorithms in remote sensing of inland waters.

Method	Name	Reference
SVR	Support Vector Regression	(X. Wang et al., 2017; Pu et al., 2019; P. Liu et al., 2019) (Hafeez et al., 2019; L. Li et al., 2019; Peterson et al., 2020) (Aldhyani et al., 2020; X. Li et al., 2021; Cui et al., 2022)]
RFR	Random Forest Regression	(Pu et al., 2019; Hafeez et al., 2019; Cui et al., 2022) (Ruescas et al., 2018; Kravitz et al., 2020; X. Sun et al., 2022) (X. Li et al., 2021)
GPR	Gaussian Processes Regression	(Blix et al., 2017, 2018; X. Sun et al., 2022)
ANN	Artificial Neural Networks	(Chowdury et al., 2019)
LSTM	Long-Short-Term Memory	(X. Wang et al., 2017; S. Lee & Lee, 2018; Yu et al., 2020) (Zou et al., 2020; Hanson et al., 2020; Barzegar et al., 2020) (L. Li et al., 2019; Aldhyani et al., 2020)
ELM	Extreme Learning Machine	(Peterson et al., 2018, 2020; Sagan et al., 2020)
CNN	Convolutional Neural Network	(Pu et al., 2019; Barzegar et al., 2020) (Sharma, Isha, & Vashisht, 2021; Cui et al., 2022)

2.3 Water quality of inland waters

Limitation of water availability is increasing in parallel with growing population because it increases pollution of water resources. The World Health Organization (WHO), estimates that 3 million people dies per year due to water pollution and eutrophication (Vollenweider, Kerekes, et al., 1982). The degradation of water quality occurs most often when a higher loads of wastewaters, heavy metals, nutrients and sediment discharges occurs into streams or waterbodies. To try to control this situation, the study of the water quality defines its status through several chemical, physical and biological properties that help to detect pollution sources that deplete water quality (Usali & Ismail, 2010).

These parameters are usually measured with fixed stations where continuous measurements or buoys are taking continuous measurements of data, but the field sampling is still limited by its spatial scale and the high frequency measurements is costly. However, the field measurements are very important because they describe the water quality status based on their values and ranges. Therefore, many of them are used as indicators of water quality. These water parameters are directly to the trophic state or the catchment processes of inland waters (Adrian et al., 2009). The selection of the indicators feasible to be measured by remote sensing is highly important because the conventional limitations are reduced by means of a remote acquisition. By remote sensing, it is possible to retrieve several water quality parameters by different means, which also alleviates cost and time requirements. One essential characteristic of water that affects the availability of water leaving radiance is water transparency (Peeters et al., 2009) and its effects are directly related to several remote sensing retrievals (as suspended matter or colored dissolve organic matter) and procedures of correction. In water, transparency affects, the bio-chemical processes as photosynthesis, the usage of light as energy to generate chemical fuels by plants and algae, and the production of other aquatic plants (macrophytes). Secchi disk depth (Figure 2.5) is widely used to measure transparency in water. Additionally, suspended matter also influences water transparency by absorbing or scattering light and carries loads of nutrients in water.

As it is intended that the leaving reflectance that is captured by the sensor should be the the water leaving reflectance, the study and analysis of water parameters by remote sensing is usually limited to its behavior on the surface. Analysis of deeper layers is difficult since requires vertical measurements from boats or divers and understanding of the vertical distribution of the parameters in the water column (Hunter, Gilvear, Tyler, Willby, & Kelly, 2010).

Figure 2.5: Conventional measurement of transparency by the author using a Secchi Disk (2013). Location: Plutarco Elias Calles Reservoir, Aguascalientes, Mexico (https://goo.gl/maps/sjjbgq9aZGUVjNZn9).

Common parameters that are measured to control water quality are turbidity (P. L. Brezonik, Olmanson, Bauer, & Kloiber, 2007; Alparslan, Coskun, & Alganci, 2009; B. He, Oki, Wang, & Oki, 2009), chlorophyll-a (Giardino et al., 2014; Lim & Choi, 2015; Santini, Alberotanza, Cavalli, & Pignatti, 2010; Tilstone et al., 2013) concentration of sediment (Bhatti, Rundquist, Nasu, & Takagi, 2008; Onderka, 2008; Sudheer, Chaubey, & Garg, 2006; G. Wu, 2003), dissolved oxygen, nutrients (Shafique, Fulk, Autrey, Flotemersch, et al., 2003; Lim & Choi, 2015; Ali, 2008; Song et al., 2012; C. Wu et al., 2010; W. He, Chen, Liu, & Chen, 2008; X. Wang, Fu, & He, 2011; Hamylton, Silverman, & Shaw, 2013). Furthermore, water temperature (Ahn, Shanmugam, Lee, & Kang, 2006; Casey, Brandon, Cornillon, & Evans, 2010; Handcock et al., 2006; Syariz et al., 2015), metals, salinity (Font et al., 2013; Martin et al., 2012; Reul et al., 2012; Vinogradova & Ponte, 2012), and other contaminants are also considered indicators of water quality (Muller-Karger, 1992) but its study is limited due its weak spectral response when present in the water. The most common water quality parameters which are investigated in remote sensing of inland waters are shown in Table 2.3.

Table 2.3: Commonly measured water quality parameters in remote sensing of inland waters.

Water Quality Parameter	Abbreviation	Units	Optical Activity
Chlorophyll-a	Chl-a	mg/L	OAC
Secchi Disk Depth	SDD	m	OAC
Temperature	T	C	OAC
Colored Dissolved Organic Matter	CDOM	mg/L	OAC
Total Organic Carbon	TOC	mg/L	OAC
Dissolved Organic Carbon	DOC	mg/L	nOAC
Total Suspended Matter	TSM	mg/L	OAC
Turbidity	TURB	NTU	OAC
Sea Surface Salinity	SSS	PSU	OAC
Total Phosphorus	TP	mg/L	nOAC
Orthophosphate	PO4	mg/L	nOAC
Chemical Oxygen Demand	COD	mg/L	nOAC
Biochemical Oxygen Demand	BOD	mg/L	nOAC
Electrical Conductivity	EC	us/cm	OAC
Ammonia Nitrogen	NH3-N	mg/L	nOAC

From these parameters it is important to stress the effect of nutrient loads that affect water quality because they favor the algal blooms and aquatic plant growth, which leads to eutrophication and consumes the dissolved oxygen necessary for fish life (Chapman, 1996). From those blooms, a certain type of cyanobacteria is known for being harmful algal bloom (HAB) organisms which are of toxic nature. On the other hand, high erosion rates deteriorate water quality because the degradation of the water channel, affects water supply structures and create erosion. Some of these parameters can be used as indicators of the water quality or trophic status of the lakes (Adrian et al., 2009).

The need of an adequate monitoring capacity is therefore present when analyzing the many parameters and factors which can be affected in water ecosystems to initiate countermeasures to avoid outbreak events and protect water from pollution. It is precisely here where the monitoring of inland water based on remote sensing approaches is of key importance.

3 Monitoring Water Quality of Valle de Bravo Reservoir, Mexico, Using Entire Lifespan of MERIS Data and Machine Learning Approaches

Arias-Rodriguez, L.F.;
Duan, Z.; Sepulveda, R.; Martinez-Martinez, S.I.; Disse, M.
Remote Sensing 2020, 12, 1586.
Received: 17 April 2020 / Accepted: 14 May 2020
https://doi.org/10.3390/rs12101586

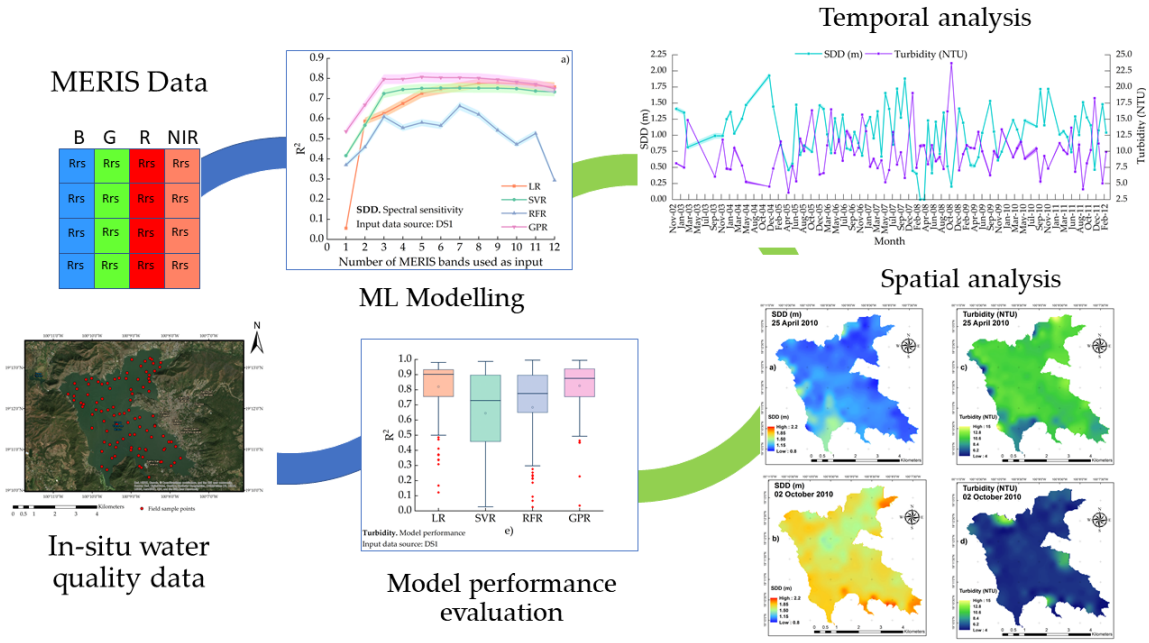

Keywords: turbidity; secchi disk depth; trophic state; remote sensing; gaussian processes regression; support vector machines; random forest regression; inland waters

Abstract

Remote-sensing-based machine learning approaches for water quality parameters estimation, Secchi Disk Depth (SDD) and Turbidity, were developed for the Valle de Bravo reservoir in central Mexico. This waterbody is a multipurpose reservoir, which provides drinking water to the metropolitan area of Mexico City. To reveal the water quality status of inland waters in the last decade, evaluation of MERIS imagery is a substantial approach.This study incorporated in-situ collected measurements across the reservoir and remote sensing reflectance data from the Medium Resolution Imaging Spectrometer (MERIS). Machine learning approaches with varying complexities were tested, and the optimal model for SDD and Turbidity was determined. Cross-validation demonstrated that the satellite-based estimates are consistent with the in-situ measurements for both SDD and Turbidity, with R^2 values of 0.81 to 0.86 and RMSE of 0.15 m and 0.95 nephelometric turbidity units (NTU). The best model was applied to time series of MERIS images to analyze the spatial and temporal variations of the reservoir's water quality from 2002 to 2012. Derived analysis revealed yearly patterns caused by dry and rainy seasons and several disruptions were identified. The reservoir varied from trophic to intermittent hypertrophic status, while SDD ranged from 0-1.93 m and Turbidity up to 23.70 NTU. Results suggest the effects of drought events in the years 2006 and 2009 on water quality were correlated with water quality detriment. The water quality displayed slow recovery through 2011 - 2012. This study demonstrates the usefulness of satellite observations for supporting inland water quality monitoring and water management in this region.

3.1 Introduction

Inland waters such as lakes, reservoirs, and rivers are important water resources; they regulate climate and hydrological flows; support soil formation, nutrient cycling, and pollination; enable food production and water supply; and provide aesthetic conditions, cultural services, and recreation (MAE, 2005). Therefore, their protection is vital and their water quality must be assured. Based on a water body's intended purpose, the parameters of water quality must achieve certain standards. Monitoring these parameters allows for the detection of sudden harmful changes and establishes opportunities for implementing preventive and restorative measures to recover healthy conditions. Conventional methods for monitoring water quality, so-called point sampling methods, determine water quality indicators by collection of samples directly from the field and their analysis in a laboratory. However, these traditional methods have important constraints. First, in-situ sampling is laborious and requires extensive time to cover large areas, which increases costs. Furthermore, investigating the spatial and temporal trends of water quality parameters in large waterbodies is not feasible due to limited sample points, which do not accurately represent the complete status of the water surface (Ritchie, Zimba, & Everitt, 2003). Moreover, the topography can play an important role in restricting access to some areas of water bodies, and errors may still exist in field and laboratory measurements. From the conventional parameters, Secchi Disk Depth (SDD) is a common measurement of water transparency, which can be evaluated using the approach developed by Pietro Angelo Secchi (Preisendorfer, 1986). In this method, a white and black disk disappears inside a water column at a certain water depth; therefore, SDD is commonly measured as a numerical variable for distance as meters (m). Additionally, SDD is inversely related to the average amount of organic and inorganic materials along the water column (Preisendorfer, 1986) and is a practical indicator of trophic conditions (Carlson, 1977; Lathrop, 1992; Cheng & Lei, 2001; Luhtala & Tolvanen, 2013). SDD is employed to study relative nutrient loads and particle contents as well as visually track the flow of suspended detritus and the displacement of sediment influxes from tributary streams and rivers.

In a eutrophication process, the water is affected by algae saturation and other aquatic plants due to excess nutrients. The remaining matter of such aquatic plants depletes oxygen from the water, causing oxygen-dependent life to deplete. Fertilizers from fields, human sewage and animal wastes are the main sources of such nutrient loads. Inland waters with high eutrophication are characterized by poor water quality, which can potentially threaten human health and constrain usage (Khan & Ansari, 2005). Turbidity in a water body is caused by suspended chemical and biological particles via scattering and absorption of light. This water quality parameter has implications for both water safety and aesthetics regarding drinking-water supplies (WHO, 2017). To measure Turbidity, an electronic turbidimeter in nephelometric turbidity units (NTU) is employed, which requires water samples.

Through Remote Sensing (RS), it is possible to acquire information from the Earth's surface. This can be achieved over different scales, regions, and periods of time. Information concerning inland waters can be utilized to retrieve physical and biochemical parameters of the water using the spectral reflectance measured by RS sensors in several bands of the electromagnetic spectrum. This procedure has helped to develop water quality monitoring with RS in the recent decades. The successful history of water quality monitoring applications has been detailed in studies by Dekker (A. Dekker & Peters, 1993), Cheng (Cheng & Lei, 2001), Odematt (Odermatt, Heege, Nieke, Kneubühler, & Itten, 2008), Matthews (Matthews, 2014) and Hansen (Hansen, Burian, Dennison, & Williams, 2017). During its period of operation (2002-2012) and beyond, the Medium Resolution Imaging Spectrometer (MERIS) provided by the European Space Agency (ESA) has been successfully employed to monitor inland waters (Giardino, Candiani, & Zilioli, 2005; Kratzer, Brockmann, & Moore, 2008), and its archives are considered a rich source of data for water research (Matthews, 2011). MERIS has outstanding advantages for monitoring water quality, including full spatial resolution of 260 x 290 m, 15 visible (VIS) and near-infrared (NIR) bands, as well as an extensive web-enabled image archive (2002-2012) (Sepulveda, 2011). MERIS also enables temporal analysis applications with its three-day temporal resolution. The current ESA satellites, the Sentinel-2 and 3 are under operation since 2015 and research of former events must be addressed using archived imagery from prior sensors. Increased use of MERIS for inland water quality analysis was visible during the years before the launch of the Sentinels (2010-2015) with a decrease after 2015. During those years, MERIS was an important source of data for inland water quality research considering the quantity of available sensors (Figure 3.1).

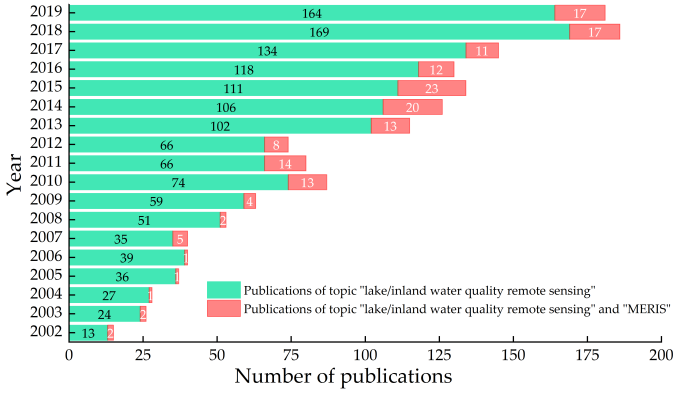

Figure 3.1: Number of publications (2002-2019) listed in the Web of Science for the terms "lake water quality remote sensing" and "inland water quality remote sensing" and the further addition of the word "MERIS" to both terms (literature published January 2020).

Currently, archived data from MERIS contain valuable information in many fields that has yet to be processed, as is the case of applications in inland water quality. This situation opens the need to further research and increases the limited number of studies analyzing the complete MERIS imagery, which leads to a broader scope and better representation of study cases. Despite the advantages of monitoring water quality using RS techniques, these methodologies are not yet broadly applied by applied by water resources and policy managers (Schaeffer et al., 2013). Further research using RS with field measurements is therefore necessary to evidence its benefits and potential in protecting water resources and promptly detecting potential hazards. To estimate water quality parameters, various approaches have been developed based on the relationship between RS reflectance and optical characteristics of water constituents. In general, these methods can be broadly divided in empirical, semi-analytical and machine learning methods (Schaeffer et al., 2013) with further sub-classifications among them.

Empirical methods employ band and band ratio as coefficients to establish relationships. Frequently, several combinations of input values are evaluated through comparison of error metrics looking for the best fit. The result is a regression algorithm that can be applied to the images of the study area and dates of interest to estimate spatial and temporal variations in water quality parameters. This approach is, to some extent, easily applicable when there are enough in-situ and RS data; however, its application is limited to the studied water body and cannot be generalized to other regions due the variations of atmosphere and water composition (Giardino et al., 2010). If an empirical method selects bands or band

ratios based on the knowledge of the physical characteristics of water components that may affect specific wavelengths, then it is classified as a semi-empirical method. On the other hand, analytical approaches use the knowledge of physics of light. They define the specific and necessary parameters of a model on the base of the optical properties of the water and atmosphere also known as inherent optical properties (IOPs). The modeling process produces theoretical absorption and backscattering values which can be separated to estimate optically active water quality constituents using an inverse equation (Hedley et al., 2016). The semi-analytical approaches implement in addition in-situ measurements, to define the parameters of the inverse equation and to reduce the difficulty of modeling complex waters. These models can derive several water quality parameters simultaneously (Giardino et al., 2019) and they can be applicable to other regions different from the original study area. However, their use require various large spectral datasets for training and computing, as well as considerable fieldwork in the regional context to develop robust algorithms (Matthews, 2011; Le et al., 2013; Feng, Hu, Han, Chen, & Qi, 2015; Kallio et al., 2015).

The machine learning (ML) techniques in the RS field were introduced to overcome the complex association between the RS data and the water constituents present in the parametric regression models as least-squares or multiple regression (P. Brezonik, Menken, & Bauer, 2005; Zheng et al., 2015). A standard procedure of regression approaches is the linear regression (LR) which is a statistical method that allows to observe the relationship between two constant numerical variables. It can be classified as an empirical approach in the water quality modeling field or as a ML basic algorithm for data analysts. During this paper we will define LR as a ML approach for further comparison. Another widely applied algorithm is the Support Vector Regression (SVR) (Vapnik, Golowich, Smola, et al., 1997; Noori et al., 2011; Mountrakis, Im, & Ogole, 2011) which is a supervised learning method trained with labeled data. As the support vector machines (SVM) used for classification, SVR algorithm includes the C hyperparameter and the kernel trick. It is useful with a limited number of samples because of its good generalization ability. Also common, the random forest is an adaptable procedure useful for classification and regression (RFR). It employs subsets of the data which are averaged for enhancement of predictive capacity, control of over-fitting and handling of large datasets. RFR has been implemented to several RS applications including water resources (Rodriguez-Galiano, Mendes, Garcia-Soldado, Chica-Olmo, & Ribeiro, 2014; M. Liu, Liu, Liu, Ding, & Jiang, 2015). A more recent method for estimation of biophysical parameters, the Gaussian Processes Regression (GPR) (Rasmussen, 2003; Verrelst, Rivera, Moreno, & Camps-Valls, 2013) provides a Bayesian approach to learn regression problems using kernels (Rasmussen, 2003). It has lately been applied for water quality parameters retrieval from remotely sensed data with high performance in its estimations (Pasolli, Melgani, & Blanzieri, 2010; Verrelst et al., 2012; Blix et al., 2018). When lacking spectral field measurements, the modeling process in ML algorithms can be implemented with less data and different assumptions for their training stage in comparison with radiative transfer models (Kim, Im, Ha, Choi, & Ha, 2014). For water quality studies, the ML approaches analyzing completely and intensively the MERIS imagery of lakes and reservoirs are sparse due to their recent development and the previous operating timeframe of MERIS. Thus, these studies using novel algorithms could take a greater advantage of the legacy of this sensor increasing the usage of such rich source of data.

The Valle de Bravo reservoir in central Mexico is a multipurpose waterbody that provides drinking water to the metropolitan area of Mexico City. It is also the most important reservoir in the country for recreational activities such as tourism, fishing, and sailing (Flores Alvarez, 2016). Most of the previous research in Valle de Bravo is limited due to the use of conventional measuring methods. These constrains are in temporal and spatial scale due to scarce measuring stations or impossibility of continuous sampling campaigns due the time and costs demands. In the last two decades, studies by Olvera-Viascan (Olvera, 1990; Olvera-Viascán, Bravo-Inclán, & Sánchez-Chávez, 1998), Ramirez-Garcia (García et al., 2002), Nandini (Nandini, Merino-Ibarra, & Sarma, 2008) and Figueroa-Sanchez (Figueroa-Sanchez, Sarma, & Sarma, 2014) analyzed the reservoir and expressed concern about its trophic state. Some authors ultimately offered strategies for improving the reservoir's water quality and reducing the presence of toxic cyanobacteria, pointing as main contributors of the degradation of water quality the scarce wastewater management, the agricultural runoff and the surrounding ecosystems factors. In Mexico, there is a national monitoring water quality program under the Sistema Nacional de Informacion del Agua (SINA) with measurement stations (around 5000) distributed across the inland waters of the country, with five fixed stations located in Valle de Bravo. However, these five stations and the measured water quality parameters can likely be insufficient for accurately representing the spatial and temporal scale of harmful events in the water, especially in cases of eutrophication or harmful algae. Moreover, the measured

parameters are limited to control the pollution from wastewaters as biochemical oxygen demand (BOD), chemical oxygen demand (COD), total suspended solids (TSS) and fecal coliforms. The major installation of monitoring stations began in 2012, which indicates there is no comprehensive water quality data about the reservoir prior to this time. As a result of the limited monitoring capacity in the reservoir, there is an increasing demand for continuous monitoring of water quality parameters in the region, especially for such important reservoirs which supply drinking water to great urban areas where millions of people reside. Furthermore, a lack of knowledge of the water quality conditions may persist in the years prior the establishment of monitoring programs. Similar limitations can likely be present in transition and developing economies either because they lack extensive survey networks or because these networks are of recent implementation and therefore no previous data can be acquired. Standard procedures which may help to overcome these limitations are needed and they are of particular benefit for such regions to improve their water quality monitoring capacity. One way to overcome these restrictions is using available resources in combination with current analysis techniques. This leads to clarification of the variations of inland water quality in recent years, together with the implications of natural and anthropogenic hazards in water quality detriment. In this way, overall conclusions of the water quality could be achieved even in lack of extensive field or surface spectral data measurements. Concerns about the water quality conditions and quantity of the water supply raised for the urban region of Mexico City during the previous decade (CNN, 2010; FCEA, 2010; Escolero, Kralisch, Martínez, & Perevochtchikova, 2016) and until today regulation in the supply is commonly applied. As the most important drinking water source for the region, the protection and continuous monitoring of Valle de Bravo reservoir is an essential duty. The understanding of disruptive events that occurred in previous years may lead to a clear comprehension of the current situation and to avoid formerly occurred threats.

To contribute to such needs in the region, this paper analyzes the water quality parameters variations in the Valle de Bravo reservoir for a period of 11 years, prior to the launch of current sensors used for water quality monitoring. Water quality measurements from sampling campaigns conducted in 2010 and RS data from matchup MERIS imagery are used as input for ML algorithms. From the analysis, the best model is selected and applied to the complete MERIS data archives (2002-2012) to examine the spatial and temporal variations of water quality. This could contribute to future research on water quality of lakes and reservoirs where limited monitoring is implemented but the resources to increase its investigation exist. The main objectives of this research are focused firstly, on the development and evaluation of a methodology based on ML approaches using MERIS spectral data and physically water quality data measured in Valle de Bravo. Secondly, on the analysis of the spatial and temporal dynamics of the water quality in the reservoir during the entire MERIS operation timeframe (11 years), which also complements the scarce number of studies taking advantage of the complete MERIS imagery. Also, as the ML techniques are commonly based on different assumptions, a further and continuous evaluation of their predicting capacity is necessary to determine which approach may be better to evaluate and map water quality in the region using MERIS data. Finally, this study also contributes to increase the use of ML techniques in the analysis of water quality parameters in lakes and reservoirs, which are of recent implementation. The results of this work will complement the existing literature for water quality evaluation in the reservoir. To our best knowledge, no comprehensive integration of insitu water quality measurements and RS techniques has yet been implemented to monitor water quality in this region for such amount of time or using ML approaches. This study aims to fill this research gap for the intended water quality parameters. The findings of this work are expected to provide guidance to policy makers on incorporating satellite RS into national insitu water quality control program.

3.2 Study area

Valle de Bravo (Figure 3.2) is a tropical (https://goo.gl/maps/9Y7nxZxZDBXs7NWw6) and high-altitude (1780 masl) reservoir. It has a surface area of 18.55 km^2 and an average depth of 20 m, with a storage capacity of 418.25 x 106 m^3 and a drainage basin of 547 km^2 (Ramirez, Olvera, Pulido, & Duran, 1998; Merino-Ibarra et al., 2008; Gaytan-Herrera, Martinez-Almeida, Oliva-Martinez, Duran-Diaz, & Ramirez-Garcia, 2011). The precipitation measures 836 mm year-1, while the mean annual evaporation measures 1620 mm year-1 (Ramírez-Zierold et al., 2010). The reservoir receives water discharge primarily from the Amanalco River and also from smaller tributaries (Molino, Gonzalez and Carrizal rivers), as well as sewage outlets from adjacent towns (Valle de Bravo and Avandaro). The Amanalco and Carrizal rivers

were formerly detected as the main sources of physical and chemical pollution causing bacterial presence due to incoming nutrient loads of phosphorus and nitrogen from their discharges. The reservoir provides most of the drinking water to Mexico City (21 million inhabitants) through the Cutzamala System -a 330 km network of open channels, tunnels, and aqueducts that brings the drinking water of neighboring reservoirs toward the capital. This network system supplies 25% (19 m^3/s) of the city's drinking water demand by pumping it a total of 1100 m from its lowest to highest point in Mexico City (2250 masl) (GOBMx, 2010). The water balance of such system depends on extractions and injections of water from other neighbor reservoirs, such as Los Colorines, El Bosque, and Tuxpan, located at the east of the reservoir. Critical periods of volume storage occurred during 2006, 2009 and again in 2013, where the reservoir lost 50% of its maximum capacity due to water scarcity. These situations posed serious issues regarding tourism, water quality (CNN, 2010), and supply of drinking water in Mexico City (FCEA, 2010), which escalated the establishment of extraordinary tariffs to control demand.

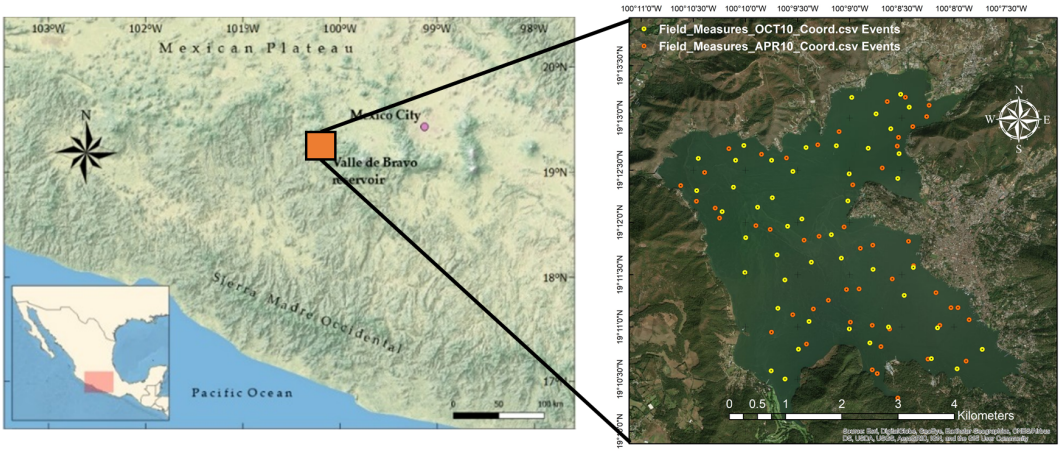

Figure 3.2: Location of the study area and water measurement locations in Valle de Bravo. Orange points indicate field measurements taken on 25 April 2010; yellow dots indicate samples taken on 2 October 2010.

3.3 Materials

3.3.1 Field campaigns

The in-situ data were acquired as part of the research program IN107710 "Water quality monitoring using remote sensing" funded by the National Autonomous University of Mexico (UNAM) through the "Support program to research and innovation technology". Sampling campaigns were performed on 25 April and 2 October 2010. Weather conditions were considered optimal with no rain or cloud coverage in the study area. A total of 96 samples (50 on April and 46 on October 2010) were collected and analyzed. SDD was measured in the field campaign and Turbidity under lab conditions. The SDD was measured using a standard 20 cm diameter acrylic disk divided in black and white quarters. For the Turbidity measurements, the collected water samples were kept in containers with ice and transported to the lab facilities of the Sanitary Engineering Department at the UNAM. The following day, the Turbidity was measured in a Hach 2100N device.

3.3.2 MERIS satellite data

MERIS full-resolution Level 1P products were collected from 2002-2012 with the MERIS FRS extraction tool (https://merisfrs-merci-ds.eo.esa.int/merci/welcome.do) with the selection criteria of low cloud coverage and period of time (image at the mid or end of each month) to ensure a fixed time reference in the analysis and allow significant changes to be visible. For model development, remote sensing reflectance (Rrs) was obtained from the processing of Level 1P MERIS products with acquisition dates on 27 April and 3 October 2010 with ±2 days to the respective field measurement dates (25 April and 2 October 2010, Table 3.1), ensuring the same water quality conditions in the reservoir.

Table 3.1: MERIS imagery corresponding to the field campaign data.

Name	Acquisition	Field Campaign
MER FRS 1PPBCM20100427	27 April 2010	25 April 2010
MER FRS 1PPBCM20101003	3 October 2010	2 October 2010

The two images present low cloud coverage (9-11%) and were processed using ESA's SNAP' software for Sentinel products, which is suitable for MERIS image analysis. The MERIS Level 1 Radiometric Processor was applied for SMILE correction, equalization and radiometric recalibration. Geometrical correction was applied using the MERIS Orthorectification Processor. Adjacency effect was corrected using the Improve Contrast over Ocean and Land processor (ICOL) (Santer, Zagolski, & Gilson, 2009). For atmospheric correction and retrieval of Rrs the Case-2 Regional CoastColour (C2RCC) Processor was implemented which is based on inversion of radiative transfer and bio-optical models using neural networks (Doerffer & Schiller, 2007).

The remote sensing reflectance was selected as output instead of the water leaving reflectance. With training ranges of 0.016-43.18 mg m-3 of Chl-a, C2RCC stands as an adequate processor for the MERIS products used in this study which provides Rrs values and retrieval of inherent optical properties concentrations. The processor is described in detail in Doerffer and Schiller (Doerffer & Schiller, 2007). For model development, to test the effect that different processing levels have in the final retrievals, two different datasets (DS1 and DS2) of Rrs were produced. The DS1 avoids the adjacency processor, as it was seen it modifies considerably the reflectance values, then the Rrs was taken directly from the C2RCC after atmospheric correction; the DS2 does include all the above described corrections. The entire image processing procedure is shown in Figure 3.3.

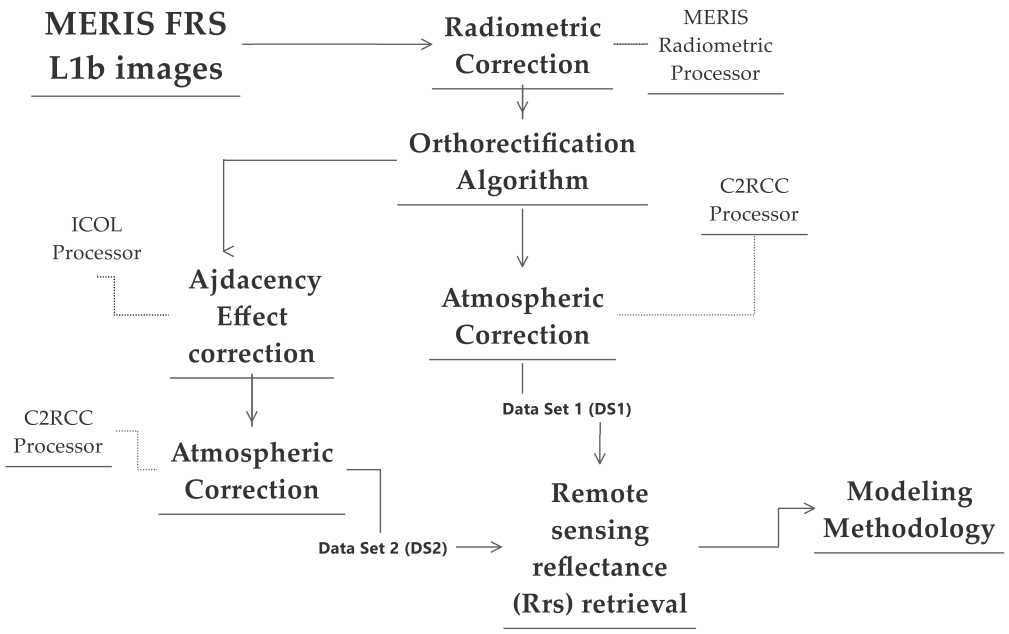

Figure 3.3: Image processing flowchart, including atmospheric correction, optional adjacency effect correction and remote sensing reflectance (Rrs) retrieval.

The Valle de Bravo reservoir (and most inland waters) was masked as land for the processor pixel-expression detection, thus the default-pixel expression was removed allowing the algorithm to process the complete scene. Additionally, the atmospherically corrected reflectance was retrieved as Rrs. All other processing parameters were used as default. The retrieved 12 Rrs bands with wavelengths (in nm) are:

b1 (412.69), b2 (442.56), b3 (489.88), b4 (509.81), b5 (559.69), b6 (619.60), b7 (664.57), b8 (680.82), b9 (708.32), b10 (753.37), b12 (778.40), b13 (864.87). The Rrs data of each measurement location and the in-situ measurements of SDD and Turbidity were used as input base for model development. The reflectance values taken from each pixel correspond to one coordinate in the image, which is already an average value of the pixel area (260 x 290 m).

3.4 Methods

Different regression algorithms were evaluated to develop the predictive model: linear regression (LR), random forest regression (RFR), support vector regression (SVR) and Gaussian processes regression (GPR). Their accuracy was further compared with cross-validation to retrieve R^2 and RMSE, selecting the best model accordingly. All the regression analysis was produced using the open-source resources of the Scikit-Learn library in a Python environment. Hyperparameter tuning results for each algorithm are shown in Section 4.5.

3.4.1 Linear regression

LR is a standard procedure used in many studies since decades (Lathrop, 1992; Cheng & Lei, 2001; H. Duan, Ma, Zhang, & Zhang, 2009) and until recently (Bonansea, Ledesma, Rodriguez, & Pinotti, 2019). It fits a linear model with coefficients to minimize the residual sum of squares between the observed targets in the dataset and the targets predicted by the linear approximation (Pedregosa et al., 2011). Its procedure allows relative straight-forward predictions and has been utilized in absence of spectral field measurements as is the case of this study. The regression analysis followed the general form expressed as:

$$y = \beta_0 + \beta_1 x_1 + \beta_2 x_2 + ... + \beta_n x_n \tag{1}$$

where y is the selected water quality parameter, x refers to the value of the reflectance of a MERIS band, and β is the coefficient band obtained from the multiple regression. Similar approaches can be observed in the studies of Härmä and Kloiber (Härmä et al., 2001; Kloiber, Brezonik, Olmanson, & Bauer, 2002) and more recently from Garaba, Toming or Alikas (Garaba, Badewien, Braun, Schulz, & Zielinski, 2014; Toming et al., 2017; Alikas & Kratzer, 2017).

3.4.2 Random forest regressor

The Random Forest algorithm has been proved as an effective ML algorithm for classification and regression in many fields, including water quality monitoring (Ruescas et al., 2018; Maier & Keller, 2019). Regression trees model non-linear relationships in data between predictors and response variables but with likely problems of overfitting. Random forest introduces randomness into individual regression trees to solve this problem (Maier & Keller, 2019). The forest is composed of decision trees with different subset features and added flexibility, as bootstrap sampling from the dataset.

Each tree is therefore trained with a random vector sampled independently with the same distribution, leading to a generalization of the error for the forest. The result is an increased accuracy using the mean of individual predictions of trees who acted as learners (James, Witten, Hastie, & Tibshirani, 2013). The algorithm of random forest for regression (Breiman, 2001) is constructed for $b = 1$ up to $b = B$ trees, then a bootstrap sample of size N from the training data is selected. After, m random variables from the initial p should be selected as well, the best variable/split-point among the m chosen, and the node split into two daughter nodes for each terminal node of the tree (Tb). The ensemble of trees is retrieved as the computed average of such B trees to make predictions in the form:

$$\hat{Y}(x_i) = \frac{1}{B} \sum_{b=1}^{B} T_b(x_i) \tag{2}$$

Hyperparameters needed to be optimized for RFR are the *n_estimators* that specifies the number of trees in the forest, the *max_depth* which sets the maximum depth of the tree, the *min_samples_split* which is the minimum number of samples required to split an internal node and the *min_samples_leaf* which is the minimum number of samples required to be at a leaf node.

3.4.3 Support vector regressor

The support vector regression (SVR), the regression version of the support vector machine (SVM) algorithm, is a well-positioned ML algorithm that has been applied for water quality studies (Kim et al., 2014) and its use is considered a standard procedure in ML evaluations. It is known for its good generalization capability, particularly with a limited number of samples (Batur & Maktav, 2018). The algorithm looks at the extremes of the datasets and draws a decision boundary defined as a *hyperplane* near those extreme points, establishing a frontier which best segregates between the classes of data. This is done with the aid of separation lines known as *support vectors* which are defined as data points that the margin pushes up against all points that are close to the opposing class. The SVR algorithm gives greater importance to the support vectors. With the hyperplanes, the SVR can be used in multidimensional datasets.

For multidimensional data, a function is used to overcome linearity and transform the data into a high dimensional space but at a higher computational demand. Therefore, a Kernel function, a function that takes vectors as inputs in the original space and returns the dot product of the vectors in the feature space, is implemented. For SVR, linear, polynomial, gaussian radial basis, or hyperbolic sigmoid functions are common. For the regression formulation, consider a set of training points, $(x_1, z_1), ..., (x_1, z_1)$, where $x_i \in R^n$ is a feature vector and $zi \in R^1$ is the target output. Under given parameters $C > 0$ and $\epsilon > 0$, the standard form of support vector regression is:

$$\frac{min}{\omega, b, \xi, \xi^*} \qquad \frac{1}{2}\omega^T\omega + C\sum_{i=1}^{1}\xi_i + C\sum_{i=1}^{1}\xi_i^* \tag{3}$$

$$\omega^T\phi(x_i) + b - z_i \leqslant \epsilon + \xi_i \tag{4}$$

$$z_i - \omega^T\phi(x_i) - b \leqslant \epsilon + \xi_i^* \tag{5}$$

$$\xi_i, \xi_i^* \geqslant 0, i = 1, ..., l \tag{6}$$

where $C > 0$ is the regularization parameter (Pedregosa et al., 2011) [58,70]. In this study the radial basis function (rbf) kernel function was adopted. Hyperparameters needed to be optimized for SVR are the C parameter that acts as a penalty measure of the term and the *gamma* parameter which is the kernel coefficient for types rbf, poly, and sigmoid.

3.4.4 Gaussian processes regressor

The GPR is a non-linear kernel method that establishes a relation between the input and the output variables, in this case, the spectral bands of MERIS and the field-measured water quality parameters, respectively. It has been applied in water quality parameters predictions with successful results and its use starts to be common in evaluation of ML approaches (Pasolli et al., 2010; Blix et al., 2017, 2018). The main objective is to describe adistribution over functions using a Gaussian process specified by its mean and covariance function. The mean $m(x)$ and the covariance function $k(x, x')$ of a real process $f(x)$ are defined as:

$$m(x) = \mathbb{E}[f(x)], \tag{7}$$

$$k(x, x') = \mathbb{E}[(f(x) - m(c))(f(x') - (m(x'))], \tag{8}$$

defining the Gaussian process as:

$$f(x) \backsim \mathbb{GP}(m(x)), k(x, x')) \tag{9}$$

where usually the mean function is considered to be zero (Rasmussen, 2003). To produce predictions in a multidimensional space, the GPR uses diverse kernel types. In this study we selected the rfb kernel together with a noise white kernel function.

Hyperparameters needed to be optimized for GPR are the *alpha* which is a value added to the diagonal of the kernel matrix during fitting; larger values correspond to increased noise level in the observations and the *n_starts_optimizer* which is the number of restarts of the optimizer for finding the kernel's parameters which maximize the log-marginal likelihood.

3.4.5 Hyperparameters tuning

The hyperparameters used on the ML algorithms play a vital role in the performance of the developing models. Fitness and error behavior are affected depending on the assigned values and thus, hyperparameter tuning is a critical and challenging step in the development of the models. In this study, a 12-fold cross-validation was implemented using a *GridSearch* on the relevant hyperparameters. The optimal values are selected from the dataset with better performance in error metrics and presented in Table 3.2. The remaining hyperparameters of each model used default values.

Table 3.2: Hyperparameters setting and results of cross-validation with GridSearch for the ML algorithms.

Method	Hyperparameter	GridSearch Values	SDD Result	Turb Result
LR	-	-	-	-
RFR	*n_estimators*	1, 10, 50, 100, 200 500, 1000, 1500, 2000	1	10
	min_samples_leaf	0.1, 0.5, 1, 5, 10	1	1
	min_samples_split	2, 5, 10, 50, 100	10	2
	bootstrap	True, False	True	True
	max_depth	2, 4, 10, 20, 50, 100, None	50	20
SVR	*C*	0.0001, 0.001, 0.005, 0.0075, 0.1, 0.5, 1, 5, 10, 15, 20, 50, 100, 1000	1000	1000
	gamma	0.0001, 0.001, 0.01, 0.1 1, 5, 10, 100, 1000	1000	1000
	alpha	0.0001, 0.001, 0.0045, 0.0055,	0.0045	1
GPR	*n_restarts_optimizer*	0.0080, 0.01, 0.1, 1, 10 0, 1, 2, 4, 8, 10, 12, 16, 20, 32, 64	2	0

3.4.6 Model evaluation

To determine the most relevant MERIS bands as input for the algorithms, all possible combinations of the 12 MERIS bands were determined through the implementation of a power set (PS) as follows:

$$PS(b) = 2^b \tag{10}$$

where b is 12, the number of MERIS bands, with a total of 4096 possible band combinations per each dataset. The evaluation of each possible combination was assessed with a 12-fold cross-validation as matching number of folds for the available data (96 samples). Conventional proportions for training and validating are in the range of 70-30% or 80-20% when having enough data. With limited data, a *leave one out cross − validation* (LOOCV) could be applied, which evaluates all the available data except for

one value. In this work we set an intermediate proportion between both above approaches, with a 12-fold cross validation, we settle for the middle between 25-20% and the extreme case of LOOCV; which brings us to a 12.5-10% of validation size.

We did not consider evaluating further cross-validation proportions to consider it out of the scope of this work. Finally, the dataset was divided into training (88 samples, 91.67% of the total) and validation sets (8 samples, 8.33% of the total) for the cross-validation. This procedure ensured extensive validation of the dataset and avoided skew results due to random sampling. The error metrics controlling the performance were the R^2 and RMSE:

$$RMSE(y, \hat{y}) = \sqrt{\frac{1}{n_{samples}} \sum_{i=0}^{n_{samples}-1} (y_i - \hat{y})^2} \tag{11}$$

$$R^2(y, \hat{y}) = 1 - \frac{\sum_{i=0}^{n_{samples}-1} (y_i - \hat{y})^2}{\sum_{i=0}^{n_{samples}-1} (y_i - \bar{y}^2} \tag{12}$$

The validations were dependent on the number of bands used as input. To allow an analysis of the spectral sensitivity, all the possible combinations using only 1 band were evaluated and the band with best error metrics determined; similarly, this process was repeated for all the combinations of 2 bands, 3 bands, until 12 bands. On each validation the R^2 and RMSE were calculated to determine the optimal number of bands and its specific wavelength.

The entire approach was applied to all the ML algorithms. When the best conditions (type and number of bands) were found for each model, a further comparison among them was performed using its best resources with several cross-validations. The model with the best metrics was selected for a posterior multitemporal analysis of MERIS data. The workflow diagram of this methodology is shown in Figure 3.4.

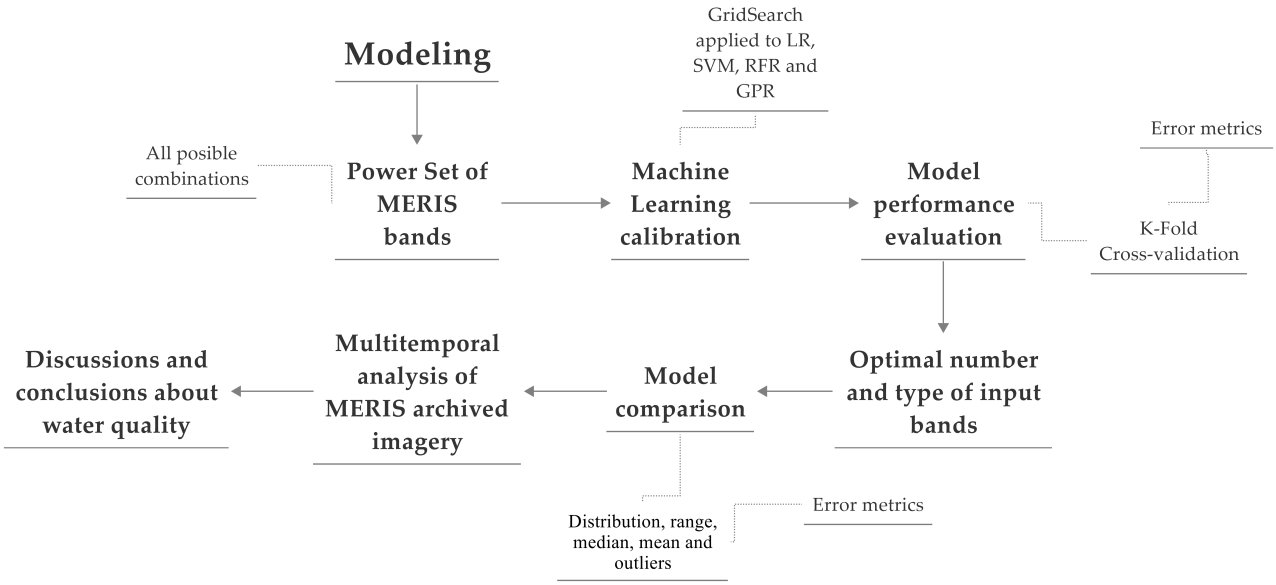

Figure 3.4: Overview of the methodology used in this study.

3.5 Results

3.5.1 In-situ measurements

The two sampling campaigns were performed during rainy (April) and dry (October) seasons. With this, the two predominant conditions of the seasons of the year were acquired. This contributed to the enrichment of the developed models. The statistical properties of the data for the SDD exhibit a mean of 1.36 m with a maximum of 2.03 m and minimum of 0.72 m. The Turbidity mean was 8.2 NTU and the maximum and minimum values were 13 NTU and 4.5 NTU, respectively. The standard deviation measured 0.38 m for the SDD and 3.1 NTU for the Turbidity.

3.5.2 Spectral sensitivity

The feature engineering is of major importance in ML model development. The main objective is to provide higher accuracy and robust results. The spectral sensitivity behavior of the tested algorithms is shown in Figure 3.5.

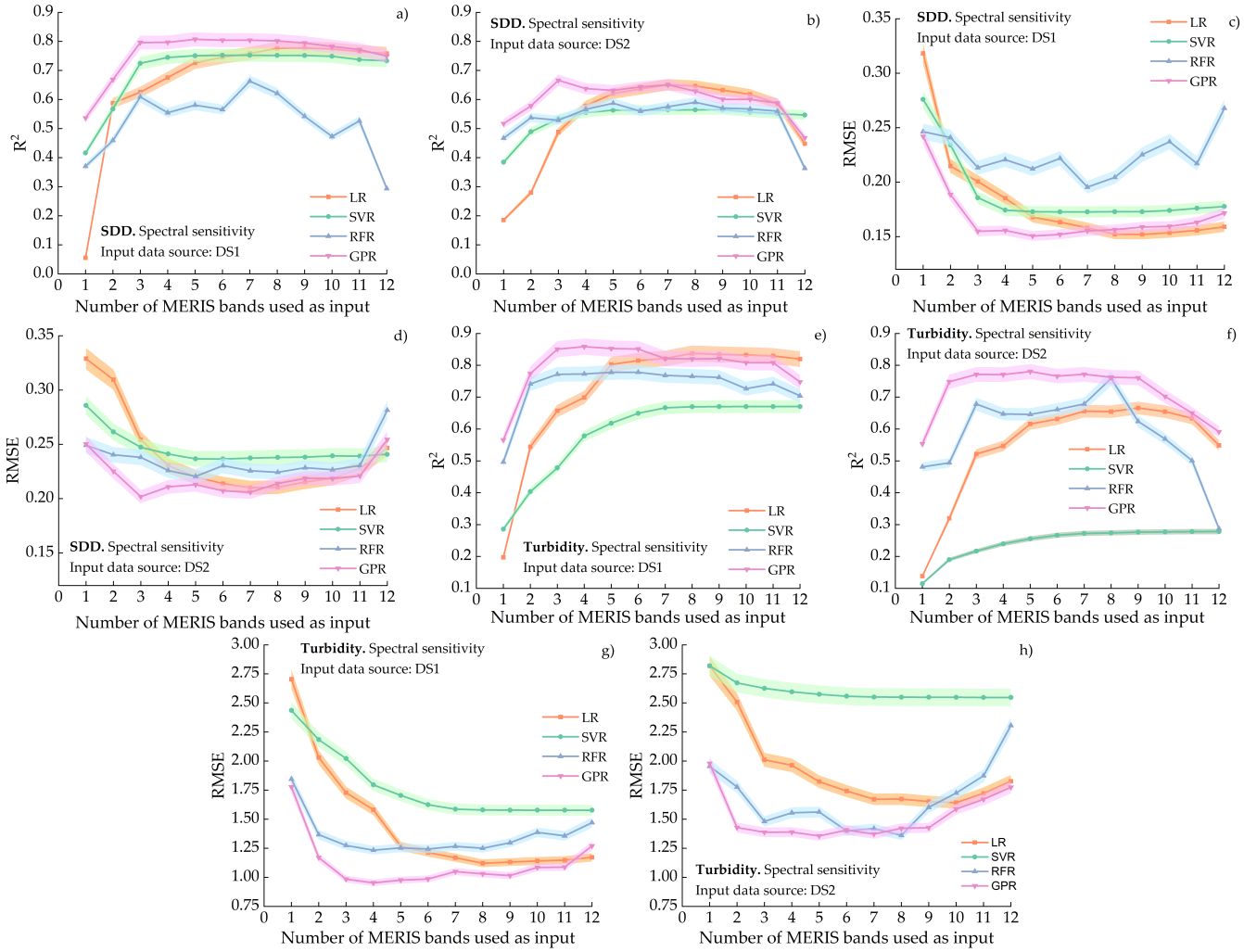

Figure 3.5: Spectral sensitivity of the ML models for different number of MERIS bands and Rrs datasets. R^2 and RMSE are displayed as error metrics. The horizontal axis represents the number of used MERIS bands, not the specific MERIS channel. Dataset origin is indicated in the graph. a) and b) show R^2 and c) and d) RMSE for SDD. Similarly, e), f) and g) and h) for Turbidity. The filling area of each model stands for the error bars.

The 12 bands of MERIS imply a rigorous assessment due to the many possibilities of different combinations as input data for intended algorithms, which also implies high computational demand. The

process is challenging due to the different nature and characteristics of the ML algorithms. To identify the optimal type and number of MERIS spectral bands required for both SDD and Turbidity, we rely on the error metrics evaluated with a rigorous 12-fold cross-validation combined with the appraisal given by the PS. For DS1, differences exist within the models with the addition of spectral bands, especially for the RFR and LR (Figure 3.5 a, c, e, g). But most important, the high collinearity and correlation of the spectral bands is present in all the ML algorithms. This is visible for the interval of 1 to 3 bands, with the high increase of accuracy and minimization of the error. This behavior is present in all the models but more constant in the GPR and less in the RFR. For both water quality parameters, SVR and GPR require only 3 bands to perform satisfactory and constant in R^2 (Figure 3.5 a, e), with no major improvement with the addition of more bands. LR performs satisfactorily ($R^2 > 0.70$) when using 6 bands or more. On the other hand, the RFR behaves inconsistently depending on the number of features added.Its maximum performance is reached with 8 bands. The turning point occurring when using 3 bands is similar for SVR and GPR, however, for SDD the SVR and the GPR start a small decrease in accuracy and error after using 5 bands. For Turbidity, the improvement is high from 1 to 3 bands and then the tendency is constant for GPR. RFR behaves constant after using 2 bands but its performance remains constant at $R^2 \approx 0.75$. SVM does not reach values of the R^2 higher than 0.7 and LR shows high performance when using more than 5 bands with its peak at 8 bands. Accordingly, the RMSE is lower for GPR in all cases (Figure 3.5 c, g). For DS2, a remarkably similar behavior is seen in the spectral sensitivity but with an important decrease in the performance of all models in R^2 and RMSE (Figure 3.5 b, d, f, g). High collinearity is also present in high degree in all the ML models but in lesser extend in RFR. Satisfactory results are not achieved for SDD nor R^2 or RMSE and the GPR stands as the best model for both water quality parameters. For Turbidity GPR and RFR perform with better error metrics (Figure 3.5 f, h) than SDD (Figure 3.5 b, d) but not improving the use of DS1 (Figure 3.5 e, g). The best results of each algorithm with different DS and water quality parameters are shown in Table 3.3. In Table 3.4 the highest error metrics of each algorithm and their optimal number and type of bands are presented and they all are product of the DS1 as result of the evaluation.

Table 3.3: Best combination and number of MERIS bands results of cross-validation. Coefficient of determination (R^2) and root mean square error (RMSE) are shown for the ML methods.

SDD								
Model	**LR**		**SVR**		**RFR**		**GPR**	
Dataset	DS1	DS2	DS1	DS2	DS1	DS2	DS1	DS2
R^2	0.78	0.65	0.75	0.57	0.66	0.59	0.81	0.67
RMSE	0.15	0.21	0.17	0.24	0.20	0.22	0.15	0.20
Turbidity								
Model	**LR**		**SVR**		**RFR**		**GPR**	
Dataset	DS1	DS2	DS1	DS2	DS1	DS2	DS1	DS2
R^2	0.84	0.67	0.67	0.28	0.78	0.76	0.86	0.78
RMSE	1.12	1.64	1.58	2.55	1.24	1.36	0.95	1.35

Table 3.4: Best combination and number of MERIS bands results of cross-validation. Coefficient of determination (R^2) and root mean square error (RMSE) are shown for the ML methods. These combinations belong to the DS1 as result of the evaluation.

Model	**SDD**			**Turbidity**		
	Band Combination	R^2	**RMSE**	**Band Combination**	R^2	**RMSE**
LR	b1, b3, b4, b5, b6, b7, b8, b9, b10	0.78	0.15	DS4	0.84	1.12
RFR	b1, b2, b4, b5, b6, b8, b10	0.66	0.20	DS4	0.78	1.24
SVR	b3, b4, b5, b6, b8	0.75	0.17	DS4	0.67	1.58
GPR	b4, b5, b6, b7, b8	0.81	0.15	DS4	0.86	0.95

The minimum number of bands required for SDD and Turbidity retrieval with relatively good accuracy

(however not the best) are recognized as 2 for GPR, 3 for SVR (SDD) and RFR, and 5 for LR. It is visible that increasing the input bands of MERIS does not significantly improves the fitness or minimizes the error of the prediction. As computational demand often increases when adding more bands to validation procedures and evaluation of further data, this result provides valuable information on how to improve the efficiency of modeling.

3.5.3 Model performance

The results from spectral sensitivity allow a standardized evaluation among the ML models using the optimum number and type of bands determined for each algorithm (Table 3.5), ensuring each model performs under its best conditions. The random sampling of training and testing datasets has a strong influence in the results retrieved for each individual training. Thus, to retrieve a representative set of results and avoid atypical responses, we executed random runs of the models to yield a dataset of 120 predicted values. The results of this process are displayed in Figure 3.6.

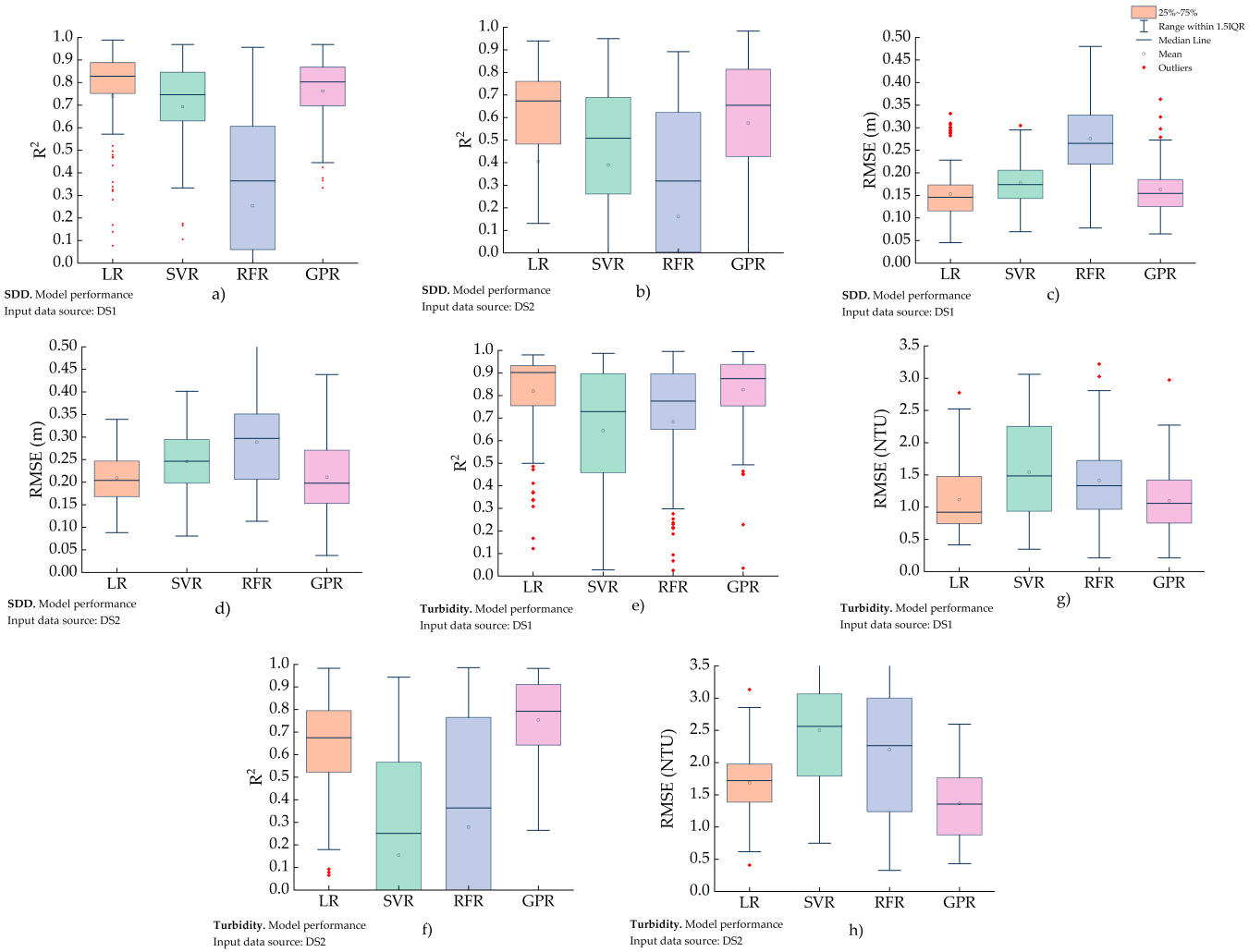

Figure 3.6: R^2 and RMSE distribution of random repetitions (120 values) between the predicted and measured SDD and Turbidity. The dataset origin is indicated in the graph (a,b) show R^2 and (c,d) RMSE for SDD, respectively. Similarly, (e-h) for Turbidity.

Similar to spectral sensitivity results, the DS1 outperforms the DS2 in all the models and error metrics. In DS1, GPR ($R^2 = 0.762, RMSE = 0.163$) and LR ($R^2 = 0.739, RMSE = 0.153$) perform better and more robust for SDD followed by SVM ($R^2 = 0.693, RMSE = 0.177$) and RFR ($R^2 = 0.253, RMSE = 0.276$) (Figure 3.6 a, c). For Turbidity, GPR performs better and surpasses the other models ($R^2 = 0.826, RMSE = 1.099$). It is important to note that RFR acts extremely poor in robustness for SDD and SVM for Turbidity. GPR and LR perform similarly for both water quality parameters. The

main differences are seen on the RMSE where GPR acts more robust (Figure 3.6 e, g). From these results, it is clear that GPR is more stable to the random sampling processes. For DS2, R^2 and RMSE models produced values that are more spread and less robust, following the tendency of the spectral sensitivity (Figure 3.6 b, d, f, h). The best results for SDD are produced using the GPR ($R^2 = 0.58, RMSE = 0.21$) as well as Turbidity ($R^2 = 0.75, RMSE = 1.36$), however, these metrics are still lower than the ones of DS1. In Table 3.5 a summary of the mean results of error metrics is shown. In general, using the DS1, GPR and LR achieved satisfactory and similar performances, which indicates they are good options for water quality parameters retrieval. SVM performed better for SDD than Turbidity and the opposite behavior is seen in RFR. From these results, GPR and LR are the potential methods for retrieval of SDD and Turbidity using MERIS spectral data in this study.

Table 3.5: Cross-validation mean results from 120 samples produced with the best combinations and number of MERIS bands. Coefficient of determination (R^2) and root mean square error (RMSE) are shown for the ML methods.

SDD								
Model	**LR**		**SVR**		**RFR**		**GPR**	
Dataset	DS1	DS2	DS1	DS2	DS1	DS2	DS1	DS2
R^2	0.74	0.41	0.69	0.39	0.25	0.16	0.76	0.58
RMSE	0.15	0.21	0.18	0.25	0.28	0.29	0.16	0.21
Turbidity								
Model	**LR**		**SVR**		**RFR**		**GPR**	
Dataset	DS1	DS2	DS1	DS2	DS1	DS2	DS1	DS2
R^2	0.82	0.63	0.64	0.15	0.68	0.26	0.83	0.75
RMSE	1.11	1.69	1.54	2.50	1.41	2.20	1.10	1.36

3.5.4 Processing efficiency

It is important to consider the processing demand during training and validation on computational resources; depending on the desired application this can play a crucial role. All the models were implemented using Python version 3.7.4. The hardware used was an Intel(R) Core(TM) i7-8665U CPU processor 1.90 GHz and 2.11 GHz, 32.0 GB of installed memory (RAM) and system type 64-bit, x64-based processor. The results of the processing performance are illustrated in Figure 3.7. The process of cross-validation on a power set of 12 predictors (bands) which includes GridSearch of several possible hyperparameters in more than 4000 cases is highly demanding. A major influencing factor is the number of iterations required on the hyperparameter tuning process and the number of predictors needed to be evaluated. A larger number of terms and type of kernel also increases the required processing time in these methods. The settings are as described in Section 4.5 and no increment was used for the *cache_size*.

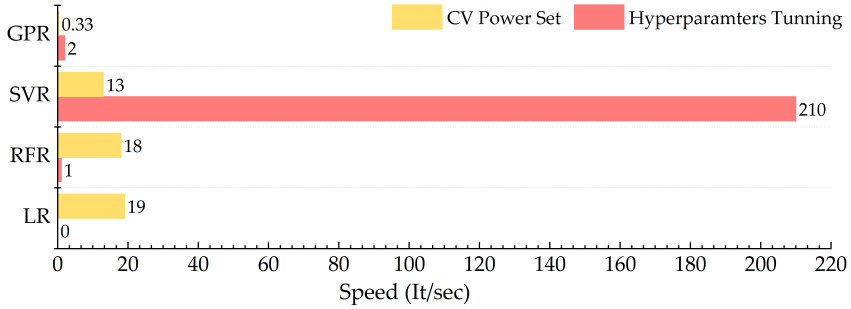

Figure 3.7: Processing performance of the ML models.

SVR immediately stands out, performing at 210 it/sec in the hyperparameter tuning process, far away

from the similar results of RFR and GRP. The LR has the advantage here of no tuning need. During the cross validation of the power set SVR, RFR and LR perform similar with 18-19 it/sec. However, GPR performs the lowest at this point with 0.33 it/sec.

3.5.5 SDD and Turbidity maps

MERIS images from the sampling campaign dates were used to produce spatial distribution maps for both water quality parameters. The GPR was selected according to previous results of model performance and processing efficiency. Figure 3.8 displays the SDD and Turbidity spatial distribution over the water surface.

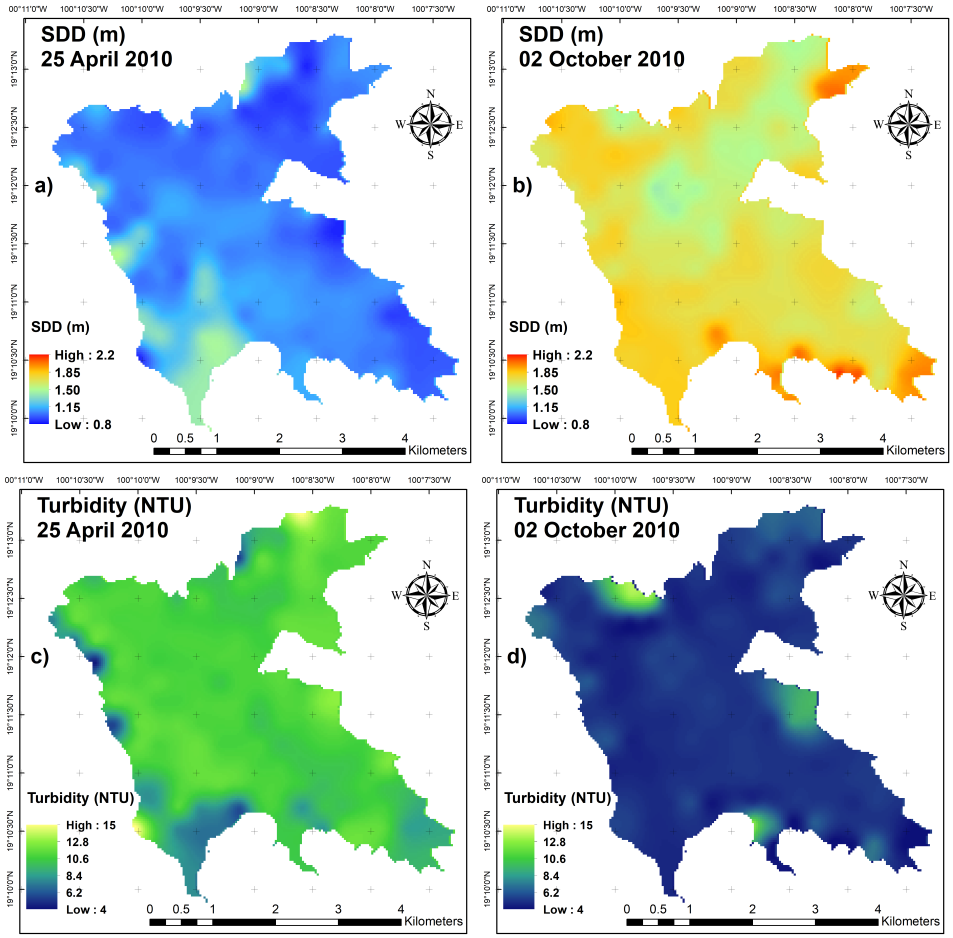

Figure 3.8: SDD and Turbidity spatial distribution maps for the sampling campaigns days in Valle de Bravo. SDD upper (a, b), and Turbidity lower (c, d).

For the spatial resolution, different levels of pixel size were tested to increase the 300 m resolution of MERIS. Interpolation with Spline with Barriers technique was applied in ArcMap'GIS software which interpolates a raster surface using barriers from points with a minimum curvature spline technique. The final resolution of the maps stands in 3 m. The maps revealed higher values of SDD during April and lower in October, the opposite pattern was observed for Turbidity in agreement with the negative correlation of the two water quality parameters. From the maps, it is visible that the higher levels of transparency and lower turbidity are present during October. In April, the southern part of the reservoir presents the higher values of SDD (Figure 3.8 a, green color) and lower Turbidity (Figure 3.8 c, clear blue color), particularly in the entrance of the incoming rivers (Carrizal, Gonzalez and Molino) and the wastewater discharges from neighbor towns. In October, the SDD (Figure 3.8 b, blue color) and Turbidity (Figure 3.8 d, clear blue color) acquire the opposite values and they are more homogenous all around the water surface.

3.5.6 Multitemporal analysis of MERIS imagery

Figure 3.9 exhibits the average monthly value for each parameter in the entire reservoir. Retrievals indicated that SDD ranged from 0 to 1.92 m and Turbidity up to 23 NTU. The correspondence between the SDD and Turbidity is clearly visible, as well as the seasonal dependence of both parameters.

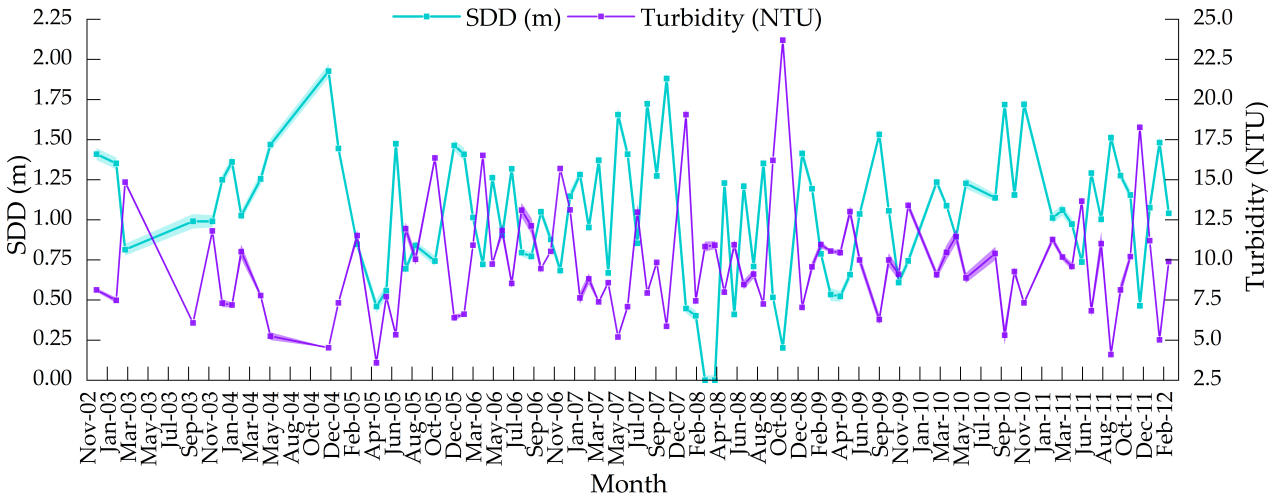

Figure 3.9: Estimated values for SDD and Turbidity in Valle de Bravo for the period 2002 - 2012.

The significant correlation between the two parameters indicates robustness in the model, since the GPR was trained for SDD and Turbidity independently. In general, high turbidity periods (Nov 2005 (16 NTU), Apr and Dec 2006 (16 NTU), Jan, Oct and Nov 2008 (10, 16 and 23 NTU) and Dec 2012 (18 NTU) correspond with low transparency ($SDD = 0.63$ m). During 2008, SDD experienced exceptionally low levels during Mar (≈ 0 m), Apr (≈ 0 m) and Nov (0.20 m). Furthermore, constant tendency of low SDD and high Turbidity were found during a long period in Apr 2005-Mar 2006 and intermittently in Feb-Oct 2008 and Apr-Dec 2009. In contrast, the estimations for the rest of the years have recognizable patterns with high clarity in dry seasons and low clarity during rainy periods. Valle de Bravo experienced the highest transparency during the years of 2004, end of 2007, 2010 and 2012 throughout the period of November reaching peak values in Dec 2004, Sep and Nov 2007 and Dec 2010. During Jan and Nov 2008 high Turbidity is observed, atypical even for other records of years. Recovery was visible from May 2010 and continued with higher SDD during 2012. A further analysis of SDD values per each month during the complete timeframe is shown in Figure 3.10 a. Each year is also displayed with the corresponding months in Figure 3.10 b. Similarly, Figure 3.10 c, d show the Turbidity values per month and year.

The MERIS coverage was poor for the months of August and during the years of 2002, 2003 and 2004. In Figure 3.10 a-d, the patterns of SDD and Turbidity are shown. The higher values of SDD are recognizable during the mid-part of the year (rainy) and the lower values during the last part (dry). The Turbidity shows a corresponding behavior. The years of 2005 (May-Jun), 2008 (Jan-Mar, Oct-Nov), and 2009 (Apr-Jun) show lower values of SDD, Figure 3.10 a, b, and higher Turbidity (2005, 2006, 2008 and 2011), Figure 3.10 c, d. An important missing part of the analysis is the record from the years of 2003-2004 where no major droughts or other emergencies were reported. Due this lack of images, the comparison of common patterns gains uncertainty and the degree of disruption of events during the remaining years remains partially unclear. As said before, the peaks in values of SDD and Turbidity were associated with the years of 2005 and 2008 and they likely represent special cases with consequences during 2006 and 2010. Therefore, these events which are not common in a period of 11 years, should be treated as serious incidents which might pose health threats from suspended solids accumulations and highly turbid water.

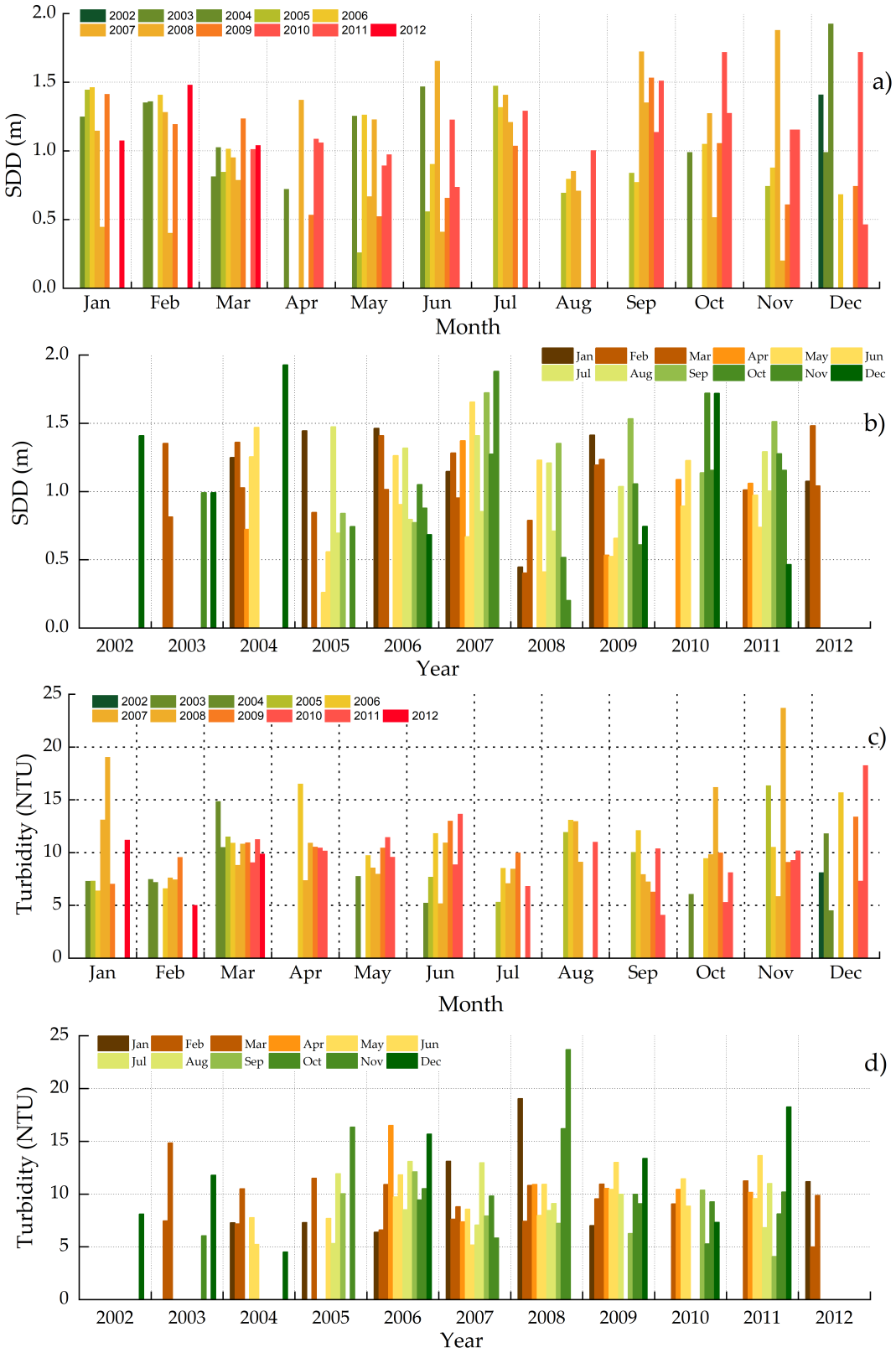

Figure 3.10: SDD and Turbidity analysis per month and year during 2002-2012. Figures 10a and 10b correspond to monthly and yearly analysis of SDD, similarly Figure 10c and 10d for Turbidity.

3.6 Discussions

3.6.1 Performance of machine learning algorithms

The great variety of ML algorithms offers great potential for development of robust models that could predict water quality parameters. This variety, however, also challenges the selection among many candidates and possible train and validation DS. Firstly, the selection of diverse DS of RS data for training is an important step which will contribute to the goodness in performance of the models. In this case, the exception of the Adjacency Effect correction using the ICOL processor in the DS1 implies an unaccounted error in the developed model that was chosen to perform the multitemporal analysis. The adjacency effect affects mainly overestimating or under-correcting the NIR bands. Nevertheless its influence may be lesser significant, thanks to the relatively good error metrics of the models here developed when validating against in-situ measurements,. The validation procedure demonstrated that DS1 produced accurate predictions with substantial improvement between 30-90% in R^2 for SDD and up to $\geq$ 100% for Turbidity over predictions retrieved with DS2 with similar dedicated training time conditions (Figure 3.7). Furthermore, the chosen model for multitemporal analysis, the GPR, only uses NIR bands for Turbidity retrieval (Table 3.4) and the error metrics associated with it remain the highest (R^2 = 0.83, $RMSE$ = 1.05) (Table 3.5). It is recommended, however, to complement the methodology with alternative correction approaches to evaluate further the adjacency effect and its associated errors when using RS in small reservoirs as this case (Brando & Dekker, 2003; Candiani, Giardino, & Brando, 2007).

Secondly, feature selection of representative bands is an important stage that should be addressed with a proper evaluation, to contrast the contributions of different spectral regions to the model. Random selection of the training dataset has a considerable influence in the performance predictions that can be reduced via cross-validation. Furthermore, the tuning of hyperparameters requires rigorous analysis due to the multiple values of a GridSearch; its proper validation should be assessed as well with a cross-validation. Finally, much of the goodness of the models will come from the quantity and quality of the field data gathered, which, in many cases, represents an important limitation. This study contributes to solve the above-mentioned constrains by applying a comprehensive methodology with state-of-the-art ML algorithms using MERIS data. Furthermore, the tuning process results of the hyperparameters are also provided, which could give more insights of typical ranges used for applications in water quality retrievals using RS data. The GPR and the LR models here developed performed with relatively good results and a similar behavior. SVR and RFR performed relatively good on only one of the predicted parameters (SDD for RFR and Turbidity for SVR). The reason for this behavior in RFR could be due to the complexity on the tuning process of the algorithm and the many hyperparameters required to be adjusted as well as the limited number of field data used. In the SVR most likely an extensive search of GridSearch values would be required. In both cases, this also implies a higher computational demand for a proper tuning process, increasing the complexity when apply it in regression applications like this study.

From the results, it is clear that there is a high correlation between the MERIS spectral bands; thus, a specific region of the electromagnetic spectrum cannot be pointed as a clear dominant for the development of the ML algorithms using MERIS due that many combinations produce similar performance (Figure 3.6). In the case of Valle de Bravo, the addition of the blue band could have had an important influence in the GPR model for the estimation of SDD when measuring VIS reflectance, however the green and red regions produce the best model. On the other hand, for Turbidity, the red and NIR bands agrees with the reflection of electromagnetic energy from suspended solids present in the water, which reflect in those regions. However, there is need of only 2-3 bands to produce relatively good performance models and the addition of bands only improves slightly the initial results for GPR. On the contrary, LR and SVM (for Turbidity) require additional bands for a better performance. Although research may tend to use only visible and NIR spectral regions that are known to contribute significantly to the absorption of water, in this study and as part of the limited data, preconceived ideas of former methodologies were not considered and all the available bands were evaluated in correlation with the field data. The result from the mathematical point of view is that, for the developed ML algorithms, some MERIS bands had a strong correlation for this study case and a limited number of bands are likely to produce relatively good results for both water quality parameters (Figure 3.6). This work contributes therefore to open a discussion about the introduction of ML, empirical and semi-empirical methods and their further integration with other existing approaches, as semi-analytical algorithms.

3.6.2 Dynamics of water quality parameters and its influencing factors

The reservoir has marked seasons with dry autumns and winters, along with rainy springs and summers (Figure 3.9). According to the results, in rainy seasons water transparency decreases and Turbidity increases. This could be explained by runoff, suspended matter, and dissolved solids carried in rainy months, enhanced by the possible growth of phytoplankton from incoming nutrients. In contrast, the autumns and winters are characterized by low rainfalls and thus experience less runoff, avoiding resuspension and instead allowing settlement of the suspended matter and dissolved solids, particularly in deeper and less turbid waters. These observations bolster findings from previous studies (Figueroa-Sanchez et al., 2014; Carnero-Bravo, Merino-Ibarra, Ruiz-Fernández, Sanchez-Cabeza, & Ghaleb, 2015). However, it would be expected that these factors are only causing the regular patterns and not the anomalies seen in a deeper analysis for the years 2006-2008 and 2010 (Figure 3.9 and Figure 3.10 b, d). In these years some rainy months exhibited high transparency ($\geq$ 1 m) and lower Turbidity ($\approx$ 10 NTU or lower) (2006: May, Jun; 2007: Jun-July, Sep; 2010: Jun, Sep) (Figure 3.10 a, b). This fluctuation affected the regular patterns also in dry months with low transparency ($\approx$ 1 m or lower) and high Turbidity ($\approx$ 10 NTU or higher) (2006: Oct-Dec; 2007: Jan, Mar; 2010: Mar) (Figure 3.10 c, d). The inconsistency in these values could also affected the observed behavior in years of recovered water volume storage (2010-2012) where SDD and Turbidity variations were clearly correlated with an inverse relationship.

As said before, different aspects such as resuspension, shoreline erosion, loads from river inputs, wind, and water depth are considered important influencers of transparency (therefore SDD) and Turbidity in reservoirs (Sokoletsky, Lunetta, Wetz, & Paerl, 2011). Furthermore, the reservoir is surrounded by neighboring hills with important altitude differences to the reservoir surface (up to 2100 masl compared to 1780 masl) on the reservoir's west and northwest side. The runoff produced by rainfall in rainy seasons carries loads of suspended materials and dissolved solids into the reservoir, causing reduction in SDD and increase in Turbidity because of light attenuation. Therefore, low SDD and high Turbidity are expected from river inflows to the east and southeast during rainy seasons. In dry seasons, the suspended materials and dissolved solids tend to form sediment, and the penetration of light is higher for deep waters. However, these events could not explain completely the change in patterns seen during 11 years of monitoring. Consequently, there is a need of further clarification for the major events affecting the water in the reservoir during this period. Researchers have studied the decrease of water availability in Valle de Bravo, extractions, droughts, and climate change (Escolero et al., 2016). In this sense, a correlation between the water scarcity and the disruption in patterns of water quality parameters may exist. According to local records (Mundial, 2015), in the period of 2006-2007 and 2009-2010, the reservoir lost up to 50% of its storage (Figure 3.11).

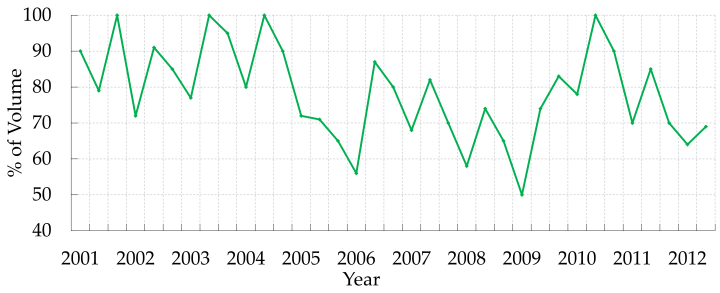

Figure 3.11: Water volume variation in Valle de Bravo (% of its maximum capacity) during the period of 2001-2012. Adapted from ProValle.

The years of critical volume storage observed in Figure 3.11 (2005-2006, 2008-2009) coincide with the periods of disturbance of SDD and Turbidity parameters, clearly recognizable in the years 2006-2009. The findings in this study suggest that there is a possible correlation between the water quality behavior and the decrease of water volume caused by low precipitation (Figure 3.12), which could lead to increased Turbidity and low SDD, particularly in the dry season (Nov-May).

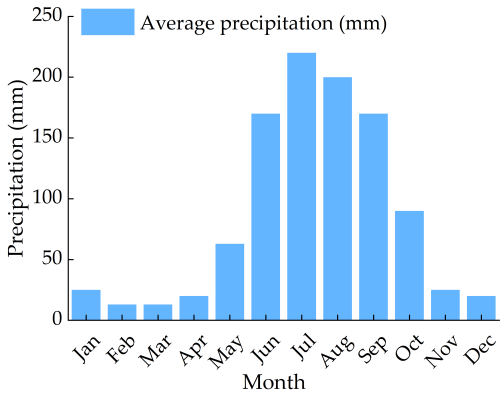

Figure 3.12: Average monthly precipitation in Valle de Bravo river basin. Adapted from CONAGUA.

3.6.3 Water quality status in the reservoir

Water Quality Status in the Reservservoir during the studied period is difficult to infer from physical type parameters as SDD and Turbidity. For an appraisal approach, biological and chemical measures as chlorophyll-a or total phosphorus would be required. However, with the available data, some correlations could be established, and useful insights of biological and chemical parameters obtained. Regarding this, a classification based on collected lake data from the international program on eutrophication of the Organization for Economic Cooperation and Development (OECD) (Vollenweider et al., 1982) is a useful resource for further categorization and an estimation can be then inferred for nutrient and load-eutrophication responses in Valle de Bravo. Applying its classification according to SDD, during most of the 2002-2012 Valle de Bravo was under a hypertrophic status with intermittent recovery in trophic conditions. The hypertrophic conditions are more evident for the period of 2005-2009 with a slight recovery in 2007 (Figure 3.13).

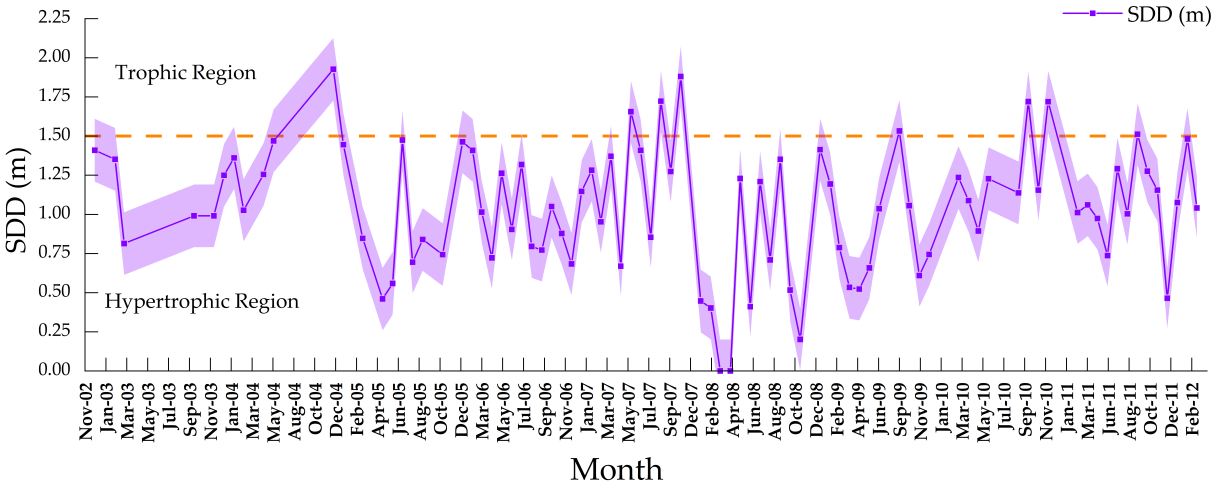

Figure 3.13: SDD (m) values and standard deviation (0.50 scaling factor) of Valle de Bravo during 2002-2012 with the corresponding regions of classification of the OECD.

Valle de Bravo experimented Eutrophic status ($3 < \text{SDD} < 1.5$ m) for 7 months (8% of the period) and Hypertrophic for 77 months (92%). For this period, total phosphorus and chlorophyll-a concentrations could be present with amounts up to 100 mg/m^3 and 25 mg/m^3 respectively according the OECD classification. High levels of phosphate and nitrate could serve as an indicator of the presence of cyanobacteria blooms, which reduces potability of drinking water. This study gathers limited data to obtain strict conclusions about the water quality conditions of the reservoir; however, the findings suggest that there is a clear correlation between the water quality behavior and the decrease of water volume caused by low precipitation.

3.7 Conclusions

Utilizing the remote sensing reflectance from MERIS data and in-situ collected samples, this study developed and validated machine learning algorithms to estimate the water quality parameters of Secchi Disk Depth (SDD) and Turbidity for Valle de Bravo reservoir in central Mexico from 2002 to 2012. Using the dataset 1 (DS1), the models performed well for estimation of both water quality parameters with satisfactory cross-validation results and with a slightly outperformance for GPR (SDD: $R^2 = 0.81$; $RMSE = 0.15$ m, Turbidity: $R^2 = 0.86$; $RMSE = 0.95$ NTU) followed by LR, SVM and RFR. With this, the contribution to the continuous analysis of MERIS imagery stored is reinforced. The results obtained confirm that ML algorithms are current useful approaches to retrieve water quality parameters from RS data.

From the temporal analysis it, is suggested that the droughts of 2006 and 2009 acted in detriment of the water quality of the reservoir. The seasonal fluctuations were affected with unusual behaviors during 2006-2009 and contributed to lower values in 2010. The water transparency measured with SDD retrieved low values ($\approx$ 1 m) during these periods. The Turbidity estimations confirmed this behavior with high values ($\approx$ 12 NTU) during the same years. The suggested classification indicated an evolution from an initial trophic stage in 2002-2005 to an intermittent hypertrophic one during 2006-2008 and 2010, before a slight recovery to trophic status during 2011-2012. The water patterns also suggest that periods with low SDD and high Turbidity coincide with the rainy months (June-October) and thus, runoff of surrounding areas could have had influence on transparency owing to the loads of suspended materials and dissolved solids. On the contrary, opposite behavior, high SDD and low Turbidity was observed in dry seasons.

The methodology applied in this study yielded results that were consistent with independent evaluations, confirming the idea that RS techniques are powerful tools for overcoming limited resources when planning monitoring programs of water quality, even across long time periods. The synchrony of field measurements and the acquisitions of the sensor is of major importance. Ideally, same day in situ data is preferred for validation of satellite products. Regarding this study, it is necessary to consider that greater uncertainties in the results may be present due the variation of $\pm$ 2 days between field and satellite data collection. To avoid this, it is recommended to conduct continuous field measurements and use sensors with enough temporal resolution. Local water quality monitoring systems are present in different countries of the world to periodically analyze the state of inland waters. Such systems have great potential for integration with RS techniques. This combination could allow extensive spatial and temporal analysis on a greater scale. Scheduled field campaigns paired with the date of image acquisition by respective satellites could be useful for data calibration, training, and validation. The continuous measurements of water quality parameters could serve as a constant source of field data. The RS resources, as the MERIS archives, offer valuable data and an important opportunity to contribute to the understanding of how diverse events influence inland waters. The study of data acquired from sensors such as MERIS is essential for the understanding of the water quality of lakes and reservoirs in the last two decades. The current operational satellites, particularly the Sentinel-2 and Sentinel-3, are the natural successors of ENVISAT with MERIS sensors; however, extensive analysis of periods of time of any inland water compelling the first 20 years of the 2000 years would require the contribution from MERIS for a wider monitoring. For the case of Valle de Bravo, this study could serve as a base for further monitoring using Sentinel data and investigate its evolution during the remaining 8 years of the decade. The full exploration of the usefulness and performance of MERIS in monitoring inland water quality would be beneficial to the development and improvement in utilization of successor satellite missions/sensors, i.e., the Sentinel-3 with OLCI instrument, that is continuity of the MERIS instrument capability. The validated good performance of estimated water quality parameters using MERIS data in this study provides confidence in combining MERIS and successor satellite missions to extend a longer term monitoring of inland water quality.

ML regression models are useful methods to retrieve water quality parameters for the first decade of the century using MERIS imagery, particularly in inland waters with special importance for human health, as seen in the encouraging accuracies retrieved. Future work will focus on (i) gather in-situ national water quality monitoring system datasets, (ii) process spectral datasets of current sensors like Landsat 8 OLCI or Sentinel satellites, (iii) extend the analysis of inland waters of the region where the most of the water quality remains uncertain at long-time period scale, (iv) assess new approaches like variations of linear regression (ridge linear regression, radius neighbor regression, elastic net regression)

or trees (gradient boost regression trees) and (v) estimate other important water quality parameters as Chl, CDOM, TSS or nutrients. All the above with the aim to contribute to the knowledge of water quality status and trophic state of inland waters in regions which have not been previously studied using remote sensing techniques.

Author Contributions: Z.D. and L.F.A.-R. conceived this study. L.F.A.-R. and Z.D. conducted data processing and analysis. L.F.A.-R wrote the original version of the manuscript with extensive guidance from Z.D. The in-situ measurements of water quality parameters for this study were provided by R.S. Constructive comments and improvements of the manuscript were provided by Z.D., S.I.M.-M. and M.D. through extensive discussion. All authors have read and agreed to the published version of the manuscript.

Funding: This article was accomplished with the financial support for research of the Mexican National Council for Science and Technology (CONACYT) and the Federal Department of Energy (SENER) through its funding "CONACYT-SENER Sustentabilidad Energetica" CVU 678957 to L.F.A.-R. Furthermore, this work was supported by the German Research Foundation (DFG) and the Technical University of Munich (TUM) in the framework of the Open Access Publishing Program.

Acknowledgments: The authors would like to thank the persons involved in the field campaigns in Valle de Bravo, with the participation of R.S. and the support of the Sanitary and Environmental Engineering Department (DISA) from the National Autonomous University of Mexico (UNAM). They would also like to thank the Technical University of Munich (TUM) and its Graduate School (TUM-GS) for providing all the institutional services and facilities used in this study. They are further grateful to the ESA for providing the necessary MERIS data and software. Additionally, they would like to acknowledge the TUM fellows A.G. Padilla, Jaime Vigil, and Maria Galli. Many thanks as well to Thomas Schneider from the TUM Chair of Aquatic Systems Biology and Marco Koerner from the TUM Chair of Remote Sensing Technology for their valuable advice and opinion about this paper. We would like finally to thank the peer reviewers for providing constructive comments, which extensively improved this manuscript.

4 Integration of Remote Sensing and Mexican Water Quality Monitoring System Using an Extreme Learning Machine

Arias-Rodriguez, L.F.;
Duan, Z.; Diaz-Torres, J.d.J.; Basilio Hazas, M.;
Huang, J.; Kumar, B.U.; Tuo, Y.; Disse, M.
Sensors 2021, 21, 4118.
Received: 21 May 2021 / Accepted: 10 Jun 2021
https://doi.org/10.3390/s21124118

Abstract

Remote Sensing, as a driver for water management decisions, needs further integration with monitoring water quality programs, especially in developing countries. Moreover, usage of remote sensing approaches has not been broadly applied in monitoring routines. Therefore, it is necessary to assess the efficacy of available sensors to complement the often limited field measurements from such programs and build models that support monitoring tasks. Here, we integrate field measurements (2013-2019) from the Mexican national water quality monitoring system (RNMCA) with data from Landsat-8 OLI, Sentinel-3 OLCI, and Sentinel-2 MSI to train an extreme learning machine (ELM), a support vector regression (SVR) and a linear regression (LR) for estimating Chlorophyll-a (Chl-a), Turbidity, Total Suspended Matter (TSM) and Secchi Disk Depth (SDD). Additionally, OLCI Level-2 Products for Chl-a and TSM are compared against the RNMCA data. We observed that OLCI Level-2 Products are poorly correlated with the RNMCA data and it is not feasible to rely only on them to support monitoring operations. However, OLCI atmospherically corrected data is useful to develop accurate models using an ELM, particularly for Turbidity ($R^2 = 0.7$). We conclude that remote sensing is useful to support monitoring systems tasks, and its progressive integration will improve the quality of water quality monitoring programs.

Keywords: Landsat 8 OLI; Sentinel 2 MSI; Sentinel 3 OLCI; water quality monitoring system; extreme learning machine; support vector regression; inland waters; turbidity; Chlorophyll-a; secchi disk depth

4.1 Introduction

Inland waters, as a source of good water quality, are essential to human health. The amount of worldwide population relying on surface water for drinking purposes ranges between 70 and 85% (Morris et al., 2003). Additionally, surface waters provide services such as irrigation, fisheries for food, hydropower, purification of wastewaters, flood protection, wetland plants for fuel and construction, as well as water and nutrient cycling provided by surface waters (UNEP, 2016). The impact of human anthropogenic activities such as discharge of waste products or increased loads of nutrients and sediments from agriculture and urban areas escalate the eutrophication of global inland waters. This situation raises concerns about the protective measures of inland water resources and how to ensure their adequate environmental quality. A fundamental task to understand and prevent environmental threats is the continuous monitoring of water quality. The information gathered during monitoring is used to warn of current and emerging risks and assent of applicable regulations by pointing to changes in trends of quality parameters. From monitoring, empirical data is provided to aid decision-making on health issues, and it provides evidence for water quality management in the long term. Currently, monitoring water quality is a growing challenge because of the difficulty in costs and time resources of sampling tasks and identifying a large number of chemicals for industry and domestic uses that make their way into inland waters. Nowadays, every country is responsible for the state of its water. In developing countries, the priority has been to supply drinking water and control wastewater. In these cases, water quality monitoring programs are designed to be conducted with conventional, boat-based, or buoy-based measuring techniques at specific times and locations and their subsequent laboratory analysis. Some national monitoring programs for inland waters are already under continuous development and operation.

In Latin America, Mexico has established a national water monitoring network (RNMCA) since 1996. Initially, with 200 stations and a sampling frequency of 2 to 3 campaigns a year for lakes, it has gradually been expanded to operate with more regularity after a major renovation in 2012. Today, 2700 stations integrate a surface water dataset with information about the location of the stations and measurement frequency. In Brazil, a similar number of stations (4500) were planned to be reached by 2020 (Iagua, 2014), but other cases are still in need of improvement, such as Argentina with 617 stations (RFMA, 2014) or Chile, where until 2009, it lacked a coordinated monitoring system at a national level (Meza, 2009). However, even with the improvement in such cases, the coverage in spatial and temporal scales of the water monitoring programs is limited by the economic costs of each sampling station and the frequency of measurement. Remote sensing offers a strong potential to monitor water quality in inland waters because it magnifies forthcoming data availability by providing radiometric measures prone to be associated with water quality parameters. Mainly visible (VIS) and near-infrared (NIR) bands of the electromagnetic spectrum have been used in several studies to obtain correlations between radiometric data acquired from sensors on board satellites and physical and biochemical constituents in water (Kloiber, Brezonik, & Bauer, 2002; Miller & McKee, 2004; Matthews et al., 2010; El-Din, Gaber, Koch, Ahmed, & Bahgat, 2013; Giardino et al., 2014; Medina-Cobo, Domínguez, Quesada, & De Hoyos, 2014; Watanabe et al., 2015; Pereira, Andes, Cox, & Ghulam, 2018). As a result of many years of research, the UN Environment Project recognizes the need to integrate remote sensing sensors in the water quality monitoring tasks (UNEP, 2016).

To reliably establish such relation from modeling, radiometric values and in-situ water quality measurement should be acquired in a coincident acquisition date. Models capable of finding a relationship between radiometric data from sensors and water quality constituents can be classified as empirical, semi-analytical, or machine learning-based (Topp et al., 2020). Empirical models fit a standard linear regression between spectral radiometric values in the form of bands or band ratios from the sensor and in-situ water quality measurements. These models are simple and transparent in their process, requiring minimal computational requirements. However, they are limited to the range and temporal scale of the input data because weather conditions and water conditions create significant alterations in observed radiometric data, bounding its regional generalization. Semi-analytical models are based on the optical properties of the water and the atmosphere, which are unrelated to the light field and are therefore called inherent optical properties (IOPs). These IOPs are used to calculate absorption and backscattering coefficients from which water quality parameters can be retrieved. Because of its physics background in the properties of water and atmosphere, these models are generalizable on a regional scale. However, there is a need for extensive in-situ data for validation. The required information about atmospheric composition

and bottom reflectance makes its application difficult where this data is missing (Malthus et al., 2012).

Machine learning (ML) incorporates the advantages of empirical modeling but with an increased computational capacity to handle complex nonlinear relationships. Similar to empirical methods, ML algorithms are limited by the range and settings of input data of its trained models. However, they present several advantages such as iterative learning to reduce the overall error and to maximize fit (Hastie et al., 2009). Due to its novelty, the use of ML is still not well understood in water quality retrievals, and its application is still necessary to further understand its behavior in remote sensing of inland waters (Arias-Rodriguez, Duan, Sepúlveda, Martinez-Martinez, & Disse, 2020). Several sensors are available for potential applications in water quality retrievals to supply these varieties of models with input data. The Operational Land Imager (OLI) onboard NASA's satellite Landsat-8 (launched 2013) has a broad background of applications in inland waters through the former Landsat missions (Meisner, 1983; Yacobi et al., 1995; P. Brezonik et al., 2005; F. Wang, Han, Kung, & Van Arsdale, 2006; Watanabe et al., 2015; E. Vermote, Justice, Claverie, & Franch, 2016; Peterson et al., 2018). Despite its original design for terrestrial applications, it is suited to inland waters due to its spatial and spectral resolution (11 spectral bands, up to 30 m spatial resolution) and with the drawback of a sparse temporal resolution for regular monitoring (16 days) (Gholizadeh et al., 2016). The use of Medium Resolution Imaging Spectrometer (MERIS) (15 bands, 300 m resolution) on board the European Space Agency (ESA) ENVISAT contributed to monitoring inland waters from 2002 to 2012 (Odermatt et al., 2008; Kratzer et al., 2008; Matthews et al., 2010; Arias-Rodriguez et al., 2020) and its archives still offer a potential data mine for further applications. The ESA designed the Ocean and Land Color Instrument (OLCI) on board the Sentinel-3 with similar and improved characteristics (21 spectral bands, up to 300 m spatial resolution) is expected to assume the legacy of MERIS and continue with suitable applications on monitoring inland waters. The MultiSpectral Instrument (MSI) onboard Sentinel-2 has suitable characteristics for water quality monitoring (13 spectral bands, up to 10 m spatial resolution) and temporal resolution (10-days single and 5-days combined constellation revisit frequency of Sentinel-2A and Sentinel-2B). Chlorophyll-a (Chl-a) concentrations have been recently investigated with MSI in different locations worldwide such as Estonia (Ansper & Alikas, 2019) or Africa (Buma & Lee, 2020). The utilization of geographic information systems (GIS) is a key resource to gather and manage field and remote sensing data. GIS merges different types of data into a common framework where layers of information are displayed to detect patterns and relations. These observations are useful to communicate, analyze and take decisions to solve complex problems. For monitoring, GIS plays a key role, because of the clear manner the changes can be detected using a variety of data (Tamm & Tamm, 2020). When monitoring inland waters by remote sensing, the patterns of water parameters are retrieved from models using sensors' data and they are commonly displayed in spatial and temporal scales, represented in maps of spatial distribution (Bonansea, Rodriguez, Pinotti, & Ferrero, 2015).

Despite the available approaches in computational modeling and remote sensing data, the consideration of such techniques when planning and executing tasks in water quality monitoring is limited. Consequently, remote sensing may not be recognized as the main driver of the design of water quality monitoring programs and decisions of water managers. This may be because local managers are not considering technical expertise in remote sensing techniques and because research integrating data from entire water monitoring programs for modeling purposes is scarce (Schaeffer et al., 2013). Therefore, an evaluation of remote sensing techniques using data from water quality monitoring programs is necessary as an initial step to foster the integration of remote sensing data into the monitoring routines. This work addresses this situation using the RNMCA in Mexico as a case study, acquiring entire time series of relevant-remote-sensing water quality parameters. This data is matched with available remote sensors and modeled through machine learning approaches to evaluate the feasibility of integrating existing monitoring data into predictive models. Additionally, we provide suggestions to improve monitoring programs with the progressive integration of remote sensing.

The specific objectives of this study are: (1) to verify the feasibility to use existing data (gathered with no considerations of remote sensing) from monitoring programs in a routine of water quality parameter retrievals by remote sensing; (2) evaluate readily-to-use (Level 2 Products) water quality remote sensing products with respect to historical water quality measurements; (3) use radiometric data from available sensors and machine learning techniques for water quality parameters estimations; (4) find feasible water quality parameters and inland waterbodies for such monitoring routine. Additionally, it is provided a

critical opinion of the main limitations and challenges when integrating these two independent sources of data. This work highlights the need of upscaling this research field using national-wide monitoring data, evaluating different available sensors, and applying multitemporal analysis with the availability of the sensor's archives.

4.2 Study area

We study five Mexican lakes identified by the Mexican water authority as the most relevant ones in terms of size and regional use, therefore we considered them as priority targets in terms of the integration of monitoring systems with remote sensing: Chapala, Cuitzeo, Patzcuaro, Yuriria, and Catemaco (CONAGUA, 2018). These are all located in the Trans-Mexican Volcanic Belt (TMVB) and have a volcanic origin, with the exception of the lake of Yuriria, which is artificial. Catemaco belongs to the Gulf-Center hydrological-administrative region, and the other four lakes are within the Lerma-Santiago-Pacific area (Figure 4.1). The sampling stations of the RNMCA are displayed in Figure 4.2.

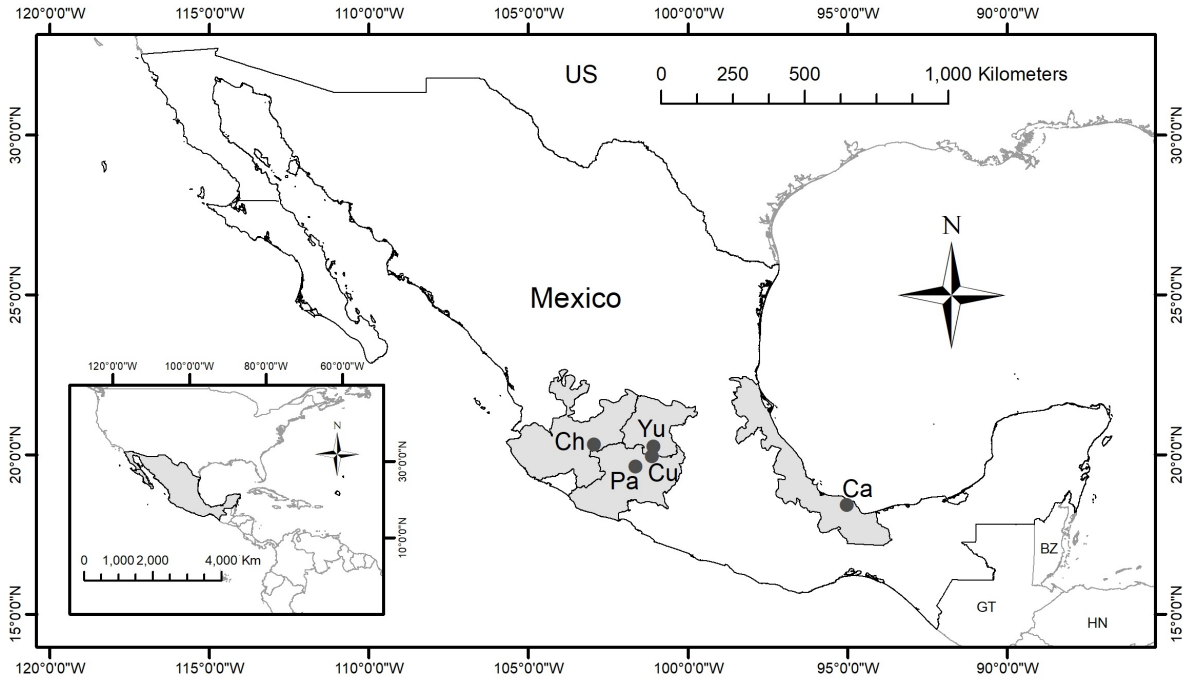

Figure 4.1: Regions and locations of the studied lakes in Mexico. Ch: Chapala, Cu: Cuitzeo, Pa: Patzcuaro, Yu: Yuriria, Ca: Catemaco.

Chapala Lake is the largest inland lake in Mexico. It covers approximately 3% of its territory with an area of 1116 km^2, and it is considered one of the largest and shallowest tropical lakes in the world (CONAGUA, 2018). It is located at 1523.8 m.a.s.l. at https://goo.gl/maps/sArLqNqPtruMGMRRA. It has a mean depth between 4 and 6 m with a maximum depth of 8 m. Its dimensions are 75 km in length and 5.5-20 km in width (López-Hernández, Ramos-Espinosa, & Carranza-Fraser, 2007; Otto et al., 2020). The lake's primary input is precipitation, but it also receives water from the water sheet and several streams, the Lerma River being its main tributary. Evaporation, pumping, and the Santiago River are the main outflows (Membrillo-Abad et al., 2016). The lake's catchment area is a mixture of lacustrine sediments with volcanic rocks and basaltic and andesitic lavas accumulated since the Miocene. Thermal springs, outcrops, and calcareous sinter are also present in the basin (de Anda, Shear, Maniak, & Valle, 2004). The weather in the catchment is mainly humid subtropical, with a mean annual precipitation of 730 mm and a uniform temperature around 24°C (Membrillo-Abad et al., 2016). Chapala lake has a high level of sediments and turbidity, partly by the geology and topology of the area that facilitates the transport of clay particles to the lake. In particular, the Lerma River can carry many sediments from areas affected by erosion (de Anda et al., 2004; Otto et al., 2020). Due to intense water extraction, dry periods, and land-use change, the lake's volume has decreased up to 42% (Membrillo-Abad et al.,

2016). In addition, the rivers and streams can transport contaminants from industrial, agricultural, and livestock activities in the catchment area (López-Hernández et al., 2007; Otto et al., 2020).

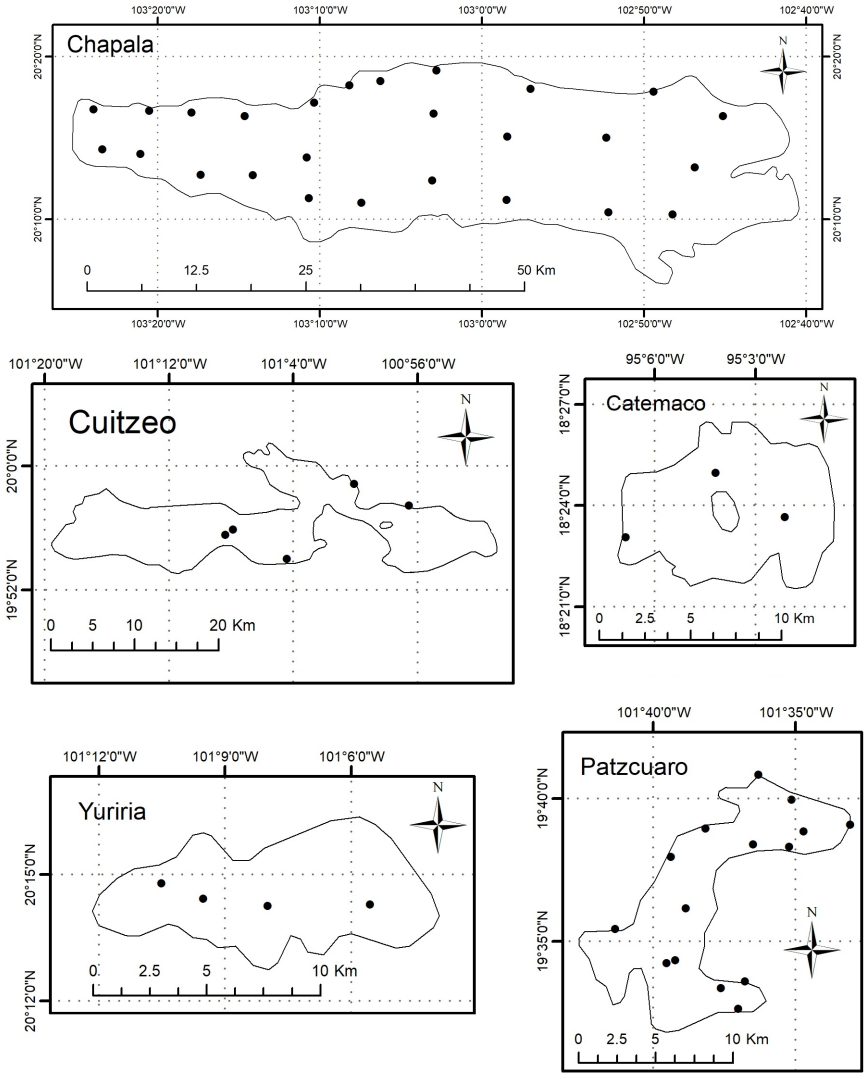

Figure 4.2: Location of the RNMCA sampling stations (black dots) in the lakes: (a) Lake Chapala, (b) Lake Cuitzeo, (c) Lake Patzcuaro, (d) Lake Yuriria, and (e) Lake Catemaco. The scale is different for each lake.

Located at 1820 m.a.s.l and in https://goo.gl/maps/Zw3ghwNfzxtvoVZ36, Lake Cuitzeo is the second largest lake in the country by surface area (M. E. Mendoza, Bocco, Bravo, Granados, & Osterkamp, 2006; Villalobos-Castañeda, Alfaro-Cuevas, Cortés-Martínez, Martínez-Miranda, & Márquez-Benavides, 2010). With a maximum potential area of 420 km^2, currently, Cuitzeo Lake consists of brackish waters of 1-2 m of depth over an area fluctuating around 300 km^2 (M. Mendoza, Bocco, López-Granados, & Bravo Espinoza, 2010; M. E. Mendoza, Granados, Geneletti, Pérez-Salicrup, & Salinas, 2011). The lake is highly susceptible to weather variations and has been closed to desiccation during at least three severe drought periods in the last century (M. E. Mendoza et al., 2006). The approximately 4000 km^2 watershed has several low and high hills originated by volcanic activity during the Miocene and Pliocene, including pyroclastic-fall deposits and fluviolacustrine plains (M. E. Mendoza et al., 2011). The Grande and Querendaro Rivers are the main tributaries (Villalobos-Castañeda et al., 2010). There is no natural outlet in the lake, although according to Soto-Galera (Soto-Galera, Paulo-Maya, López-López, Serna-Hernández, & Lyons, 1999), it could have been connected to the Lerma River during the Holocene. The climate in the catchment is moderate, with temperatures ranging from 10°C to 28°C. Annual precipitation can vary from 765 to 1200 mm and it is concentrated in the summer, from May to October (Soto-Galera et al., 1999; Villalobos-Castañeda et al., 2010; M. E. Mendoza et al., 2011). As the quality and quantity

of the water feeding the lake have decreased (e.g., waters coming from municipal and industrial activities or agricultural runoffs), the lake is in a hypertrophic state. Furthermore, it also has detectable arsenic levels coming from geothermal boreholes around the lake and a thermal spring located on a magmatic chamber (Villalobos-Castañeda et al., 2010).

Patzcuaro Lake is located at https://goo.gl/maps/wmV37adP5EsuF6HG7 and 3035 m.a.s.l. It has a maximum surface area of 116 km^2 with an average depth of 5 m, although certain zones can have up to 12 m (Ramírez-Herrejón et al., 2014). The lake and its four islands originated from volcanic activity during the Pleistocene about 1 million years ago (Osorio-Ocampo et al., 2018). The lake is well mixed, not stratified, and it is maintained mainly by small springs of shallow groundwater and by local runoff (Bradbury, 2000; Metcalfe et al., 2007). The drainage basin covers 929 km^2 and, while the system today is endorheic, it could have drained to the Lerma River 25,000 years ago. Two seasons dominate the weather: rainfall in summer and stable dry conditions in winter with a mean annual precipitation of 950 mm (Bradbury, 2000). Patzcuaro Lake has been subject to several paleoenvironmental studies where the extracted cores contain lacustrine sediments that record climate change, human impact, volcanic activity and earthquakes for periods up to 48,000 years ago (O'Hara, Street-Perrott, & Burt, 1993; Bradbury, 2000; Metcalfe et al., 2007; Osorio-Ocampo et al., 2018). In recent years, fish biodiversity in the lake has decreased due to anthropogenic activities (Bradbury, 2000; Metcalfe et al., 2007; Ramírez-Herrejón et al., 2014). Yuriria Lake is located at https://goo.gl/maps/dow4yuWpdXfAPkgPA at 1740 m.a.s.l. (FIR, 2004). With 13.79 km in length and 5.88 km wide, it has a surface of 66 km^2 and a maximum depth of 3.2 m (Espinal Carreón, Sedeño Díaz, & López López, 2013). It is an artificial lake considered the first post-Columbian hydraulic work, as it was formed after building a deviating water channel from the Lerma River in 1548. The silty clay on the surface avoids water leakage to the aquifer (FIR, 2004). The channel from the Lerma river is still the main tributary of the lake (Espinal Carreón et al., 2013), although precipitation and runoff also contribute to it. The mean annual temperature in the area is 18 C and the rainy season is from May to September, with annual precipitation that can vary from 669 to 797 mm. The lake supports migratory and resident birds, and the area is considered a Wetland of International Importance (RAMSAR) since 2004 (FIR, 2004). Espinal Carreon et al. (Espinal Carreón et al., 2013) identified eutrophication and contamination levels that may be dangerous for fish biodiversity and recreation. Catemaco Lake is located at 322 m.a.s.l. and in https://goo.gl/maps/xs6fHcGEQTQK9P2x6, between San Martin Tuxtla Volcano and the Sierra de Santa Marta. It is part of the subcatchment of the San Juan River, a tributary of the Papaloapan River, the second most fast-flowing river in Mexico (Florescano, Ortiz Escamilla, Benítez Badillo, Welsh Rodríguez, & Córdova, 2010). With an approximately squared layout, Catemaco Lake has an area of about 75 km^2. The mean depth is 7.6 m, but while the lake basin is mainly a plateau of 11 m deep maximum, there are three pits that reach up to 22 m depth (Pérez-Rojas & Torres-Orozco, 1992). The lake receives water from at least 10 tributaries, and it is also fed by groundwater and precipitation, which can be up to 5000 m per year. Its main effluent is the Grande de Catemaco River, a tributary of the San Juan River (Guevara, Laborde, & Sánchez-Ríos, 2004; Gutiérrez Quevedo et al., 2014). Catemaco Lake is considered a warm polymictic lake, there is no stratification, and the concentration of dissolved oxygen is constant across the water column. The light penetration between 0.53 and 2 m depth and its temperature ranges from 23° to 28° C (Berry & Lind, 2010). The catchment area of Catemaco covers 322.2 km^2. It has escarpments, cinder cones, and maars resulting from volcanic activity in the late Miocene ($\approx$ 7 million years ago) and having the latest eruptions in the XVIII century. In fact, the lake formed when several cinder cones blocked the drainage to the north, and the lake contains many islands formed by subaquatic vulcanism (García-Aguirre, Álvarez, Dirzo, Ortiz, & Eng, 2010). Catemaco Lake is in the tropical rain forest and has high biodiversity. Divided by the NW-SE axis, approximately half of the lake borders with the Natural Reserve of Los Tuxtlas (Guevara et al., 2004). However, the area is affected by deforestation, water abstraction, and water pollution due to agriculture and livestock farming (Guevara et al., 2004). With coliform, organic matter, hydrogen sulfur, water lilies, and phosphorous, the lake has been classified as eutrophic (Gutiérrez Quevedo et al., 2014).

In general, the lakes are affected by well-known stressors caused by anthropogenic activities. Furthermore, they are exposed to a certain degree of diversions and removals of water for agricultural, livestock, and industrial activities (Otto et al., 2020), numerous discharges of untreated industrial and municipal wastes, and a growing urban population (Soto-Galera et al., 1999). This has disruptive effects, such as drying up and refilling by sediments from erosion and runoff from deforested uplands due to poor management of soil resources (Espinal Carreón et al., 2013), loss of surface area, reduction of the water

column, lower water transparency and hyper-eutrophication, erosion, or nutrient loads (Chacon-Torres, Ross, Beveridge, & Watson, 1992; Berry & Lind, 2010). As the lakes are surrounded by large urban areas or are close to industrially developed regions, the spectral signature is contaminated to some degree by atmospheric effects caused by aerosols and other gases. Hence, the optical properties and identification of various optical water types are challenging.

4.3 Materials

4.3.1 In-situ data

This work utilizes the dataset available from the national water monitoring network (RNMCA) managed by the Mexico's national water council (CONAGUA), which is the primary source of water quality data in the country. The historical-series data contain daily physic-chemical data taken in different intervals between 2012 and 2018 using in-situ field campaigns with exact sampling dates. The information is open access under http://sina.conagua.gob.mx/sina/ (accessed on 8 June 2020) The water quality measures are taken on monitoring stations operated by CONAGUA all over the country, which in 2019 had more than 4000 fixed locations. The biggest lakes of the country analyzed in this study counted with 30 in Chapala, 15 in Cuitzeo, 10 in Patzcuaro, 8 in Yuriria, and 4 in Catemaco, and frequency of measurement is also limited to 2 to 3 times per year. From the available parameters, this study focuses on Chlorophyll-a (Chl-a), Turbidity, Total suspended matter (TSM), and Secchi disk depth (SDD) as these are important for water quality and present in remote sensing of inland waters studies (Gholizadeh et al., 2016; Giardino et al., 2019; Topp et al., 2020). CONAGUA manages the RNMCA to obtain the water quality parameter following national and international standards to the parameter determinations. In this sense, the Chl-a measurement derived from the extraction method 10200-H described in the American Public Health Association (APHA, 2005); turbidity determination follows the nephelometry method referred in the NMX-AA-038-SCFI-2001 (NOM, 2004), while the TSS are determinate under the Mexican standard NMX-AA-034-SCFI-2015 (NOM, 2015a) procedures; SDD is measured following the 30 cm Secchi Disk procedure (APHA, 2005). These Mexican standards follow the general criteria for controlling the quality of analytical results from NMX-AA-115-SCFI-2015 (NOM, 2015b). When the usage of water is for the supply of drinking water, the relevant norm for sampling in surface and groundwater for water quality parameters is the NOM-014-SSA1-1993 (NOM, 1993) which indicated measures should be taken with the bottle immersed in the water with the neck facing down, up to 15 to 30 cm deep. Unfortunately, no measurements of radiometric data are available from RNMCA. Descriptive statistics of the water quality dataset are shown in Table ST1.

4.3.2 Satellite data and processing

The general characteristics of the sensors used in this study are shown in Table 4.1. Landsat-8 OLI multispectral images were downloaded from the United States Geological Service (USGS) website (earthexplorer.usgs.gov (accessed on 10 June 2021), Collection 1 Level 2, on-demand products). Sentinel-3 OLCI Level 1 Full Resolution images were downloaded from the European Organization for the Exploitation of Meteorological Satellites EUMETSAT Data Centre website https://archive.eumetsat.int/usc/ (accessed on 10 September 2020). Sentinel-2 MSI Level-1C (L1C) images were downloaded from the Copernicus Open Access Hub https://scihub.copernicus.eu/dhus/#/home (accessed on 12 October 2020) using the Sen2r package (Ranghetti, Boschetti, Nutini, & Busetto, 2020). Additionally, Sentinel-3 OLCI Level-2 Full Resolution Water Products (OLCI WFR) were considered for further comparison of its Chl-a and TSM layers. Table ST2 displays the selected bands from the sensors used in this study.

Synchronized field and satellite data were identified with the allowance of ± 3 days of difference. For OLI, 41 matches were found, while 47 for OLCI and 31 for MSI. The number of sampling points present on each image and more details of the synchronized data are shown in Table ST3. Pixel averaging was not considered since the sampling stations are well located and the resolution is considered adequate for all the sensors (Otto et al., 2020). OLI Collection 1 Surface Reflectance includes the use of the Land Surface Reflectance Code (LaSRC) (version 1.4.1), which produces Top of Atmosphere (TOA) Reflectance and TOA Brightness Temperature (BT) using calibration parameters from the metadata. These TOA

products are further corrected with water vapor and ozone data from the Moderate Resolution Imaging Spectroradiometer (MODIS) and digital elevation derived from the Earth Topography Five Minute Grid (ETOP05) to generate surface reflectance (SR) (E. Vermote et al., 2016). Atmospheric correction of OLCI L1b radiances was based on the well-known Case 2 Regional CoastColour (C2RCC) processor available as plug-in in SNAP (v7.0). This selection was made based on the standard and recurrent application of the C2RCC in literature and its use as a standard atmospheric corrector, which helped develop the methodology with certainty. The C2RCC retrieves directly remote sensing reflectance (Rrs). Sentinel-2 MSI images were resampled to 60 m with the Resampling (v2.0) tool to give the same base for each AC processor. Similarly, C2RCC (v0.15) was applied to Sentinel-2 products and the retrieved Rrs.

Table 4.1: Characteristics of the optical sensors used in this study.

Satellite	Revisit (Days)	Spatial Resolution (m)	Launched on	Spectral Bands
Landsat-8 OLI	16	30	2013	11
Sentinel-3A and 3B	2-3	300	3A: 2016, 3B: 2018	21
Sentinel-2A and 2B	5	10 and 20	3A: 2015, 3B: 2017	13

4.4 Modeling methodology

Dimensionality reduction was necessary due to the many scenarios to analyze with different lakes (5), sensors (3), algorithms (3), hyperparameters and bands as predictors, and the cross-validation necessary on each model. Selecting a subset with the relevant predictors was desirable to prevent overfitting and enhance the generalization and avoid collinearity conditions, commonly present in nearby bands situated next to each other (Matthews, 2011). The advantages of this reduction are fewer training periods and fewer computational demands. Investigated bands were inside the VIS, and NIR regions as these are well documented for having spectral relation to the studied water parameters (Blix et al., 2018; Topp et al., 2020) and work well when developing algorithms for Case 2 waters. To gain hints about further relevant wavelengths to use for every sensor, the correlation between bands and field data was inspected utilizing its distribution and scatterplots. Attributes were also tested with logarithmic, exponential, and cubic transformation for visual analysis. Linear relationships between predictors and parameters were using Pearson's correlation. The correlations were further displayed in a heatmap matrix to inspect further and enhance the most correlated bands. The bands of every sensor with stronger correlation to the field data were selected to further be analyzed as input for the models. Different ML algorithms were trained with the field and radiometric data. Recent trends are focused on applying neural network techniques in the remote sensing of inland waters (Peterson et al., 2018, 2020; Sagan et al., 2020) for its robust results and capacity to detect nonlinear patterns between radiometric data and water quality parameters. A novel approach is the extreme learning machine (ELM). Its basic form is a feedforward neural network with a single hidden layer that adjusts randomly the weights of the hidden layer with no iterative optimization, reducing the computational demand of a traditional feedforward neural network (Huang, Zhu, & Siew, 2006). With a d number of nodes, L as the input layer and m as the output layer, for training samples as X, where X, the matrix of the network is expressed as:

$$H\beta = T \tag{13}$$

being

$$H = \begin{bmatrix} g(w_1, b_1, x_1) & \cdots & g(w_l, b_L, x_1) \\ \vdots & \vdots & \vdots \\ g(w_1, b_1, x_N) & \cdots & g(w_L, b_L, x_N) \end{bmatrix}_{NxL}, \quad \beta = \begin{bmatrix} \beta_1^T \\ \vdots \\ \beta_L^T \end{bmatrix}_{Lxm} \quad and \quad T = \begin{bmatrix} t_1^T \\ \vdots \\ \beta_L^T \end{bmatrix}_{Lxm} \tag{14}$$

where W is the vector of the input weights of the node i and bi is the bias, with both wi and bi randomly

generated; bi is the output weight vector and g the activation function. The least-square solution of the outputs weights in the hidden layer is found to train the ELM. The b is expressed as:

$$\beta = H^{\dagger}T \tag{15}$$

where $H^{\dagger}$ is the Moore-Penrose generalized inverse of H (Huang et al., 2006). Hyperparameters to tune for the ELM are the number of neurons in the hidden layer and the activation function. We evaluated different logarithmic ranges for the number of hidden neurons. All the available activation functions (Mouselimis & Gosso, 2018) for the ELM implementation were evaluated for the different options of hidden neurons. Additional algorithms were tested to gain insights into the ELM performance against algorithms with previous applications in the region. Support vector regression (SVR) and least-squares linear regression (LR) demonstrated a good performance when retrieving Turbidity and SDD (Samui, 2008; Pasolli et al., 2010; Azamathulla & Wu, 2011; Verrelst et al., 2012; Blix et al., 2018) in central Mexico (Arias-Rodriguez et al., 2020). Both SVR and LR algorithms have been applied in predicting water quality parameters with successful results, and their use starts to be common in the evaluation of ML approaches. To tune the hyperparameters of the SVR, the radial basis, sigmoidal and linear kernel together with the regularization parameter and the kernel coefficient in logarithmic ranges were evaluated. The rest of the hyperparameters were used as default. More details of the SVR can be found at Vapnik et al. (Vapnik et al., 1997) or in previous applications (Arias-Rodriguez et al., 2020). To search the optimal hyperparameters of each algorithm, a grid of predefined values was analyzed using leave-one-out cross-validation (LOOCV) to evaluate all possible combinations due to the limited matches between field and satellite data used in training and validations. In this process, a score of performance is calculated for each set, and a later function displays the values reaching the highest score to select the most adequate hyperparameters combination. The individual and synergistic behavior of the investigated bands was evaluated, analyzing all the possible combinations of the remaining predictors by implementing a power set (PS) to perform a spectral sensitivity analysis to finally select the number and kind of predictors retrieving the best error metrics. The power set is defined as follows:

$$PS(b) = 2^{b} \tag{16}$$

where b is the number of predictors for that specific dataset. After dimensionality reduction, tuning of hyperparameters and optimal number of predictors, the ELM, SVR and LR models were evaluated against each other using their best configurations through a LOOCV for each sensor, lake, and parameter. The training size used for each LOOCV varied depending on the resulting dataset of each lake and sensor, and a correlation analysis, and for all cases it was equal to N. From the three models, the one with best performance was selected as the ideal to model the specific parameter used for a specific sensor. For this we use different controlling metrics, the coefficient of determination (R^2), the root mean squared error (RMSE), and the mean absolute error (MAE), defined as:

$$RMSE(y, \hat{y}) = \sqrt{\frac{1}{n_{samples}} \sum_{i=0}^{n_{samples}-1} (y_i - \hat{y})^2} \tag{17}$$

$$R^2(y, \hat{y}) = 1 - \frac{\sum_{i=0}^{n_{samples}-1} (y_i - \hat{y})^2}{\sum_{i=0}^{n_{samples}-1} (y_i - \bar{y}^2} \tag{18}$$

$$MAE(y, \hat{y}) = \frac{1}{n_{samples}} \sum_{i=0}^{n_{samples}-1} |y_i - \hat{y_i}|^2 \tag{19}$$

where yi is the estimated value, yi is the observed value and nsamples is the number of samples. Usage of ELM was performed via the *Caret* library (Kuhn, 2008) in R, which applies the *elmNNRcpp* package from Mouselimis (Mouselimis & Gosso, 2018) based on the implementation of Gosso (Gosso & Martinez-de Pison, 2012). The base codes of ELM can be found at: https://www3.ntu.edu.sg/home/egbhuang/elm_codes.html (accessed on 12 February 2021). SVR and LR were implemented using the *Scikit − Learn* library (0.20.1) (Pedregosa et al., 2011) in Python (v.3.8.3).

4.5 Results

4.5.1 OLCI water products compared to RNMCA

OLCI Water Products Compared to RNMCA Chl-a and TSM values estimated with OLCI WFR were compared against all the insitu data (Figure 4.3.)

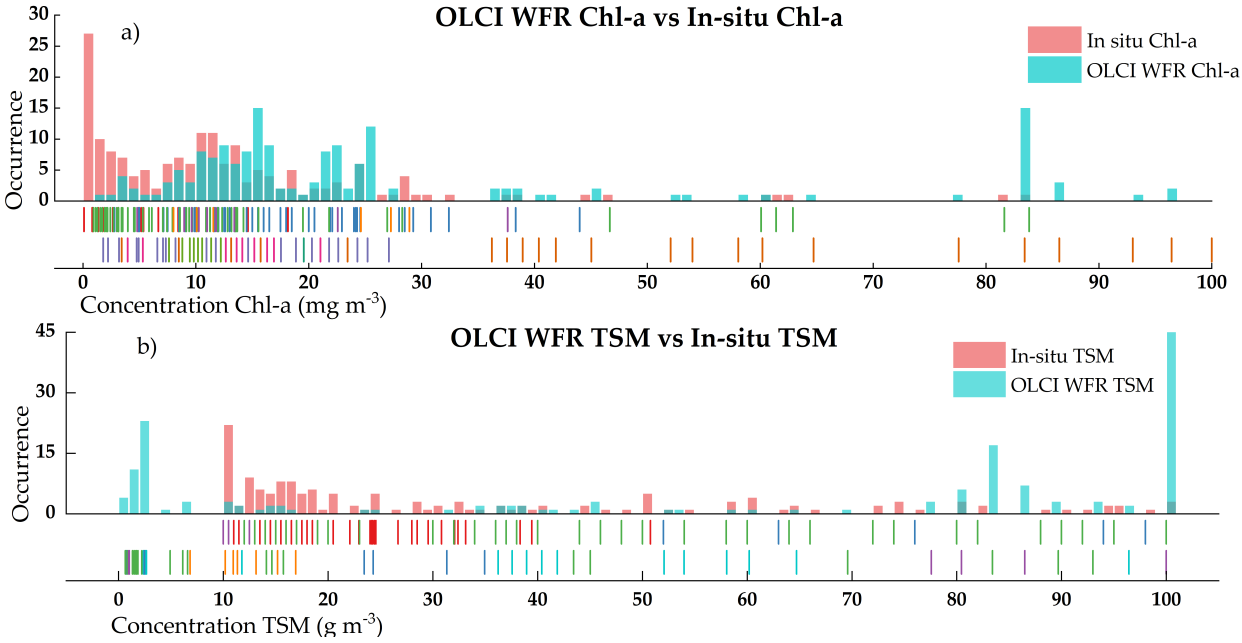

Figure 4.3: Histograms of OLCI WFR Chl-a (a) and TSM (b) estimations overlapped to RNMCA measurements. Marks along the x-axis as perpendicular rugs display single qualitative data and its distribution.

The overlap between histograms shows significant differences for both water parameters when compared with in-situ data. Chl-a field concentrations are usually low (avg: 14 mg m-3) compared to the OLCI products (avg: 30 mg m-3). Furthermore, the distribution of the OLCI derivations from Chl-a seems to have a closely normal distribution shape spread in the range 5-30 mg m-3. The averages values for field TSM (avg: 53 g m-3) and OLCI derived (avg: 53 g m-3) are very close to each other; however, the constraints from the TSM layer relies on the frequent prediction of values close to either 0 or 100 g m-3, as seen in Figure 4.3 b. The complete overlap of histograms by lake is shown in Figure SF1. Figure 4.4 shows the scatterplots of the OLCI water products in-situ data.

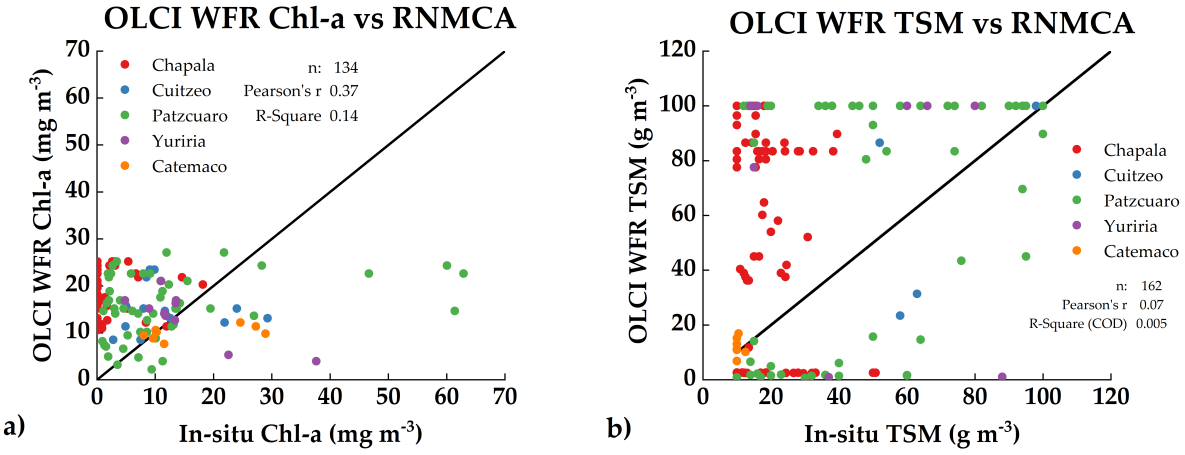

Figure 4.4: In-situ and S3 derived water quality parameters. (a) OLCI WFR Chl-a vs in-situ measurements, (b) OLCI WFR tsm_nn vs. in-situ measurements.

The Pearson's correlation of both data remains low, particularly for TSM (r = 0.07), where the differences of extreme predictors between 0 and 100 g m-3 values display scattered values. On the other hand, Chl-a water products were underestimated above 30 mg m-3. Individually, Chl-a retrievals were overestimated in Chapala. Patzcuaro had little agreement with under and overestimation before and after 15 mg m-3. Catemaco showed a better agreement. For TSM, Patzcuaro, Chapala and Yuriria suffered poor agreement, and Catemaco again showed the best correlations at lower concentrations.

4.5.2 Data evaluation and model performance

Generally, the exploratory analysis on a single set per sensor containing all the water quality data of each lake did not present strong correlations between reflectance from sensors and RNMCA data (Figure 4.5).

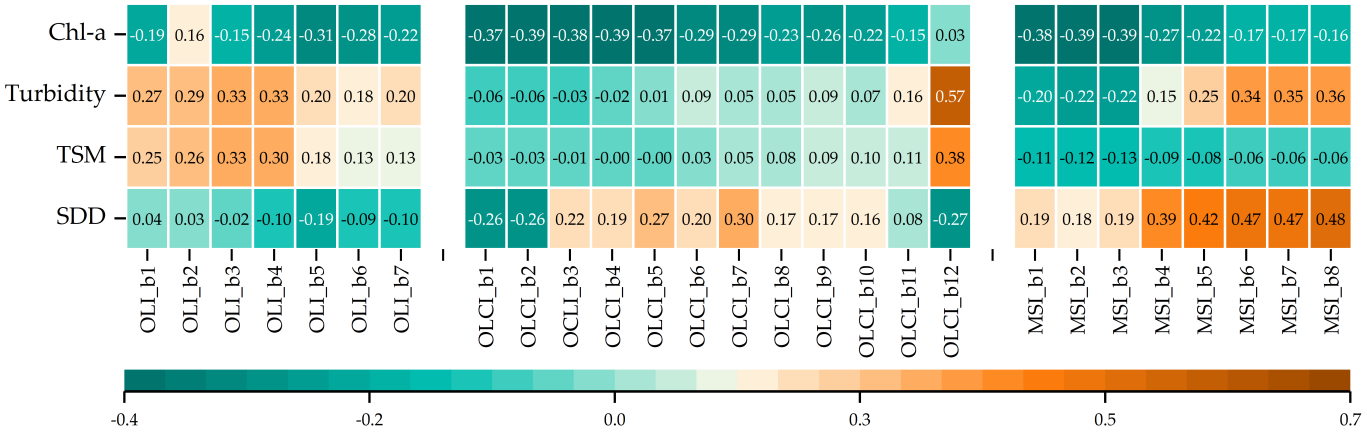

Figure 4.5: Correlation matrix heatmap of reflectance values of the analyzed bands and water quality parameters. Bands of the Operational Land Imager (OLI) are shown at left, Ocean and Land Color Instrument (OLCI) are shown at the center, and Multi Spectral Instrument (MSI) are shown at the right.

For OLI, higher correlations were seen in the VIS for Turbidity and TSM (R ≈ 0.30) and b5 for Chl-a (R ≈ 0.31). OLCI displayed slightly better correlations in the VIS for Chla (R ≈ 0.38) and b12 for Turbidity and TSM (R ≈ 0.57 and R ≈ 0.38) alongside b1, b2, and b12 for SDD. MSI displayed higher correlations in VIS bands with Chla (R ≈ -0.38), NIR with Turbidity (R ≈ 0.35) and SDD (R ≈ 0.47). TSM showed the weakest correlations in OLCI (R ≈ 0.03) and MSI (R ≈ 0.12) and slightly better for OLCI (R ≈ 0.30). Further analysis of Pearson's coefficient was performed, analyzing each data set separate by sensor and lake with an additional cleaning process of noise values prior to model training. From a practical point of view, Sentinel-3 OLCI presents the strongest correlation for all the target parameters except SDD. Scatter plots of all the in-situ parameters and best models for each sensor resulting from the LOOCV are shown in Figure 4.6. Modelled algorithms varied in every sensor and lake depending on the approach and hyperparameters. The additional factor of varying training sample size due to the different matched samples and the remotion of noisy values influenced further the error evaluation. Averages showed that OLI performs better for Cuitzeo (R^2 = 0.55) than the other lakes, behaving the worst in Yuriria (R^2 = 0.21). Its best prediction is obtained for Turbidity (R^2 = 0.42). OLCI performs better in Cuitzeo (R^2 = 0.67) and Yuriria (R^2 = 0.52) and better predicts Turbidity (R^2 = 0.69) and SDD (R^2 = 0.50). MSI has on average higher performances due to a low number of training samples in Cuitzeo, Yuriria, and Catemaco, due to poor image coverage in sampling dates and cloud coverage in the few matching images (Table ST3). The comparison is feasible only with Chapala where its performance is similar (R^2 = 0.45) and Patzcuaro where it is the poorest (R^2 = 0.21). An easier comparison comes from analyzing the model performances by water parameter. Turbidity resulted in a higher performance (R^2 = 0.71) with also relatively good Chl-a and SDD (R^2 = 0.64 and R^2 = 0.61). From the water parameters, TSM showed to be the most challenging parameter to model as seen in the poor performance in terms of error metrics for all sensors (OLI: R^2 = 0.42, OLCI: R^2 = 0.35,

MSI: $R^2 = 0.48$). Additionally, Chl-a was also poorly correlated for OLI and OLCI (OLI: $R^2 = 0.18$, OLCI: $R^2 = 0.36$). Turbidity models displayed the best performances for Chapala, Cuitzeo Patzcuaro, and Yuriria, shown in Tables Table ST4, Table ST5 and Table ST6. Individually no model could retrieve a good correlation for TSM in Yuriria in any sensor (OLI: $R^2 = 0.19$, OLCI: $R^2 = 0.34$, MSI: $R^2 = 0.11$), Chl-a in Patzcuaro (OLI: $R^2 = 0.14$, OLCI: $R^2 = 0.38$, MSI: $R^2 = 0.21$) in Table ST4, Table ST5 and Table ST6. For the 5 lakes and 4 parameters to the model, ELM occurrence (37 times) for better performance was the highest among all sensors, followed by LR (15 times) and SVR (8 times) (Table 4.4). The average error metrics by lake and parameter are shown in Table 4.2 and Table 4.3 as an overview of the performance in error metrics of lakes and water parameters. The complete validation of models displaying error metrics, the best algorithm for each lake, sensor, and water parameter together with tuned hyperparameters and training size is shown in Table ST4, Table ST5 and Table ST6.

Table 4.2: Average coefficient of determination (R^2) of the developed models by sensor and lake together with the average number of samples (n). Operational Land Imager (OLI) (left), Ocean and Land Color Instrument (OLCI) (center), and Multi Spectral Instrument (MSI) (right).

Lake	OLI		OLCI		MSI	
	R^2	n	R^2	n	R^2	n
Chapala	0.37	141	0.45	75	0.45	44
Cuitzeo	0.55	23	0.67	19	0.90	7
Patzcuaro	0.37	43	0.42	31	0.21	39
Yuriria	0.21	16	0.52	17	0.60	11
Catemaco	0.27	17	0.32	17	0.88	7

Table 4.3: Average error metrics of the trained models by sensor and water parameter. Error metrics of all lakes are included on each water parameters RMSE: Chla in mg m-3, Turbidity in NTU, TSM in g m-3, SDD in m. The number of samples is also displayed on average.

Parameter	OLI				OLCI				MSI			
	R^2	RMSE	MAE	n	R^2	RMSE	MAE	n	R^2	RMSE	MAE	n
Chl-a	0.18	19.99	13.81	40	0.36	21.27	8.86	32	0.64	8.47	6.23	20
Turbidity	0.48	35.23	23.31	51	0.69	17.80	30.99	30	0.71	17.24	47.40	22
TSM	0.42	107.31	40.37	49	0.35	33.12	28.10	32	0.48	118.21	24.70	23
SDD	0.33	0.08	0.05	52	0.50	0.26	0.18	32	0.61	0.45	0.36	23

Table 4.4: Model occurrence in every sensor as a result of better predictive capabilities.

Model	**OLI**	**OLCI**	**MSI**	**Total**
ELM	10	14	13	37
SVR	5	3	-	8
LR	5	3	7	15
Total	20	20	20	60

ELM was better suited for OLCI data, and LR was useful in few samples (MSI). SVR showed not to be suited for MSI, most likely because of the combination of limited data and better suitability of ELM and LR (Table ST4, Table ST5 and Table ST6).

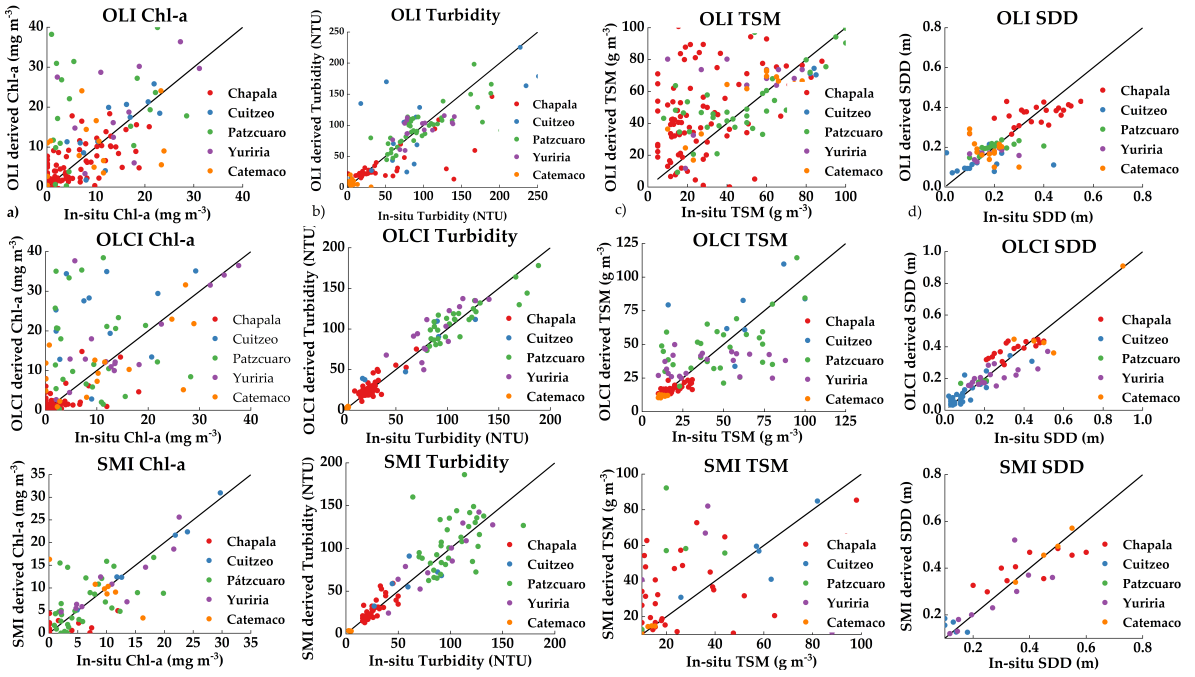

Figure 4.6: Comparison of estimated Chlorophyll-a (Chl-a, column (a)), Turbidity (column (b)), total suspended matter (TSM, column (c)) and Secchi disk depth (SDD, column (d)) by sensor. Individual estimations by lake are displayed on each figure: Operational Land Imager (OLI) (top), Ocean and Land Color Instrument (OLCI) (center) and Multi Spectral Instrument (MSI)(bottom).

4.5.3 Spatial patterns from Sentinel-3 OLCI WFR and estimated parameters

Locally calibrated models were used to produce spatial distribution maps of Chl-a and TSM. These maps were also compared against the OLCI WFR retrievals. The map product of the modeling, regardless of the uncertainties associated with its empirical nature, contribute to a higher understanding of the spatial distribution of water parameters in comparison with being based on sampling stations. The complete maps for all lakes are shown in Figure 4.7. For display purposes, a random image was selected for its usefulness for visual analysis on every lake.Derived maps suggest different interpretations in terms of magnitude and distribution of the parameters between both types of derivations. In Lake Chapala, Chl-a concentrations from OLCI products are generally overestimated, which is visible in most of the lake surface where no significant changes are observed. The east part of the lake shows more variations in the quality in agreement with the location of river discharges discussed in the study area. In agreement with the previous histograms, OLCI TSM presents fixed values near 100 g m-3 mainly in the east part of the lake (Figure 4.7 a-d). Similarly, Lake Cuitzeo varies from homogeneous distribution of Chl-a and TSM from OLCI products to a higher variability depending on the section of the lake with apparent underestimation from OLCI (Figure 4.7 e). Lake Patzcuaro displayed similitudes between OLCI and modelled Chl-a, with visible differences only near the shores of the lake, especially in the southwest (Figure 4.7 i,j). OLCI TSM for Lake Patzcuaro also shows overestimation compared with modelled TSM (Figure 4.7 k,l). Lake Yuriria shows the different spatial distribution of both Chl-a and TSM. However, the patterns of river discharges carrying suspended solids (Figure 4.7 p) are clearly distinguishable only in the maps derived from the models. For Lake Catemaco (Figure 4.7 q) and Lake Patzcuaro (Figure 4.7 i), lower differences are observable for Chl-a OLCI products and maps from models. However, TSM showed higher variability in Patzcuaro from 85 g m-3 for OLCI products to lower values of 50 g m-3 in the calibrated models. As a general observation, more refined details and distinguishable patterns can be discernible in the maps from the trained models; for Chl-a estimations, for example, regions with higher Chl-a content seem to be revealed in areas where primary productivity may be expected to occur as in river discharge or nutrients deposit. Additionally, further characteristics of each lake not studied in this work, such as wind direction, bathymetry, hydrodynamic and morphological features, might induce strong influence in the distribution and magnitude of both parameters.

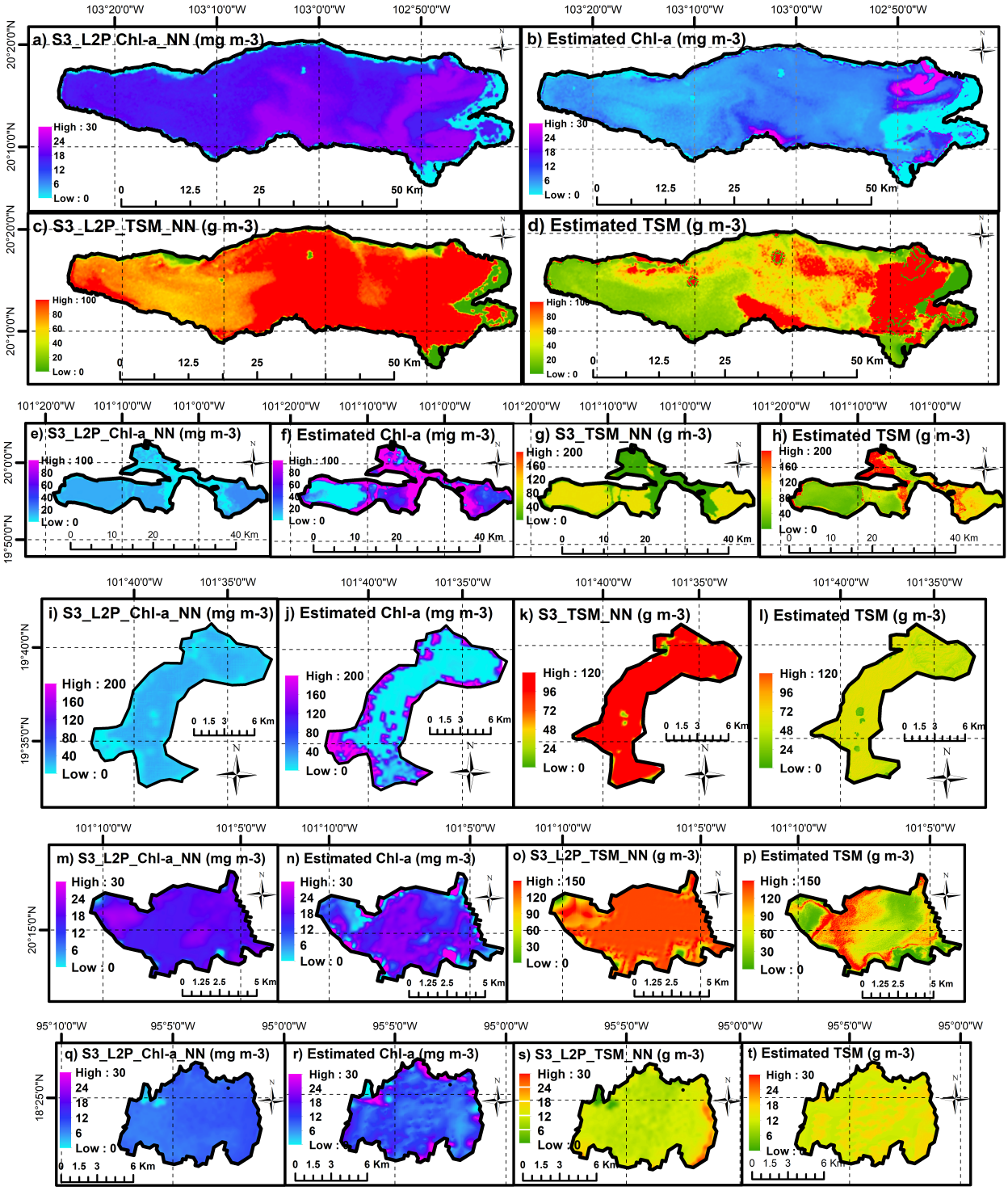

Figure 4.7: Comparison of Chlorophyll-a (Chl-a) and total suspended matter (TSM) estimations by OLCI WFR products and developed the models in this study for all lakes.

4.6 Discussions

4.6.1 OLCI water products

Significant limitations exist when integrating remote sensing available products to support the monitoring system in Mexico. A substantial mismatch between OLCI WFR and field measurements was found (Figure 4.3). OLCI product tends to overestimate Chl-a and TSM values. A deeper analysis on each lake individually displayed little correspondence, except for Chl-a and TSM in Lake Yuriria (Figure 4.7). Furthermore, an analysis of the spatial distribution of such parameters based on single images showed that patterns regarding the path and concentration of these parameters are difficult to detect via OLCI WFR layers. Likewise, the surface of the lakes appears to be highly homogeneous, while significant spatial variations were identified via local modeling (Figure 4.7). It is vital to notice that OLCI L2 algal pigment concentration is conceived for ocean products, and its range varies from 0.01 to 100 mg m-3 in Case 2 waters. The lakes in this study had lower concentrations, particularly Lake Chapala (Table ST1) and therefore an overestimation of Chl-a is not surprising. A similar situation occurs with TSM. These findings suggest that, to rely only on these products to support monitoring program tasks is unfeasible, and therefore there is the need for locally trained models. Even with the disagreement between OLCI WFR and field data from the RNMCA, OLCI L1C products were found to be among the most reasonable sensors to use when monitoring big enough inland waters in the region.

4.6.2 Comparison of sensors

OLI has outstanding features in terms of spatial resolution and adequate preprocessing routines. In this study, these features contributed to keeping spectral information from proximal stations to water shores. Additionally, its launch in 2013 increased the number of matched images with RNMCA substantially. Its application is further endorsed by years of legacy from the Landsat constellation and its perpetual presence in research of remote sensing of inland waters (Meisner, 1983; Zilioli & Brivio, 1997; P. Brezonik et al., 2005; Han & Jordan, 2005; Papoutsa, Retalis, Toulios, & Hadjimitsis, 2014). Therefore, it was expected to retrieve better results from models trained with its radiometric data, although essential restrictions constrained its application. The temporal resolution (16 days) limits the number of matches with the existing field data. Despite its longevity, the retrieved datasets were of similar size to OLCI and the large archive advantage was not compelling to gain a privileged place as the best sensor (Table ST4 and Table ST5). This limitation was already appointed by Mandanici (Mandanici & Bitelli, 2016) who compared OLI and MSI, finding limitations in OLI temporal resolution for continuous water quality monitoring. Furthermore, as OLI is designed to observe the main features in earth and not water resources; except for the NIR-band, the spectral amplitude and spectral coverage of the other bands in the VIS region measured by OLI sensor represent a common limitation to carry out specific studies related to the water quality assessment. In other words, OLI is not designed to observe characteristics and features of important parameters involving algae blooms such as Chl-a, commonly used as a proxy of the trophic state of inland waters.

In the sense of the above, the spectral resolution of OLCI is higher (21 bands) than OLI (11 bands), and the bands are located in relevant regions of the spectra for water quality monitoring. Specifically, wavelengths at 681 nm or at the range 700-710 nm allowed the development of Chl-a based algorithms as the fluorescent line height (FLH) (Gower, 1980) or the maximum chlorophyll index (MCI) (Alikas, Kangro, & Reinart, 2010). Furthermore, the location of many bands in the Red and NIR regions (b8-12) allowed Turbidity and TSM patterns to be detected. The temporal resolution is reinforced with both S3-A and S3-B, which could have potentiated the found matching data. Unfortunately, the availability of Sentinel-3B was limited when investigating matching dates of the RNMCA, and the data remained limited to S3-A except for a couple of S3-B images. The major limiting factor was possibly the spatial resolution when working with stations close to shores, as some existed in the RNMCA. Due to the size of a single pixel (300 x 300 m) which averages the shore radiances with the ones of adjacent water, such stations were rejected and data availability constrained. If considered, these stations could lead to adjacency error (AE) which would add further uncertainty to the models. For this study and considering the target lakes as the biggest in the country, the resolution of OLCI did not represent a limiting factor as enough pixels were constantly retrieved from the surface of the lakes. However, if OLCI is intended to be used in routinary monitoring tasks, the resolution will likely be a program for small inland waters.

It was recently demonstrated that available atmospheric correction procedures, including the C2RCC, for OLCI have difficulties when removing atmospheric disturbances over small inland waters (Kravitz et al., 2020). This is particularly challenging when there are many small lakes as in central Mexico (CONAGUA, 2018), and no radiometric data is measured as part of the RNMCA routines. To improve the methodology applied here, a more comprehensive evaluation needs to analyze different AC or errors associated to different radiometric data as TOA radiances. In terms of model performance from OLCI data, the error metrics (Table 4.3 and Table 4.4) even when far from perfect fitting, showed reasonable performances with enough data in most of the lakes and parameters, which may also indicate a good generalization ability.

MSI combines high spatial and temporal resolution due to the availability of both S2-A and S2-B, and expectations with its data were high. Unfortunately, coverage of MSI for the sampling dates and regions of the lakes analyzed in this study was limited and only some images matched with the RNMCA (Table ST3). Furthermore, cloud coverage also impeded the processing of some of those few images. This resulted in a limited number of matched points, especially for Lakes Cuitzeo, Yuriria, and Catemaco (Table ST6). These factors played an important role. and models using MSI data are likely to lack the generalization ability out of the range of the limited training data. Moreover, similarly to OLI, its design is based on terrestrial and vegetation applications. Therefore current AC processes for S2 are still a matter of research to further validate the quality of the corrected radiometric data over different inland waters (Ansper & Alikas, 2019).

4.6.3 Data analytics and machine learning modeling

The data analytics routine demonstrated to be useful, as seen in the developed models using spectral and RNMCA data. As seen in the exploratory data, not all the bands or band ratios of the sensors strongly correlated with the water quality parameters (Figure 4.3). This was corroborated with poor performances from the models in specific lakes or parameters (Table ST4, Table ST5 and Table ST6). However, good agreements were also found and models with strong correlations were developed for each sensor, particularly for turbidity, which exhibited constant high performance in every lake. The usage of shallow algorithms as LR and SVR is shown to be a good base for modeling tasks in inland waters, since they provide straightforward results that can serve as a proxy for test modeling. Regarding ELM, it is a state-of-the-art shallow algorithm that is in constant development and starts to be applied in evaluations of remote sensing of inland waters (Peterson et al., 2018, 2020). Furthermore, the usage of ELM in this study resulted in being useful to develop more accurate models in certain cases. Since it is expected that acquisitions from the RNMCA will continue, further validation and calibration should complement and adapt the models developed here and open new doors for more accurate algorithms. This is especially valid for the use in research of machine learning models, which are in constant change and evolution. Additionally, the evaluation of machine learning models against approaches as empirical-based or bio-optical models is important to further understand the more suitable methodology for remote sensing of inland waters. The promising performance of machine learning models was found in this study. To go further, alternatives such as Deep Learning has already been pointed out in recent research (Peterson et al., 2020; Sagan et al., 2020) as an adequate methodology to deal with the challenges of working with enormous amounts of data storage (as satellite images could be) and water quality datasets. In addition, although different approaches may lead to more robust or generalizable models, its application may be complex and could require large amounts of in-situ data for calibration (Matthews, 2011). These requirements greatly restrict the application of semi-analytical models, favoring empirical approaches. Here is where machine learning offers a good balance between computational power and straightforward application. In this study, machine learning approaches were a useful methodology applied to consistently evaluate the available data from RNMCA. The results suggest that these models are adequate approaches to support the monitoring tasks in emerging economies like Mexico.

The challenges in the application of machine learning approaches are primarily due to the calibration of the hyperparameters. LR has the advantage of not requiring this calibration, but the relationships between water quality parameters and radiometric data are often not linear. Therefore, the importance of a good calibration of SVR and ELM is to reveal non-linear patterns or non-normally distributed data as water quality parameters. Regarding SVR, its application resulted in being straightforward due to the considered hyperparameters calibrated. Nevertheless, if a broad spectra of hyperparameters are consid-

ered, this can lead to long training time. To reduce the computing time, the usage of known kernels and particular values for the regularization parameter (C) and the kernel coefficient (Y) based on powers of 10 resulted in a comprehensive grid that covered a wide range of possible combinations. The case of ELM was further challenging due to the many activation functions available for neural networks and the large number of hidden neurons that can be taken. Ideally, considerations regarding the convergence speed of the ELM with the activation function or perseverance of normalization. These were evaluated by considering training times and normalization of the data before training. However, activation functions did not influence training times as much in Caret using the RNMCA and radiometric data, but more challenging was determining the number of hidden neurons in the hidden layer. From Huang et al. (Huang et al., 2006), it is known that the generalization performance is stable on a wide range of number of the hidden neurons. Therefore, a range of values based on powers of 10 resulted again in an effective way to find variations in the ELM performance. A small number of neurons (≈ 10) retrieved results tending to the mean of the training samples. A number of neurons greater than 15,000 or 20,000, together with training data of $n > 100$ and a LOOCV, resulted in hours of training and minimum improvement of the error metrics, which is not the optimal performance of an ELM. The range of hidden neurons in this study was found to be optimally varied between 1000 and 10,000. A further sensitivity analysis of the number of neurons to better set a range of the ideal number of neurons of an ELM using remote sensing and water quality data is recommended. In addition, it is important to consider that there are additional model capability limitations from radiometric data product of time delay in matching satellite and water quality data (Otto et al., 2020) and the limited amount of matching data, which leads to small datasets for model training. To face these challenges, we exclude region/pixels which may be corrupted by clouds or adjacency effects, and therefore possible uncertainties and the model routines are evaluated with strict LOOCV. However, this study used data from a single atmospheric correction and did not evaluate further possibilities nor estimate the uncertainties.

4.6.4 Integration of remote sensing and the RNMCA

The performed analysis of the selected parameters using OLI, OLCI, and MSI stresses the complications of retrieving accurate estimations of water quality in the region using the available data. From the investigated parameters, turbidity is the parameter better positioned to be estimated using optical and RNMCA data. Different and varied factors may enhance difficulties in estimations. Limitations regarding the nature of the RNMCA and the modeling itself were present in the development of this work and pose challenges for future integration of remote sensing and water quality data.

The current state of the RNMCA data and its acquisitions routines is independent of the satellite acquisitions. Consequently, a lack of synchronization between the field campaigns to measure in-situ data and the satellite overpasses leads to the rejection of data for being too sparse in time (Table ST3). Similarly, only some fixed stations on each lake are regularly sampled in field campaigns. For specific dates, there are no measurements of all the stations, most likely subject to different priorities, and limiting the availability of data. Moreover, in-situ radiometric measurements are not routinely measured, impeding validation of the reflectance of the sensor and identification of the optical water types or consideration of further modeling approaches. In addition, the frequency of field campaigns limiting because it was observed to be limited to a couple of times every year or in single campaigns spread over several days. This detaches samples from the date of satellite acquisition, leading to reduction of usable data. This situation affected to a minor degree to Lake Chapala or Lake Catemaco, but it was observed more frequently in Lake Yuriria and Lake Catemaco. In the studied lakes, some sampling stations are located near the shores, which leads to adjacency effects on the acquired radiometric energy in that location and induces errors in the modeling process. Therefore, in this study, these stations were rejected due to its proximity to the land. Access to the data is also of major importance. For instance, the complete dataset of all the measured parameters in the last decade was available only until late 2019. Before this, the available information was limited to information regarding biological oxygen demand (BOD5), chemical oxygen demand (COD), and total suspended matters (TSM). Since the water quality information from the RNMCA focused on displaying the results rather than its acquisition and usage, application and research from it were limited. By the beginning of 2020, the increase of data availability and the possibility to use it in an adequate format improved conditions for monitoring research. Currently, this data is also already available in the global freshwater quality database portal (GEMStat), where until the writing of this paper, Mexico leads the amount of data water quality data available for inland waters (UNEP, 2021).

There are also inherent challenges regarding the methodologies in field campaigns, the use of radiometric data or the wind and temperature conditions in the lakes. From field measurements methodologies in the data description, we assume that samples collect water from the surface up to a maximal depth of 15-30 cm. For those parameters which require less water volume in sampling, such as turbidity (100 mL), it is likely that the sample is filled at a lower depth than for those that require more, such as TSM or Chl-a (1000 mL), but for all cases the limit is between 15 and 30 cm. This lead us to the assumption that, for Chl-a, turbidity, and TSM, possible discrepancies due to NIR bands are not relevant or relevant in a lower degree. Still, the depth of sampling and the effective depth of remote sensing reflectance might not match, which surely add some uncertainties, however, this is a common issue in the remote sensing studies. In our case, this is supported by the fact that turbidity showed the better metrics for all parameters and its models include NIR bands consistently (Table ST4 and Table ST6) or the use of NIR bands in studies where similar parameters are studied (Otto et al., 2020) or even at deeper measurements (Han & Jordan, 2005; Oyama, Matsushita, & Fukushima, 2015). Partial discrepancies due to sampling methods are, however, very likely for SDD. For example, Secchi Disk Depth is based on a subjective measure from the operator, and it reflects the total depth in which the disk is lost from sight, therefore, it is not representing a property of a shallow layer of water directly. Furthermore, the SDD in average is higher than the NIR penetration rate in water of 10 cm (Table ST1). In this case, the use of NIR bands may represent a bias in the developed models, which use these bands. Therefore, results for SDD should be taken with caution and not be conclusive. Prevailing winds are capable of generating dispersion phenomena as a result of forcing or friction on the water surface that induces waves, as well as the generation of aerosols due to natural evaporation processes. Additionally, vertical mixing induces movement of waters due to temperature gradients and this may conditionate the satellite measurements. The study areas are located in low wind zones (Hernández-Escobedo, Manzano-Agugliaro, & Zapata-Sierra, 2010), but the wind patterns or prevailing winds should be considered as a challenge for toe reliability of results (Anatoliy, Tereshchenko, Monzon, Avalos-Cueva, & Pantoja-González, 2016). Determination of temperature profiles to find mixing areas would also contribute to increase the reliability of the estimations and the determination of the associated uncertainties. The atmospheric correction has several challenges to deal with, as the many variables influencing the radiance spectra used to train the models. Low signal-to-noise-ratio product of the small amount of reflected light in water bodies requires an accurate correction for atmospheric contributions (W. Moses, Ogashawara, Montes, De Keukelaere, & Knaeps, 2017). The predominance of the effect of a specific constituent over another in the water may create the masking effect and avoid estimating the non-dominant constituent in the water with enough confidence (Giardino et al., 2019). Since turbidity depends strongly on TSM and Chl-a, and given that all the lakes (except Lake Catemaco) preserve relative high concentrations of both parameters; turbidity was the parameter better positioned among the investigated parameters. On the other side, radiometric data may be improved through pre-processing. An additional glint-correction on the image may help to improve the response derived from the sub-surface water layer, retrieving a more reliable water-leaving radiance this may help to diminish the dispersion effect produced by the reflection of the wind-waves, aerosols associated to natural evaporation in the air-water layer.

To include remote sensing into the RNMCA routines, it is important to understand the obstacles of integration. One of the main reasons is the lack of awareness or expertise from local managers of remote sensing techniques. Schaeffer et al. (Schaeffer et al., 2013) assessed this situation in a local study in the US. According to their findings, local managers commonly lack the knowledge to interpret and use the technical descriptions of remote sensing and modeling techniques to retrieve water parameters. Therefore dialog between researchers and resource managers is essential and applications that foster the embracing of remote sensing are necessary to show its full potential continuously. After the limitations described in this work, it is clear that requirements for the applications of remote sensing approaches should be considered when designing sampling campaigns. For example, the field campaigns may consider synchronization with satellite acquisitions after a revision of the most adequate sensor and considering the spatial and temporal requirements. Scales of days are needed and resolutions below 300 m and 30 m are adequate for big and small lakes, respectively. The number of field campaigns and sampling stations are equally important. A minimum of four field campaigns per year is recommended for the United Nations Environment Program (UNEP, 2016), one for each season. In Catemaco or Yuriria, the fourth and fifth biggest lakes in the country only have five and four stations, respectively. The loss of one or two stations are due to shore proximity or incomplete sampling limits data availability. Furthermore, the inclusion of

in-situ radiometric data measurements to validate the satellite's sensors reflectance spectra and further classify the optical water types. For this, upwelling radiance from water and downwelling sky radiance are key parameters. Routines of calibration should then be applied to normalize this data to downwelling irradiance. The derivation of remote sensing reflectance can be then done through known procedures (C. D. Mobley, 1999).

The benefits for water managers are well known. Costs regarding time consumption in field campaigns and human resources can be mitigated, and the enhancement of spatial and temporal information is highly significant compared to field campaigns alone. The recommendation for integration is already suggested by the UNEP, where the advice is to schedule and adapt the field campaigns considering the use of remote sensing for water monitoring (UNEP, 2016). The initial step could be the most challenging since it will require an assumption from the highest level of water managers to direct how the field campaigns are being taken. Meanwhile, the data from the RNMCA are highly valuable and set the basis for an extensive network for water quality monitoring. The identification of fixed stations, the high variety of water parameters measured (around 30 in the complete dataset), and its endurance through the years will likely allow high-quality and comprehensive data to be available for practical and research applications. Besides, it should be clear that a hypothetical integration of remote sensing into the design of management routines will be in continuous evolution. It is expected that the routines are adapted with the availability of future sensors, which can incorporate better features suited for inland water quality monitoring. Furthermore, resources such as cloud computing should be taken into account to develop large applications that process great amounts of data as a monitoring water system at a national level or satellite imagery. Cloud computing infrastructure and applications based on AI may facilitate water quality monitoring through access to NASA, USGS, and ESA archives.

4.7 Conclusions

This work focuses on the implications of the lack of integration of remote sensing in water quality monitoring routines, taking as a study case the existing monitoring system (RNMCA) of the five biggest lakes in the country. Available ready-to-use products from Sentinel-3, OLCI WFR, tend to overestimate or underestimate field values for Chl-a and TSM, and validation results indicate a need for alternative approaches based on field data. Through a routine based on data analytics and machine learning algorithms, Landsat-8 OLI, Sentinel-3 OLCI, and Sentinel-2 MSI sensors were studied to investigate their suitability to monitor water quality in the region. ELM resulted in the most used methodology for modeling followed by LR and SVR. The results ranged widely in performance, from weak to strong relationships. From the three sensors, Sentinel-3 OLCI showed a moderate better performance over Landsat-8 and Sentinel-2 MSI for these study areas with good results for turbidity and moderate correlations for Chl-a, TSM, and SDD. The current state of the data and the fact that the RNMCA is developed independently and without considering remote sensing techniques placed different difficulties in the processing methodology and led to considerable losses of in-situ data. It is recommended to study the local needs and available in-situ data when choosing a sensor for monitoring water quality or design routinely field campaigns based on the acquisition calendar of only one sensor. Due to their design, it is not possible to select a sensor for monitoring inland waters. To magnify their use and full potential, synergistic applications should be developed to combine the strengths of various sensors and mitigate their limitations. This work contributes to creating awareness of the misuse and absent application of remote sensing by water managers in emerging economies for water monitoring routines. The progress of remote sensing for inland waters is bound to its usage to improve existing monitoring tasks, which will impact management and protection of water resources.

Author Contributions: Conceptualization, L.F.A.-R., Z.D. and M.D.; methodology, L.F.A.-R., Z.D. and J.d.J.D.-T.; software, L.F.A.-R., J.d.J.D.-T. and B.U.K.; validation, L.F.A.-R. and J.d.J.D.-T.; formal analysis, L.F.A.-R. and B.U.K.; investigation, L.F.A.-R., J.d.J.D.-T. and M.B.H.; resources, L.F.A.-R., Z.D., M.B.H. and J.H.; data curation, L.F.A.-R. and B.U.K.; writing-original draft preparation, L.F.A.-R.; writing-review and editing, L.F.A.-R., Z.D., J.d.J.D.-T., M.B.H., J.H. and Y.T.; visualization, L.F.A.-R.; supervision, Z.D., Y.T., M.D.; project administration, M.D.; funding acquisition, L.F.A.-R. All authors have read and agreed to the published version of the manuscript.

Funding: This work was supported by the Mexican National Council for Science and Technology (CONACYT) and the Mexican Federal Department of Energy (SENER) through the program "CONACYT-SENER Sustentabilidad Energetica" CVU 678957. Publication costs were covered by the German Research Foundation (DFG) and the library of the Technical University of Munich (TUM) in the framework of the Open Access Publishing Program.

Acknowledgments: We thank the United Stated Geological Service (USGS) and the European Space Agency (ESA) for providing the necessary OLI, OLCI, and MSI spectral data and software for this study. We are further grateful to the Mexican National Water Council (CONAGUA) for providing the field water quality measurements through the Mexican Water Quality Monitoring System (RNMCA). Additionally, we would like to acknowledge Gabriele Chiogna and Francesca Perosa from the TUM Chair of Hydrology and River Basin Management for their valuable advice and discussions about this work. We would like to thank the Technical University of Munich (TUM) and its Graduate School (TUM-GS) for providing all the institutional services and facilities used in this study. Finally, we would like to thank the peer reviewers for providing constructive comments, which greatly improved this manuscript.

5 Holistic Approach for Estimating Water Quality Ecosystem Services of Danube Floodplains: Field Measures, Remote Sensing, and Machine Learning

Hoyek, A.; Arias-Rodriguez, L.F.; Perosa, F.
Hydrobiology 2022, 1, 211-231.
Received: 31 March 2022 / Accepted: 11 May 2022
https://doi.org/10.3390/hydrobiology1020016

Abstract

Human pressure has caused river ecosystems to be severely damaged. To improve river ecosystems, "working with nature", i.e., nature-based Solutions (NbS), should be supported. The purpose of this paper is to evaluate the effects of a specific NbS, i.e., floodplain restoration, which provides, among others, the ecosystem service of nutrient retention. For these, an in-depth time series analysis of different nutrients' concentrations and water physiochemical parameters was performed to obtain Water Quality Indices (WQI), which were calculated along the river. To estimate water quality from remote sensing data and to generate water quality maps along the river, Sentinel-2 water products were validated against in situ data, and linear regression (LR), random forest (RF), and support vector regression (SVR) were trained with atmospherically corrected data for chlorophyll-a and TSM. The results show different outcomes in diverse floodplains in terms of improvement of the water quality downstream of the floodplains. RF demonstrated higher performance to model Chl-a, and LR demonstrated higher performance to model TSM. Based on this, we provide an insightful discussion about the benefits of NbS. These methodologies contribute to the evaluation of already existing NbS on the Danube River based on a quantitative analysis of the effects of floodplain ecosystems to water quality.

Keywords: Danube; floodplain; ecosystem services (ES); water quality; remote sensing; Sentinel-2; machine learning (ML)

5.1 Introduction

Nature-based solutions (NbS) are "actions which are inspired by, supported by or copied from nature", that are potentially "energy and resource-efficient and resilient to change" (EC., 2015,). NbS can solve water management problems, restore ecosystems, and increase sustainability (EC., 2015,; Nesshöver et al., 2017; UN, 2018,). An ecosystem is at the center of the NbS implementation areas. Human pressures have caused river ecosystems to be seriously damaged in the entire world. Over the past 50 years, pollution, nutrient enrichments, dam constructions, and unsustainable exploitations have led to rivers' deterioration. For example, the interruption of migratory routes of fish species by dam and weir constructions has led to a critical decrease of these fish species or even for their extinction (Zingraff-Hamed et al., 2018). One major cause of river ecosystems' degradation is nutrient pollution. It is causing growth of dangerous algal blooms in new river locations, where they have different toxicity levels, and they are lasting for longer hours (Glibert & Burford, 2017). Agricultural practices, river modifications, bank erosions, and fertilizer applications have caused a huge increase in nutrient loads in rivers, mainly from nitrogen (N) and phosphorus (P) (Goolsby et al., 1999; Galloway, 2002; Alexander et al., 2008; Howarth, 2008; Glibert & Burford, 2017). Nitrogen is present in waterways by the forms of nitrite (NO2), nitrate (NO3), ammonium (NH4), and organic N; phosphorus is present as particulate P, and soluble reactive P (SRP).

A good example for an NbS dealing with the degradation of river ecosystems is floodplain restoration. Floodplains are a space alongside a watercourse, which are typically developed by deposition of solid particles in the course of floods of different magnitude (Lewin, 1978; Nardi, Vivoni, & Grimaldi, 2006), where water, nutrient, sediment, and organism exchanges are happening (Amoros & Bornette, 2002; Benjankar, Egger, Jorde, Goodwin, & Glenn, 2011). Flooding events, ranging from frequent and very low discharge events to less frequent and high discharge events, support the dynamics of the floodplain ecosystem and impact multiple biophysical features (e.g., hydro-morphological features and soil hydrology). Additionally, floodplains play an important role for the natural functioning of a river (Poff et al., 1997; Whiting, 2002), and provide ecosystem functions and ecosystem services (ES), i.e., "the quantifiable or qualitative benefits of ecosystem functioning to the overall environment, including the products, services, and other benefits humans receive from natural, regulated, or otherwise perturbed ecosystems" (Assessment, 2005). One of the most important ES of floodplains is the transformation and retention of nutrients in river streams (Sanon, Hein, Douven, & Winkler, 2012; Schindler et al., 2014; Weigelhofer & Hein, 2015), identified by nitrate-N, total particulate P, the Water Quality Index (WQI), or concentrations of chlorophyll-a (Chl-a) and total suspended matter (TSM).

5.1.1 Background

Nitrate-N and total particulate P are the two primary forms of N and P in floodplain studies (Hardison, O'Driscoll, DeLoatch, Howard, & Brinson, 2009), and are retained by denitrification for N (Xue et al., 1999) and sedimentation for P (Knighton, 2014). WQI is generally used to assess the quality of both groundwater and surface water (e.g., rivers), and it is very important to compute when dealing with water resources management (Debels, Figueroa, Urrutia, Barra, & Niell, 2005; Lumb, Sharma, & Bibeault, 2011; Sutadian, Muttil, Yilmaz, & Perera, 2016). WQI consists of combining multiple natural parameters (e.g., nutrients in water concentration and water physiochemical parameters), and translate them efficiently into a single value, reflecting the quality of water. Satellite remote sensing is an approach to retrieve water quality parameters such as Chl-a and TSM (Giardino et al., 2013), which according to the Water Framework Directive (WFD), are very important to monitor, since they are one of the lead parameters that described the trophic state of water, in addition to phytoplankton biomass (Y. Zhang et al., 2008; W. J. Moses, Gitelson, Berdnikov, & Povazhnyy, 2009; Wozniak, Bradtke, & Kreeezel, 2014) and water clarity (Salem et al., 2017).

One example of a satellite remote sensing tool is the MultiSpectral Instrument (MSI) onboard Sentinel-2 (S2), which has a high resolution of up to 10 m, and it has shown very good results in estimating the Chl-a and TSM concentrations in lakes (Bresciani et al., 2018). For complex waterbodies, additional studies for atmospheric correction (AC) algorithms can be developed (Grendaitė, Stonevičius, Karosienė, Savadova, & Kasperovičienė, 2018). For this reason, the Copernicus Program developed an open source database for satellite imagery to improve monitoring (Klein, Nilsson, Persson, & Haakansson, 2017) through mod-

eling. In fact, modeling can be used to set up a relation between the radiometric values obtained from satellite images and the in situ measurements acquired in a matching date. These relationships can be sorted as empirical, semi-analytical, or based on machine learning (ML) (Topp et al., 2020), e.g., through multivariate linear regression (MLR), random forest (RF), support vector regression (SVR), or neuronal networks models. ML is considered a novel field of study, hence it is still not very efficient in water quality estimation, and it is very important to understand its behavior in remote sensing for a better estimation of inland water qualities (Arias-Rodriguez et al., 2021).

5.1.2 Research objective

To understand the effects of nutrient retention in potential floodplain restoration NbS, we investigated the situation of water quality along the Danube River in time and space, and analyzed the effects of already existing, i.e., active, floodplains. Estimating the actual effect of floodplains on the retention of nutrients is a laborious process, which requires a high amount of measured data and/or proper modeling. Therefore, with this study, we aim at observing nutrient retention on the Danube, by analyzing nitrate-N, total particulate P, WQI, Chl-a, and TSM, and estimating their changes along the Danube floodplains. To reach this main goal, different sub-objectives were set:

- Displaying the behavior of specific parameters with a temporal analysis of water quality with field data from 1996 to 2017
- Investigating particular changes of the water quality at the spatial level through all active floodplains along the Danube River
- Assessing the effect of floodplains' nutrient retention and water quality improvement by means of time series analysis of nutrients, physiochemical parameters, and WQI
- Analyzing the relationship between the river discharge and river water quality through correlation analysis between the nutrients' retention values and the river discharge, as well as between the water quality improvement and the river discharge

Moreover, remote sensing-based ML models (MLR, RF, and SVR) were trained using field measurements and Sentinel-2 products, to investigate the situation of water quality using satellite imagery and to generate water quality maps, describing the situation of water quality through all active floodplains along the Danube River. The Danube River was chosen in our study because nearly all the floodplains of the large rivers located in Central Europe (e.g., the Rhine, Elbe, Danube, and Oder) have suffered degradation due to agricultural activities, structural flood protection measures, dam constructions, and land-use changes (urbanization and transport infrastructure) (Holubova, Hey, & Lisicky, 2003; Brunotte, Dister, Gunther-Diringer, Koenzen, & Mehl, 2009; Marren, Grove, Webb, & Stewardson, 2014).

5.2 Study area

We investigated floodplains located along the Danube River (Table 5.1). The river originates in West Germany and its outlet is in the Black Sea. In total, 17 active floodplains within the Danube River Basin were selected as targets. These were derived within the Danube Floodplain Project (Figure 5.1), which defined active floodplains as inundated areas (hydraulically active) during a flood event with a return period of 100 years (HQ100), and identified them through a ratio factor between the widths of floodplain and river, a minimum threshold to the size, and hydraulic characteristics of the floodplain (e.g., flow paths, stages, and natural flow characteristics should be maintained) (DTP, 2021).

This area is relevant since the Danube has lost 80 of its former floodplains due to anthropogenic influence (Schwarz, 2011). To monitor water quality dynamics in the river, field data measurements were acquired from multiple stations located in the vicinity of each floodplain. To analyze changes in water quality before and after each floodplain, we classified these stations as "upstream" and "downstream". The restoration demand of each floodplain was reported as estimated from the Danube Floodplain Project https://www.interreg-danube.eu/approved-projects/danube-floodplain (accessed on 10 December 2021) (DTP, 2020), indicating the level of restoration needed of each floodplain to regain its maximum functionality (e.g., providing groundwater recharge, filtering contaminants, supporting habitats, or transporting nutrients) (Table 5.1).

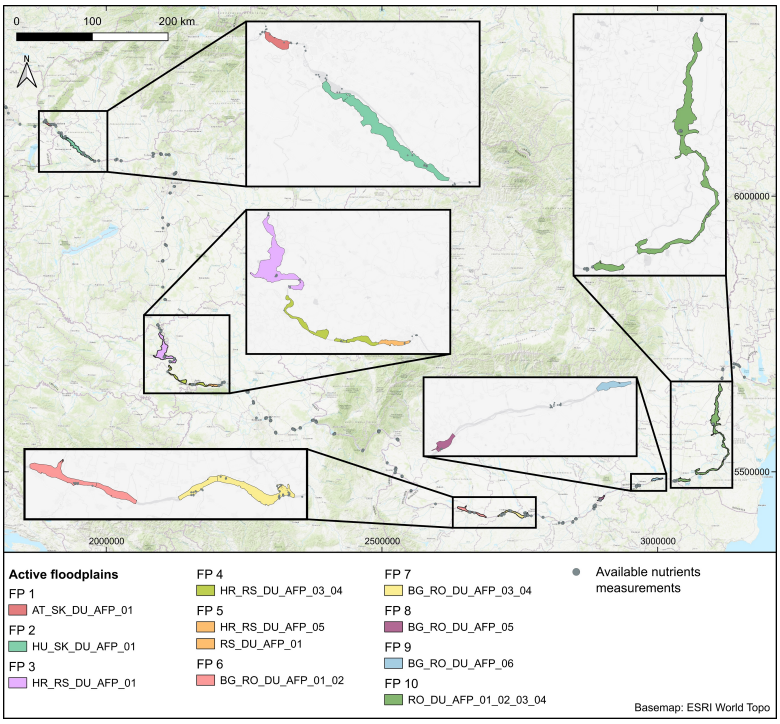

Figure 5.1: The active floodplains (FP) of the Danube River used in this study.

Table 5.1: Floodplain keywords, locations, upstream and downstream gauging stations, morphometric data, and their restoration demand, as assessed according to the Danube Floodplain Project.

Floodplain Keyword	Restoration Demand	Location	Area Size (km^2)	Floodplain Length (km)	River Kilometer (km)	Countries	Upstream Stations Code	Downstream Stations Code
FP1	High	48.144 N 17.025 E	19.8	9.8	1880 - 1871.5	Austria Slovakia	AT6	AT4 SK1
FP2	Low	47.889 N 17.476 E	140.2	51.4	1851.8 - 1797	Hungary Slovakia	AT4 SK1	HU1 SK2
FP3	Low	45.61 4N 18.905 E	279.9	70.1	1425 - 1354.2	Serbia Croatia	HU5 HR1	HR2 RS2
FP4	High Medium	45.323 N 19.084 E 45.268 N 19.226 E	24.6 30	16.8 9.3	1334 - 1318 1318 - 1308.4	Serbia Croatia	HR2 RS2	RS9 HR11
FP5	High High	43.779 N 23.811 E 43.716 N 24.069 E	49.2 34.8	27.2 16.8	1304 - 1276 1276 - 1258	Serbia Croatia	RS9 HR11	RS3
FP6	Medium Medium	43.779 N 23.811 E 43.716 N 24.069 E	60.1 32.3	25.2 15.6	703 - 677 677 - 661	Bulgaria Romania	RO18 RS8 RO2 BG1	BG2
FP7	Medium Medium	43.736 N 24.433 E 43.725 N 24.697 E	29.3 81.6	15.4 30.9	646- 630 630 - 600	Bulgaria Romania	BG4 BG8 BG15	RO3
FP8	Medium	43.911 N 26.033 E	25.3	10.3	490 - 479.5	Bulgaria Romania	G4 BG8 BG15	RO3
FP9	Medium	44.136 N 26.93 E	33.6	14.9	412 - 395.5	Bulgaria Romania	RO3	RO4 BG5
FP10	Medium Medium Low Low	44.125 N 27.37 E 44.226 N 27.714 E 44.475 N 28.031 E 44.901 N 27.903 E	50.3 79.4 93.6 298.8	17.7 31.2 58.6 77.9	375 - 356 345 - 313.5 313.5 - 252.5 252.5 - 172	Romania	RO4 BG5	RO11 RO5 UA1

5.3 Materials and methods

5.3.1 Evolution of water quality in the Danube River

Information on the active floodplains and their restoration demand were retrieved from the open-source GIS website (http://www.geo.u-szeged.hu/dfgis/ (accessed on 10 December 2021) which provides spatial results of the Danube Floodplain Project (DTP, 2021). Field data were retrieved from the Danube River Basin Water Quality Database (DTP, 2021). Field measurements of hydrological variables are provided together with concentrations of different nutrients and other water physiochemical parameters. The water parameters used are river discharge, concentrations of ammonium, chlorophyll-a, nitrates, total nitrogen, and total phosphorus, in addition to conductivity, dissolved oxygen, pH, and total suspended matter. To understand the evolution of water parameters, time series graphs for each active floodplain (upstream and downstream) were analyzed. The values were aggregated to monthly and yearly averages, and important flood events were highlighted in the respective time frame to better understand the influence of these extreme events on the respective floodplains (ICPDR, 2021). Complete time series plots for all floodplains and water parameters are provided in Figure S1 Figure S10. Time series values were used to compute the nutrient retention, calculate the WQI, and compute the water quality improvements between upstream and downstream locations in relation to each active floodplain of the Danube River. Based on data availability for each floodplain, nutrient retention and WQI were computed. Among all the floodplains analyzed (Table 5.1), we calculated the nutrient retention for both nitrogen and phosphorus for floodplains FP1, FP2, FP3, FP9, and FP10. As for the WQI, this was calculated for floodplains FP2, FP3, FP6, FP7, FP8, FP9, and FP10.

The evaluation of water quality can be achieved by monitoring nutrient concentrations, and especially the nutrients that can provide information on the river's trophic status, such as nitrogen (N) and phosphorus (P). To evaluate the contribution of a river, or in our case, a floodplain, to the nutrient balance of a system, nutrient loads and improvement or deterioration of water quality should be monitored (Kronvang & Bruhn, 1996). However, there are no methods to measure nutrient loads directly (Zweynert, 2008). Computing in-stream nutrient loads depends on the availability of data for the corresponding nutrients, and it can be done by different calculation methods. In general, they are the product of the nutrient concentration and the river discharge value (Zweynert, 2008). Nutrient retention in floodplains can be then calculated by subtracting the nutrient load exiting the floodplain from the nutrient load entering it. Still, uncertainties in computation must be considered, since previous studies showed that nutrient loads computed from continuous river discharges and monthly nutrient concentrations (as in our case) deviate by 25 from the true values (Zessner, 2008). These deviations are caused by missing nutrient concentration peaks due to low frequency measurements (one time per month) and can lead to under- or over-estimation (Zessner, 2008). In our study, we computed the nitrate-N retention, as it is the primary form of nitrogen (Hardison et al., 2009) and the total phosphorus retention in the different active floodplains of the Danube River, using the values generated from the time series analysis. Generally, nutrient retention in floodplains is computed per unit area of floodplain. For this study, the major interest was in the effects of nutrient retention in the active floodplains along the Danube River and not in retention rate per unit area. Therefore, only retentions in terms of nutrient loads were computed.

WQI is a simple and efficient method to monitor the quality status. To describe the effect of floodplains in river restoration, we calculated the WQI upstream and downstream of each floodplain, and the WQI improvement in each floodplain. The WQI was calculated using Equation (1), developed to assess river water quality by Rodriguez de Bascaran (Fernández-Vítora, Ripoll, Ripoll, & Garro, 1997; Moscuzza, Volpedo, Ojeda, & Cirelli, 2007), and the water parameters generated as described in Section 3.1.2.:

$$WQI = \frac{\sum C_i W_i}{\sum W_i} \tag{20}$$

where C_i represents a normalized assigned value (in percent) for each parameter value and W_i represents a weight for each parameter, ranging from 1 to 4, where 1 represents a minor importance for the ecological life and 3 represents a major importance. Two of the parameters used in the calculation of the WQI developed by Rodriguez de Bascaran (Fernández-Vítora et al., 1997; Moscuzza et al., 2007) are

the Chemical Oxygen Demand (COD) and the Total Dissolved Solids (TDS). Since COD and TDS are not available in our dataset, COD was replaced by Chl-a because a significant positive correlation was shown between COD and Chl-a (Y. Zhang et al., 2008). Additionally, TDS was replaced by TSM, since it is the only parameter describing the hardness quality of water in our data (Salem et al., 2017). This decision was supported by previous studies where TSM was used in the calculation of the WQI (Yogendra & Puttaiah, 2008; Etim, Odoh, Itodo, Umoh, & Lawal, 2013).

An active floodplain is a hydraulically active area inundated by flood event with return period of 100 years (ICPDR, 2021). Since the aim of this study is to understand the nutrient retention effect in active floodplains, it was important to focus on the river discharge values leading to a floodplain being active. For this matter, a correlation analysis was conducted between the nutrient retention in floodplains and the river discharge values, in addition to another correlation analysis between the water quality improvement values (using the WQI improvement values) and the river discharge values. The analysis was done by calculating the Pearson's correlation coefficient. This analysis was used to determine the relationship between the discharge values and the water quality.

5.3.2 Modeling water quality dynamics with remote sensing

Different products available from remote sensing sensors can be used to monitor water quality parameters. We focused on Chl-a and TSM, and analyzed their concentrations. These two variables, considered important indicators for water environmental quality evaluation (Tundisi & Tundisi, 2016; Silveira Kupssinsku et al., 2020), can be monitored by remote sensing sensors since they are considered optically active components (Giardino et al., 2019), and ready-to-use products are available from atmospherically corrected procedures. There are several studies showing that the capabilities of Sentinel-2 products are suitable to estimate Chl-a and TSM in water (Tundisi & Tundisi, 2016; Bresciani et al., 2018; Ansper & Alikas, 2019; Giardino et al., 2019), but with some challenges in retrieving accurate data (Grendaitė et al., 2018). Sentinel-2 temporal (5 days) and spatial (10 m) resolutions contribute to consider this satellite as one the few suited to analyze a narrow water body as a river, but still wide enough as the Danube River. To evaluate the usefulness of available remote sensing products, we compared remotely derived Chl-a and TSM against field-measured parameters. To further model water quality changes in the river surface, atmospherically corrected remote sensing reflectance and several spectral-derived features were used as input features to supply ML algorithms, and produce further spatial and temporal analyses.

The field measurement data for the Chl-a and TSM concentrations were retrieved from the Danube River Basin Water Quality Database by the International Commission for the Protection of the Danube River (ICPDR) (ICPDR, 2021). The Copernicus Open Access Hub (`https://scihub.copernicus.eu/`, accessed on 16 December 2021) was used to download cloud free Sentinel-2 S2 MSI Level-1C (L1C) data for the period 2014-2017 over the area of interest. An allowed period of a ± 3 day difference between the S2 image and its corresponding in situ measurement was taken into consideration while matching up data (Topp et al., 2020). Then, the images were processed using SNAP (v8.0.0.0), the open access toolbox for processing Sentinel missions. A standard atmospheric correction was applied to account for the scattered signal of the atmosphere, and retrieve remote sensing reflectance (Rrs) to further modeling process (Brockmann et al., 2016; Giardino et al., 2019). The Level 1C data from Sentinel-2 was processed using the Case 2 Regional Coast Color (C2RCC) algorithm (Brockmann et al., 2016), which uses a large database of Chl-a and TSM concentrations trained with neural network, as well as using extreme ranges of scattering and absorption properties. The C2RCC processor is adequate for optically complex Case 2 waters (as the Danube River) which also retrieves layers of Chl-a and TSM concentrations (Arias-Rodriguez et al., 2020). These products are evaluated against available in situ data using conventional error metrics, such as the coefficient of determination (R^2) and the Root Mean Squared Error (RSME).

After C2RCC product validation, modeling was conducted by means of three ML algorithms, which were assembled and trained to estimate the Chl-a and TSM as targets. The input features were the remote sensing reflectance bands from C2RCC and further derived radio spectral features. MLR (Cheng & Lei, 2001; Kloiber, Brezonik, & Bauer, 2002; H. Duan et al., 2009; Garaba et al., 2014; Bonansea et al., 2019), RF (Breiman, 2001; Ruescas et al., 2018; Maier & Keller, 2019), and the SVR (Chang & Lin, 2011; Kim et al., 2014; Batur & Maktav, 2018) were considered since they are becoming standard algorithms in ML modeling of water quality (Ruescas et al., 2018). All ML algorithms were implemented in Python

3.10.0 using the Scikit-Learn 1.0.2 library. Feature engineering was used to develop additional predictors to test more modeling scenarios (Matthews, 2011; Gholizadeh et al., 2016; Peterson et al., 2020; Topp et al., 2020). The complete additional feature combinations were also tested in related research of remote sensing of inland waters (Peterson et al., 2020). To select the most adequate predictors, all the predictors were tested with the Pearson's correlation against Chl-a and TSM. The highest correlated features were then selected as input for the algorithms. To tune algorithm hyperparameters, we used a Grid Search with predefined values. The final dataset of remote sensing reflectance and target parameters was divided into train and test splits and evaluated using a leave one out cross-validation (LOOCV) (Arias-Rodriguez et al., 2021). LOOCV is a specific case of a K-fold cross-validation where K equals N (the number of data points), which eliminates biases that a single split in the dataset may cause by using this technique. This method partitioned the dataset into K-fold of freely selected observations. Every model was trained for each of the K possible training-test splits, and the reported values for R^2 and RMSE were the average of these K runs. Finally, the model with the best error metrics values was chosen for estimating Chl-a and TSM over the surface of the Danube River to visualize spatial distributions based on specific dates and locations detected in the time series and WQI variations on each floodplain. The complete process which summarizes the methodology applied in this work is shown in Figure 5.2.

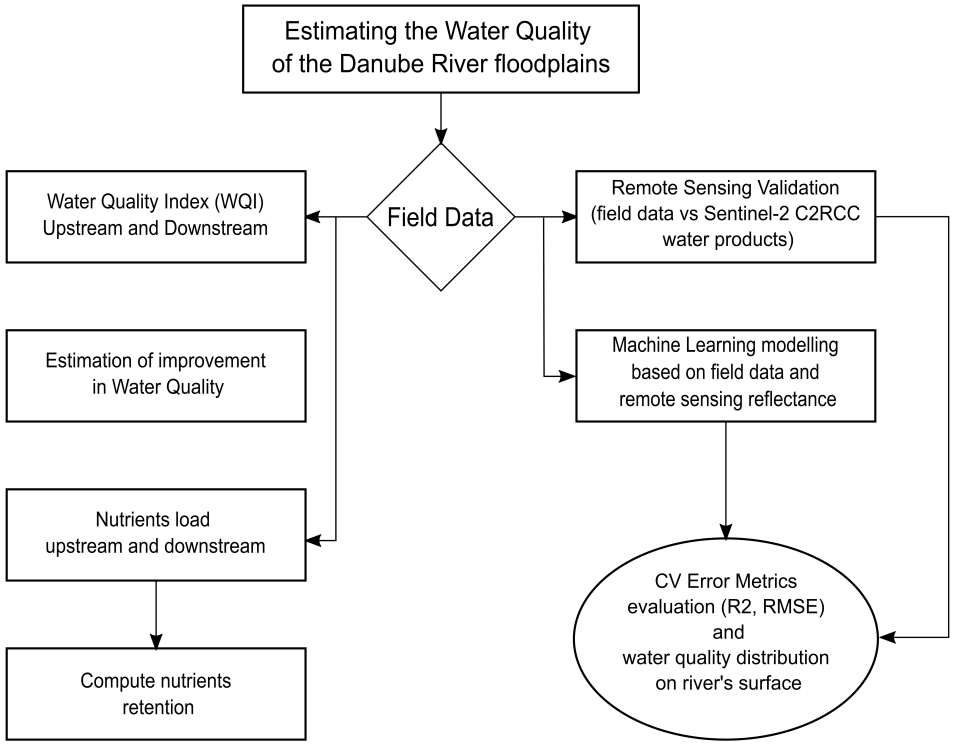

Figure 5.2: Flowchart describing the methodology applied in this work.

5.4 Results

5.4.1 Results on water quality index (WQI)

Results indicate, in general, that floodplains act positively by improving water quality in floodplains (Figure 5.3). We can notice an improvement in water quality between upstream and downstream for the majority of years in FP2, FP6, FP7, FP8, and FP9. Floodplain FP3 also shows an improvement in water quality for some years, however, it displays very little data. Floodplain FP10 acts quite the opposite to the other floodplains, as it does not show any improvement of water quality downstream of the floodplain in any year. The percentage of improvement of WQI is still conservative and is usually below 8 for the whole period of analysis, with exception to FP8, which shows improvements of up to 20 (in 2015). Similarly, a decrease in WQI reaches maximum 7 for all floodplains except for FP10, which displayed WQI reductions up to 11.

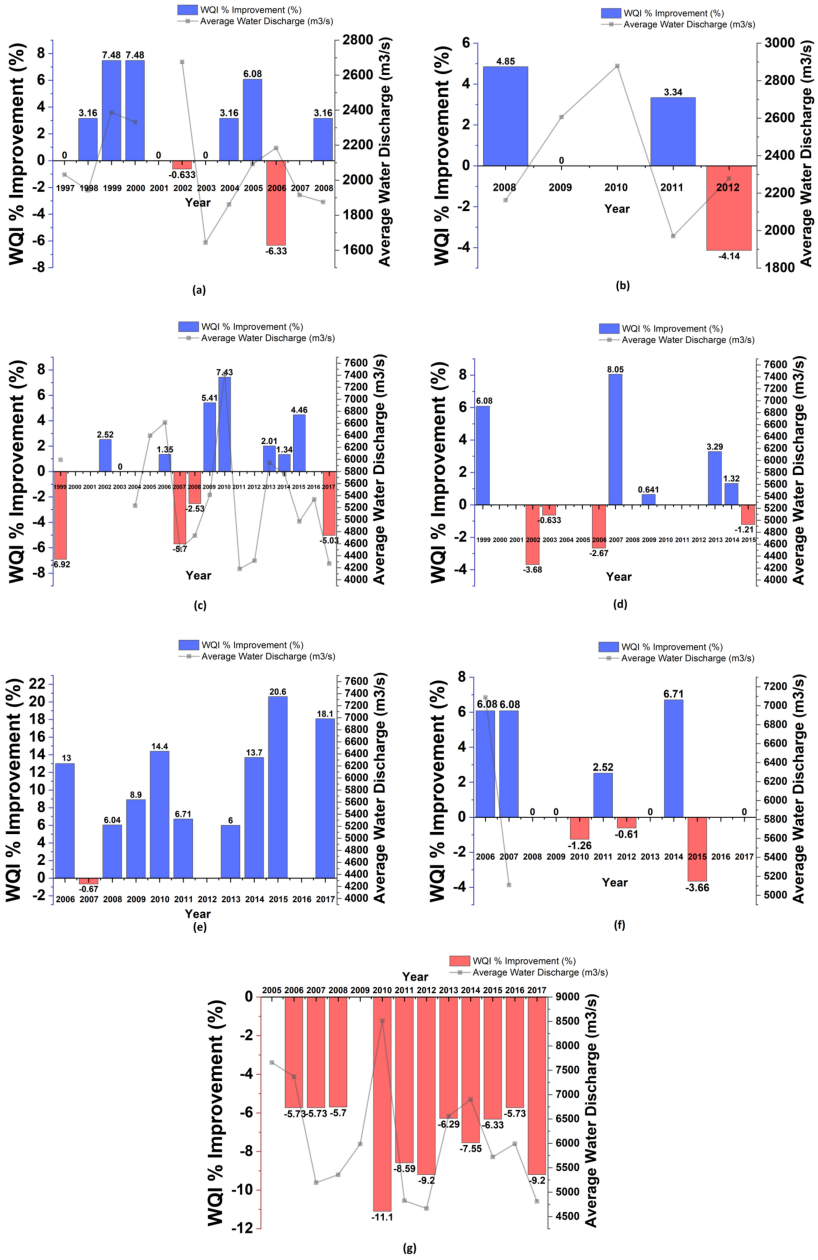

Figure 5.3: WQI percentual improvement and river discharge time series in: (a) FP2; (b) FP3; (c) FP6; (d) FP7; (e) FP8; (f) FP9; (g) FP10.

5.4.2 Nitrogen and phosphorus retention

Average yearly retention values for nitrates and phosphorus are shown in Figure 5.4. It can be seen that both FP2 and FP10 retain nutrients, whereas neither FP3 nor FP9 promote retention. On the other hand, FP1 retains very small amounts of nitrate but does not fortify phosphorus retention in cases when the retention load is too large.

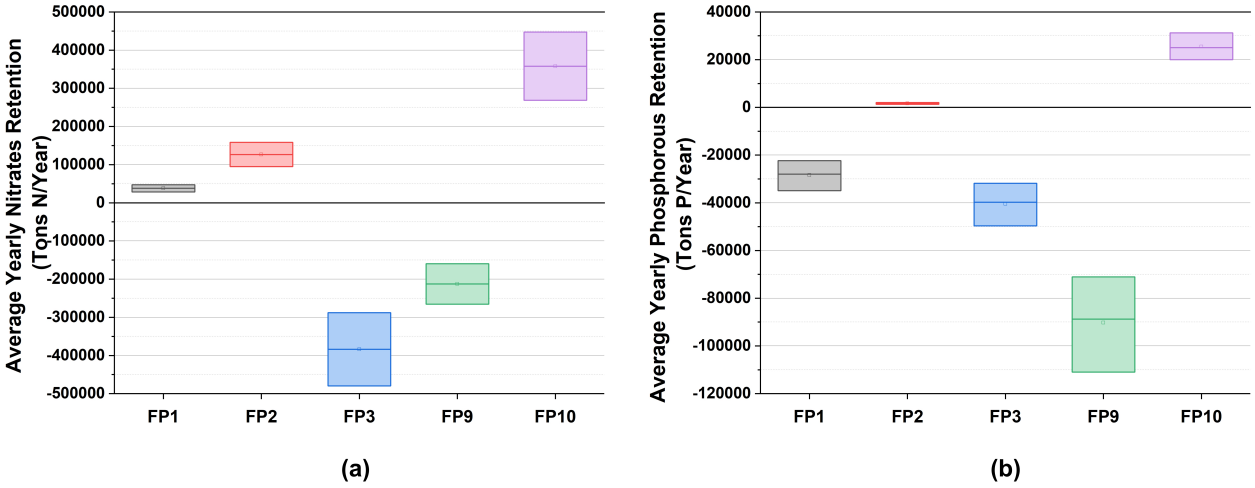

Figure 5.4: Average yearly retention values of the analyzed floodplains (FP) for: (a) Nitrogen; (b) Phosphorus.

5.4.3 Water quality variations

By averaging the improvement and worsening results of WQI, it is possible to have an overall view of the water quality variations. Results of this exercise are shown in Figure 5.5. Except for FP10, all floodplains show an average annual water quality improvement downstream of the corresponding floodplain. It is also noticeable that the extreme cases for improvement and worsening are the FP8 and FP10, respectively.

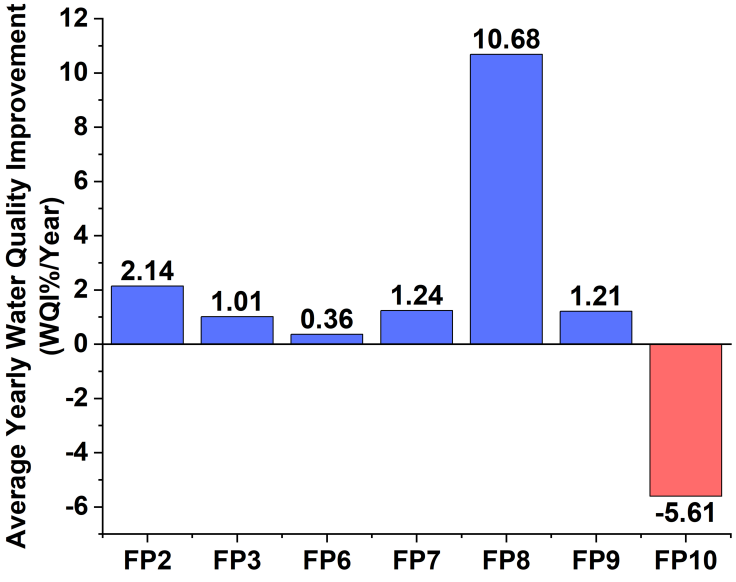

Figure 5.5: Average yearly water quality improvement of the analyzed floodplains (FP).

5.4.4 Water quality and correlation with river discharge

Complete Pearson's correlation plots between average yearly nutrient retention and river discharge, as well as correlation plots between water quality improvement and river discharge value are provided online here: https://www.mdpi.com/article/10.3390/hydrobiology1020016/s1. These plots determine the relationship between the discharge values and the water quality. They can also explain the different behaviors of floodplains towards improving the water quality.

5.4.5 Remote sensing-based machine learning models

Complete Pearson's correlation plots between average yearly nutrient retention and river discharge, as well as correlation plots between water quality improvement and river discharge value are provided in Figure S11-Figure S13 (https://www.mdpi.com/article/10.3390/hydrobiology1020016/s1). These plots determine the relationship between the discharge values and the water quality. They can also explain the different behaviors of floodplains towards improving the water quality. Correlation between C2RCC and in situ measurements is displayed in Figure 5.6.

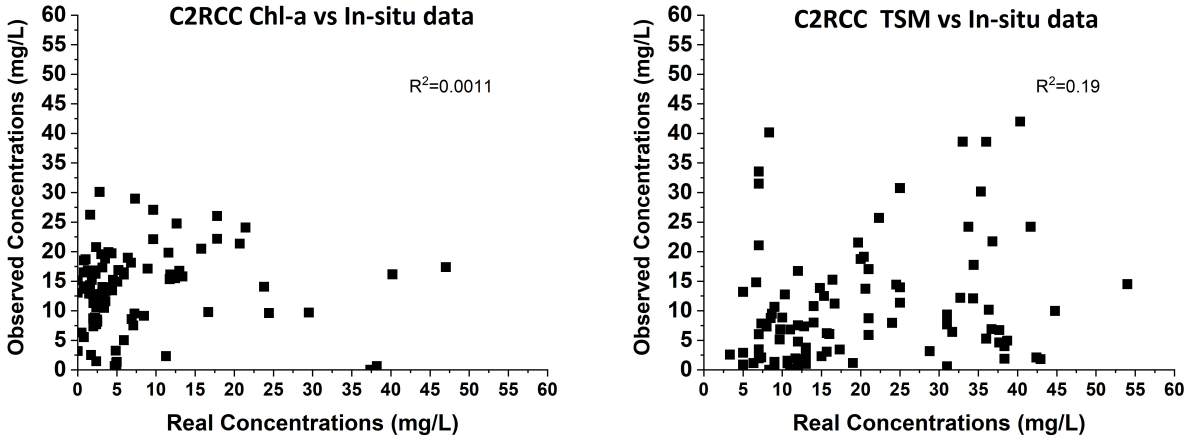

Figure 5.6: In situ validation for Case 2 Regional Coast Color (C2RCC) algorithm results with in situ measurements: (a) Chlorophyll-a (Chl-a); (b) Total Suspended Matter (TSM).

Poor results for both Chl-a and TSM products are retrieved, particularly for Chl-a, for which an overestimation occurs in the range of 0-10 mg/L. TSM shows underestimation for almost all the range of the concentration but a slightly better correlation $R^2 = 0.19$. These results justify further modeling using Rrs and locally-tuned machine learning approaches in an effort to estimate accurately Chl-a and TSM. After the tuning of hyperparameters, the feature engineering process and the LOOCV, average error metrics were calculated and the three models were compared against each other. Results for Chl-a and TSM are displayed in Table 5.2 and Table 5.3.

Table 5.2: Machine learning models' results for best runs of each algorithm for Chl-a estimation.

Model	R^2	RMSE	Number of Features
MLR	0.31	7.76	1
RF	0.60	5.90	2
SVR	0.57	6.10	5

Chl-a ML models perform better with better results for Random Forest $R^2 = 0.60$ and RMSE = 5.90 against SVM ($R^2 = 0.57$ and RMSE = 6.10). TSM ML models perform very poorly, and only LR reach an $R^2 > 0.10$. We chose, therefore, RFR for further estimation of Chl-a and LR for TSM. We assumed, however, that for TSM, we would retrieve highly uncertain results due to the very weak performance of TSM models. The results of water quality from modeling over the surface of Danube River confirm the

Table 5.3: Machine learning models' results for best runs of each algorithm for TSM estimation.

Model	R^2	RMSE	Number of Features
MLR	0.12	15.62	1
RF	0.08	15.99	2
SVR	0.08	21.07	1

previous results from Figure 5.6. Chl-a spatial variations are shown in Figure 5.7 for FP2 (Figure 5.7a), FP6 and FP7 (Figure 5.7b), and FP8 (Figure 5.7c). The selected dates of the image acquisition to display spatial variations were based on the time series analysis and WQI analysis. Similarly, TSM spatial variations are shown in Figure 5.8. From Figure 5.7, it is visible that upstream regions of FP 2 show a higher concentration of Chl-a (up to 23-27 mg/L), and downstream region reduces its concentration (<=3 mg/L). Similar scenarios are visible in Figure 5.7b for FP6 and FP7, except for the region at the extreme East, where a plume with high Chl-a concentrations is visible (Figure 5.7b, downstream). In Figure 5.7c, a clear difference is visible between upstream and downstream concentrations as well. Despite the low performance of TSM models, the estimations are in agreement with the average water quality improvement from Figure 5.5 for FP2 (Figure 5.8a), FP 6 and FP7 (Figure 5.8b), and FP 8 (Figure 5.8c) where upstream higher concentrations are reduced after the floodplain regions.

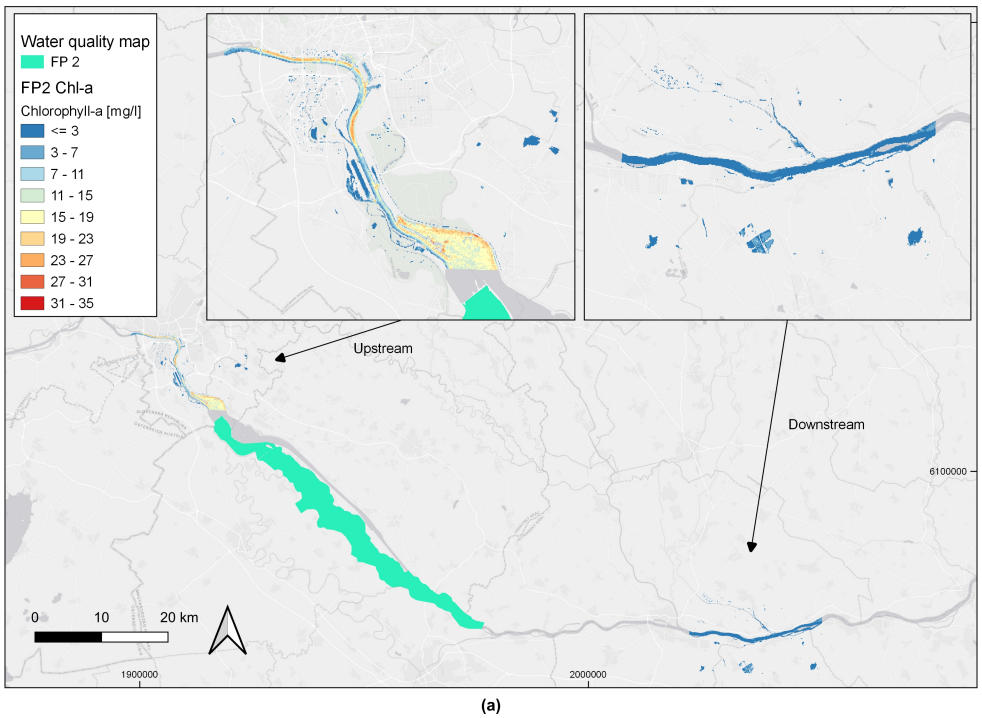

(a)

Figure 5.7: Cont.

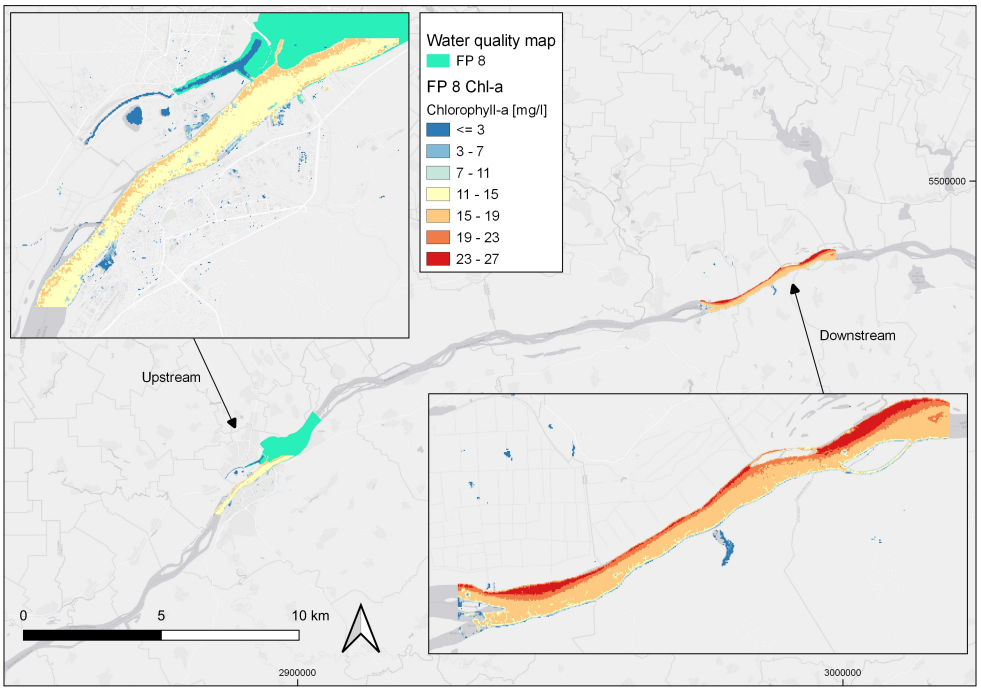

(c)

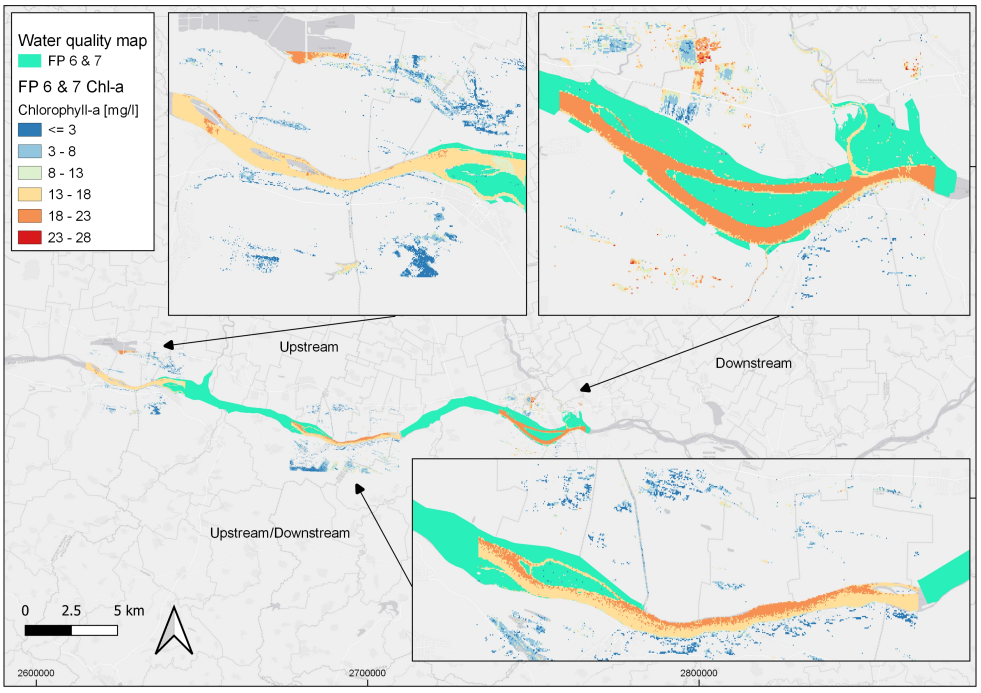

(b)

Figure 5.7: Water quality maps for Chlorophyll-a expressed in mg/L for the three areas that correspond to (a) floodplain 2 (S2 image acquired on: 13 April 2016); (b) floodplains 6 and 7 (S2 image acquired on: 28 February 2017); (c) floodplain 8 (S2 image acquired on: upstream on 26 May 2017 and downstream on 15 May 2017). Basemap: ESRI Gray. EPSG: 3857. Figure 7. Water quality maps for Chlorophyll-a expressed in mg/L for the three areas that correspond to (a) floodplain 2 (S2 image acquired on: 13 April 2016); (b) floodplains 6 and 7 (S2 image acquired on: 28 February 2017); (c) floodplain 8 (S2 image acquired on: upstream on 26 May 2017 and downstream on 15 May 2017). Basemap: ESRI Gray. EPSG: 3857.

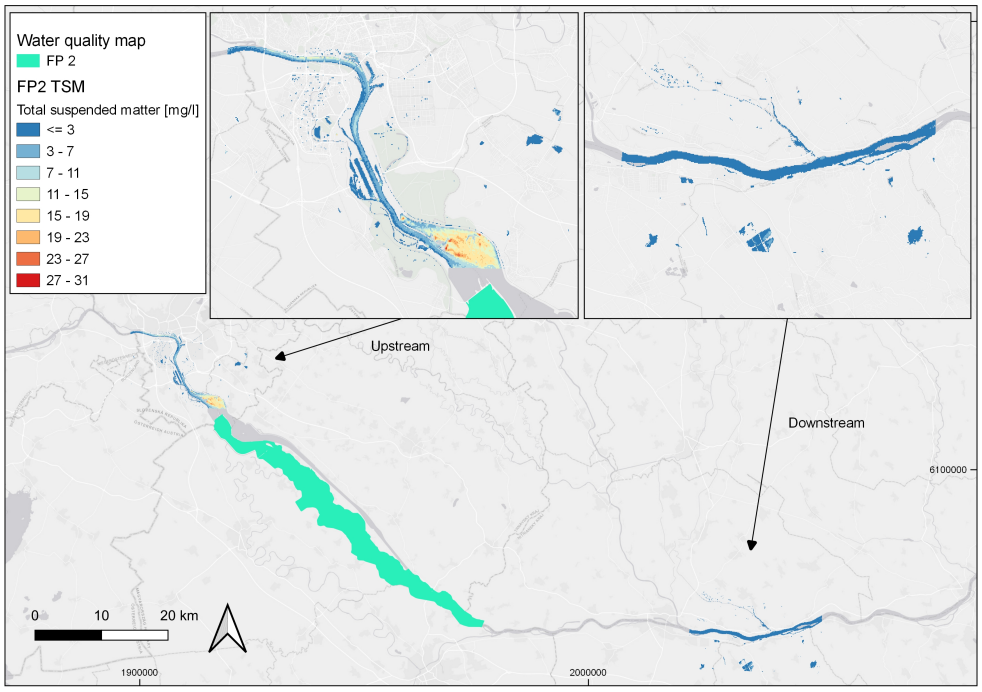

(a)

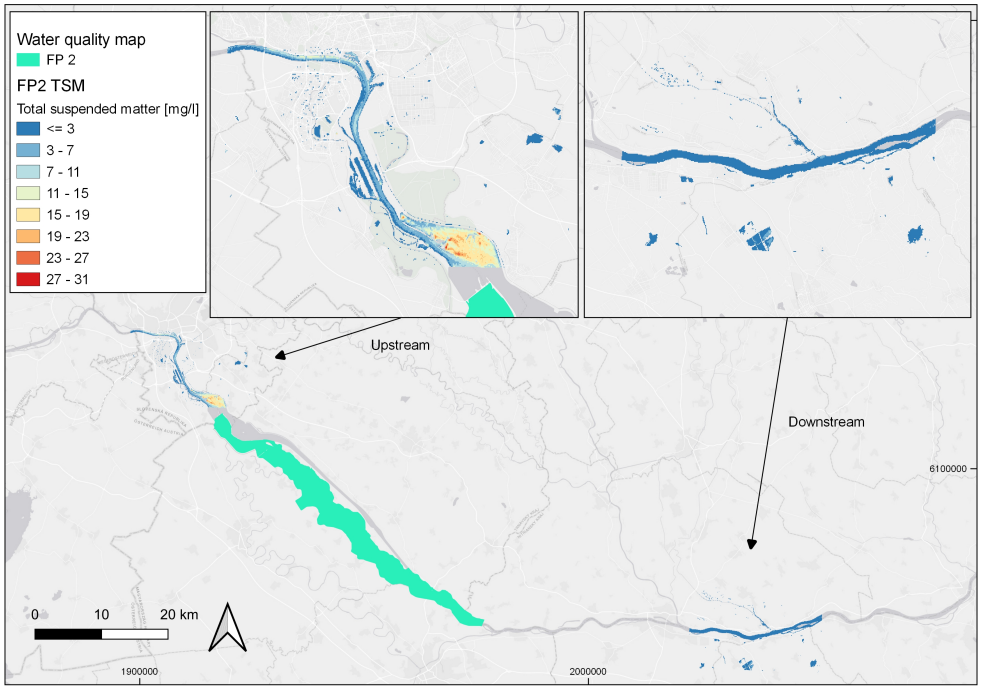

(a)

Figure 5.8: Cont.

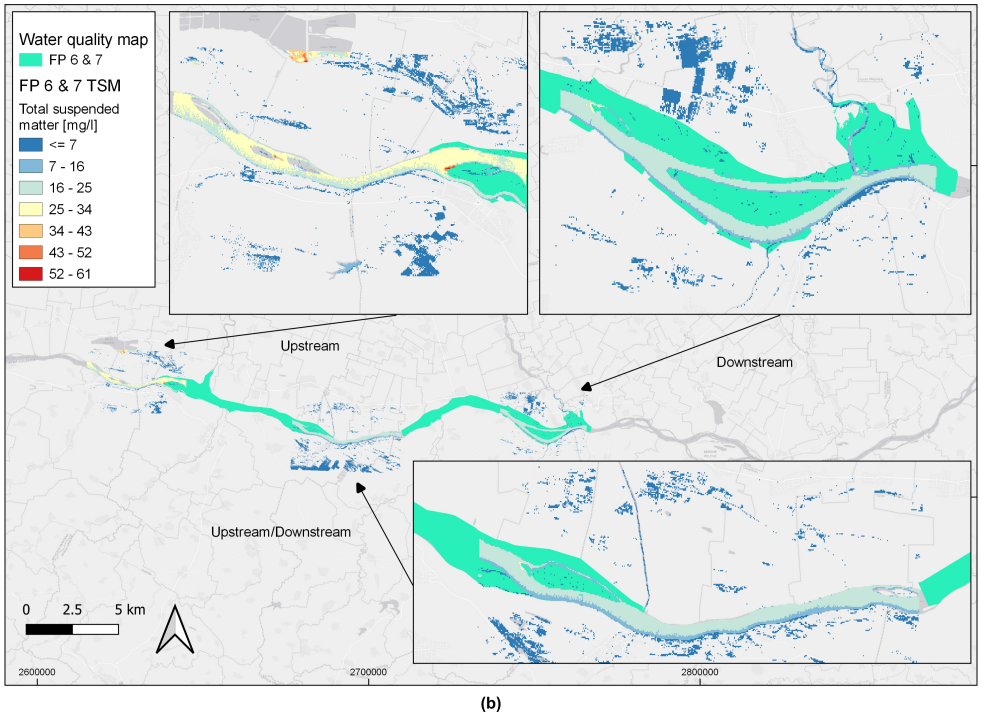

Figure 5.8: Water quality maps for total suspended matter (TSM) expressed in mg/L for the three areas that correspond to (a) floodplain 2 (S2 image acquired on: 13 April 2016); (b) floodplains 6 and 7 (S2 image acquired on: 28 February 2017); (c) floodplain 8 (S2 image acquired on: upstream on 26 April 2017 and downstream on 15 May 2017). Basemap: ESRI Gray. EPSG: 3857.

5.5 Discussions

5.5.1 Water quality and nutrient retention

Not all floodplains could be analyzed in our study since there was a lack of field measurements for important nutrients in some stations or an absence of discharge data in other stations. Floodplains showing a positive behavior in improving the water quality downstream of the floodplain were described to have a low to medium restoration demand, showing that these floodplains' functionality of filtering contaminants and improving water quality is active, and also, it can be improved further for FP6, FP7, FP8, and FP9, having a medium restoration demand. On the other hand, one floodplain (FP10) did not show a water quality improvement at any year, despite having a medium restoration demand. Still, it is possible that other functionalities are active in this floodplain, such as providing groundwater recharge or supporting habitats, but the improvement of water quality function is not active and needs to be restored. Moreover, among the floodplains showing a pattern of retaining nutrients, we can notice that 83 of the years in which a flood occurred, the yearly average improvement of water quality was positive. This explains that during flooding years, the water quality improvement function of floodplains is more active. Regarding the nutrient retention, only five floodplains had enough data to conduct the analysis. Some of the floodplains that showed a retention behavior in the general water quality analysis did not retain nutrients, and also acted quite poor in terms of nutrient retention and vice versa. This is due to other valuable parameters that are taken into consideration when computing water quality, such as Chl-a, TSM, and the Dissolved Oxygen concentrations. Therefore, sometimes, a floodplain may not serve for nutrient retention but it will improve other water quality parameters, leading to a better quality of water downstream. The poor nutrient retention in floodplains can be caused by a release of nutrients greater than retention capacity. Sometimes, nutrient storages are not permanent due to the dynamic nature of floodplains. Some studies showed floodplains releasing nutrients or sometimes re-suspending them due to scouring currents occurring in the river. Other studies showed a net release of phosphorus or even an increase in both nitrogen and phosphorus amounts in the river channel next to a floodplain (Sparks, 1995; Kadlec & Wallace, 2008). Additionally, in some cases, it is important to consider the presence of

soluble reactive phosphorus (SRP), which can act disproportionally to downstream eutrophication (Xue et al., 1999). Moreover, it is important to consider the nutrients that can be returned to the river via lateral stream migration and erosions from stream banks over long time periods, which can shrink the size of the floodplain each year as well (Philippot, Hallin, & Schloter, 2007; Knighton, 2014).

Finally, it is very important to consider river discharge in floodplains because it is the river discharge values that determine the hydraulically connected area of an active floodplain (DTP, 2020). The correlation between the water quality improvement or the nutrient retention and the river discharge values was not strong, except for some floodplains. In these floodplains, it is important to consider the hydraulic load and the water depth while designing flow rate recommendations for effective treatment, because they play critical roles in the effectiveness of nutrient removal (Batjes, 2011). The poor correlation between discharge rate and retention could be explained by a limited range on the available data and a small difference among inflow concentrations (Walling, He, Blake, et al., 2000). Finally, some floodplains showed a negative correlation, i.e., showing higher retentions during small river discharges. This can be explained by the fact that during low discharge periods, longer water residence times are expected, promoting nutrient retentions such as denitrification and other types of soil accumulation (Jarvie et al., 2017). Additionally, we have to mention that some floodplains did not have enough sample points in order to do a significant correlation analysis. For example, FP3 and FP9 for both nitrates and phosphorus had only 5 sample points each, which is a small amount of data to make an accurate analysis.

5.5.2 Machine learning models based on remote sensing

Modeling water quality parameters over inland waters, and specifically over large fluvial systems, has been demonstrated to be possible, even when there are challenges and uncertainties associated with the process (Peterson et al., 2018; Y. Zhang et al., 2020). In this work, the poor correlation with available water products from C2RCC justified further modeling and provide continuous spatial coverage of both Chl-a and TSM. From the error metrics evaluation, Chl-a displayed good performance ($R^2 = 0.61$) and therefore, modeling spatial variation along the river is more certain. However, TSM performance is very weak ($R^2 = 0.12$), although the spatial patterns are in line with the WQI improvements seen in Figure 5.5. Still, a complete agreement between these two results is not possible to be demonstrated based on this exercise, since the quality maps represent only one snapshot in a specific moment of interest for the floodplain of interest. Feature engineering was also a useful process that helped to develop better ML models and could be extended in the future. Although modeling water quality parameters using satellite images and remote sensing has been demonstrated to be possible, we still face many associated challenges and limitations (Peterson et al., 2018; Y. Zhang et al., 2020). These include the narrow stream channels of a river, requiring a higher spatial resolution of satellite image data (Bukata, Jerome, Kondratyev, & Pozdnyakov, 2018). Another challenge is the high variation of sediment concentrations in time and space (Bukata et al., 2018). Moreover, our modeling was based on remote sensing data, which adds further limitations because of the need to match satellite acquisitions and field measurements. This adds up as a significant limitation in the temporal resolution (Peterson et al., 2018). Given that Sentinel-2 imagery during the time of interest had a frequency of 1 image every 10 days (low frequency compared to 1 image every 5 days nowadays), a high number of images were eliminated during the filtering process because they did not match the date of field measurements. Other images were eliminated due to cloud cover. This problem can be solved by using multiple satellites. Even so, we believe that the potential of remote sensing is high to evaluate changes in water quality, as done in several studies (Peterson et al., 2018; Topp et al., 2020), allowing to develop predictive models that can be extrapolated in time (multitemporal analysis) or over space scales (water surface distribution of water parameters).

5.5.3 Human intervention and floodplain reconnections

Anthropogenic interventions had a direct and major impact on floodplain ecosystems causing them to degrade (Batjes, 2011), especially in urban areas. There, the floodplain areas are artificially constructed and therefore show reduced ecosystem functions, due to a loss of connectivity between the river and the historically natural floodplain (Nelson, Redmond, Sparks, et al., 1995). In our study, half of the floodplains in the Danube River (especially the upper part) are not fully reconnected (Llewellyn et al., 1996) and need to be restored. Maximizing the function of a floodplain can be done by fully reconnecting

the floodplains and designing them with the optimum river discharge value (Walling et al., 2000), so that they can retain a higher amount of nutrients from rivers and streams (Walling et al., 2000).

5.6 Conclusions and outlook

Anthropogenic influence has led to disconnected Danube floodplains, which lost 80 of their original size (Schwarz, 2011), although they are a source of multiple ES. The restoration of lost floodplains is a well-known NbS, used to deal with river water quality issues. We looked for approaches in alternatives to water quality modeling and field measurements, and combined multiple methods to understand the potential of floodplain restoration to improve water quality along the Danube River. The main conclusions on the effect of floodplains on Chl-a, TSM, nitrate nitrogen, total phosphorus, and water quality can be summarized as follows:

- At the annual scale, most areas downstream of active floodplains have better WQI than the corresponding upstream section, while nitrate and total phosphorus retention do not show a relevant trend (the effect is rather dependent on the single floodplain)
- There is the need for more sophisticated analyses of remote sensing data, as shown by poor results for in situ validation of Sentinel-2 C2RCC water products; on the other hand, remote sensing-based ML modeling shows more certain results for Chl-a, but is still lacking certainty in the modeling of TSM
- The comparison of remote sensing ML approaches (water quality maps) and in situ data analysis (WQI variation shown by the time series) shows an agreement of two independent methodologies

Based on these observations, we conclude that no homogeneous improvement of water quality downstream of floodplains can be demonstrated with the applied methodologies (data series analysis and remote sensing-based ML), due to missing statistical relevance of the data. Therefore, we can only partially determine the benefits of floodplains along the Danube River. More effort should be put into predicting the potential of floodplains for water quality improvement. One way to do so is the study of active floodplains and their effects on water quality, as done in this work at the full river-length scale. Other ways to predict the potential of nutrient retention are to work at the floodplain scale by implementing in situ measurements (M. T. T. Natho S.; Hein, 2022), or to conduct water quality modeling, as done in multiple ways in the Danube River Basin (Garnier et al., 2002; Venohr et al., 2011; Malago, Bouraoui, Vigiak, Grizzetti, & Pastori, 2017; S. Natho, Tschikof, Bondar-Kunze, & Hein, 2020). Instead of focusing on only one of these approaches, we recommend researchers to combine their skills and efforts to conduct interdisciplinary work, so that methodologies based on different backgrounds can be compared, and results can be double-checked. For example, spatially highly dense sub-daily field measurements implemented on one floodplain could be combined with physically-based or statistical models for upscaling calibrated parameters on a whole river basin. Water quality estimations on rivers based on remote sensing still presents some limitations (Peterson et al., 2018), such as the low performance of the models for TSM, or the dependence on the temporal resolution of the chosen satellites. Nevertheless, this publication is, to the authors' knowledge, the first attempt to analyze floodplain benefits in terms of water quality through a holistic set of approaches, which also includes satellite remote sensing. We call for other researchers, as done by (Y. Zhang et al., 2020) or (Peterson et al., 2018), to explore the potential of remote sensing to evaluate floodplains' ecosystem services, not only limiting to nutrient retention, but also analyzing carbon sequestration, flood mitigation, or nature-based recreation.

Additionally, future research should focus on developing other ML techniques with hydrological and remote sensing applications, such as the extreme learning machine (ELM), or hybrid methods such as the hybrid back propagation neural network (BPNN). ELM has demonstrated to produce high accurate models that can provide stakeholders with important and precise sediments' information with a continuous and finer spatial resolution (Peterson et al., 2018). In addition, ELM outperformed traditional monitoring methods, leading to better results (Peterson et al., 2018). Moreover, ELM can be further refined with Sentinel-2 sensors, resulting in finer and more accurate estimates of concentrations (Peterson et al., 2018). On the other hand, hybrid methods such as the hybrid BPNN can be trained with a little amount of data and still outperform other models (Y. Zhang et al., 2020). In conclusion, ML still has a lot of room for improvement, especially in hydrological applications, and further studies should be made to improve ML

models in remote sensing. For future analyses on floodplain restoration NbS, special attention should be put into further estimating the effect of hydrological connectivity, as this has been shown to be a main driver determining the amounts of nutrients retained by floodplains (S. Natho et al., 2020). In fact, frequent inundations and complete reconnection of side arms would lead to higher nutrient retention (S. Natho et al., 2020), and simultaneously increase typical floodplain habitat provisioning, whose degree of biodiversity and primary productivity is higher than purely terrestrial or aquatic ecosystems (Tockner & Stanford, 2002). In fact, even with less than 2 of Earth's land surface, floodplains furnish nearly 25 of all ES, excluding marine ecosystems (Akanbi, Lian, Soong, et al., 1999). Finally, more investments should be put into the restoration of floodplains and other ecosystems, such as peatlands and forests, as, for example, announced for Germany with the Action Program "Natural Climate Protection" by the Federal Government, which plans to invest 4 billion Euros for NbS for climate protection between 2022 and 2026 (fur Umwelt, 2021).

Author Contributions: Conceptualization, F.P. and L.F.A.-R.; methodology, F.P. and L.F.A.-R.; software, validation, formal analysis, investigation, resources, data curation, writing-original draft preparation A.H., writing-review and editing, visualization, supervision, project administration, F.P. and L.F.A.-R. All authors have read and agreed to the published version of the manuscript.

Funding: This research received no external funding.

Acknowledgments: We would like to thank all Danube Floodplain project's partners for providing necessary input data and useful insights regarding the study areas, especially the International Commission for the Protection of the Danube River (ICPDR), the University of Szeged (USZ), and the University of Natural Resources and Life Sciences (BOKU). Additionally, we would like to thank the Chair of Hydrology and River Basin Management (Disse) of the Technical University of Munich for providing administrative and technical support. We thank the peer reviewers for providing constructive comments, which extensively improved this manuscript. Finally, we would like to thank the Mexican National Council for Science and Technology (CONACYT).

6 Global Water Quality of Inland Waters with Harmonized Landsat-8 and Sentinel-2 Data using Cloud-Computed Machine Learning

Arias-Rodriguez, L.F.;
Tuzun, U.F., Duan, Z.; Huang, J.; Tuo, Y.; Disse, M.
For peer review

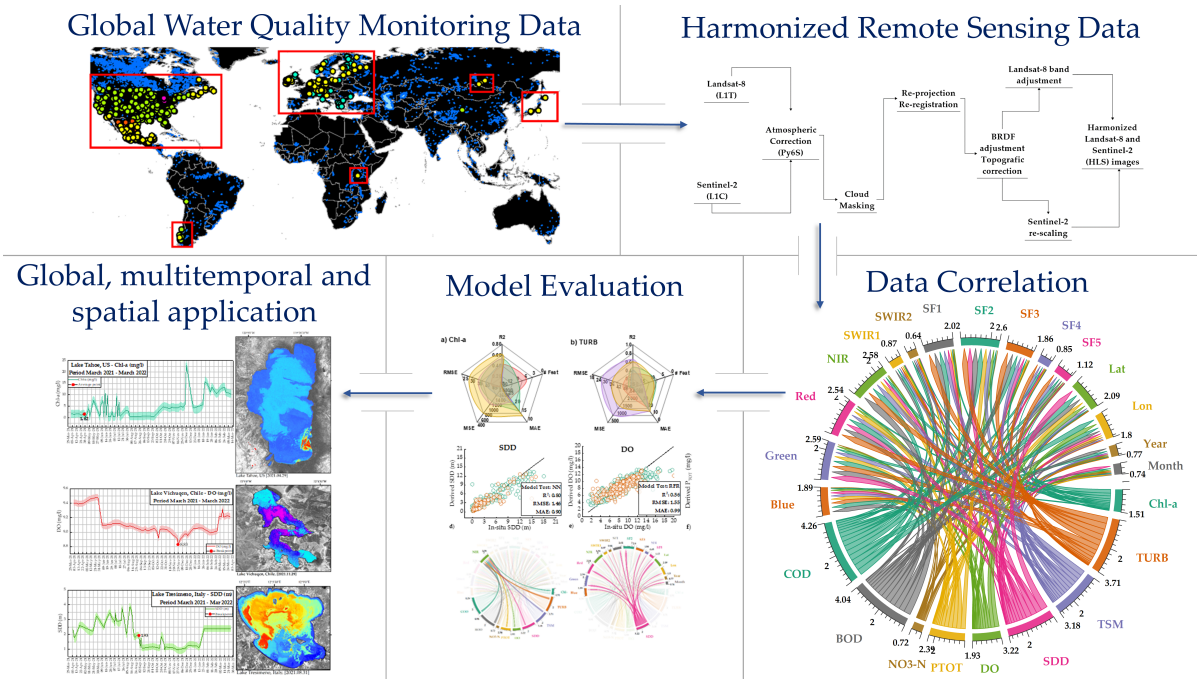

Highlights:

- Modeling of water quality in inland waters at global scale
- Water quality data from more than 18 countries were analyzed
- Harmonized remote sensing data produced for water quality predictions
- Time series and quality maps for lakes in different continents
- Model performance reaches up to $R^2 = 0.70$ for specific parameters

Keywords: Landsat 8 OLI; Sentinel 2 MSI; Sentinel 3 OLCI; water quality monitoring system; extreme learning machine; support vector regression; inland waters; turbidity; Chlorophyll-a; secchi disk depth

Abstract

Modeling water quality in inland waters by remote sensing has demonstrated its capacity to retrieve water parameters and support monitoring tasks. However, limitations still exist for applicability in divers regions around the world and retrieval non-optically active parameters (nOAC). Increased data availability offers opportunities to challenge these limitations. Remote sensing and field data count with methods that increment usable data for water modeling. For example, data processing from water monitoring programs around the world and harmonization of satellite data. Furthermore, Machine Learning (ML) and Cloud Computing provide resources to process vast amounts of data. Currently, there is a lack of research that incorporates water quality data from monitoring systems across the world and remote sensing data from operational satellites for a synergistic analysis. To overcome this, this study gathers global water measurements and pair them with Harmonized RS data of Landsat-8 and Sentinel-2, with the aim to increase data availability and build a dataset with worldwide lake characteristics to be processed with ML. The results show that trained models retrieve high correlations for SDD, TURB and BOD (R^2 = 0.68) and lower performances for TSM and NO3-N (R^2 = 0.43). The Extreme Learning Machine (ELM) and the Random Forest Regression (RFR) shown the higher performance. Additionally, time series and quality maps for lakes in different continents were produced. Results indicate that ML algorithms are capable to process remote sensing data and additional inherent features to model water quality at global scale and contribute to overcome limitations of transferability and retrieval of nOAC. However, important limitations need to be improved are present, namely the harmonization process and atmospheric correction would require to be developed specifically for water quality applications. We highlight the need of international contribution to global water quality datasets capable to supply extensive and homogeneous water data for improvement of global water monitoring.

6.1 Introduction

Monitoring water quality of inland waters in different countries is mostly done individually by each nation. Global integration of their data is often constrained by a lack of worldwide projects or collaborations (UNEP, 2016). When possible, the countries measure the water quality mainly inside their borders through their monitoring systems and stored locally. Therefore, an important quantity of data that is collected every year is usually not available or it is of difficult access for external researchers or international institutions. Currently, there are international projects that aim to integrate homogeneously water quality data from several countries for applications in water resources (UNEP, 2021). However, these programs are in early stages and until now there no comprehensive and unique source for global and homogeneous water quality data. At the same time, the global coverage of operational monitoring stations is insufficient or lacks acceptable levels of confidence and precision (UMA, 1998; EPA, 2006; UNEP, 2016). This situation limits considerably the application of current data-driven methods that use big datasets to learn from water quality patterns. Therefore, monitoring water quality remains limited by only conventional analysis as collection water samples in field and laboratory analysis (Matthews, 2011; Gholizadeh et al., 2016). Conventional methods are highly accurate, but also expensive, time demanding and limited in spatial and temporal coverages. Additionally, it is complex to develop a representative understanding of the water quality status in a waterbody from punctual field measurements or limited field campaigns over the course of large periods of time. A solution to increase the scope and capabilities of monitoring water quality is the use of remote sensing data, which contributes to provide data from remote sensors that couple field data and increase the analysis in time and space. International institutions such as the United Nations encourage already the coupling of monitoring systems with remote sensed technologies through its Environment Program (UNEP, 2016). When paired with field data, combined water and remote sensing measurements allow monitoring at a larger scope since they have the potential to analyze waterbodies at regional or global locations. This is done by studying water quality from indicator parameters and dealing with better cost-benefit methods in comparison with the extensive spatial and temporal scales that is analyzed. Several modeling techniques associate remote-sensed signal, mostly in the visible and near-infrared wavelengths (400-900 nm), with the water parameter of interest to derive information of the waterbody. The relation originates from the interaction of the surface radiation that interacts by absorption and scattering with the optically active constituents (OAC) as Chlorophyl-a (Chl-a), Total Suspended Matter (TSM) (Giardino et al., 2019), etc. Remote Sensing is suited to analyze these relationships because of the high sensitivity in the radiometric resolution of several satellite sensors. As

water absorbs within the visible spectrum, low reflectance occurs in the water column in contrast to the high reflectance of land. Therefore, high sensitivity in the spectral sensors is required to detect the slight changes in water reflectance that surpass the absorption of water (Sathyendranath et al., 2000; Doxaran et al., 2002). Currently, sensors such as Landsat-8 OLI and Sentinel-2 MSI are suited to provide remote sensed data for water quality monitoring because of their radiometric and temporal resolutions (Claverie et al., 2018). While remote sensing-based models can reproduce the patters and dynamics of key water parameters, it becomes relevant to improve confidence and accuracy of such methodologies and the data that is provided to calibrate them. From the different approaches developed in the last decades, machine learning algorithms currently offers accurate and precise models for water quality monitoring (Y. Zhang, Ma, Duan, Loiselle, & Xu, 2014; Bonansea et al., 2015; Peterson et al., 2018, 2020). Machine learning comprises statistical methods which are able to learn from the data they are provided through iterative processes of error adjustment between training and prediction datasets. The process involves providing data to the selected algorithm which is trained with known or predefined features or objects that allow detection, classification, or pattern recognition in semi-automated or automated learning. Methodologies combining machine learning with remote sensing data have been used to successfully model water quality (Y. Chen et al., 2019; J. He, Chen, Wu, Stow, & Christakos, 2020; K. Chen et al., 2020; Y. Li, Wang, Zhao, Han, & Liu, 2020; Xu, Coco, & Neale, 2020; Peterson et al., 2020; Y. Zhang, Wu, Deng, & Ouyang, 2021; Pyo et al., 2021). Some algorithms are considered standard for machine learning evaluations like support vector machines (SVR) and random forest regression (RFR) (Arias-Rodriguez et al., 2020). Furthermore, deep learning, a subset of machine learning based on neural networks, has demonstrated higher accuracy than other methodologies used to model water quality as bio-optical or band/ratio models (Peterson et al., 2018; Hartling, Sagan, Sidike, Maimaitijiang, & Carron, 2019; Sidike et al., 2019; Maimaitijiang et al., 2020; Pahlevan et al., 2020). Due to its novelty, there are still open challenges in the application of machine learning which require further research (L. Zhang, Zhang, & Du, 2016; Ball, Anderson, & Chan Sr, 2017; Alom et al., 2019; Ma et al., 2019; Sidike et al., 2019).

The availability of paired remote-sensed and field-water-quality data is highly limited because of the independent nature of acquiring both types of data. Monitoring water quality programs in different countries was not designed to take into consideration remote sensing acquisitions or satellite overpasses. Therefore, an important percentage of field data is not feasible to be coupled with remote sensing images (Arias-Rodriguez et al., 2021). Moreover, remote sensing data originates from multiple instruments with different characteristics. This heterogeneous data, in terms of frequency, spatial and radiometric resolution, demands further data pre-treatment and better machine learning models to reveal meaningful information and may difficult model transferability. Inherent challenges regarding modeling processes also exist, in particular for deep learning. Yet, a deeper neural network may retrieve more accurate results but at a higher computational cost and with associated risks of overfitting. To determine optimal conditions and parameters of these elements is still a crucial research question (Szegedy et al., 2015). Also, important water quality parameters such as nutrient concentrations, indicators of oxygen levels or organic compounds are not feasible to be directly retrieved by remote sensing because of their inaction over the spectral response of the water when dissolved and are therefore known as non-optically active compounds (nOAC). Current research poses the possibilities to determine these parameters on indirect correlations with other optically active components such as Chlorophyll-a, Turbidity, or Suspended Solids (Sagan et al., 2020). Finally, due to the nature of machine learning models trained with remote sensing data being inherently empirical, they are expected to be valid mainly in the region from where their training data are originated, and most of these models are applicable only at their specific regions or waterbodies. As these models rely on optical characteristics, which may vary from waterbody to water body in complex waters, their transferability is further limited to the origin of their training data. However, a key characteristic of machine learning methodologies is that they learn patterns and behaviors from great amounts of data. Therefore, a worldwide-integrated dataset of water quality and remote sensing data arises the possibility to develop a data-driven approach with the capacity for global estimations of water quality by comprising global lake characteristics in a single dataset. In this study we aim to create this dataset with the available resources for remote sensing image processing and open access field water quality measurements. Harmonization of remote sensing data contributes increase data availability by combining remote sensing data from different sensors. A recent example is the harmonization process for Landsat-8 OLI and Sentinel-2 MSI which have been subject to treatment to homogenize their spectral response and spatial resolution (Claverie et al., 2018; Nguyen, Baez-Villanueva, Bui, Nguyen, & Ribbe, 2020; Peterson et al., 2020). To couple water quality and remote sensing as much as possible, we search for available

water quality monitoring systems around the world that offer fully open access to its records, enabling the possibility to use collectively field data samples worldwide. This integration of global water quality data is a necessary step towards fully developed models that can predict water quality in any region of the world.

To contribute to clarify the above challenges, this work aims to: (i) to gather open-access water quality monitoring datasets of the relevant parameters from different regions in the world for its synergistic use with remote sensing, (ii) to maximize the data availability of coupled field and sensor acquisitions by using an image homogenization process for L8 and S2 and produce harmonized image products from both satellites enabling both sensors to be used synergistically, increasing the size available spectral data, (iii) build a comprehensive coupled dataset created from the coupling of the global data set and the harmonized remote sensing products, and (iv) to model relevant water quality parameters using machine learning and validate the use of the developed models for global water quality predictions. In addition, we investigate the results using this dataset and machine learning approaches to understand better the optimal balance between computational demand and retrieved accuracy as well as the possibilities of nOAC direct or indirect retrievals.

6.2 Methods

6.2.1 Sources of the global water quality dataset

The main source of field data are the open-access data portals from water and environment national agencies of different countries which make public their archives of field measurements and monitoring activities. A summary of agencies and links of acquisition is provided in Table 6.1. In its raw form, the dataset contained almost 300,000 total samples. A summary of the number of observations and lakes by region is displayed in Table 6.2. The global location of all the stations from the above-mentioned data sources is shown in Figure 6.1. The objective was to integrate most of the globally available water quality datasets. A recent research of Thorslund and van Vliet (Thorslund & van Vliet, 2020), indicates that the current state of the global water quality stations monitoring lakes and reservoirs is focused mainly on the U.S. followed by Europe, Mexico and South Africa. Australia counts with a great number of stations near 90,000 but most of them are for groundwater and, only 5 are located on lakes or reservoirs.

Table 6.1: Source of national and international water quality datasets acquired in this study.

Source	Data Location	Region
Water Quality Portal (WQP)	https://www.waterqualitydata.us/	United States
European Environment Agency (EEA) Waterbase	https://www.eea.europa.eu/data-and-maps/data/waterbase-water-quality-icm-1	Europe
Mexican National Water Monitoring Network	https://www.gob.mx/conagua/articulos/calidad-del-agua	Mexico
Open Government Portal of Canada	https://search.open.canada.ca/en/od/	Canada
General Chilean Water Directorade	https://dga.mop.gob.cl/servicioshidrometeorologicos/Paginas/default.aspx	Chile
Global Freshwater Quality Database (GEMStat)	https://gemstat.org/data/	Global

Table 6.2: Overview of the number of observations and lakes per region in the raw data set.

Region	n	Lakes
United States	263,699	43
Europe	17,681	64
Mexico	9,086	32
Canada	5,412	2
Japan	1,292	3
Chile	897	16
Russia	32	1

For this study, the gross part of the data components comes from the U.S. and European sources since their data archives are open-access and easy to acquire through their respective portals.

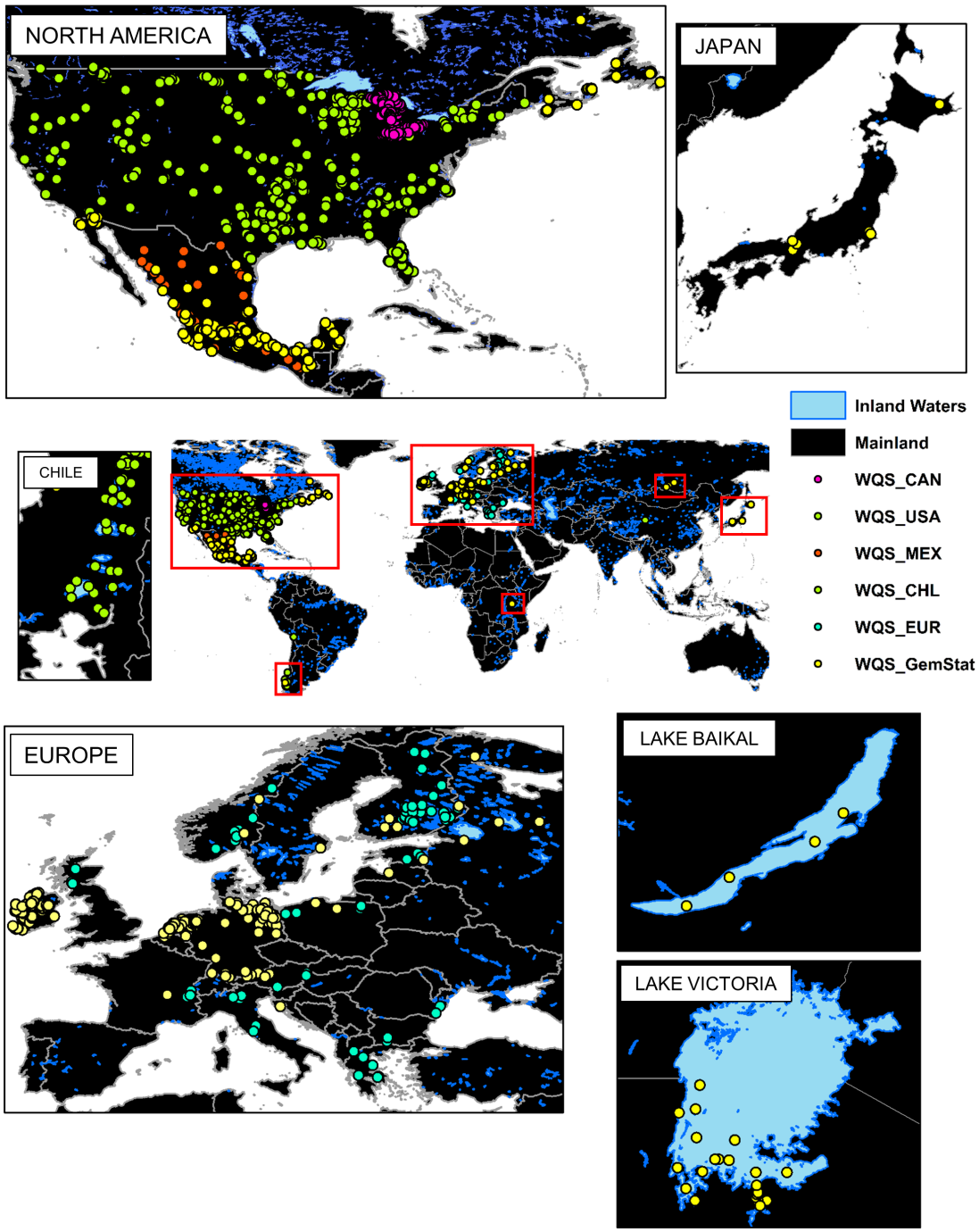

Figure 6.1: The global location of all the stations from the above-mentioned data sources in raw form.

The U.S. data were acquired from the Water Quality Portal (WQP, 2021), which is a cooperative service sponsored by the United States Geological Survey (USGS), the Environmental Protection Agency (EPA) and the National Water Quality Monitoring Council (NWQMC) that integrates publicly available water quality data from the USGS National Water Information System (NWIS) the EPA STOrage and RETrieval (STORET) Data Warehouse, and the USDA ARS Sustaining The Earth's Watersheds - Agricultural Research Database System (STEWARDS) (https://www.waterqualitydata.us/). Data from the European continent were acquired through the European Environment Agency (EEA) Waterbase (https://www.eea.europa.eu/data-and-maps/data/waterbase-water-quality-icm-1), which contains time series of nutrients, organic matter, hazardous substances and other chemicals in rivers, lakes, groundwater, transitional, coastal and marine waters (EEA, 2021). Additionally, datasets from the National Water Monitoring Network of Mexico (https://www.gob.mx/conagua/articulos/calidad-del-agua)

(GOBMX, 2021), the Canadian Great Lakes (https://search.open.canada.ca/en/od/) (GOBCA, 2021), and the Chilean General Water Directory (DGA) lake's database (GOBCHL, 2021) were also acquired (https://dga.mop.gob.cl/servicioshidrometeorologicos/Paginas/default.aspx).

Finally, the Global Freshwater Quality Database (UNEP, 2021) (https://gemstat.org/data/), which is a GEMS/Water Programme of the United Nations Environment Programme (UNEP), was also acquired to account as much as possible for remaining global data around the world. The GEMStat is hosted by the GEMS/Water Data Centre (GWDC) within the International Centre for Water Resources and Global Change (ICWRGC) in Koblenz, Germany (UNEP, 2021).

6.2.2 Field dataset compliance by lake selection, satellite coincidence and data curation

For lake selection, the minimum surface area to consider a waterbody was set to 20 km^2. This size ensures to avoid adjacency errors in the NIR region from the surrounding land surfaces and bottom reflectance in the sensor acquisitions (Bulgarelli, Kiselev, & Zibordi, 2017). At the same time, this area is on the limit to retrieve an adequate number of pixels from the image acquisition based on the spatial resolution per pixel (30 x 30 m) of the intended OLI and MSI sensors to be used as the source of radiometric data.

We used the Level-1 and Level-2 database from the Global Lakes and Wetlands Database (GLWD) developed by the World Wildlife Fund (WWF) and the Center for Environmental Systems Research, University of Kassel, Germany (https://www.worldwildlife.org/pages/global-lakes-and-wetlands-database) (Lehner & Döll, 2004) to apply lake's selection. The first GLDW product, GLWD-1, comprises 3067 lakes (area > 50 km^2) and 654 reservoirs (storage capacity > 0.5 km^3) worldwide, and includes extensive attribute data. The second GLDW product, GLWD-2, comprises permanent open water bodies with surface area larger than 0.1 km^2, from which the minimum area of 20 km^2 was established. Additionally, we apply a rigorous data cleaning process which involved the rejection of samples that (i) predate the launch of Landsat-8 and Sentinel-2, (ii) are not within the ± 3 days range of L8 and S2 images, (iii) taken deeper than 1.0 meter, (iv) are duplicate records, (v) are labeled as of poor or suspect data quality, (vi) are below and above the detection limits for every parameter, (vii) have fill values, (viii) are detected as outliers and faulty study parameter measurements, (ix) belong to not-studied parameters.

In its cleaned form the dataset contained almost 7,000 total samples. An overview of the number of observations and lakes per region in the cleaned data set and their respective number of samples per parameter are shown in Table 6.3 and Table 6.4, respectively. Descriptive statistics of the parameters are provided in Table 6.5. Although we initially had some samples from China and Africa, they did not pass the initial screenings and thereby were not used in the final dataset.

Table 6.3: Overview of the number of observations and lakes per region in the cleaned data set.

Region	n	Lakes
United States	2,032	33
Europe	1,540	54
Mexico	2,875	32
Canada	16	2
Japan	202	3
Chile	206	14
Russia	13	1

Table 6.4: Overview of the number of observations per parameter in the cleaned data set.

Region	n	Lakes
Chl-a (ug/L)	1,080	OAC
TURB (NTU)	554	OAC
TSM (mg/L)	291	OAC
SDD (m)	694	OAC
DO (mg/L)	1872	nOAC
PTOT (mg/L)	987	nOAC
NO3-N (mg/L)	711	nOAC
BOD (mg/L)	214	nOAC
COD (mg/L)	481	nOAC

Table 6.5: Descriptive statistics of our study parameters.

Parameter	Chl-a	TURB	TSM	SDD	DO	PTOT	NO3-N	BOD	COD
Count	1080	554	291	694	1872	987	711	214	481
Mean	26.87	24.48	40.65	2.73	8.80	0.20	2.89	11.25	30.39
St.Dev.	52.53	55.11	54.71	3.31	2.24	0.39	23.98	12.65	27.98
Min	0.00	0.10	1.00	0.00	1.30	0.00	0.00	0.50	2.10
25 Perc.	1.90	2.30	12.00	0.67	7.60	0.03	0.04	3.42	13.00
Median	6.80	5.30	20.00	1.20	8.90	0.07	0.18	5.99	22.00
75 Perc.	22.90	18.00	43.72	3.20	10.00	0.18	1.41	17.00	39.00
Max	561.07	578.70	520.00	18.00	27.00	5.73	443.00	94	270.00

6.2.3 Harmonization of Landsat-8 and Sentinel-2 data

To increment data availability, harmonization of data from different remote sensors was applied as a feasible solution to increase availability of remote sensing data and therefore, to increase the possibilities to match up with available water quality measurements. Harmonization is a novel approach, and its implementation has been in development for general applications as land or crop modeling. Recently, harmonization of Landsat-8 and Sentinel-2 data has been applied for water quality retrievals with promising results (Peterson et al., 2020; Sagan et al., 2020). However, this process is still challenging and requires several stages of image processing (Storey et al., 2016), especially when it is intended to be used at a global scale and using entire collections of remote sensors as in this study. For the purposes of this study, there is the need of an implementation in a cloud platform capable to process the complete imagery of both Landsat-8 and Sentinel-2. Additionally, atmospheric correction applicable to all images is also necessary to retrieve remote sensing reflectance (Rrs). Google Earth Engine (GEE) is a cloud platform that provide excellent access to complete archives of both Landsat and Sentinel data and allows operations and corrections over the entire imagery.

Currently, there is an application of the harmonization process and atmospheric correction in GEE which is described in (Nguyen et al., 2020) based on the original methodology by (Claverie et al., 2018). Following the above mentioned methodology, the collections of Landsat-8 (L8) Top-of-Atmosphere (TOA) and Sentinel-2 (S2) Level-1C (L1C) were acquired via Google Earth Engine (GEE) for the studied lakes and dates of measurement. Images were then atmospherically corrected using the Second Simulation of the Satellite Signal in the Solar Spectrum (6S) developed by (E. F. Vermote, Tanré, Deuze, Herman, & Morcette, 1997), which uses Radiative Transfer Models (RTMs) to simulate the passage of solar radiation across the atmosphere. The 6S algorithm is adapted to a Python (Py6S) interface (Wilson, 2021) and implemented recently for its use with Google Earth Engine (Murphy, 2018) via a Python API and Docker container. Cloud and detection in L8 images, we applied the CFMask algorithm on GEE based on the implementation of (Nguyen et al., 2020). Cloud detection in S2 images was conducted by the

cloud scoring algorithm developed by (Poortinga et al., 2019) that exploits the spectral and thermal properties of bright and cold clouds that excludes snow (Housman, Chastain, & Finco, 2018). Cloud shadow detection was done via the Temporal Dark Outlier Mask (TDOM) (Nguyen et al., 2020), which is a version adapted from (Poortinga et al., 2019). TDOM applies dark pixel anomaly (Housman et al., 2018) to predict the position and the extent of a cloud's shadows by using the cloud's shape, height, and position of the sun at that time (Hollstein, Segl, Guanter, Brell, & Enesco, 2016). Co-registration was performed by measuring the misalignment between L8 and S2 images (up to 38 m) (Storey et al., 2016) and aligning the L8 with its corresponding S2 (GEE, 2022b). Afterwards, reprojection was applied to account for possible differences in band scale and projection (Gao, Masek, & Wolfe, 2009). L8 bands from B2 through B7 were reprojected with respect to the red band of S2 (WGS84), and each band's resolution was rescaled to 30 m using bicubic interpolation (Keys, 1981; GEE, 2022a). Bidirectional Reflectance Distribution Functions (BRDF) model developed by (Poortinga et al., 2019) was applied to reduce the directional effects due to the differences in solar and view angles between L8 and S2 (Claverie et al., 2018). This correction is based on fixed c-factors provided by (Roy et al., 2016), where the view angle is set to nadir and the illumination is set based on the center latitude of the tile (Claverie et al., 2018). The implementation of BRDF correction in GEE is based on results from different studies (Roy et al., 2016, 2017). Topographic correction, which accounts for variations in reflectance due to slope, aspect, and elevation, was implemented using the SRTM V3 (30 m SRTM Plus) and GTOPO30 (Global 30 ArcSecond Elevation) products to cover all Earth regions (Soenen, Peddle, & Coburn, 2005). Adjustment in L8 bands was performed using cross-sensor transformation coefficients from (Chastain, Housman, Goldstein, Finco, & Tenneson, 2019) to solve spectral differences with S2 due to independent radiometric and geometric calibration processes. In (Chastain et al., 2019) the absolute difference metrics and major axis linear regression analysis over 10,000 image pairs across the conterminous United States was used to obtain these transformation coefficients.

The above process retrieves Harmonized Landsat-8 and Sentinel-2 (HLS) images which are corrected surface reflectance with equal spectral and spatial characteristics. A detailed overview of the Harmonization process is shown in Figure 6.2. Pixel extraction of the remote sensing Reflectance (Rrs) was performed from the described location (Latitude and Longitude) of the field stations. We selected the main six bands from the visible, infrared and shortwave infrared, which are relevant for remote sensing of inland waters to reduce processing time.

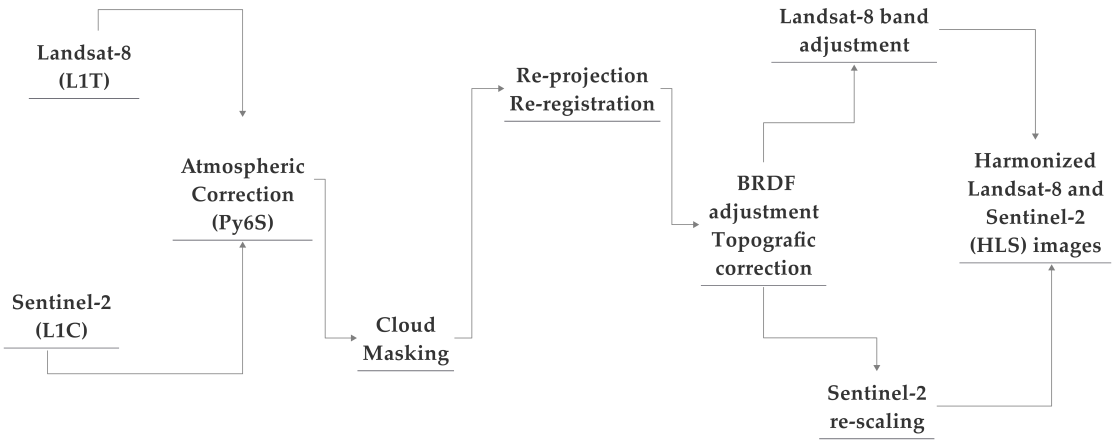

Figure 6.2: Overview of the HLS processing.

6.2.4 Feature engineering and dataset arrangement

Additional features were derived from the HLS dataset in search of stronger correlations. Similarly, the effect of adding additional features on the model performance was also evaluated. To this end, different types of datasets were tested. Each dataset contained different engineered features and inherent

characteristics of each lake. The main differences were based on the usage of common band ratios applied to remote sensing bands (Lathrop & Lillesand, 1989; A. G. Dekker et al., 1991; Doxaran et al., 2002; Ritchie et al., 2003; Svab, Tyler, Preston, Presing, & Balogh, 2005; Sudheer et al., 2006; Odermatt et al., 2012) and additional non-radiometric features such as time and location characteristics (latitude, longitude, month, year). Data were scaled to account for better performances in the modeling process. Additional features specifications are shown in Table 6.6. Four different datasets were evaluated: (i) The harmonized bands (HB) dataset contained purely the HLS bands; (ii) the feature engineering (FE) dataset contained the HLS bands plus the additional band ratios; (iii) the harmonized bands plus region and time (HBRT) dataset which contained the harmonized bands dataset in addition to time and space features, and (iv) the feature engineering plus region and time (FERT) dataset which contained the feature engineering data plus region and time. A summary of each dataset description is provided in Table 6.7.

Table 6.6: List of additional features derived from the HLS dataset and lakes inherent characteristics.

Feature	Formula	Naming
Ratio of Red and Green plus Near Infrared	Red/Green + NIR	SF1
Average of Green plus Red	(Green + Red)/2	SF2
Ration of Green and Red	Green/Red	SF3
Ratio of Red and Green	Red/Green	SF4
Radio of Near Infrared and Green	NIR/Green	SF5
Latitude	-	Lat
Longitude	-	Lon
Month	-	Month
Year	-	Year

Table 6.7: Summary of the studied datasets.

Dataset	Features	Description
HB (Harmonized bands)	HLS bands	Original harmonized Landsat-Sentinel bands
FE (Feature engineering)	H-bands, Red/Green + NIR, (Green + Red)/2, Green/Red, Red/Green, NIR/Green	HLS bands, and the radiometric band ratios
HBRT (HLS Bands, Region, Time)	HB, latitude, longitude, year, month	HB dataset, region and time
FERT (Engineering, Region, Time)	FE, latitude, longitude, year, month	FE dataset, region and time

6.2.5 Machine learning algorithms

Machine Learning algorithms are data-driven methods and therefore, they require enough in-situ water quality observations that contribute to the *learning* of the model. In this process, the models establish a relationship between water leaving radiance acquired remotely (Dörnhöfer & Oppelt, 2016) and the in-situ observations (Sagan et al., 2020). Hence, there is an inherent empirical relationship established between target parameters and predicting features. The learning characteristic of machine learning algorithms is further evaluated in this study by considering additional predicting features that, such as

the water leaving reflectance of a specific measuring point, are also intrinsic to each waterbody. This could help to improve retrievals from purely remote sensing features, which often suffer from high correlation and collinearity between them (Matthews, 2011). Recently applied regression models in research of remote sensing of inland waters were used as modeling approaches. Supervised learning algorithms considered were the linear regression (LR) (Cheng & Lei, 2001; H. Duan et al., 2009; Hicks, Stichbury, Brabyn, Allan, & Ashraf, 2013; Bonansea et al., 2019), support vector regression (SVR) (Vapnik et al., 1997; Samui, 2008; X. Wang, Ma, & Wang, 2010; Azamathulla & Wu, 2011; Maier & Keller, 2018), and random forest (RF) (Breiman, 2001; Hastie et al., 2009; Ruescas et al., 2018; Arias-Rodriguez et al., 2020). Additionally, we employed deep learning algorithms, which have been less commonly applied in the field, from which we focused on the extreme learning machine (ELM) (Huang et al., 2006; Peterson et al., 2018; Arias-Rodriguez et al., 2021), and the multilayer perceptron regressor (MLP) (Keiner, 1999; Panda, Garg, & Chaubey, 2004; Giardino et al., 2013; Peterson et al., 2020).

For every target parameter, each of the above models and hyperparameter optimization with common values in GridSearch was trained and tested. Intensive hyperparameter tuning was not mainly addressed since the primary goal was to evaluate differences in datasets for machine learning models in similar conditions. The settings of the LR model consider an intercept. Hyperparameters for SVR used a radial basis function (rbf) kernel, regularization parameter of C = 1.0, and epsilon = 0.1. We employed RFR with squared error criterion as a function to measure the quality of a split. Different activation functions were tested for ELM depending on the training data ($sig, sin, radbas, hardlim, purelin, tansig$), with common occurrences of sigmoidal function and hidden nodes ranging from 50 - 1000 for different parameters. MLP was used having five hidden layers with the ADAM activation function, learning rate of 0.01, and utilized Bayesian regularized backpropagation to train the model. The modeling approach was done using SciKit Learn (v1.0.2) in Python (v.3.10,3) and the Caret package (v2019.03.27) in R (41.3). Google CoLab was used as the cloud computing platform to perform all calculations.

6.2.6 Model evaluation

Cross-validation with k = 5 folds was selected as our main method of model evaluation. The train/test split ratio was 80 training and 20 testing. Random selection of samples in each iteration was performed to ensure representative selection of data in the training and testing stages. The presence of multicollinearity in the predictors was addressed by an initial feature selection with mutual info regression as the scoring function and a second-degree polynomial feature to account for the non-linearity in the data. To ascertain model performance, we used the following quantitative error metrics: the mean absolute error (i), mean squared error (ii), root mean squared error (iii), and R^2 (iv) in our study. Additionally, we consider the number of features (v) used as a metric for overall comparison among the models. It was considered that the model with the need for fewer predictors has an advantage in terms of required computing power. The error metrics were calculated for both the training and independent testing dataset. Respectively, each performance metric is defined as:

$$R^2(y, \hat{y}) = 1 - \frac{\sum_{i=0}^{n_{samples}-1}(y_i - \hat{y})^2}{\sum_{i=0}^{n_{samples}-1}(y_i - \bar{y}^2)} \tag{21}$$

$$RMSE(y, \hat{y}) = \sqrt{\frac{1}{n_{samples}} \sum_{i=0}^{n_{samples}-1} (y_i - \hat{y})^2} \tag{22}$$

$$MAE(y, \hat{y}) = \frac{1}{n_{samples}} \sum_{i=0}^{n_{samples}-1} |y_i - \hat{y}_i|^2 \tag{23}$$

where y_i is the estimated value, y_i is the observed value and $n_(samples)$ is the number of samples.

6.3 Results

6.3.1 Correlation of water parameters and derived predictors

The correlation between target parameters and predicting features was investigated by the Pearson's coefficient. The range of the coefficient for all features is shown in Figure 6.3. The bigger thickness in the arrow indicates a higher correlation with a specific predictors. Individual plots of nodes and arrows, and their correlation matrix are provided in the supplementary material. Overall, the highest positive and negative correlations are in the order of $r \approx 0.50$ and $r \approx -0.48$. The Green band is moderately correlated ($r \approx 0.38$) with Turbidity, SDD, BOD and COD. Red band has a slightly higher correlation ($r \approx 0.42$) with TURB, SDD and COD. NIR band presented the highest correlations in average ($r \approx 0.43$) with TURB, TSM, BOD and COD. The SWIR bands displayed very weak correlations ($0.17 < r < -0.07$).

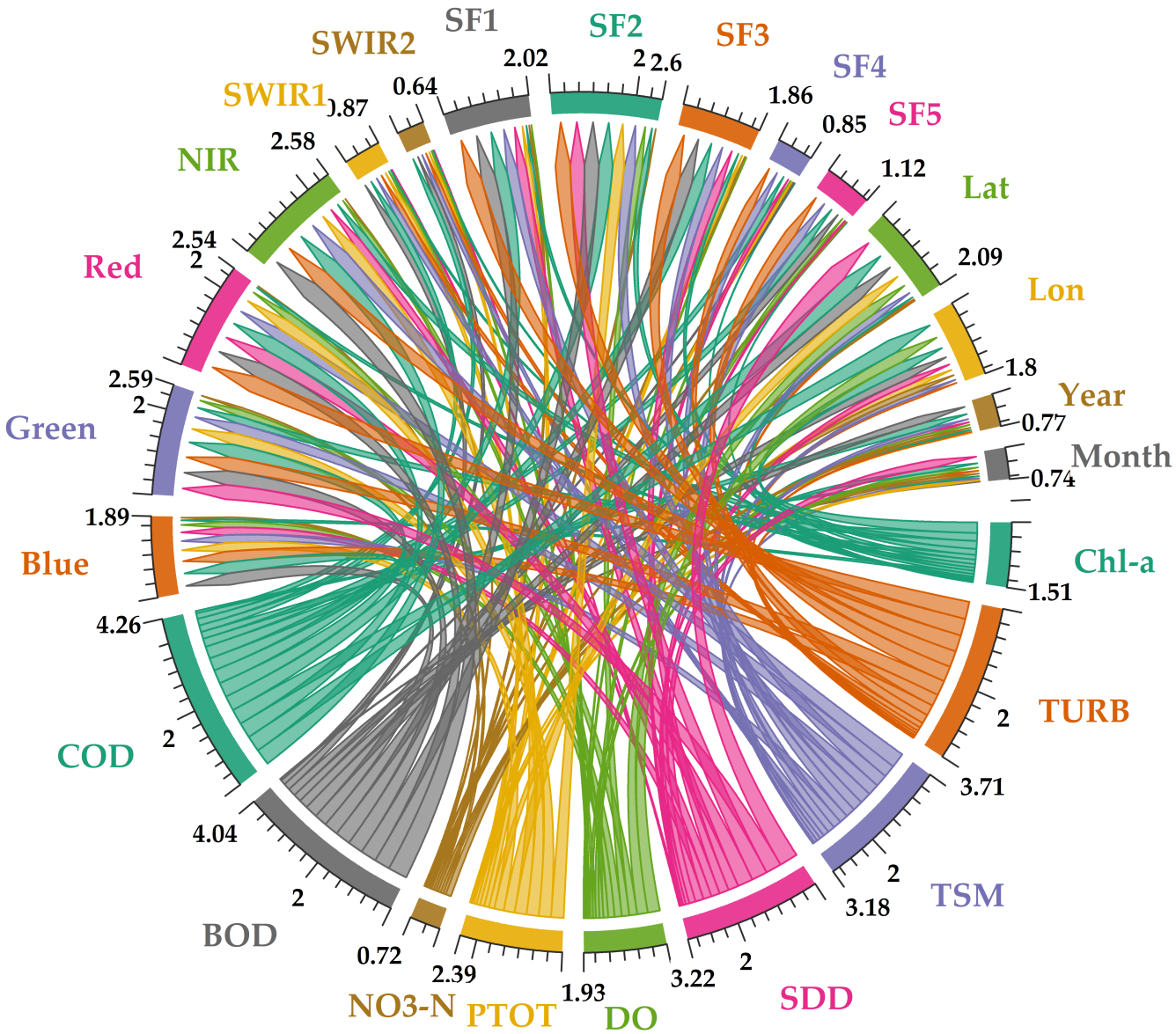

Figure 6.3: Sum and individual correlations of the water quality parameters with predicting features. The total of each node represents the sum of absolute value of positive and negative correlations between all the parameters with all predictors.

From the band ratios, the SF1 and SF2 had a considerable correlations with the targets. SF1 displayed ($r \approx 0.39$) with TURB, SDD, BOD and COD. SF4 and SF5 were poorly correlated ($0.20 < r < -0.20$) with all the parameters, except for an $r = -0.30$ and $r = 0.27$ for TURB. From the SF predictors, SF2 and SF3 showed a higher correlations ($r \approx 0.39$ and $r \approx 0.36$) with TURB, SDD, BOD and COD. Latitude and Longitude were also moderately correlated with SDD, PTOT, BOD and COD, specially Latitude ($r \approx 0.37$). Year and Month were poorly correlated with all analyzed predictors ($0.20 < r < -0.20$). Overall, the most correlated features were the ones of the visible and near-infrared regions, which showed higher correlation in comparison with the spectral features and the region and time features. Green, red, and near-infrared bands showed the higher correlations with TURB, SDD and BOD and COD. Short wave infrared bands 1 and 2 almost completely lacked of any significant correlation. Stronger are weaker correlations are displayed in Figure 6.4. NIR band and SDD parameters show the highest correlations for a predictive feature and a target parameter (Figure 6.4a-b). Similarly, NO3-N and DO show the lower correlations for a feature and target correspondingly.

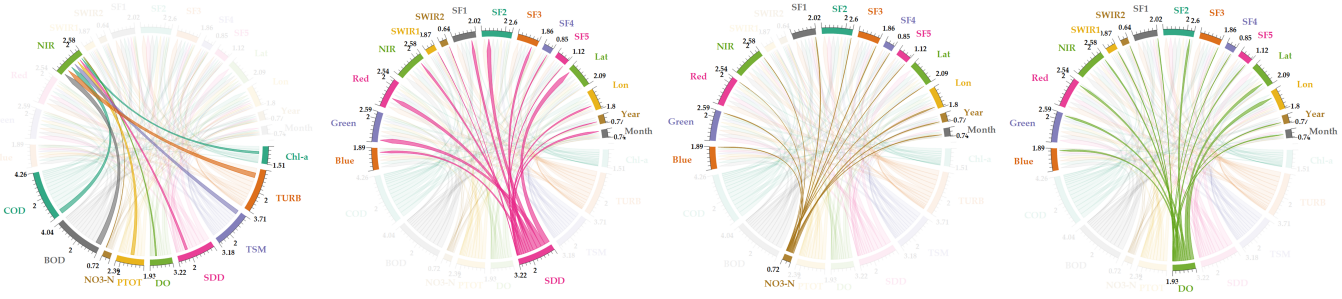

Figure 6.4: Higher and lower correlations for targets and predictors.

6.3.2 Model and dataset evaluation

Training and test phases were evaluated using the 4 available datasets (HB, FE, HBRT, FERT) for each algorithm (LR, SVR, RFR, ELM and MLP). The best dataset for each model is then shown in the table alongside the error metrics of better performance. This evaluation was performed for every target parameter. The entire modeling results are summarized in Table 6.8. In general, LR retrieved low performance models ($R^2 = 0.33$). It performed better on SDD and COD. However, lower performance for TSS and TURB. SVR performed better than LR in most of the parameters, both for the nOACs and OACs, with the exception of COD and Chl-a. Regarding NO3-N, most of the models performed poorly, only SVR attaining reasonable results by retrieving $R^2 = 0.42$ using the HBRT dataset. In the beginning of the calibration process, RFR tended to overfit the data, even with a relatively low number of estimators in each random forest ($n_{estimators} = 5000$). This was addressed by tuning the maximum depth of each tree and the minimum number of samples required for a split.

From this routine, RFR improved greatly and retrieved most of the parameters in acceptable values mostly by using best on HBRT, with the exception of NO3-N, RFR performed satisfactorily for DO ($R^2 = 0.56$) and PTOT ($R^2 = 0.56$). Regarding the development of the deep learning models, it was expected to establish a baseline routine of calibrated models with LR and improve it based on the SVR and RFR training methodologies to finally surpass ensemble learning models with neural networks as ELM and MLP. Overall, ELM performed satisfactorily in most of the analyzed parameters. Specifically, ELM outperformed all algorithms when retrieving Chl-a ($R^2 = 0.53$), TURB ($R^2 = 0.65$), TSM ($R^2 = 0.43$), SDD ($R^2 = 0.72$), BOD ($R^2 = 0.65$) and COD ($R^2 = 0.57$). However, the results we obtained from the MLP were subpar in comparison with ELM or RFR. MLP was trained with relatively high learning rates ($1e^{-2}$ to $1e^{-5}$) and test of up to deep 10 layers were used together with the Adam optimizer. Weights were initialized with random normal as it retrieved better results than Xavier initialization. Except for TURB, MLP results generally have less accuracy than ELM and RFR.

Table 6.8: Summary of the best performing dataset for all models and all parameters in train and test stages. Units: Chl-a: mg/L, TURB:NTU, TSM: mg/L, SDD:m, DO:mg/L, PTOT:mg/L, NO2-N:mg/L, BOD:mg/L COD:mg/L.

			Training					Validation					
	Model	**Dataset**	R^2	**RMSE**	**MSE**	**MAE**	**Feat**	**Dataset**	R^2	**RMSE**	**MSE**	**MAE**	**Feat**
Chl-a													
	LR	HBRT	0.48	38.42	1475.96	20.58	9	HB	0.43	42.25	1784.68	23.34	6
	SVR	FERT	0.63	33.66	1132.83	13.87	15	FERT	0.42	38.76	1502.37	19.74	15
	RFR	FERT	0.81	23.92	572.21	9.60	10	HBRT	0.53	35.11	1232.70	16.18	9
	ELM	FERT	0.53	36.20	1310.31	19.08	15	FERT	0.53	33.61	1129.74	21.77	15
	MLP	FERT	0.62	60.43	3652.16	25.86	15	FERT	0.37	27.53	758.13	13.53	15
TURB													
	LR	HBRT	0.70	27.53	757.80	13.29	9	HBRT	0.32	45.40	2060.82	21.37	9
	SVR	FERT	0.97	9.21	84.77	1.60	15	FERT	0.41	52.32	2737.40	19.22	15
	RFR	HBRT	0.82	22.01	484.41	7.59	9	HBRT	0.47	50.05	2504.73	16.50	9
	ELM	HBRT	0.43	44.33	1964.97	20.43	10	FERT	0.65	26.97	727.41	16.06	15
	MLP	HBRT	0.60	30.11	906.71	13.46	15	HBRT	0.61	40.44	1635.66	17.40	10
TSM													
	LR	HB	0.51	32.96	1086.33	22.13	6	HB	0.22	40.58	1646.95	26.72	6
	SVR	FERT	0.89	16.02	256.70	4.07	15	HBRT	0.28	54.79	3001.95	25.55	10
	RFR	FERT	0.79	24.18	584.45	15.11	4	HBRT	0.30	52.04	2708.02	28.09	4
	ELM	FERT	0.30	48.57	2358.74	28.39	15	FE	0.43	40.23	1618.31	25.52	11
	MLP	HB	0.28	36.27	1315.51	22.28	6	HB	0.30	48.39	2341.57	26.06	6
SDD													
	LR	HBRT	0.70	1.81	3.28	1.18	9	FERT	0.56	2.26	5.10	1.42	12
	SVR	FERT	0.82	1.39	1.92	0.49	15	HBRT	0.69	2.03	4.14	1.10	7
	RFR	FERT	0.88	1.18	1.40	0.58	14	HBRT	0.72	1.93	3.73	1.02	6
	ELM	FERT	0.70	1.84	3.39	1.20	15	HBRT	0.72	1.69	2.84	1.17	15
	MLP	FERT	0.80	2.62	6.87	1.54	15	FERT	0.58	1.65	2.73	0.94	15
DO													
	LR	HBRT	0.40	1.69	2.84	1.17	8	HBRT	0.37	1.75	3.07	1.25	8
	SVR	HBRT	0.44	1.64	2.68	1.06	6	HBRT	0.39	1.76	3.08	1.19	6
	RFR	HBRT	0.83	0.94	0.88	0.58	4	HBRT	0.56	1.55	2.39	0.99	4
	ELM	FERT	0.40	1.72	2.96	1.24	15	FERT	0.32	1.78	3.18	1.32	15
	MLP	HBRT	0.53	1.88	3.53	1.33	10	FERT	0.37	1.69	2.86	1.19	10
PTOT													
	LR	HBRT	0.52	0.25	0.06	0.14	9	HB	0.22	0.43	0.18	0.17	6
	SVR	HBRT	0.79	0.17	0.03	0.05	9	HBRT	0.47	0.26	0.07	0.11	9
	RFR	FERT	0.84	0.15	0.02	0.05	14	FERT	0.56	0.24	0.06	0.09	14
	ELM	FERT	0.57	0.22	0.05	0.13	15	FE	0.41	0.27	0.07	0.16	11
	MLP	FERT	0.58	0.31	0.09	0.14	15	FERT	0.40	0.25	0.06	0.10	15
NO3-N													
	LR	HBRT	0.30	4.66	21.71	0.30	2	FERT	0.03	37.25	1387.90	6.07	1
	SVR	HBRT	0.82	2.48	6.17	0.94	9	FERT	0.42	26.32	692.88	2.96	14
	RFR	HBRT	0.78	2.64	6.98	0.77	2	FERT	-1.52	26.86	721.55	3.19	1
	ELM	FERT	0.42	14.57	212.43	6.58	15	HBRT	0.43	31.31	980.11	6.96	15
	MLP	FE	0.05	4.94	24.40	2.61	11	FE	0.21	25.99	675.47	3.93	11
BOD													
	LR	HB	0.56	7.33	53.80	4.96	5	HB	0.32	10.08	101.54	6.00	5
	SVR	HBRT	0.71	6.01	36.15	2.58	9	FERT	0.41	10.55	111.33	5.68	14
	RFR	HBRT	0.87	4.21	17.72	2.17	7	HBRT	0.56	9.44	89.12	4.74	7
	ELM	FERT	0.42	9.95	98.96	6.16	15	FERT	0.65	7.41	54.96	5.12	15
	MLP	HB	0.57	9.67	93.51	7.09	6	HBRT	0.39	9.19	84.44	5.33	10
COD													
	LR	HBRT	0.52	19.21	368.94	12.45	8	HBRT	0.48	21.11	445.72	13.34	8
	SVR	FERT	0.64	17.86	319.10	8.47	15	HBRT	0.40	20.21	408.63	12.20	6
	RFR	HBRT	0.83	11.75	138.15	6.07	8	HBRT	0.54	17.94	321.67	10.56	8
	ELM	FERT	0.38	22.15	490.49	13.92	15	FERT	0.57	16.83	283.16	11.95	15
	MLP	HBRT	0.39	31.23	975.36	15.72	10	HBRT	0.21	20.09	403.41	13.39	10

At this point, the main metrics for model performance were R^2, RMSE, MSE, MAE and the number of features utilized to reach optimal error performance in the test phase ($\#Feat$). We compared these metrics in a comprehensive evaluation to determine the best model for each parameter. The five algorithms (LR, SVR, RFR, ELM and MLP) were trained using the best dataset determined in Table 6.8 to calibrate each model in its best conditions. The results of this evaluation are displayed in radial graphs in Figure 6.5.

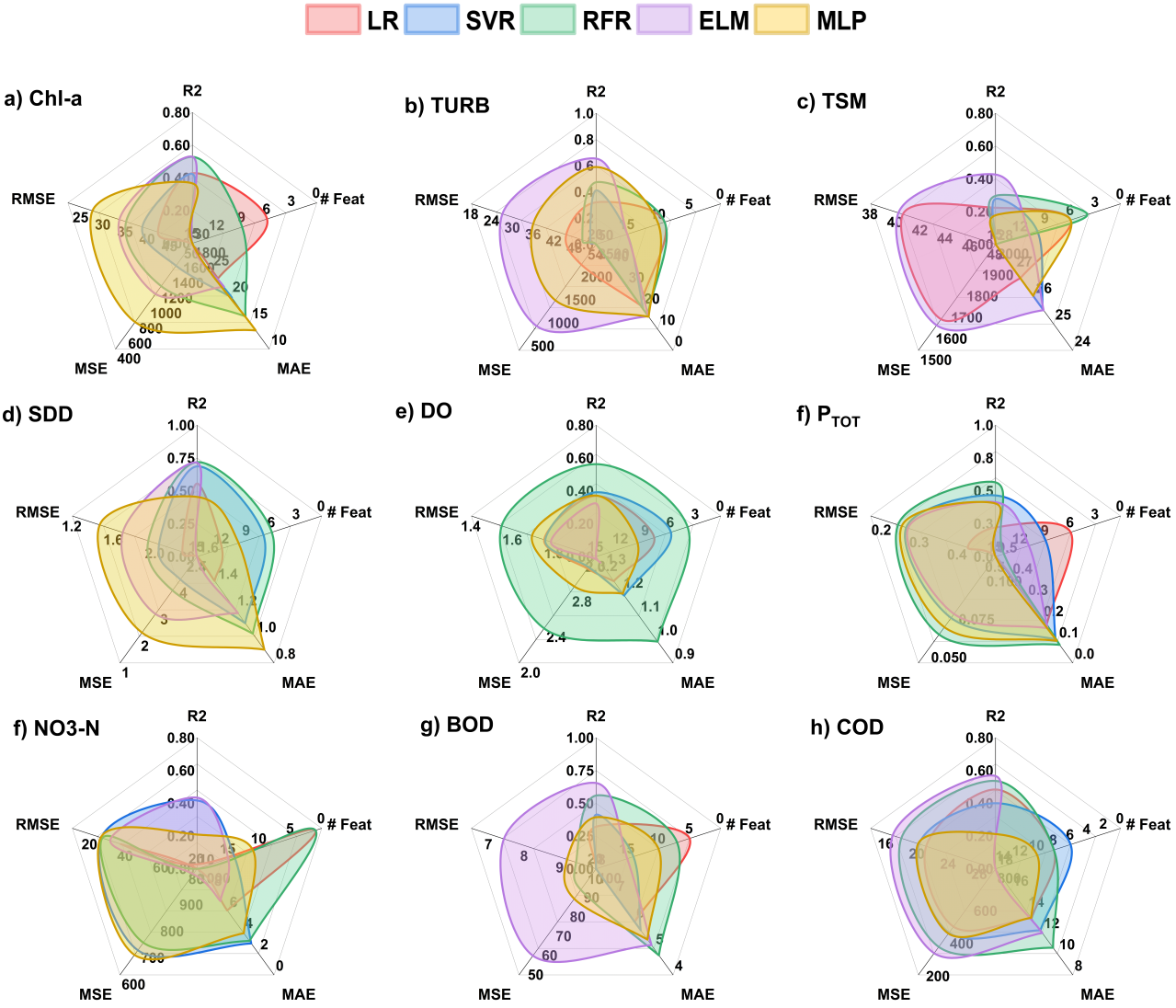

Figure 6.5: Comprehensive evaluation of tested algorithms based on the relevant error metrics for optimal performance. The algorithms use the best source dataset in all cases.

In general ELM and RFR resulted in the best models which outperformed the rest of the machine learning techniques for the majority of the water parameters (Chl-a, TURB, TSM, SDD, PTOT, BOD and COD) from a comprehensive perspective. SVR performed better for the challenging NO3-N respectively.

Scatter plots of target parameters using the models calibrated with the best corresponding dataset are shown in Figure 6.6 for both Train and Test datasets. From the scatterplots is visible that TSM, NO3-N and in lesser degree TSM were the most challenging parameter to model and that SDD was able to be modelled with high accuracy by the ELM ($R^2 = 0.72$) as seen in the performance in terms of error metrics in Table 6.8.

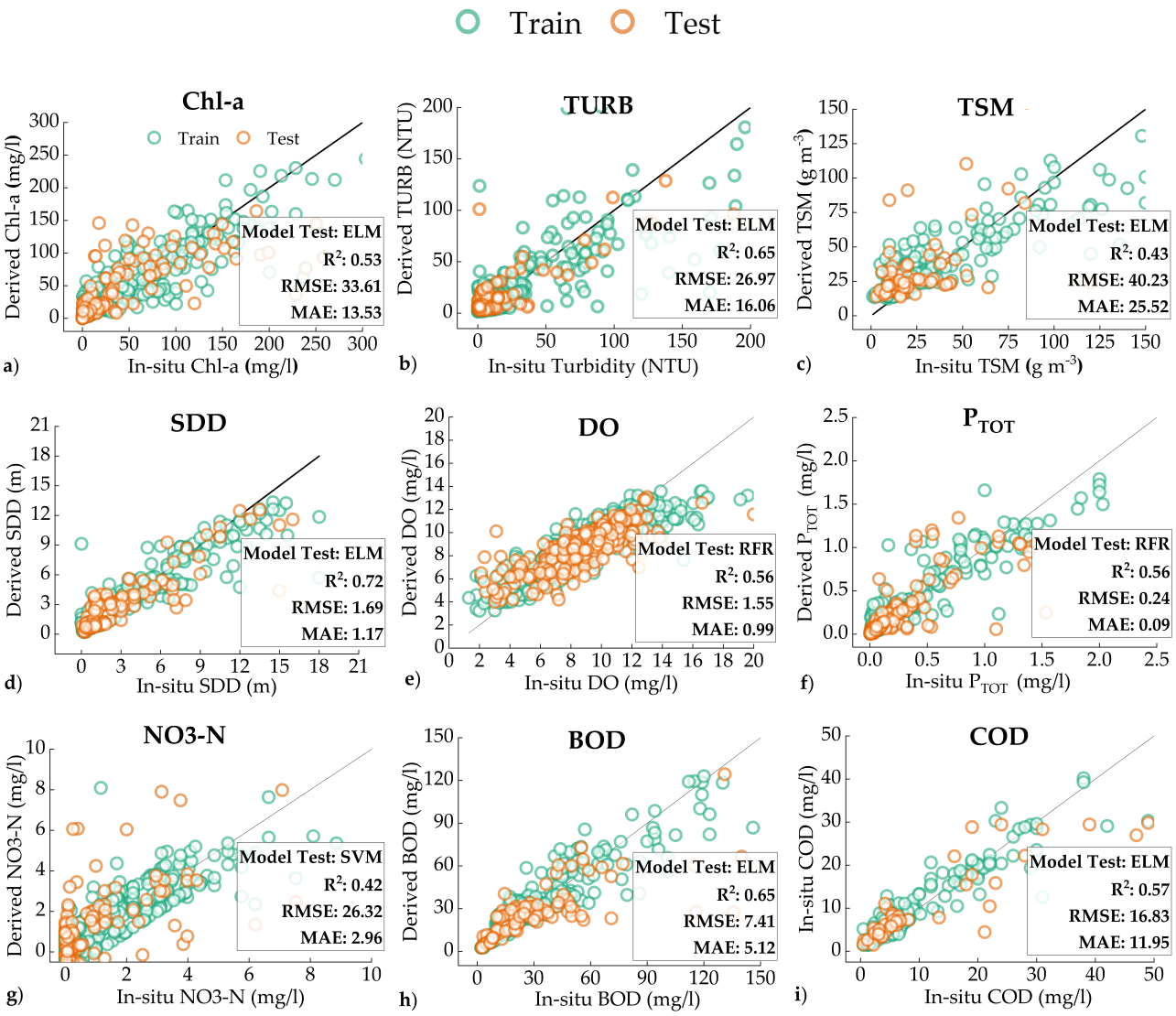

Figure 6.6: Scatterplots of modelled and measured water quality parameters in the test datasetcases.

The results also showed that the big majority of the models for all the water parameters performed better when using any of the two datasets aware of region and time (HBRT and FERT). Therefore, a deeper analysis was performed in this direction by comparing the R^2 of each dataset and the performance of each model when trained with different datasets.

Figure 6.7 shows the average R^2 for the complete modeling process, which includes not only the best results summarized in Table 6.8 but the rest of the models as well. Figure 6.7a stress how the performance of both HBRT and FERT is superior to HB and FE for train and test evaluations. Similarly, Figure 6.7b, shows the performance of the algorithms, when using different datasets. When trained with HBRT or FERT datasets (Figure 6.7a, red lines; Figure 6.7b increased tendency from left to right), all the algorithms reached always higher correlations than when trained with HB or FE (Figure 6.7a, blue lines; Figure 6.7b decreasing tendency from right to left).

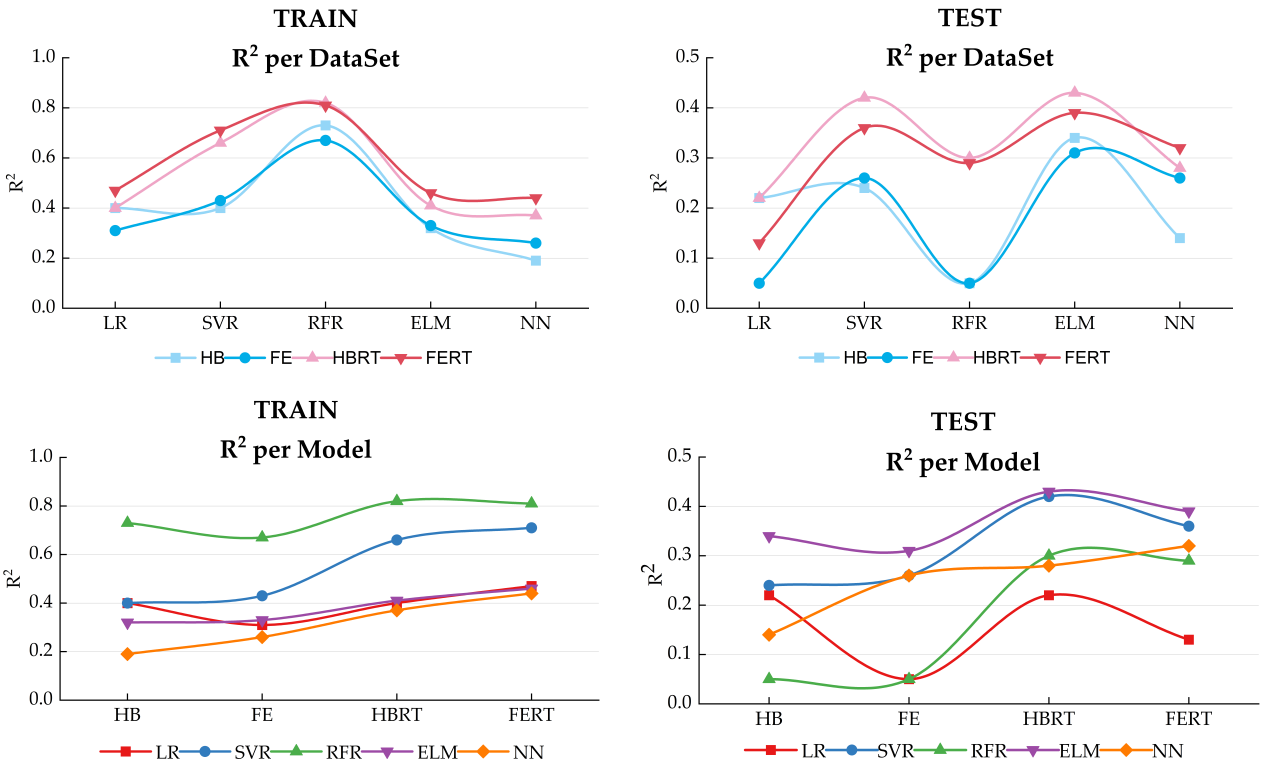

Figure 6.7: Train and Test average R^2 for each algorithm and dataset.

6.3.3 Model capabilities

To stage model capabilities, we apply the methodology using Harmonized products for the period March 2021 - March 2022 to estimate time series of specific parameters (Chl-a, DO and SDD) and to model their variations throughout a year. The points marked in the evolution of the targets were used as a suitable date and to map spatial distribution. We selected different lakes around the world to test the transferability of the models. Specifically, Lake Tahoe (US, https://goo.gl/maps/AZrmNJAhjUALMRfv8), Lake Trasimeno (Italy, https://goo.gl/maps/1LDUMqYyxMEJPrHG7) and Lake Vichuquen (Chile, https://goo.gl/maps/zoarjSNAqee8LATU6) were selected for Chl-a, DO and SDD respectively based on field data availability. Time series and parameter maps are shown in Figure 6.8. Chl-a in Lake Tahoe shows concentrations between 5 - 10 ug/L for most of the year, but after a breaking point in December 2021, where the concentration reached its highest level above 20 ug/L, it gradually decreased and kept a range between (10 - 15 ug/L). DO shows low variability during the year, and it is in a range of 8.8 - 9.5 mg/L in Lake Vichuquen.

The lowest concentration is reached by the end of November 2021, from which it starts a recovery to higher concentrations above 9 mg/L. March, April and mid-May seem to be the months of higher availability of DO in the area. The spatial resolution of 30 m from the Harmonized products allows adequate visualization of the distribution of DO even in a relatively small lake as Vichuquen (40 km^2). From the map, it is visible that DO availability is higher in the outlet and inlets, located at north and south respectively, likely cause by the turbulence and stirring of the incoming and leaving water flows. SDD in Lake Trasimeno ranges in average from 1 to 4 m during the year. The lowest transparency is seen after August 2021 ($\approx$ 1 m) and remains in this range until its recovery in January 2022 of 2.5 m. The breaking point in August is selected as the date of interest for a spatial visualization (2021.08.31). The surface distribution of SDD reveals a big cluster of lower transparency in the northwest part of the lake. The south part, which is an open bay, remains clearer.

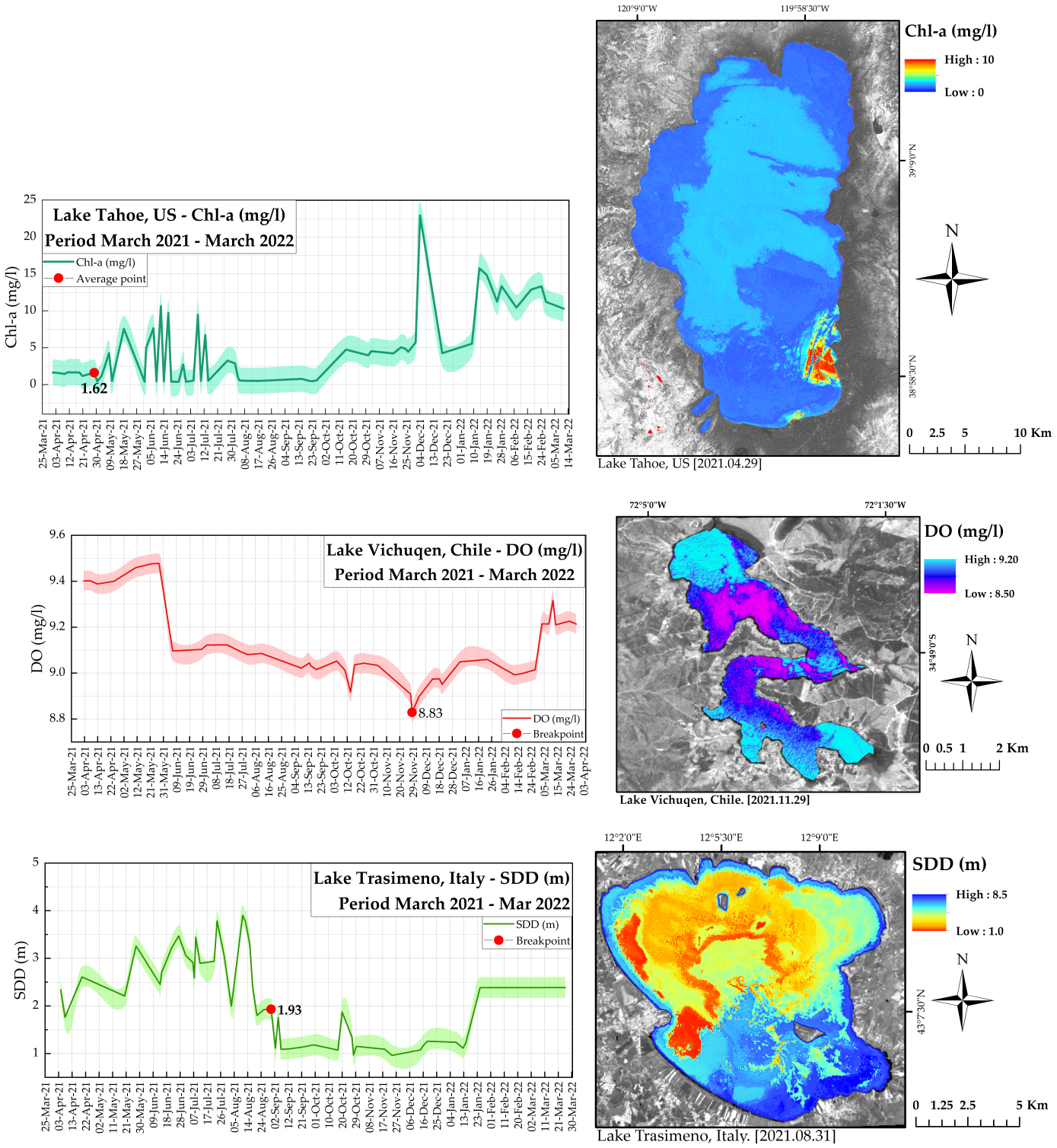

Figure 6.8: Time series and spatial distribution of a) Chl-a in Lake Tahoe (US, 2021.11.29), b) DO in Lake Vichuquen (Chile, 2021.11.29) and c) SDD for Lake Trasimeno (Italy, 2021.08.31). Background image: Harmonized Red band in greyscale.

6.3.4 Correlation between OAC and nOAC

For the specific case of nOAC (DO, NO3-N, PTOT, BOD, COD), their estimation resulted in a challenging approach as seen in the results of Table 6.8, Figure 6.5 and Figure 6.6. For NO3-N only SVR was able to produce reasonable results ($R^2 = 0.42$). To further evaluate the possibility of estimating nOAC using indirect means, a correlation analysis between OAC and nOAC was performed and is displayed in Figure 6.9.

Similarly to Figure 6.3, each node of the Chor diagram shows the sum of absolute values of Pearsons' correlation. Separate individual nodes are available in the supplementary material. From the results, no significant correlations between OAC and nOAC were retrieved, as seen in the total absolute value of the nodes in Figure 6.9, which barely overpass $r \approx 0.20$ for SDD (Figure 6.9a), BOD (Figure 6.9b) and TSM (Figure 6.9c). These results stress the difficulty of estimating nOAC from indirect methods which could rely on relevant correlations with OAC that can be computed via remote sensing.

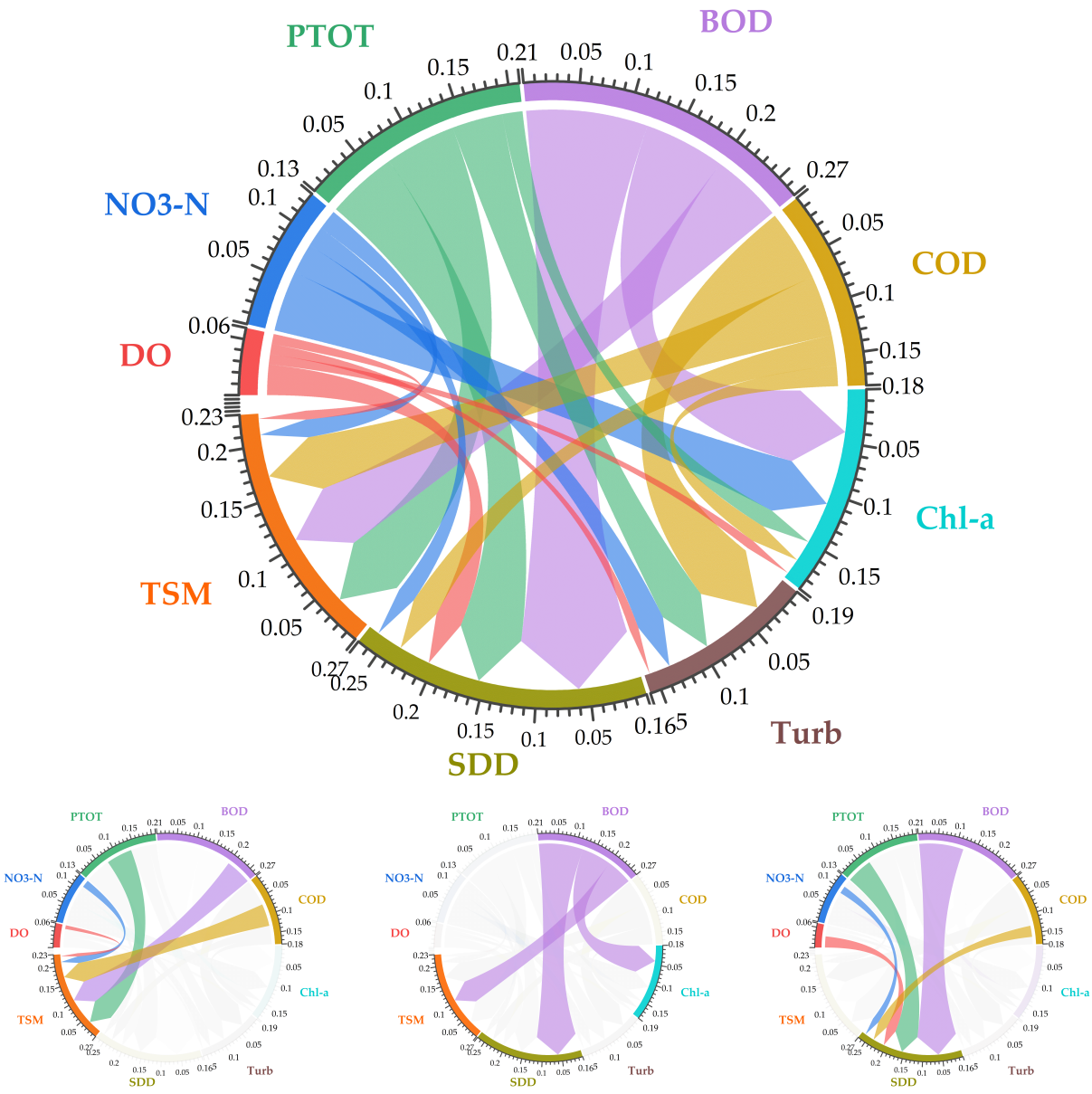

Figure 6.9: Sum and individual correlations of the OAC with nOAC.

6.4 Discussions

6.4.1 Global Water Quality Data Availability

The availability of water quality data at a global scale that can be used in synergy with remote sensing data is still very limited. In this study, the raw gathered data was filtered substantially and went from initial 300,000 measurements of all the parameters around the globe to a final dataset of around 7,000 samples after data selection. This is still an important amount of data in comparison with the available data in previous years or other studies of water quality in inland waters (Bonansea et al., 2015; Ruescas et al., 2018; Blix et al., 2018; Delgado et al., 2018; Arias-Rodriguez et al., 2021). However, it cannot be denied that the water availability at a global level is limited by several factors that can be improved based on the inter-cooperation of different instances and technical issues. For example, measuring stations at the global level are limited to certain areas around the world. In this work, we notice a lack of water information for large parts of the planet, particularly in South America, Africa and Asia. As exposed on Section 2, the study of Thorslund and van Vliet (Thorslund & van Vliet, 2020) indicates that most of the measuring water stations for lakes and reservoirs were located in North America (with big difference) and Europe. This exposes how a very important amount of inland waters are not being monitored. Additionally, the integration of global data is constrained by the fact that every nation is responsible for the technical requirements of water monitoring and making data publicly. Therefore, it is likely that already monitored data from several regions in the world is not yet available to a greater extent due limitations in this direction, and therefore its usage may be missed for global applications. In worse cases gathering global data could even be limited by trifling facts as ignorance of foreign languages. Thus, international cooperation is then needed to team-work on data availability. In this sense, initiatives as the Global Freshwater Quality Database (GEMStat) from the UN Environmental Programme (UNEP, 2016) offers an adequate framework for the previously mentioned challenges.

6.4.2 Harmonized remote sensing data for water quality estimation

Additionally to field data availability, remote sensing also has important limitations to model in full potential water quality at the global scale. For instance, temporal resolution limits the coupling of spectral and field data. In this study, we addressed this limitation up to a certain degree by harmonizing Landsat-8 and Sentinel-2 data, which increased data availability. This allowed to use coupled satellite data in a singular dataset, which was one the main objective of this study. However, the current harmonization process is not specifically designed for inland waters. Similarly, the atmospheric correction used in (Nguyen et al., 2020), the Second Simulation of the Satellite Signal in the Solar Spectrum (6S) is also not designed for waterbodies, as it occurs with other corrections designed for inland waters as C2RCC. Therefore, the results based on this methodology should be taken with caution since discrepancies from a harmonization process and an atmospheric correction for different applications than water quality retrievals are likely to exist.

The main reason this study applied these methodologies was the existing implementation in the cloud platform used for image processing. There is no current harmonization process or atmospheric correction developed for cloud computing in GEE that is design for to enhance the spectral characteristics of water surfaces and to work with the entire collections of Landsat and Sentinel satellites was not feasible using local computational resources. To develop both a harmonization procedures and an atmospheric correction for the cloud platform was out of the objectives of this research. However, the harmonization procedure is still in development and it is likely to account for water surface characteristics in the future (NASA, 2022). Likewise, the 6S atmospheric correction is a common procedure in remote sensing and it has already been implemented in mapping and water quality monitoring (Kwong, Wong, & Fung, 2022). Adopting the above describe methodology allowed to build a global dataset for model development and contribute to understand until which extend machine learning can benefit from increased data availability. Nevertheless, non-coupled satellite acquisitions and dates of water measurements was one of the main filters that avoided the usage of a great portion of the gathered data. The spatial resolution also constrains availability when the resolution is not enough to retrieve enough pixels from very small reservoirs. The pixel size of Harmonized data is 30 x 30 m, which allows consideration of a big amount

of lakes and reservoirs. However, it may not be the best resolution for inland waters below surfaces of 20 km^2 due to possible errors caused by bottom reflection and adjacency errors caused by land next to shores. Therefore the revisit time of harmonized data (3 days), even when it may be considered adequate in the field, is probably not good enough to monitor changes in water parameters that could exhibit great variations even during one single day and to account for great part of the available field data as seen in this study. Therefore, the tendency to improve temporal and spatial resolutions is highly important, as some ground-based high-frequency sensors already demonstrate (Castrillo & García, 2020).

6.4.3 Machine learning models and cloud computing

ML models provide research in water quality the possibility to model and estimate different water parameters with a high degree of accuracy based on adequate data availability (Niroumand-Jadidi, Bovolo, & Bruzzone, 2020; Y. Zhang et al., 2020, 2021). Also, the variety and distinct nature of available ML algorithms for modeling purposes foster rigorous evaluation of the methodology and contribute to reaching stronger and more developed models (Peterson et al., 2020; Sagan et al., 2020). In this study, we focused on the "learning" advantage of ML models and tried to provide as much data as possible by means of global measurements and remote sensing data fusion techniques, with the goal of reaching robust models that could retrieve water quality parameters accurately. As in previous research using ML approaches, we could develop models that predict water quality parameters with reasonable results. Furthermore, a key improvement in the direction of modeling at the global scale was achieved, which has been one of the main limitations of modeling water quality of inland waters (Matthews, 2011; Giardino et al., 2019) and that was only addressed before by bio-optical models with more complex approaches in terms of development (Giardino et al., 2019; Topp et al., 2020; Sagan et al., 2020). The extent of the regionalization modeling is precisely the advantage that ML models offer when providing enough and high-quality data. In this study we showed how the contribution of enough high-quality input data and adequate calibration of ML models could start pushing existing research barriers. In this sense, the potential for improvement of the ML models is still enormous, particularly with the progressive increment in data availability coming from more frequent field campaigns, better acquisition sensors and disclosure of non-public data. Therefore, modeling global water quality in inland waters should be considered as a continuous area of research and development with the goal to achieve models that improve continuously from constant monitoring. Besides the above-mentioned limitations, challenges regarding computational power and storage space existed. The large number of models to be tested plus even small calibration techniques resulted in extensive computing periods which could not be covered by our locally available hardware resources. Therefore, a cloud-computing platform (Google Colab) was required to address this problem and proceed with model evaluation. Cloud computing allows parallel computing while focusing cloud servers only for computational tasks. This methodology distributes more efficiently available resources and should be considered for similar tasks, especially when dealing with large datasets. Similarly, the usage of Google Earth Engine also allowed working efficiently with the vast quantity of remote sensing data product of the match ups with field measurements, and thanks to previous knowledge of state-of-the-art applications on the harmonizing process (Roy et al., 2016; Claverie et al., 2018; Poortinga et al., 2019; Nguyen et al., 2020; Peterson et al., 2020), these limitations were diminished.

The potential for global monitoring was already addressed by (Kravitz et al., 2020) with a synthetic dataset of top-of-atmosphere and bottom-of-atmosphere reflectances to comprise optical variability present in inland waters. Regarding field data measured on earth, and to the extent of the authors' knowledge, this is the first attempt to model water quality on a global scale using remote sensing data based on machine learning algorithms. Therefore, the comparison of the models developed here is complicated because, until the submission of this paper, there are no similar studies that attempt similar modeling scales. However, based on the well-established validation methodology applied, the reasonable performance of the models and its adequate application in time series and water quality maps, we convey our methodology is on the way to establishing a basis for future development in this research area. With the distances apart and for an exercise of comparison, the results here yielded were compared with novel publications that have successfully developed ML models for inland water quality. For example, error metrics of Chl-a ($R^2 = 0.53$), TURB ($R^2 = 0.65$) and DO ($R^2 = 0.56$) from ELM and RFR, are comparable with modeling results observed in (Sagan et al., 2020) Chl-a ($R^2 = 0.48$), TURB ($R^2 = 0.44$) and DO ($R^2 = 0.21$). In the other hand, PTOT ($R^2 = 0.56$), NO3-N ($R^2 = 0.42$), BOD ($R^2 = 0.65$) and COD ($R^2 = 0.57$) are comparable with the results of (Y. Zhang et al., 2020) Phosphorus ($R^2 = 0.94$),

Nitrogen ($R^2 = 0.95$), BOD ($R^2 = 0.91$) and COD ($R^2 = 0.95$) which were retrieved from hyperspectral images. Regarding the poor performance of the MLP, the strategy was to build neural nets deep and wide enough to first overfit the data and then reduce it through. However, this operation could not be totally completed due to a lack of dedicated GPUs (even in the Cloud server) and time constraints. Even in the best performing parameter (TURB), most of the MLP results were in the underfitting range, and train and test splits shown similar error metrics. These results may provide a clear picture of the behavior of a partially optimized MLP.

6.4.4 Estimation of OAC and nOAC

The estimation of OAC with remote sensing has been addressed extensively in research since for least two decades (Lathrop & Lillesand, 1989; Chacon-Torres et al., 1992; Pattiaratchi, Lavery, Wyllie, & Hick, 1994; Zilioli & Brivio, 1997; Kallio et al., 2001; P. Brezonik et al., 2005; F. Wang et al., 2006; Odermatt et al., 2008; Gómez, Alonso, & García, 2011; El-Din et al., 2013; Bonansea et al., 2015; Blix et al., 2018; Arias-Rodriguez et al., 2020; Y. Li et al., 2020). Particularly, parameters such as SDD, Turbidity or Chl-a and TSM have been studies with great detail, and their estimation has been the target of different modeling approaches, from empirical to semi-analytical models (Gower, 1980; Allee & Johnson, 1999; Kallio, Koponen, & Pulliainen, 2003; P. Brezonik et al., 2005; Han & Jordan, 2005; Turner, 2010; Alikas et al., 2010; Papoutsa et al., 2014; Palmer et al., 2015; Bi et al., 2018; Pereira et al., 2018; Delgado et al., 2018; Buma & Lee, 2020; Pahlevan et al., 2020). nOAC, however, represented a greater challenge because of its lack of response to absorption or scattering of the electromagnetic light (Giardino et al., 2019). A direct estimation of nOAC from RS data has been previously investigated. For example (X. Wang et al., 2010) used SVM and SPOT5 data for potassium permanganate index (CODmn), ammonia nitrogen (NH3-N), chemical oxygen demand (COD) and dissolved oxygen (DO) in Weihe River with better performance than the statistical regression. Recently, (Guo et al., 2021) used ML models for spatial distributions of the annual and monthly DO variability in Lake Huron from Landsat and MODIS data with consistent values of $R^2 = 0.88$. Similarly, (Y. Zhang et al., 2020) used a Bayesian probabilistic neural network to predict phosphorus, nitrogen, chemical oxygen demand (COD), biochemical oxygen demand (BOD), and chlorophyll a from hyperspectral images in a river from multispectral images. We compared the average R^2 summary of the OAC (Chl-a, TURB. TSM, SDD) and nOAC (DO, PTOT, NO3-N, BOD and COD) to contrast how the results also show that in general nOAC presents more challenges than OAC (Figure 6.10). All the models achieved higher results in OAC but at the same time nOAC results were reasonable and did not show an incapacity to model these parameters. This reinforces the fact that ML models are also suited to deal with parameters with no-liner relationships between remote sensing data or inherent lake characteristics, contributing to the improvement of modeling nOAC.

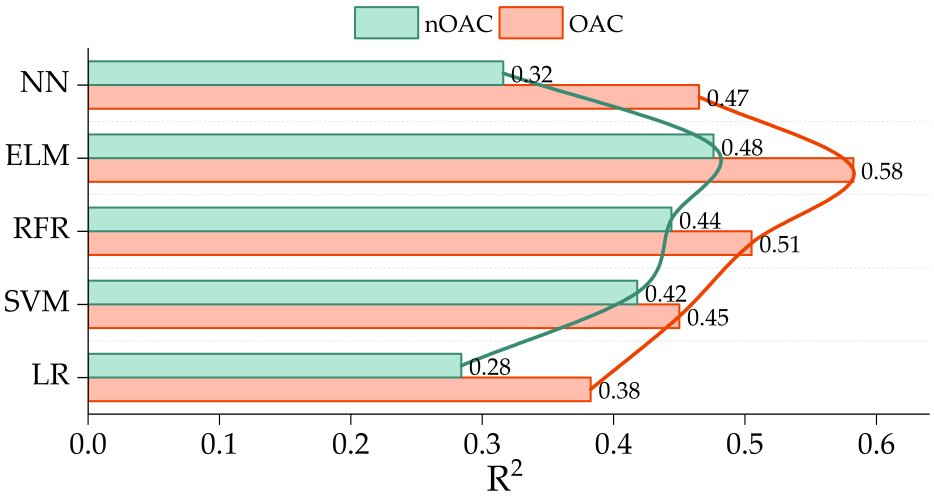

Figure 6.10: Average R^2 for all the models by the nature of the target parameters. OAC: Chl-a, TURB, TSM and SDD. nOAC: DO, PTOT, NO3-N, BOD and COD.

6.4.5 Inherent characteristics of lakes as model enhancers

Typically, semi-empirical models in the field of remote sensing of inland waters do rely on the physics knowledge of the optics in the water and how the response of water or water constituents' response to the interaction with the electromagnetic energy. One main objective of this study was to evaluate this conventional approach against more unconventional methodology that could rely more on the learning capability of the ML algorithms. On the basis that these algorithms work better with a higher number of observations and adequate predictors that explain better the behavior of the targets, we selected additional characteristics of each lake to evaluate possible improvements in comparison with purely radiometric remote sensing bands or band ratios already tested in previous literature. The cautious evaluation of the impact on model performance that the addition of these characteristics would have led to the creation of four different datasets: HB, FE, HBRT and FERT. Region and time were the selected characteristics added to the original datasets, the product of the remote sensing data. The correlation analysis revealed a moderate correlation with the water parameters for latitude and longitude and very weak correlations for Year and Month. Figure 6.11 stress this situation.

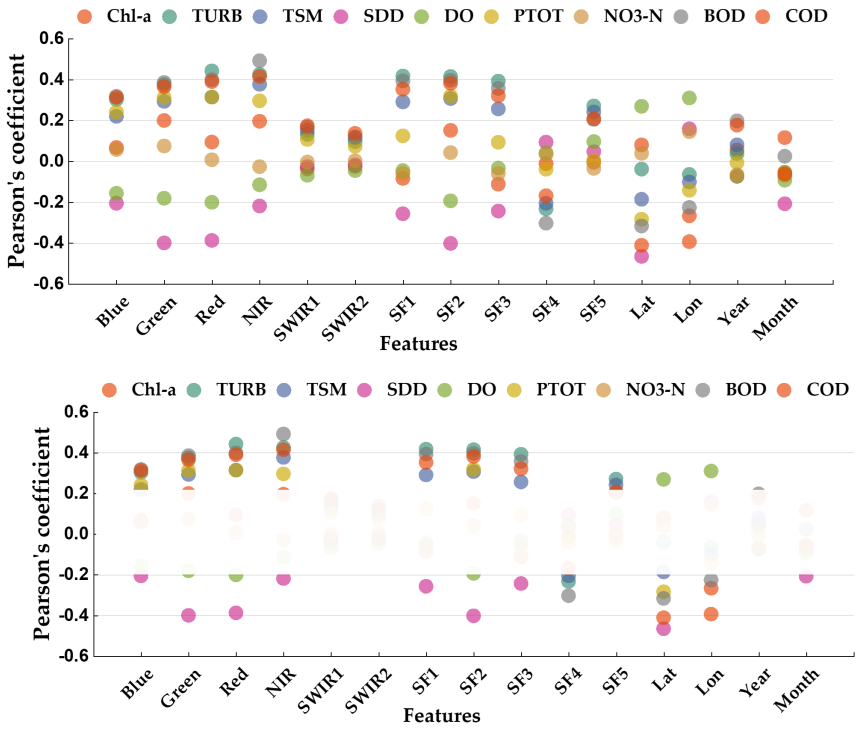

Figure 6.11: Individual correlation of each predictor with water quality parameters.

In Figure 6.11a it is seen how the visible bands and band ratios show a higher correlation, and how SWIR bands and Year and Month are in a very weak range as displayed in Figure 6.11b where the region $-0.20 < r < 0.20$ is covered to highlight stronger correlations. The occurrence that Lat and Lon are having a stronger correlation than Year and Month and therefore, a greater utility in model development could be due to the fact that Year and Month are not strictly inherent characteristics of a waterbody and its inclusion was mainly motivated because of the fact that the time and seasonality have an important influence on the behavior of certain water quality, like the blooming of algae or the arrival of storms that discharge waters with sediment creating turbidity. Nevertheless, the improvement in error metrics of all the water parameters when ML models used HB and FERT datasets was evident and validated in our methodology (Figure 6.12). This leads us to the conclusion that this approach resulted in an effective improvement of the modeling of water quality parameters by the addition of inherent lake characteristics that can be useful for ML algorithms.

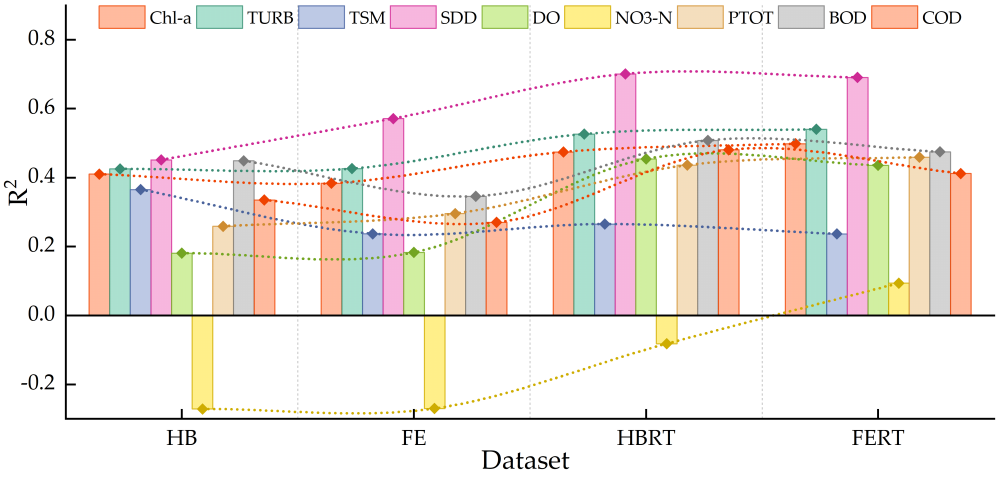

Figure 6.12: Improvement of temporally and spatially aware models. Increment in R^2 towards right is highlighted with the dot line.

Therefore, research in this direction is needed to keep the improvement of the modeling process and to develop more accurate models. There are several inherent characteristics that may be useful for such purposes and that can be found in constant patterns in time as trophic state, chemical, biological, physical, limnological or morphological features. Time features can be improved or added as labels for the season of the year as seen in (Guo et al., 2021).

6.5 Conclusions

This work developed machine learning models for water quality retrieval at a global scale using remote homogenized multimodal remote sensing data. This contributed to overcoming the present state of knowledge in which transferability of models is limited by the origin of field data and modeling water quality in inland waters at different locations was constrained. These findings directly impact the increment of our ability to analyze lakes and reservoirs globally, particularly for several water parameters of different nature and characteristics, which are key in the overall understanding of water quality in lakes and reservoirs. This work is limited by the amount and origin of the field data gathered and the extent of the remote sensing archives processed. The application of the models developed here was demonstrated at the global scale in different lakes separated by continental distances. However, the usage of these models in regions from where there was no data in the calibration process is likely to be poorly accurate and would lack reliability in results. Therefore, the methodology should be improved by gathering data from more and different sources around the world, particularly from the African, Asian and South American continents. Remote Sensing data can be increased by harmonizing data from older satellites, such as the Landsat constellation, and extending the current dataset. Thus, future work should focus on increasing the data availability of both Remote Sensing and global data in field, and incorporate the advances in remote sensing research as correction of adjacency errors and improvement of atmospheric correction.

Author Contributions: L.F.A.-R. conceived this study. U.F.T. conducted main data processing and analysis of the Harmonized RS data. U.F.T. and L.F.A.-R. conducted data processing and modeling analysis. L.F.A.-R wrote the original version of the manuscript. Constructive comments and improvements of the manuscript were provided by Z.D., J.H, Y.T. and M.D. through extensive discussion. All authors have read and agreed to the published version of the manuscript.

Funding: This article was accomplished with the financial support for research of the Mexican National Council for Science and Technology (CONACYT) and the Federal Department of Energy (SENER) through its funding "CONACYT-SENER Sustentabilidad Energetica". In addition, this work was supported by the German Research Foundation (DFG) and the Technical University of Munich (TUM) in

the framework of the Open Access Publishing Program.

Acknowledgments: The authors thank to all the national and international agencies and the personal involved in the acquisition of field water quality data around the world. They would also thank the Technical University of Munich (TUM) and its Graduate School (TUM-GS) for the institutional services and facilities necessary to perform this study. We also thank the ESA, NASA and USGS agencies for providing the necessary radiometric data and software to process it. Additionally, they acknowledge Marco Koerner from the TUM Chair of Remote Sensing Technology for valuable discussions about the methodology.

7 Conclusions and Outlook

7.1 Overall conclusions

The general goal of the dissertation is:

> *"The optimum utilization of remote sensing data and machine learning algorithms to develop predictive models that enhance temporal and spatial monitoring water quality in inland waters worldwide"*

To reach this objective, four research objectives have been pursued:

(i) Archived remote sensing imagery applied to the detection of hazard events using machine learning

(ii) Improve water quality monitoring systems by the integration of remote sensing and machine learning using the RNMCA data

(iii) Estimation of changes in water quality along the Danube River using Sentinel-2 data

(iv) Development of a global water quality and remote sensing dataset applied to worldwide water quality monitoring

Based on the work presented in this dissertation, the following conclusions can be drawn:

Conclusion 1: Heritage imagery is crucial to extend monitoring to a longer-term

The archived remote sensing data from the last decades is an unvaluable resource to contribute to understand the impact of outbreak events in inland waters. This was demonstrated by the usage of MERIS data when analyzing the Valle de Bravo reservoir (section 3). In similar applications for the same period of time (the first 10 years of the 2000's), it is likely MERIS data would be supporting wider monitoring studies.

This also apply for other sensors with extensive archives as MODIS and the Landsat constellation. Additionally, the utilization of these sensors is also beneficial for coupled applications with successor sensors, as current Landsat-8, Sentinel-2 and Sentinel-3.

Conclusion 2: Ready-to-use remote sensing water products are not fully developed for water quality monitoring in inland waters

Several ready-to-use remote sensing products are available for water quality monitoring. In remote sensing of inland waters, the standard products come from the Sentinel-3 OLCI sensor, the water full resolution products (WFR). Additionally, water products can be derived from the C2RCC atmospheric corrector for Sentinel-3 and Sentinel-2 MSI. However, the findings here demonstrated a substantial mismatch between OLCI WFR and field measurements for the data of the Mexican water quality monitoring system.

The main issues are overestimation of Chl-a and TSM. Additionally, spatial distribution of such parameters from ready-to-use images showed that patterns are difficult to detect as the water surface appears homogeneous in contrast with significant spatial variations identified in this research. (Figure 4.7). To have ready-to-use products is one of the end goals of monitoring water quality in inland waters. However, it has been demonstrated repeatedly that the available products lack high accuracy in comparison with acquired field measures around the world (Blix et al., 2018; Arias-Rodriguez et al., 2021; Hoyek, Arias-Rodriguez, & Perosa, 2022). Therefore, it would be precipitate to rely only on these products to monitor inland waters.

Conclusion 3: Integration of field and remote sensing data face inherent limitations

The difficulties found to use optical sensor and integrate it with field data from monitoring systems at this big scale are of diverse nature. The first factor is the limited field measurements, which for the study case presented are not extensive but also represent a typical case for an emerging country which has already an established monitoring water quality system. In other regions, the situation is unfortunately not better.

The situation is aggravated because it is necessary to find a matching image acquisitions from remote sensors and rejection of data for being too sparse in time occurs, in addition to the already limited field data. Since the acquisitions routines of the monitoring systems are independent of the satellite overpasses, this situation is unlikely to change. Additional constraints as limited measured stations, periodicity of field campaigns, lack of in-situ radiometric measurements for sensor validation, also exist. At end, this significantly reduces the available data for model developing.

There are several sensors with potential to support water quality monitoring tasks at national level. Even so, a deep analysis and evaluation of the most commonly used sensors (the OLI, OLCI, and MSI) emphasizes the difficulties to retrieve accurate estimations. The accuracy also varies depending on the parameter to estimate. Turbidity shows to be the most reliable water parameter to be estimated with remote sensing data and OLCI has the potential to monitor large water bodies (as MERIS was in the past) with relatively high accuracy due its higher temporal scale.

Conclusion 4: Developed methodology enables to monitor water quality changes in river at large spatial scale

The use of remote sensing and machine learning allows to detect variations in water quality in inland waters, particularly rivers, and relate these changes with the presence of river restoration measures. The study case that analyses water quality variations of the Danube River shows how the floodplains in the river have a favorable effect on water quality. In an annual scale, most areas downstream of active floodplains show better water quality than their corresponding upstream sections.

This supports the utilization of remote sensing and machine learning to support monitoring water quality for diverse applications, as the behavior in a continental river as the Danube River or the effect of floodplain restoration. Once again, the analysis of ready-to-use water products justified the development of locally trained models, that are better calibrated for the area of study.

Conclusion 5: Global water quality monitoring has its basis on data availability, both from field and remote sensing sources

A common source of the field water quality data comes from local water authorities, which manage the monitoring systems present in different countries. Such systems own the basis to reach the full potential for integration with remote sensing techniques.

As seen in section 6, this combination increases spatial and temporal analysis in a greater scale. But enough measurements and periodicity of field campaigns is not enough. Apart from the analysis of section 4, section 6 shows that measuring stations at the global level are limited to certain areas around the world, mostly the developed countries. There is an important lack of water information mainly in South America, Africa and Asia. Lack of data availability was described previously, however, the global application developed in this thesis shows how, in a greater scale, most of the available data worldwide do not match with remote sensing acquisitions. This causes that usable field measurements sink tremendously: only 7,000 out of 300,000 global water quality measurements were useful due this issue. Therefore, scheduled field campaigns paired with image acquisition are necessary for calibration, training, and validation of predictive models.

A partial solution to this issue is addressed in this thesis by harmonizing Landsat-8 and Sentinel-2 data, which increased data availability because the combined temporal resolution (3 days) of both sensors allows to consider more field measurements. Very small inland waters are unfortunately limited for potential monitoring. The spatial resolution also constrains data availability because pixels size may not be enough for small lakes and reservoirs. The resolution of harmonized data is 30 x 30 m but this may not be enough for accurate results for smaller surfaces of 20 km^2 because of bottom reflection and adjacency errors.

Conclusion 6: Machine learning applications have the potential for predicting accurately and timely water quality at the required level

Machine learning models allow to develop predictive models for water quality estimations with high accuracy. As seen in all the study cases in this thesis, this was useful to model spatial and temporal variations of water quality in very different levels of applicability. Additionally, the variety of existing algorithms contributes to find versatile models that can adapt to the needs that specific datasets can pose. Furthermore, the election one particular model over others based on error metrics ensures that the most accurate and adaptative (generalizable) model is selected and used for multi-temporal or spatial upscaling applications. The learning capacity of this models is perhaps the most useful feature because it stands the possibility to escalate applicability to many levels.

As seen in the history of this dissertation, machine learning algorithms performed reasonably good when the adequate conditions of enough data supplied and training time were met. This performance was in most cases overcoming conventional linear regression results. This leads to the understanding that based on an adequate data input for calibration, reliable predictions can be obtained. Therefore, it is crucial to overcome challenges in field data availability and remote sensing data fusion. Machine learning algorithms perhaps have reached a point in which the models can fit well to training data, but without an adequate number of samples to learn from or enough time for calibration, the key ability to generalize in unseen predictions will not be fully developed. This was evident in the usage of the NN in (section 6), where neural networks overfit to the calibration data. A contribution for water quality monitoring at global scale was achieved. But to fully develop this potential, it is necessary to feed machine learning models with a far greater number of high-quality observations as inputs, both in quantity and quality from both field and sensor sources.

One of the main contributions of this thesis shows how machine learning models can generalize its predictions for a variety of inland waters around the world, providing quality data.

This pushes the limits of water quality monitoring beyond the former state and allows to focus on more compelling issues as data availability. Additionally, cloud computing stands as the most adequate approach to undertake modeling in remote sensing of inland waters. The immense quantity of remote sensing data challenges singular computer equipment and storage of entire collection of imagery is only possible online. At the same time, calibration and validation of large datasets is often not only timely efficient when processing online. Therefore, the potential for improvement of the machine learning models for water monitoring is still vast because they will learn and generalize better when we are capable to coordinate an adequate management of the field data necessary for their learning capacity.

7.2 Outlook

Based on the current status of remote sensing of inland waters presented in this work, further research topics are summarized and mainly concern:

(i) Field data accessibility

(ii) Remote sensing data fusion

(iii) Atmospheric correction and adjacency error

(iv) Understanding of the nOAC spectral properties

(v) Improved machine learning modeling for water quality modeling

7.2.1 Field data accessibility

Comprehensive and large datasets that adequately represent water quality at global scale, paired with remote sensing data is imperative to fully reach the potential of machine learning. This data scarcity impedes further development of research in the field and obligate scientist to focus also on data gathering instead of methodology improvement. This can be partially solved by making more of the existing data publicly available and shared in the adequate forums for utilization by researchers.

Additionally quality data is also necessary because models acquire the ability to learn not only from large but also representative and varied datasets that contain heterogeneity of water quality measurements. Ensuring this is only partially cover by conscious validation tasks. Also, creation and usage of synthetic data to train machine learning models is a potential resource to solve data scarcity and improve model calibration.

7.2.2 Remote sensing data fusion

Data fusion of the most adequate sensors for water quality monitoring was used in this thesis as a key resource for global water quality estimations. Landsat-8 and Sentinel-2 present the adequate characteristics to be subject of a harmonization methodology that enables the simultaneous use in single applications.

Future sensors to be launched or in design can therefore be able to be included in the harmonization routines, continuing with the expanded temporal coverage that homogenization brings. Additionally, this resource may be investigated as well to use former sensors still in operation or archived imagery.

7.2.3 Atmospheric correction and adjacency errors

Effects of sun glint in water surface and scattering in atmospheric constituents (Giardino et al., 2019) can considerably modify the spectral response of water surface, which can lead to errors in the modeling process due to incorrect spectral signal and therefore, an incorrect establishment of the relationship between radiometric and field data. Unfortunately, there is no standard method to treat remote sensing images to produce specifically water leaving reflectance. Additionally, the surface surrounding the water surface also affects the signal captured by the sensors since the radiance captured in the near-infrared bands can increase up to 50% (Odermatt et al., 2008), leading again to inadequately develop model relationships when using this spectral region.

Research already developed these challenge is known since decades and even when there are several atmospheric and adjacency correction methods (Sagan et al., 2020), an agreement for a standard procedure is necessary (Giardino et al., 2019; Sagan et al., 2020; Topp et al., 2020) to increase reliability in correction and increase comparability of diverse studies which until now may be using different correction methods.

7.2.4 Spectral characteristics of nOAC

As not all water quality parameters respond similarly to the electromagnetic radiation, the most challenging parameters, the non-optically active parameters such as nutrients, pathogens or other biochemical parameters should be subject of dedicated research to improve their modeling and estimation from remote sensing data. The study of these parameters may follow a similar path as followed with other water constituents, as chlorophyll-a, where specific algorithms were developed for this parameter based on its spectral response.

The spectral signature which describes the shape and wavelengths in which reflectance behaves may be key for this research, particularly if a correlation with other important optically active parameters directly derived as chlorophyll-a or suspended matter and develop indirect methods for nOAC estimation. This may be a challenging task that can take years in research to develop, however, the path is set in current research (Sagan et al., 2020).

7.2.5 Improved machine learning modeling for water quality modeling

The great limitation of data availability in the field of remote sensing of inland waters may still take time to be fully covered and applications can completely rely on ready-to-use datasets for water estimations. The field of machine learning has demonstrated to be adaptative and versatile when facing diverse types of challenges in modeling development. The many algorithm architectures available often offer an adequate modeling methodology depending on the specific application.

These needs may lead to the development of machine learning methodologies that can perform reliable with low number of observations, relying mainly in the quality of the input data rather than the quantity. Quality of data may be developed based on different methodologies, for example, this thesis successfully used additional non-radiometric features for water quality estimation, which increased considerable the performance of the machine learning models. Other features should be tested for its usage as water predictors. Different characteristics can have in greater or lesser degree a direct or indirect relationship with water quality as trophic state, chemical, biological, physical, limnological or morphological features, and act therefore as improvers of developed models in absence of field measures of remote sensing matchups. As the case of Chl-a and TSS (Sagan et al., 2020).

Machine learning applications, and in particular deep learning methodologies, often require substantial computational resources and consume large amounts of time for training and testing. Additionally, remote sensing images often require high volume capacity. Conventional computational resources, as desktop or notebook computers are often unable to tackle this tasks. Therefore, it is crucial that future applications are developed on cloud-based platforms that enable online data processing, modeling and data storage.

Nowadays, Google with Colab or Earth Engine, and Amazon with Amazon Web Services platforms offer remote sensing catalogs of satellite imagery available online, a valuable resource to optimize applications for water quality monitoring. Additionally, incorporation of machine learning implementations on these platforms and atmospheric correction is a need to be developed for a fully usage of cloud computing.

7.3 Final remarks

The findings from this dissertation indicate the general applicability of remote sensing data in combination with field water quality measured in estimation of water quality from local to global purposes. Machine learning models proved effective in estimating dynamics over a wide range of water quality parameters, exhibiting reasonable accuracy mainly in prediction of optically active constituents. However, results indicate that developed models still have potential to improve accuracy in estimations of non-optically active water constituents. Since machine learning performance generally relies on data availability, a reasonable solution can be approached by homogenization of spectral data fusion from multiple sensors and feature engineering that includes additional predictors to improve quality of available datasets.

Future research should focus on gather field data from missing regions and investigate the performance of machine learning models, particularly deep learning when extensive datasets are available. Finally, since data scarcity is still likely to be a challenge in the near future, the generation of synthetic datasets and features improving dataset quality for a better model performance should be considered further to allow a better assessment of the challenges in remote sensing of inland waters.

8 Supplementary Material

Additional figures and tables are provided here as supporting material.

8.1 Supplementary Tables

Table ST1: Descriptive statistics of the RNMCA dataset used in section 3. Units are: Chl-a: mg/m3, TURB:NTU, TSM: mg/L, SDD:m

Lake	Stations	Parameter	Count	Mean	St.Dev.	Min	25%	50%	75%	Max
Chapala	26	Chl-a	307	8.3	21.7	0.0	0.1	0.9	8.3	218.4
		Turbidity	387	36.2	51.1	0.3	18.0	24.0	34.0	750.0
		TSM	388	49.5	61.4	10.0	18.0	30.1	52.0	475.0
		SDD	388	0.4	0.2	0.1	0.3	0.4	0.5	2.3
Cuitzeo	9	Chl-a	116	35.7	41.7	0.1	8.0	20.3	50.3	247.5
		Turbidity	120	181.4	191.5	2.5	52.8	122.5	238.5	1176.0
		TSM	118	152.4	159.9	10.0	56.3	96.5	170.0	790
		SDD	121	0.1	0.1	0.0	0.1	0.1	0.2	0.7
Patzcuaro	17	Chl-a	266	27.3	39.9	0.4	7.6	15.8	26.2	395.4
		Turbidity	268	92.2	43.6	4.5	62.2	87.3	115.2	302.7
		TSM	268	47.6	36.1	6.0	20.0	38.5	64.0	250.0
		SDD	268	0.2	0.1	0.0	0.2	0.2	0.2	0.5
Yuriria	6	Chl-a	75	21.4	20.5	0.1	7.3	13.5	30.7	91.3
		Turbidity	76	92.3	45.6	26.4	65.9	82.5	115.6	262.7
		TSM	76	65.3	69.7	8.0	21.5	41.0	73.3	330.0
		SDD	76	0.2	0.1	0.1	0.2	0.2	0.2	0.5
Catemaco	4	Chl-a	57	26.1	62.8	0.0	0.1	10.1	28.3	345.8
		Turbidity	58	4.9	4.2	1.0	3.1	3.8	5.1	31.3
		TSM	58	17.4	14.8	10.0	10.0	12.5	17.5	90.0
		SDD	57	0.8	1.3	0.2	0.5	0.6	0.8	10.0

Table ST2: Summary of the MERIS bands used used in section 3

OLI	b1	b2	b3	b4	b5	b6	b7					
Wavelenght (nm)	0.43-0.45	0.45-0.51	0.53-0.59	0.64-0.67	0.85-0.88	1.57-1.65	2.11-2.29					
Resolution (m)	30	30	30	30	30	30	30					
OLCI	Oa01	Oa02	Oa03	Oa04	Oa05	Oa06	Oa07	Oa08	Oa09	Oa10	Oa11	Oa12
Center(nm)	400	415.5	442.5	490	510	560	620	665	673.75	681.25	708.75	753.75
Resolution (m)	300	300	300	300	300	300	300	300	300	300	300	300
MSI	b1	b2	b3	b4	b5	b6	b7	b8	b8a			
Center(nm)	442.7	492.4	559.8	664.6	704.1	740.5	782.8	832.8	864.7			
Resolution (m)	60	10	10	10	20	20	20	10	20			

Table ST3: Matching satellite acquisitions and RNMCA sampling dates used in section 3

Sensor	**Lake**	**Matching Images**	**Total**
OLI	Chapala	13	
	Cuitzeo	11	
	Patzcuaro	4	
	Yuriria	4	
	Catemaco	9	41
OLCI	Chapala	12	
	Cuitzeo	13	
	Patzcuaro	6	
	Yuriria	9	
	Catemaco	7	47
SMI	Chapala	10	
	Cuitzeo	4	
	Patzcuaro	5	
	Yuriria	9	
	Catemaco	3	31

Table ST4: OLI Model validation and predictive capability results for all datasets including coefficient of determination (R^2), root mean square error (RMSE), mean absolute error (MAE), and the number of samples (n) used in section 3.

Sensor	Lake	Parameter	Model	Hyperparameters	Bands	R^2	RMSE	MAE	n
OLI	Chapala	Chl-a	ELM	af=hardlims hn=10,000	All	0.38	4.63	3.22	100
		Turbidity	LR	-	b2,b4,b5,b6	0.66	20.17	8.80	154
		TSM	ELM	af=hardlims hn=10,000	All	0.21	417.07	115.89	154
		SDD	SVR	C=100, y=0.01 k = sigmoid	logb1, logb2 log b4, logb5 logb6, logb7	0.3	0.11	0.08	154
	Cuitzeo	Chl-a	ELM	af = hardlim hn=10,000	All	0.13	34.55	20.38	22
		Turbidity	LR	-	b2, b5, b6, b7	0.74	97.64	64.38	22
		TSM	ELM	af=hardlims hn=15,000	All	0.91	60.86	41.18	14
		SDD	SVR	C=10, y=5	logb4,logb5 logb6, logb7	0.41	0.1	0.06	33
	Patzcuaro	Chl-a	ELM	af=hardlims hn=1000	All	0.14	34.98	25.43	43
		Turbidity	SVR	C=500 y=5	All	0.56	27.75	19.21	43
		TSM	SVR	C=1000 y=500	b2,b4	0.38	19.9	14.85	43
		SDD	SVR	C=0.5 y=500	b3,b4,b5	0.42	0.04	0.03	43
	Yuriria	Chl-a	ELM	af=hardlims hn=5,000	All	0.11	15.88	12.56	16
		Turbidity	LR	-	b1, b3, b5, b7	0.32	21.42	18.23	16
		TSM	SVR	C=0.5, y=1 k=linear	logb5	0.19	20.83	15.73	16
		SDD	LR	-	b1, b4	0.22	0.046	0.031	16
	Catemaco	Chl-a	ELM	af=hardlim hn=10000	All	0.15	9.90	7.47	18
		Turbidity	ELM	af=hardlims hn=10000	All	0.12	9.16	5.91	18
		TSM	ELM	af=hardlim hn=8000	All	0.42	17.87	14.20	16
		SDD	ELM	af=hardlims hn=100	All	0.40	0.09	0.07	16

Table ST5: OLCI Model validation and predictive capability results for all datasets including coefficient of determination (R^2), root mean square error (RMSE), mean absolute error (MAE), and the number of samples (n) used in section 3.

Sensor	Lake	Parameter	Model	Hyperparameters	Bands	R^2	RMSE	MAE	n
OLCI	Chapala	Chl-a	ELM	af=hardlims hn=500	All	0.25	3.07	1.92	77
		Turbidity	ELM	af=hardlims hn=500	-	0.67	6.08	4.47	72
		TSM	ELM	af=hardlims hn=500	All	0.20	14.47	9.63	74
		SDD	SVR	C=10, y=0.1 k=sigmoid	b8	0.67	0.06	0.05	77
	Cuitzeo	Chl-a	ELM	af=purelin hn=10	All	0.47	59.94	16.20	20
		Turbidity	ELM	af=harlim hn=10,000	All	0.82	44.99	35.75	13
		TSM	LR	-	b1, b10, b11 b3, b4, b5, b6 b7, b9	0.58	77.83	55.09	21
		SDD	ELM	af=poslin hn=10,000	All	0.82	0.04	0.12	21
	Patzcuaro	Chl-a	ELM	af=hardlims hn=10,000	All	0.38	26.74	16.19	31
		Turbidity	LR	-	b7, b8	0.77	14.08	10.62	31
		TSM	SVR	C=500 y=500	logb1, logb2, logb3 logb4, logb5, logb6 logb7	0.36	20.32	15.86	31
		SDD	ELM	af=purelin hn=5	All	0.18	0.02	0.02	29
	Yuriria	Chl-a	SVR	C=500, gamma=1 k=rfb	logb1, logb2, logb3 logb4, logb5	0.32	8.61	4.373	17
		Turbidity	ELM	af=tribas hn=15,000	All	0.83	23.32	100.85	18
		TSM	ELM	af=tansig hn=10	All	0.34	51.12	48.06	17
		SDD	ELM	af=purelin hn=12,500	All	0.60	0.11	0.25	17
	Catemaco	Chl-a	LR	-	b1, b4, b6, b7	0.38	8.01	5.63	17
		Turbidity	ELM	af=hardlim hn=10,000	All	0.36	0.54	3.27	16
		TSM	ELM	af=hardlim hn=1,000	All	0.26	1.86	11.89	17
		SDD	ELM	af=tribas hn=12,500	All	0.26	1.04	0.45	16

Table ST6: MSI Model validation and predictive capability results for all datasets including coefficient of determination (R^2), root mean square error (RMSE), mean absolute error (MAE), and the number of samples (n) used in section 3.

Sensor	Lake	Parameter	Model	Hyperparameters	Bands	R^2	RMSE	MAE	n
MSI	Chapala	Chl-a	ELM	af=hardlims hn=10,000	All	0.24	2.68	1.51	26
		Turbidity	ELM	af=hardlims hn=10,000	All	0.60	7.37	25.62	47
		TSM	ELM	af=satlins hn=15,000	All	0.43	45.08	38.69	52
		SDD	LR	-	logb3, logb4, logb6 logb7, logb8	0.53	0.08	0.06	52
	Cuitzeo	Chl-a	LR	-	logb3, logb6, logb1 logb7, logb8	0.98	0.98	0.76	7
		Turbidity	LR	-	b1, b2, b3 b4, b6	0.91	18.53	16.35	7
		TSM	LR	-	b1, b2, b3 b4, b7	0.94	13.4	9.81	7
		SDD	ELM	af=hardlim hn=5000	All	0.78	0.07	0.07	7
	Patzcuaro	Chl-a	ELM	af=radbas hn=500	All	0.21	25.91	10.15	47
		Turbidity	ELM	af=tribas hn=5000	All	0.36	44.90	104.14	36
		TSM	ELM	af=poslin hn=10,000	All	0.14	426.63	35.25	36
		SDD	LR	-	logb6, logb7	0.15	1.96	1.6	36
	Yuriria	Chl-a	ELM	af=hardlims hn=10,000	All	0.81	4.85	13.57	11
		Turbidity	ELM	af=poslin hn=10,000	All	0.82	14.63	90.41	11
		TSM	ELM	af=satlins hn=1500	All	0.11	107.57	38.64	11
		SDD	LR	-	logb1, logb3, logb4 logb5, logb6, logb7 logb8	0.68	0.07	0.05	11
	Catemaco	Chl-a	ELM	af=hardlims hn=15,000	All	0.95	7.97	5.14	7
		Turbidity	ELM	af=hardlim hn=1,000	All	0.85	0.79	0.50	7
		TSM	ELM	af=poslin hn=1,000	All	0.81	1.34	1.09	7
		SDD	LR	-	logb1, logb2, logb5 logb6, logb7	0.91	0.09	0.04	7

8.2 Supplementary Figures

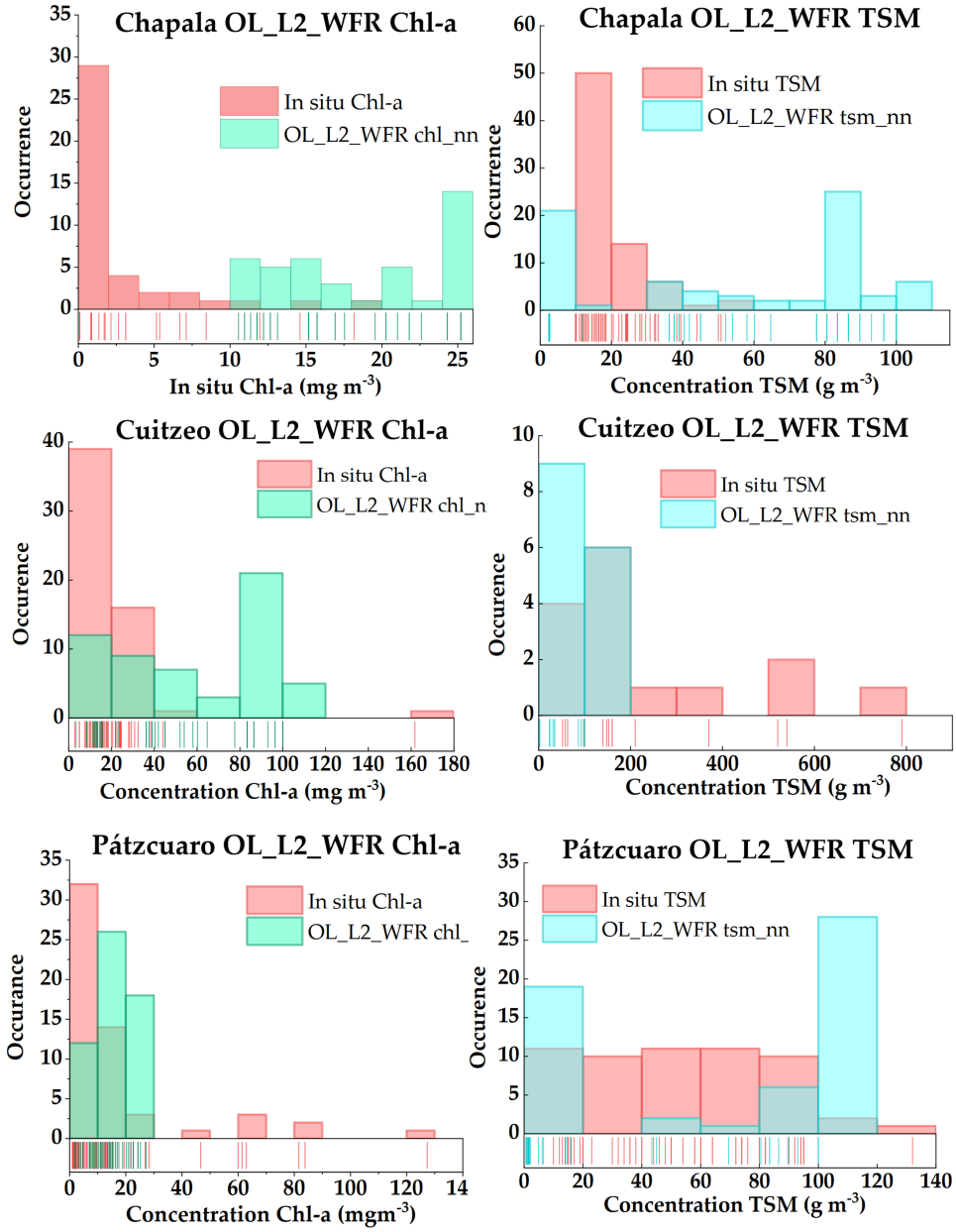

Figure SF1: Cont.

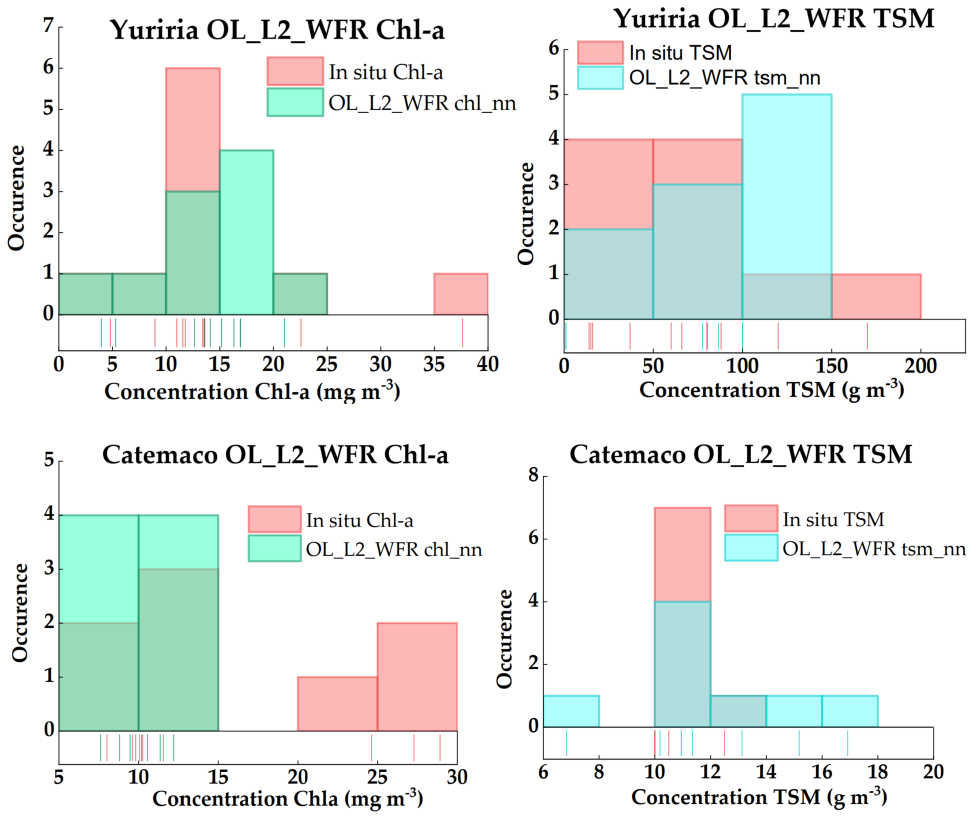

Figure SF1: In-situ and S3 derived water quality parameters vs. field data from RNMCA by lake. The upper row shows the Chl-a comparison, the lower row shows TSM.

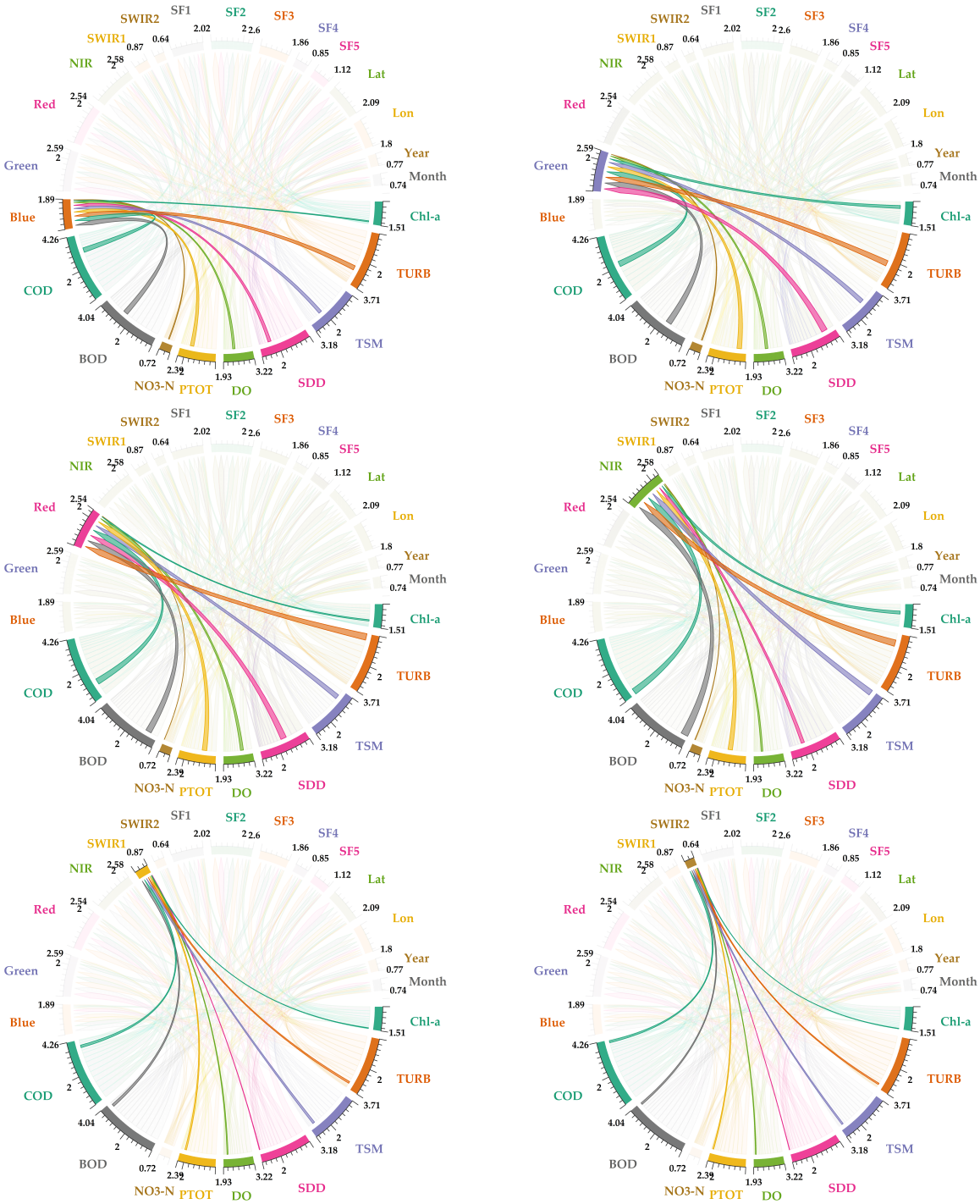

Figure SF2: Cont.

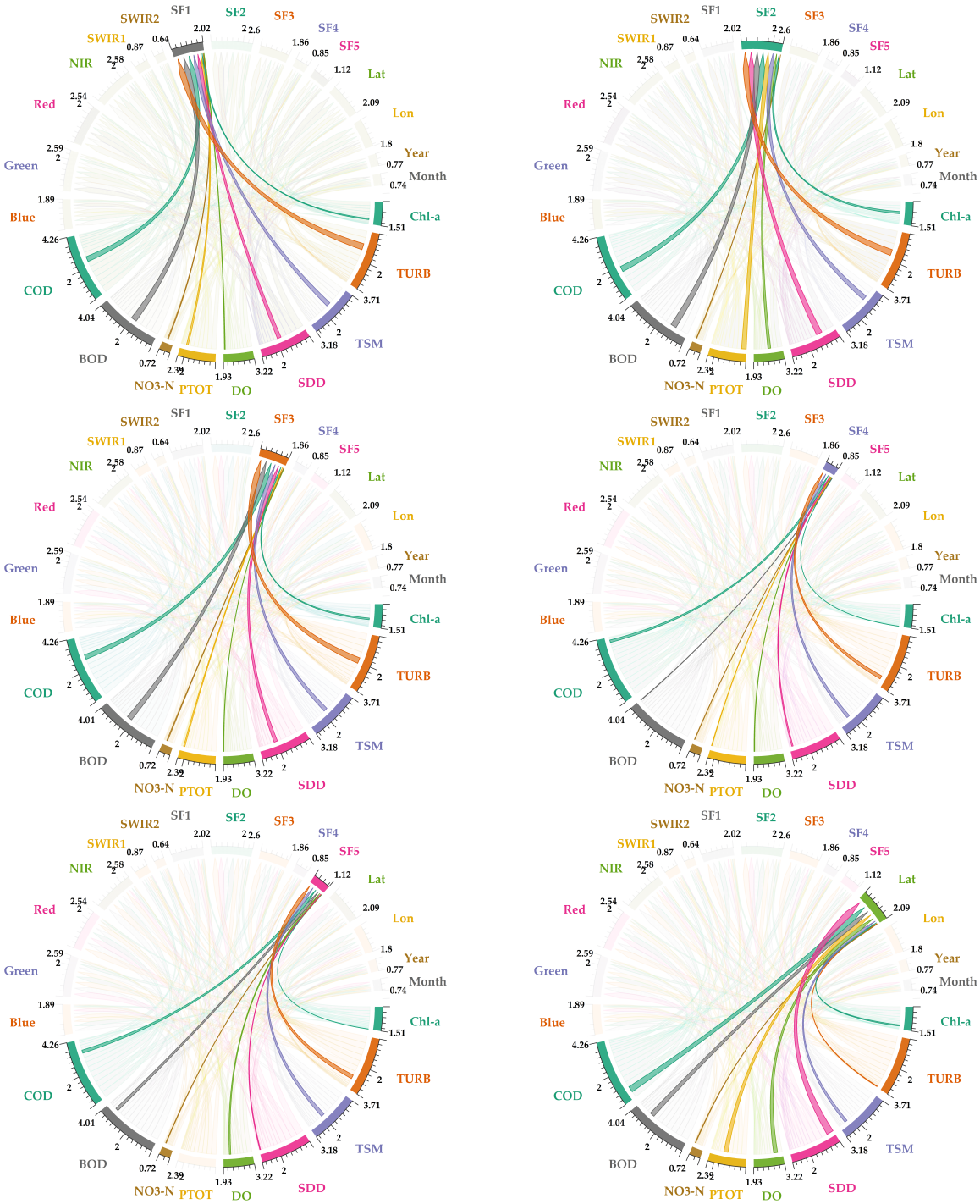

Figure SF2: Cont.

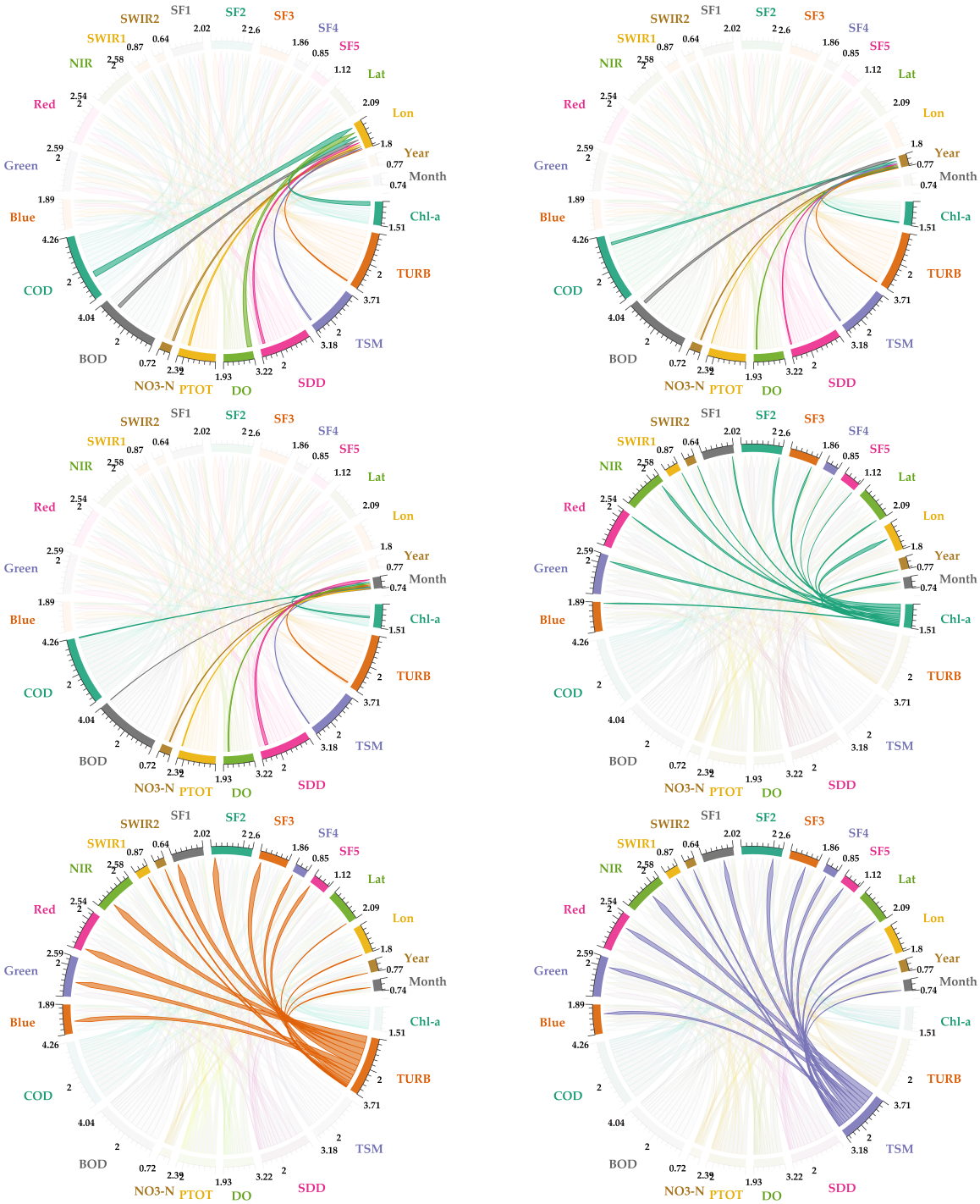

Figure SF2: Cont.

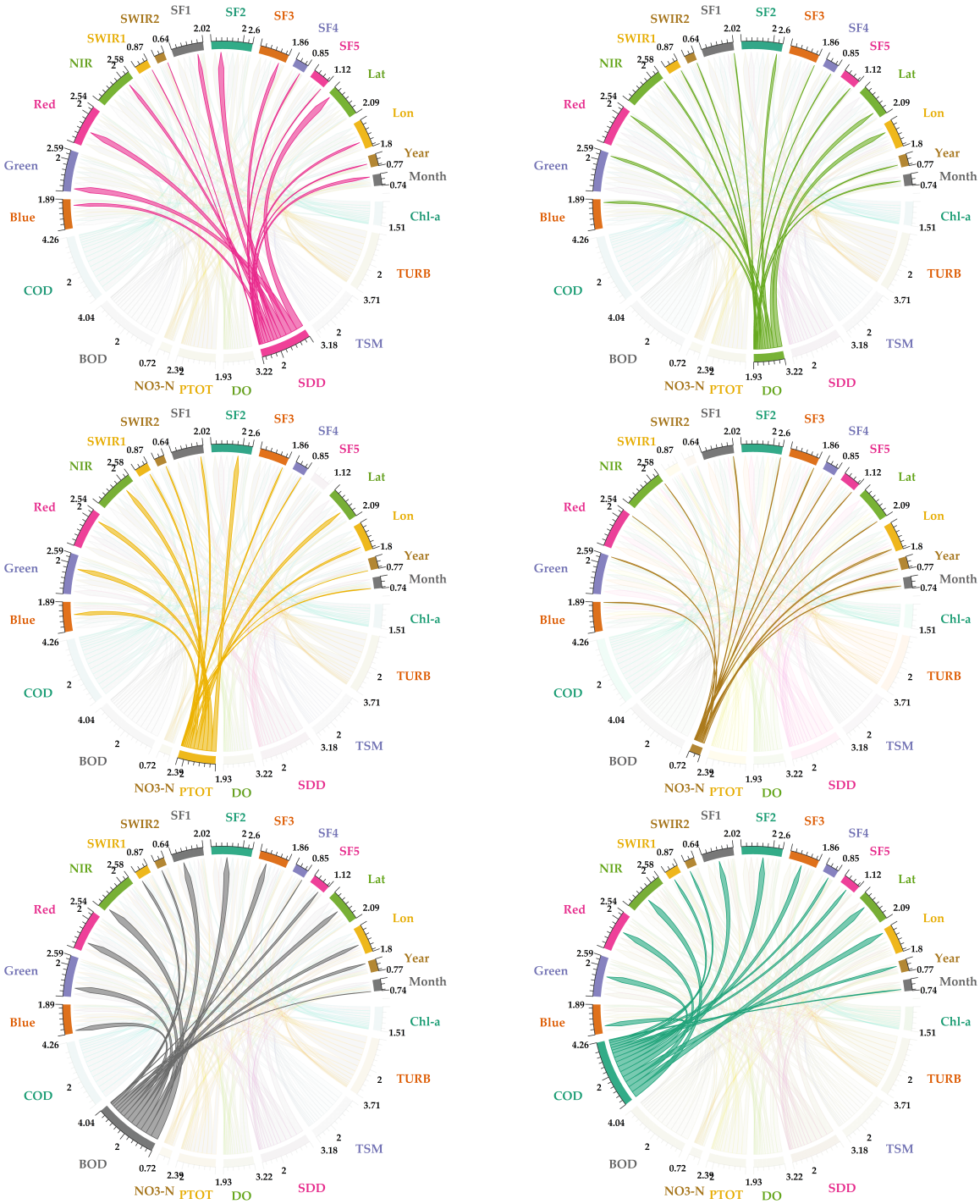

Figure SF2: Individual sum of correlations of each predictor and target in form of Chor diagram.

References

Adamo, M., Matta, E., Bresciani, M., De Carolis, G., Vaiciute, D., Giardino, C., & Pasquariello, G. (2013). On the synergistic use of sar and optical imagery to monitor cyanobacteria blooms: the curonian lagoon case study. *European Journal of Remote Sensing*, *46*(1), 789–805.

Adrian, R., O'Reilly, C. M., Zagarese, H., Baines, S. B., Hessen, D. O., Keller, W., ... others (2009). Lakes as sentinels of climate change. *Limnology and oceanography*, *54*(6part2), 2283–2297.

Africa, D. (1998). *National water act no. 36.* Pretoria Government.

Ahn, Y.-H., Shanmugam, P., Lee, J.-H., & Kang, Y. Q. (2006). Application of satellite infrared data for mapping of thermal plume contamination in coastal ecosystem of korea. *Marine environmental research*, *61*(2), 186–201.

Akanbi, A. A., Lian, Y., Soong, D. T., et al. (1999). An analysis of managed flood storage options for selected levees along the lower illinois river for enhancing flood protection report no. 4: flood storage reservoirs and flooding on the lower illinois river. *ISWS Contract Report CR 645*.

Aldhyani, T. H., et al. (2020). Water quality prediction using artificial intelligence algorithms. *Applied Bionics and Biomechanics*, *2020*.

Alexander, R. B., Smith, R. A., Schwarz, G. E., Boyer, E. W., Nolan, J. V., & Brakebill, J. W. (2008). Differences in phosphorus and nitrogen delivery to the gulf of mexico from the mississippi river basin. *Environmental science & technology*, *42*(3), 822–830.

Ali, B. (2008). Assessing water quality in the beysehir lake (turkey) by the application of gis, geostatistics and remote sensing.

Alikas, K., Kangro, K., & Reinart, A. (2010). Detecting cyanobacterial blooms in large north european lakes using the maximum chlorophyll index. *Oceanologia*, *52*(2), 237–257.

Alikas, K., & Kratzer, S. (2017). Improved retrieval of secchi depth for optically-complex waters using remote sensing data. *Ecological indicators*, *77*, 218–227.

Allee, R., & Johnson, J. (1999). Use of satellite imagery to estimate surface chlorophyll a and secchi disc depth of bull shoals reservoir, arkansas, usa. *International Journal of Remote Sensing*, *20*(6), 1057–1072.

Alom, M. Z., Taha, T. M., Yakopcic, C., Westberg, S., Sidike, P., Nasrin, M. S., ... Asari, V. K. (2019). A state-of-the-art survey on deep learning theory and architectures. *Electronics*, *8*(3), 292.

Alparslan, E., Coskun, H. G., & Alganci, U. (2009). Water quality determination of küçükçekmece lake, turkey by using multispectral satellite data. *TheScientificWorldJOURNAL*, *9*, 1215–1229.

Amoros, C., & Bornette, G. (2002). Connectivity and biocomplexity in waterbodies of riverine floodplains. *Freshwater biology*, *47*(4), 761–776.

Anatoliy, F., Tereshchenko, I., Monzon, C., Avalos-Cueva, D., & Pantoja-González, D. (2016). Climatic change in a large shallow tropical lake chapala, mexico. *Lake Sciences and Climate Change*, 1.

Ansper, A., & Alikas, K. (2019). Retrieval of chlorophyll a from sentinel-2 msi data for the european union water framework directive reporting purposes. *Remote Sensing*, *11*(1), 64.

APHA. (2005). Standard methods for the examination of water and wastewater. *American Public Health Association (APHA): Washington, DC, USA*.

Arias-Rodriguez, L. F., Duan, Z., Díaz-Torres, J. d. J., Basilio Hazas, M., Huang, J., Kumar, B. U., ... Disse, M. (2021). Integration of remote sensing and mexican water quality

monitoring system using an extreme learning machine. *Sensors*, *21*(12), 4118.

Arias-Rodriguez, L. F., Duan, Z., Sepúlveda, R., Martinez-Martinez, S. I., & Disse, M. (2020). Monitoring water quality of valle de bravo reservoir, mexico, using entire lifespan of meris data and machine learning approaches. *Remote Sensing*, *12*(10), 1586.

Assessment, M. E. (2005). *Ecosystems and human well-being: wetlands and water*. World resources institute.

Azamathulla, H. M., & Wu, F.-C. (2011). Support vector machine approach for longitudinal dispersion coefficients in natural streams. *Applied Soft Computing*, *11*(2), 2902–2905.

Ball, J. E., Anderson, D. T., & Chan Sr, C. S. (2017). Comprehensive survey of deep learning in remote sensing: theories, tools, and challenges for the community. *Journal of applied remote sensing*, *11*(4), 042609.

Barzegar, R., et al. (2020). Short-term water quality variable prediction using a hybrid cnn–lstm deep learning model. *Stochastic Environmental Research and Risk Assessment*, *34*(2), 415–433.

Batjes, N. (2011). *Global distribution of soil phosphorus retention potential* (Tech. Rep.). ISRIC-World Soil Information.

Batur, E., & Maktav, D. (2018). Assessment of surface water quality by using satellite images fusion based on pca method in the lake gala, turkey. *IEEE Transactions on Geoscience and Remote Sensing*, *57*(5), 2983–2989.

Benjankar, R., Egger, G., Jorde, K., Goodwin, P., & Glenn, N. F. (2011). Dynamic floodplain vegetation model development for the kootenai river, usa. *Journal of Environmental Management*, *92*(12), 3058–3070.

Berry, J. P., & Lind, O. (2010). First evidence of "paralytic shellfish toxins" and cylindrospermopsin in a mexican freshwater system, lago catemaco, and apparent bioaccumulation of the toxins in "tegogolo" snails (pomacea patula catemacensis). *Toxicon*, *55*(5), 930–938.

Bhatti, A. M., Rundquist, D. C., Nasu, S., & Takagi, M. (2008). Assessing the potential of remotely sensed data for water quality monitoring of coastal and inland waters.

Bi, S., Li, Y., Wang, Q., Lyu, H., Liu, G., Zheng, Z., ... others (2018). Inland water atmospheric correction based on turbidity classification using olci and slstr synergistic observations. *Remote Sensing*, *10*(7), 1002.

Blix, K., et al. (2017). Gaussian process sensitivity analysis for oceanic chlorophyll estimation. *IEEE Journal of Selected Topics in Applied Earth Observations and Remote Sensing*, *10*(4), 1265–1277.

Blix, K., et al. (2018). Remote sensing of water quality parameters over lake balaton by using sentinel-3 olci. *Water*, *10*(10), 1428.

Bonansea, M., Ledesma, M., Rodriguez, C., & Pinotti, L. (2019). Using new remote sensing satellites for assessing water quality in a reservoir. *Hydrological sciences journal*, *64*(1), 34–44.

Bonansea, M., Rodriguez, M. C., Pinotti, L., & Ferrero, S. (2015). Using multi-temporal landsat imagery and linear mixed models for assessing water quality parameters in río tercero reservoir (argentina). *Remote Sensing of Environment*, *158*, 28–41.

Bradbury, J. P. (2000). Limnologic history of lago de patzcuaro, michoacan, mexico for the past 48,000 years: impacts of climate and man. *Palaeogeography, Palaeoclimatology, Palaeoecology*, *163*(1-2), 69–95.

Brando, V. E., & Dekker, A. G. (2003). Satellite hyperspectral remote sensing for estimating estuarine and coastal water quality. *IEEE transactions on geoscience and remote sensing*, *41*(6), 1378–1387.

Breiman, L. (2001). Random forests. *Machine learning*, *45*(1), 5–32.

Bresciani, M., Cazzaniga, I., Austoni, M., Sforzi, T., Buzzi, F., Morabito, G., & Giardino, C. (2018). Mapping phytoplankton blooms in deep subalpine lakes from sentinel-2a and

landsat-8. *Hydrobiologia*, *824*(1), 197–214.

Bresciani, M., Stroppiana, D., Odermatt, D., Morabito, G., & Giardino, C. (2011). Assessing remotely sensed chlorophyll-a for the implementation of the water framework directive in european perialpine lakes. *Science of the Total Environment*, *409*(17), 3083–3091.

Bresciani, M., Vascellari, M., Giardino, C., & Matta, E. (2012). Remote sensing supports the definition of the water quality status of lake omodeo (italy). *European Journal of Remote Sensing*, *45*(1), 349–360.

Brezonik, P., Menken, K. D., & Bauer, M. (2005). Landsat-based remote sensing of lake water quality characteristics, including chlorophyll and colored dissolved organic matter (cdom). *Lake and Reservoir Management*, *21*(4), 373–382.

Brezonik, P. L., Olmanson, L. G., Bauer, M. E., & Kloiber, S. M. (2007). Measuring water clarity and quality in minnesota lakes and rivers: A census-based approach using remote-sensing techniques. *Cura Reporter*, *37*(3), 3–313.

Brockmann, C., Doerffer, R., Peters, M., Kerstin, S., Embacher, S., & Ruescas, A. (2016). Evolution of the c2rcc neural network for sentinel 2 and 3 for the retrieval of ocean colour products in normal and extreme optically complex waters. In *Living planet symposium* (Vol. 740, p. 54).

Brunotte, E., Dister, E., Gunther-Diringer, D., Koenzen, U., & Mehl, D. (2009). *Flussauen in deutschland: Erfassung und bewertung des auenzustandes*. BfN-Schriftenvertrieb im Landwirtschaftsverlag.

Bukata, R. P., Jerome, J. H., Kondratyev, K. Y., & Pozdnyakov, D. V. (2018). *Optical properties and remote sensing of inland and coastal waters*. CRC press.

Bulgarelli, B., Kiselev, V., & Zibordi, G. (2017). Adjacency effects in satellite radiometric products from coastal waters: a theoretical analysis for the northern adriatic sea. *Applied optics*, *56*(4), 854–869.

Buma, W. G., & Lee, S.-I. (2020). Evaluation of sentinel-2 and landsat 8 images for estimating chlorophyll-a concentrations in lake chad, africa. *Remote Sensing*, *12*(15), 2437.

Camps-Valls, G. (2009). Machine learning in remote sensing data processing. In *2009 ieee international workshop on machine learning for signal processing* (pp. 1–6).

Candiani, G., Giardino, C., & Brando, V. E. (2007). Adjacency effects and bio-optical model regionalisation: Meris data to assess lake water quality in the subalpine ecoregion. In *Proc. envisat symposium, montreux, switzerland* (pp. 23–27).

Carlson, R. E. (1977). A trophic state index for lakes 1. *Limnology and oceanography*, *22*(2), 361–369.

Carnero-Bravo, V., Merino-Ibarra, M., Ruiz-Fernández, A. C., Sanchez-Cabeza, J. A., & Ghaleb, B. (2015). Sedimentary record of water column trophic conditions and sediment carbon fluxes in a tropical water reservoir (valle de bravo, mexico). *Environmental Science and Pollution Research*, *22*(6), 4680–4694.

Casey, K. S., Brandon, T. B., Cornillon, P., & Evans, R. (2010). The past, present, and future of the avhrr pathfinder sst program. In *Oceanography from space* (pp. 273–287). Springer.

Castrillo, M., & García, Á. L. (2020). Estimation of high frequency nutrient concentrations from water quality surrogates using machine learning methods. *Water Research*, *172*, 115490.

Chacon-Torres, A., Ross, L., Beveridge, M., & Watson, A. (1992). The application of spot multispectral imagery for the assessment of water quality in lake patzcuaro, mexico. *International Journal of Remote Sensing*, *13*(4), 587–603.

Chang, C.-C., & Lin, C.-J. (2011). Libsvm: a library for support vector machines. *ACM transactions on intelligent systems and technology (TIST)*, *2*(3), 1–27.

Chapman, S. L. (1996). Soil and solid poultry waste nutrient management and water quality. *Poultry Science*, *75*(7), 862–866.

Chastain, R., Housman, I., Goldstein, J., Finco, M., & Tenneson, K. (2019). Empirical cross

sensor comparison of sentinel-2a and 2b msi, landsat-8 oli, and landsat-7 etm+ top of atmosphere spectral characteristics over the conterminous united states. *Remote sensing of environment*, *221*, 274–285.

Chen, K., Chen, H., Zhou, C., Huang, Y., Qi, X., Shen, R., ... others (2020). Comparative analysis of surface water quality prediction performance and identification of key water parameters using different machine learning models based on big data. *Water research*, *171*, 115454.

Chen, Y., Arnold, W. A., Griffin, C. G., Olmanson, L. G., Brezonik, P. L., & Hozalski, R. M. (2019). Assessment of the chlorine demand and disinfection byproduct formation potential of surface waters via satellite remote sensing. *Water Research*, *165*, 115001.

Cheng, K.-S., & Lei, T.-C. (2001). Reservoir trophic state evaluation using lanisat tm images 1. *JAWRA Journal of the American Water Resources Association*, *37*(5), 1321–1334.

Chowdury, M. S. U., et al. (2019). Iot based real-time river water quality monitoring system. *Procedia Computer Science*, *155*, 161–168.

Claverie, M., Ju, J., Masek, J. G., Dungan, J. L., Vermote, E. F., Roger, J.-C., ... Justice, C. (2018). The harmonized landsat and sentinel-2 surface reflectance data set. *Remote sensing of environment*, *219*, 145–161.

CNN. (2010). La ciudad de mexico, en crisis de agua. *Expansion in Alliance*.

CONAGUA. (2018). *Atlas del agua en mexico.* https://agua.org.mx/wp-content/uploads/2019/04/AAM_2018.pdf. (Online; accessed on 10 June 2021)

Cui, Y., et al. (2022). Deep learning–based remote sensing estimation of water transparency in shallow lakes by combining landsat 8 and sentinel 2 images. *Environmental Science and Pollution Research*, *29*(3), 4401–4413.

de Anda, J., Shear, H., Maniak, U., & Valle, P. F. Z.-d. (2004). Solids distribution in lake chapala, mexico. *JAWRA Journal of the American Water Resources Association*, *40*(1), 97–109.

Debels, P., Figueroa, R., Urrutia, R., Barra, R., & Niell, X. (2005). Evaluation of water quality in the chillán river (central chile) using physicochemical parameters and a modified water quality index. *Environmental monitoring and assessment*, *110*(1), 301–322.

Dekker, A., & Peters, S. (1993). The use of the thematic mapper for the analysis of eutrophic lakes: a case study in the netherlands. *International Journal of Remote Sensing*, *14*(5), 799–821.

Dekker, A. G., Brando, V. E., Anstee, J. M., Pinnel, N., Kutser, T., Hoogenboom, E. J., ... others (2002). Imaging spectrometry of water. In *Imaging spectrometry* (pp. 307–359). Springer.

Dekker, A. G., Malthus, T. J., & Seyhan, E. (1991). Quantitative modeling of inland water quality for high-resolution mss systems. *IEEE Transactions on Geoscience and Remote Sensing*, *29*(1), 89–95.

Delgado, A. L., Pratolongo, P. D., Gossn, J. I., Dogliotti, A. I., Arena, M., Villagran, D., & Fernandez Severini, M. (2018). Evaluation of derived total suspended matter products from ocean and land colour instrument imagery (olci) in the inner and mid-shelf of buenos aires province (argentina).

Doerffer, R., & Schiller, H. (2007). The meris case 2 water algorithm. *International Journal of Remote Sensing*, *28*(3-4), 517–535.

Dörnhöfer, K., & Oppelt, N. (2016). Remote sensing for lake research and monitoring–recent advances. *Ecological Indicators*, *64*, 105–122.

Doxaran, D., Froidefond, J.-M., Lavender, S., & Castaing, P. (2002). Spectral signature of highly turbid waters: Application with spot data to quantify suspended particulate matter concentrations. *Remote sensing of Environment*, *81*(1), 149–161.

DTP. (2020). *Danube transnational programme, interreg danube floodplain: Reducing the flood*

risk through floodplain restoration along the danube river and tributaries.

DTP. (2021). *Danube transnational programme, danube floodplain output 3.1: Evaluated and ranked danube floodplains.*

Duan, H., Ma, R., Zhang, Y., & Zhang, B. (2009). Remote-sensing assessment of regional inland lake water clarity in northeast china. *Limnology*, *10*(2), 135–141.

Duan, H., Zhang, Y., Zhang, B., Song, K., & Wang, Z. (2007). Assessment of chlorophyll-a concentration and trophic state for lake chagan using landsat tm and field spectral data. *Environmental monitoring and assessment*, *129*(1), 295–308.

Duan, W., He, B., Takara, K., Luo, P., Nover, D., Sahu, N., & Yamashiki, Y. (2013). Spatiotemporal evaluation of water quality incidents in japan between 1996 and 2007. *Chemosphere*, *93*(6), 946–953.

Duan, W., Takara, K., He, B., Luo, P., Nover, D., & Yamashiki, Y. (2013). Spatial and temporal trends in estimates of nutrient and suspended sediment loads in the ishikari river, japan, 1985 to 2010. *Science of the Total Environment*, *461*, 499–508.

EC. (2015,). *European commission brussel nature-based solutions and re-naturing cities.*

EEA. (2021). *European environment agency, data and maps.* https://www.eea.europa.eu/data-and-maps. (Online; accessed on 15 November 2021)

El-Din, M. S., Gaber, A., Koch, M., Ahmed, R. S., & Bahgat, I. (2013). Remote sensing application for water quality assessment in lake timsah, suez canal, egypt. *Journal of Remote Sensing Technology*, *1*(3), 61.

EPA. (2006). Elements of a state water monitoring and assessment program for wetlands.

Escolero, O., Kralisch, S., Martínez, S. E., & Perevochtchikova, M. (2016). Diagnóstico y análisis de los factores que influyen en la vulnerabilidad de las fuentes de abastecimiento de agua potable a la ciudad de méxico, méxico. *Boletín de la Sociedad Geológica Mexicana*, *68*(3), 409–427.

Espinal Carreón, T., Sedeño Díaz, J. E., & López López, E. (2013). Evaluación de la calidad del agua en la laguna de yuriria, guanajuato, méxico, mediante técnicas multivariadas: un análisis de valoración para dos épocas 2005, 2009-2010. *Revista internacional de contaminación ambiental*, *29*(3), 147–163.

Etim, E., Odoh, R., Itodo, A., Umoh, S., & Lawal, U. (2013). Water quality index for the assessment of water quality from different sources in the niger delta region of nigeria. *Frontiers in science*, *3*(3), 89–95.

Falcini, F., Khan, N. S., Macelloni, L., Horton, B. P., Lutken, C. B., McKee, K. L., ... others (2012). Linking the historic 2011 mississippi river flood to coastal wetland sedimentation. *Nature Geoscience*, *5*(11), 803–807.

FCEA. (2010). Recorte en el suministro de agua del sistema cutzamala. *Fondo para la Comunicacion y la Educacion Ambiental A.C., (accessed on 10 September 2018).*

Feng, L., Hu, C., Han, X., Chen, X., & Qi, L. (2015). Long-term distribution patterns of chlorophyll-a concentration in china's largest freshwater lake: Meris full-resolution observations with a practical approach. *remote sensing*, *7*(1), 275–299.

Fernández-Vítora, V. C., Ripoll, V. C., Ripoll, L. A. C., & Garro, V. R. (1997). *Guía metodológica para la evaluación del impacto ambiental* (No. PA 333.72 C66.). Mundiprensa.

Figueroa-Sanchez, M. A., Sarma, N., & Sarma, S. (2014). Zooplankton community structure in the presence of low levels of cyanotoxins: a case study in a high altitude tropical reservoir (valle de bravo, mexico. *Journal of Limnology*, *73*(1).

FIR. (2004). *Ficha informativa de los humedales de ramsar.* https://rsis.ramsar.org/RISapp/files/RISrep/MX1361RIS.pdf?language=en. (Online; accessed on 10 June 2021)

Flores Alvarez, A. W. (2016). Diagnostico socioeconomico y estrategias de desarrollo del mu-

nicipio de valle de bravo, 2005-2012.

Florescano, E., Ortiz Escamilla, J., Benítez Badillo, G., Welsh Rodríguez, C., & Córdova, R. (2010). *Atlas del patrimonio natural, histórico y cultural de veracruz* (No. Sirsi) i9786079513153). Universidad Veracruzana. Gobierno del Estado de Veracruz.

Font, J., Boutin, J., Reul, N., Spurgeon, P., Ballabrera-Poy, J., Chuprin, A., ... others (2013). Smos first data analysis for sea surface salinity determination. *International Journal of Remote Sensing*, *34*(9-10), 3654–3670.

fur Umwelt, B. (2021). *Nukleare sicherheit und verbracherschutz: Eckpunktepapier. aktionsprogramm naturlicher klimaschutz.*

Gall, C. L. (1974). *Canada water act.* (Unpublished doctoral dissertation). Carleton University.

Galloway, J. N. (2002). Cowling, eb, reactive nitrogen and the world: 200 years of change. *Ambio*, *31*, 64–71.

Gao, F., Masek, J. G., & Wolfe, R. E. (2009). Automated registration and orthorectification package for landsat and landsat-like data processing. *Journal of Applied Remote Sensing*, *3*(1), 033515.

Garaba, S., Badewien, T., Braun, A., Schulz, A.-C., & Zielinski, O. (2014). Using ocean colour remote sensing products to estimate turbidity at the wadden sea time series station spiekeroog. *Journal of the European Optical Society-Rapid publications*, *9*.

García, P. R., Nandini, S., Sarma, S., Valderrama, E. R., Cuesta, I., & Hurtado, M. D. (2002). Seasonal variations of zooplankton abundance in the freshwater reservoir valle de bravo (mexico). *Hydrobiologia*, *467*(1), 99–108.

García-Aguirre, M. C., Álvarez, R., Dirzo, R., Ortiz, M. A., & Eng, M. M. (2010). Delineation of biogeomorphic land units across a tropical natural and humanized terrain in los tuxtlas, veracruz, mexico. *Geomorphology*, *121*(3-4), 245–256.

Garnier, J., Billen, G., Hannon, E., Fonbonne, S., Videnina, Y., & Soulie, M. (2002). Modelling the transfer and retention of nutrients in the drainage network of the danube river. *Estuarine, Coastal and Shelf Science*, *54*(3), 285–308.

Gaytan-Herrera, M. L., Martinez-Almeida, V., Oliva-Martinez, M. G., Duran-Diaz, A., & Ramirez-Garcia, P. (2011). Temporal variation of phytoplankton from the tropical reservoir valle de bravo, mexico. *Journal of Environmental Biology*, *32*(1), 117–126.

GEE. (2022a). *Projections on google earth engine.* https://developers.google.com/earthengine/guides/projections.

GEE. (2022b). *Registering images on google earth engine.* https://developers.google.com/earthengine/guides/register.

Gholizadeh, M. H., Melesse, A. M., & Reddi, L. (2016). A comprehensive review on water quality parameters estimation using remote sensing techniques. *Sensors*, *16*(8), 1298.

Giardino, C., Brando, V., Gege, P., Pinnel, N., Hochberg, E., Knaeps, E., ... others (2019). Imaging spectrometry of inland and coastal waters: state of the art, achievements and perspectives. *Surveys in Geophysics*, *40*(3), 401–429.

Giardino, C., Bresciani, M., Cazzaniga, I., Di Nicolantonio, W., Cacciari, A., Matta, E., ... Ober, G. (2013). Combining in situ and multi-sensor satellite data to assess the impact of atmospheric deposition in lake garda. In *2013 european space agency living planet symposium* (pp. 1–5).

Giardino, C., Bresciani, M., Cazzaniga, I., Schenk, K., Rieger, P., Braga, F., ... Brando, V. E. (2014). Evaluation of multi-resolution satellite sensors for assessing water quality and bottom depth of lake garda. *Sensors*, *14*(12), 24116–24131.

Giardino, C., Candiani, G., & Zilioli, E. (2005). Detecting chlorophyll-a in lake garda using toa meris radiances. *Photogrammetric Engineering & Remote Sensing*, *71*(9), 1045–1051.

Giardino, C., Oggioni, A., Bresciani, M., & Yan, H. (2010). Remote sensing of suspended particulate matter in himalayan lakes. *Mountain Research and Development*, *30*(2), 157–

168.

Gitelson, A., & Kondratyev, K. Y. (1991). Optical models of mesotrophic and eutrophic water bodies. *International Journal of Remote Sensing*, *12*(3), 373–385.

Glibert, P. M., & Burford, M. A. (2017). Globally changing nutrient loads and harmful algal blooms: recent advances, new paradigms, and continuing challenges. *Oceanography*, *30*(1), 58–69.

GOBCA. (2021). *Open government portal.* https://search.open.canada.ca/en/od/. (Online; accessed on 15 November 2021)

GOBCHL. (2021). *EstadÃsticas estaciones dga.* https://search.open.canada.ca/en/od/. (Online; accessed on 15 November 2021)

GOBMx. (2010). Sistema cutzamala, la llave de agua del valle de mexico. *www.gob.mx*.

GOBMX. (2021). *Calidad del agua en mÃ@xico.* https://www.gob.mx/conagua/articulos/calidad-del-agua. (Online; accessed on 15 November 2021)

Gómez, J. A. D., Alonso, C. A., & García, A. A. (2011). Remote sensing as a tool for monitoring water quality parameters for mediterranean lakes of european union water framework directive (wfd) and as a system of surveillance of cyanobacterial harmful algae blooms (scyanohabs). *Environmental monitoring and assessment*, *181*(1), 317–334.

Goolsby, D. A., Battaglin, W. A., Lawrence, G. B., Artz, R. S., Aulenbach, B. T., Hooper, R. P., ... Stensland, G. J. (1999). Flux and sources of nutrients in the mississippi-atchafalaya river basin: Topic 3 report for the integrated assessment on hypoxia in the gulf of mexico.

Gosso, A., & Martinez-de Pison, F. (2012). elmnn: Implementation of elm (extreme learning machine) algorithm for slfn (single hidden layer feedforward neural networks). *R package version*, *1*(0).

Gower, J. (1980). Observations of in situ fluorescence of chlorophyll-a in saanich inlet. *Boundary-Layer Meteorology*, *18*(3), 235–245.

Gower, J., King, S., Borstad, G., & Brown, L. (2005). Detection of intense plankton blooms using the 709 nm band of the meris imaging spectrometer. *International Journal of Remote Sensing*, *26*(9), 2005–2012.

Grendaitė, D., Stonevičius, E., Karosienė, J., Savadova, K., & Kasperovičienė, J. (2018). Chlorophyll-a concentration retrieval in eutrophic lakes in lithuania from sentinel-2 data. *Geologija. Geografija*, *4*(1).

Guevara, S., Laborde, J., & Sánchez-Ríos, G. (2004). Los tuxtlas, el paisaje de la sierra. instituto de ecología.

Guo, H., Huang, J. J., Zhu, X., Wang, B., Tian, S., Xu, W., & Mai, Y. (2021). A generalized machine learning approach for dissolved oxygen estimation at multiple spatiotemporal scales using remote sensing. *Environmental Pollution*, *288*, 117734.

Gutiérrez Quevedo, M., et al. (2014). Contribución al estudio de la diversidad del zooplancton en tres lagos tropicales y sus relación con el uso de suelo en los tuxtlas, veracruz.

Hafeez, S., et al. (2019). Comparison of machine learning algorithms for retrieval of water quality indicators in case-ii waters: A case study of hong kong. *Remote sensing*, *11*(6), 617.

Hamylton, S., Silverman, J., & Shaw, E. (2013). The use of remote sensing to scale up measures of carbonate production on reef systems: a comparison of hydrochemical and census-based estimation methods. *International Journal of Remote Sensing*, *34*(18), 6451–6465.

Han, L., & Jordan, K. J. (2005). Estimating and mapping chlorophyll-a concentration in pensacola bay, florida using landsat etm+ data. *International Journal of Remote Sensing*, *26*(23), 5245–5254.

Handcock, R., Gillespie, A., Cherkauer, K., Kay, J., Burges, S., & Kampf, S. (2006). Accuracy and uncertainty of thermal-infrared remote sensing of stream temperatures at multiple

spatial scales. *Remote Sensing of Environment*, *100*(4), 427–440.

Hansen, C. H., Burian, S. J., Dennison, P. E., & Williams, G. P. (2017). Spatiotemporal variability of lake water quality in the context of remote sensing models. *Remote Sensing*, *9*(5), 409. doi: https://doi.org/10.3390/rs9050409

Hanson, P. C., et al. (2020). Predicting lake surface water phosphorus dynamics using process-guided machine learning. *Ecological Modelling*, *430*, 109136.

Hardison, E. C., O'Driscoll, M. A., DeLoatch, J. P., Howard, R. J., & Brinson, M. M. (2009). Urban land use, channel incision, and water table decline along coastal plain streams, north carolina 1. *JAWRA Journal of the American Water Resources Association*, *45*(4), 1032–1046.

Härmä, P., Vepsäläinen, J., Hannonen, T., Pyhälahti, T., Kämäri, J., Kallio, K., ... Koponen, S. (2001). Detection of water quality using simulated satellite data and semi-empirical algorithms in finland. *Science of the Total Environment*, *268*(1-3), 107–121.

Hartling, S., Sagan, V., Sidike, P., Maimaitijiang, M., & Carron, J. (2019). Urban tree species classification using a worldview-2/3 and lidar data fusion approach and deep learning. *Sensors*, *19*(6), 1284.

Hartmann, D. L., Tank, A. M. K., Rusticucci, M., Alexander, L. V., Brönnimann, S., Charabi, Y. A. R., ... others (2013). Observations: atmosphere and surface. In *Climate change 2013 the physical science basis: Working group i contribution to the fifth assessment report of the intergovernmental panel on climate change* (pp. 159–254). Cambridge University Press.

Hastie, T., Tibshirani, R., & Friedman, J. (2009). The elements of statistical learning. *Cited on*, 33.

He, B., Oki, K., Wang, Y., & Oki, T. (2009). Using remotely sensed imagery to estimate potential annual pollutant loads in river basins. *Water Science and Technology*, *60*(8), 2009–2015.

He, J., Chen, Y., Wu, J., Stow, D. A., & Christakos, G. (2020). Space-time chlorophyll-a retrieval in optically complex waters that accounts for remote sensing and modeling uncertainties and improves remote estimation accuracy. *Water Research*, *171*, 115403.

He, W., Chen, S., Liu, X., & Chen, J. (2008). Water quality monitoring in a slightly-polluted inland water body through remote sensing - case study of the guanting reservoir in beijing, china. *Frontiers of Environmental Science & Engineering in China*, *2*(2), 163–171.

Hedley, J., Roelfsema, C., Chollett, I., Harborne, A., Heron, S., Weeks, S., ... others (2016). *Remote sensing of coral reefs for monitoring and management: a review. remote sens. 8, 118.*

Heege, T., Kiselev, V., Wettle, M., & Hung, N. N. (2014). Operational multi-sensor monitoring of turbidity for the entire mekong delta. *International Journal of Remote Sensing*, *35*(8), 2910–2926.

Hernández-Escobedo, Q., Manzano-Agugliaro, F., & Zapata-Sierra, A. (2010). The wind power of mexico. *Renewable and Sustainable Energy Reviews*, *14*(9), 2830–2840.

Hicks, B. J., Stichbury, G. A., Brabyn, L. K., Allan, M. G., & Ashraf, S. (2013). Hindcasting water clarity from landsat satellite images of unmonitored shallow lakes in the waikato region, new zealand. *Environmental Monitoring and Assessment*, *185*(9), 7245–7261.

Hollstein, A., Segl, K., Guanter, L., Brell, M., & Enesco, M. (2016). Ready-to-use methods for the detection of clouds, cirrus, snow, shadow, water and clear sky pixels in sentinel-2 msi images. *Remote Sensing*, *8*(8), 666.

Holubova, K., Hey, R., & Lisicky, M. (2003). Middle danube tributaries: Constraints and opportunities in lowland river restoration. *Large Rivers*, 507–519.

Housman, I. W., Chastain, R. A., & Finco, M. V. (2018). An evaluation of forest health insect and disease survey data and satellite-based remote sensing forest change detection

methods: Case studies in the united states. *Remote Sensing*, *10*(8), 1184.

Howarth, R. W. (2008). Coastal nitrogen pollution: a review of sources and trends globally and regionally. *Harmful algae*, *8*(1), 14–20.

Hoyek, A., Arias-Rodriguez, L. F., & Perosa, F. (2022). Holistic approach for estimating water quality ecosystem services of danube floodplains: Field measures, remote sensing, and machine learning. *Hydrobiology*, *1*(2), 211–231.

Hu, C. (2009). A novel ocean color index to detect floating algae in the global oceans. *Remote Sensing of Environment*, *113*(10), 2118–2129.

Huang, G.-B., Zhu, Q.-Y., & Siew, C.-K. (2006). Extreme learning machine: theory and applications. *Neurocomputing*, *70*(1-3), 489–501.

Hunter, P., Gilvear, D., Tyler, A., Willby, N., & Kelly, A. (2010). Mapping macrophytic vegetation in shallow lakes using the compact airborne spectrographic imager (casi). *Aquatic Conservation: Marine and Freshwater Ecosystems*, *20*(7), 717–727.

Hutchinson, G. E. (1973). Marginalia: Eutrophication: The scientific background of a contemporary practical problem. *American scientist*, *61*(3), 269–279.

Iagua. (2014). Brazil launches the national water quality monitoring network. *iagua*.

ICPDR. (2021). *International commission for the protection of the danube river: The danube river basin district management plan.* https://www.icpdr.org/main/wfd-fd-plans-published-2021.

Imen, S., Chang, N.-B., & Yang, Y. J. (2015). Developing the remote sensing-based early warning system for monitoring tss concentrations in lake mead. *Journal of environmental management*, *160*, 73–89.

James, G., Witten, D., Hastie, T., & Tibshirani, R. (2013). *An introduction to statistical learning* (Vol. 112). Springer.

Jarvie, H. P., Johnson, L. T., Sharpley, A. N., Smith, D. R., Baker, D. B., Bruulsema, T. W., & Confesor, R. (2017). Increased soluble phosphorus loads to lake erie: Unintended consequences of conservation practices. *Journal of Environmental Quality*, *46*(1), 123–132.

Kadlec, R. H., & Wallace, S. (2008). *Treatment wetlands*. CRC press.

Kallio, K., Koponen, S., & Pulliainen, J. (2003). Feasibility of airborne imaging spectrometry for lake monitoring - a case study of spatial chlorophyll a distribution in two meso-eutrophic lakes. *International Journal of Remote Sensing*, *24*(19), 3771–3790.

Kallio, K., Koponen, S., Ylöstalo, P., Kervinen, M., Pyhälahti, T., & Attila, J. (2015). Validation of meris spectral inversion processors using reflectance, iop and water quality measurements in boreal lakes. *Remote Sensing of Environment*, *157*, 147–157.

Kallio, K., Kutser, T., Hannonen, T., Koponen, S., Pulliainen, J., Vepsäläinen, J., & Pyhälahti, T. (2001). Retrieval of water quality from airborne imaging spectrometry of various lake types in different seasons. *Science of the Total Environment*, *268*(1-3), 59–77.

Keiner, L. (1999). Estimating oceanic chlorophyll concentrations with neural networks. *International Journal of Remote Sensing*, *20*(1), 189–194.

Keys, R. (1981). Cubic convolution interpolation for digital image processing. *IEEE transactions on acoustics, speech, and signal processing*, *29*(6), 1153–1160.

Khan, F. A., & Ansari, A. A. (2005). Eutrophication: an ecological vision. *The botanical review*, *71*(4), 449–482.

Kim, Y. H., Im, J., Ha, H. K., Choi, J.-K., & Ha, S. (2014). Machine learning approaches to coastal water quality monitoring using goci satellite data. *GIScience & Remote Sensing*, *51*(2), 158–174.

Klein, T., Nilsson, M., Persson, A., & Haakansson, B. (2017). From open data to open analyses - new opportunities for environmental applications. *Environments*, *4*(2), 32.

Kloiber, S. M., Brezonik, P. L., & Bauer, M. E. (2002). Application of landsat imagery to regional-scale assessments of lake clarity. *Water research*, *36*(17), 4330–4340.

Kloiber, S. M., Brezonik, P. L., Olmanson, L. G., & Bauer, M. E. (2002). A procedure for regional lake water clarity assessment using landsat multispectral data. *Remote sensing of Environment*, *82*(1), 38–47.

Knighton, D. (2014). *Fluvial forms and processes: a new perspective*. Routledge.

Kratzer, S., Brockmann, C., & Moore, G. (2008). Using meris full resolution data to monitor coastal waters?a case study from himmerfjärden, a fjord-like bay in the northwestern baltic sea. *Remote Sensing of Environment*, *112*(5), 2284–2300.

Kravitz, J., et al. (2020). Application of sentinel 3 olci for chl-a retrieval over small inland water targets: Successes and challenges. *Remote Sensing of Environment*, *237*, 111562.

Kronvang, B., & Bruhn, A. (1996). Choice of sampling strategy and estimation method for calculating nitrogen and phosphorus transport in small lowland streams. *Hydrological processes*, *10*(11), 1483–1501.

Kuhn, M. (2008). Building predictive models in r using the caret package. *Journal of statistical software*, *28*(1), 1–26.

Kutser, T., & Arst, H. (1994). Remote sensing reflectance model of optically-active components of turbid waters. In *Oceanic remote sensing and sea ice monitoring* (Vol. 2319, pp. 85–91).

Kutser, T., Paavel, B., Verpoorter, C., Ligi, M., Soomets, T., Toming, K., & Casal, G. (2016). Remote sensing of black lakes and using 810 nm reflectance peak for retrieving water quality parameters of optically complex waters. *Remote Sensing*, *8*(6), 497.

Kwong, I. H., Wong, F. K., & Fung, T. (2022). Automatic mapping and monitoring of marine water quality parameters in hong kong using sentinel-2 image time-series and google earth engine cloud computing. *Frontiers in Marine Science*, 609.

Lary, D. J., Alavi, A. H., Gandomi, A. H., & Walker, A. L. (2016). Machine learning in geosciences and remote sensing. *Geoscience Frontiers*, *7*(1), 3–10.

Lathrop, R. G. (1992). Landsat thematic mapper monitoring of turbid inland water quality. *Photogrammetric Engineering & Remote Sensing*, *58*(4), 465–470.

Lathrop, R. G., & Lillesand, T. M. (1989). Monitoring water quality and river plume transport in green bay, lake michigan with spot-1 imagery. *Photogrammetric Engineering & Remote Sensing*, *55*(3), 349–354.

Le, C., Hu, C., Cannizzaro, J., English, D., Muller-Karger, F., & Lee, Z. (2013). Evaluation of chlorophyll-a remote sensing algorithms for an optically complex estuary. *Remote Sensing of Environment*, *129*, 75–89.

Lee, S., & Lee, D. (2018). Improved prediction of harmful algal blooms in four major south korea's rivers using deep learning models. *International journal of environmental research and public health*, *15*(7), 1322.

Lee, Z., Arnone, R., Boyce, D., Franz, B., Greb, S., Hu, C., ... others (2018). Global water clarity: Continuing a century-long monitoring. *Eos*, *99*(May), 1–10.

Lee, Z., Shang, S., Qi, L., Yan, J., & Lin, G. (2016). A semi-analytical scheme to estimate secchi-disk depth from landsat-8 measurements. *Remote sensing of environment*, *177*, 101–106.

Lehner, B., & Döll, P. (2004). Development and validation of a global database of lakes, reservoirs and wetlands. *Journal of hydrology*, *296*(1-4), 1–22.

Lewin, J. (1978). Floodplain geomorphology. *Progress in Physical Geography*, *2*(3), 408–437.

Li, L., et al. (2019). Water quality prediction based on recurrent neural network and improved evidence theory: a case study of qiantang river, china. *Environmental Science and Pollution Research*, *26*(19), 19879–19896.

Li, X., et al. (2021). Machine learning method for quick identification of water quality index (wqi) based on sentinel-2 msi data: Ebinur lake case study. *Water Supply*, *21*(3), 1291–

1312.

Li, Y., Wang, X., Zhao, Z., Han, S., & Liu, Z. (2020). Lagoon water quality monitoring based on digital image analysis and machine learning estimators. *Water research*, *172*, 115471.

Lim, J., & Choi, M. (2015). Assessment of water quality based on landsat 8 operational land imager associated with human activities in korea. *Environmental monitoring and assessment*, *187*(6), 1–17.

Lin, S., Novitski, L. N., Qi, J., & Stevenson, R. J. (2018). Landsat tm/etm+ and machine-learning algorithms for limnological studies and algal bloom management of inland lakes. *Journal of Applied Remote Sensing*, *12*(2), 026003.

Liu, M., Liu, X., Liu, D., Ding, C., & Jiang, J. (2015). Multivariable integration method for estimating sea surface salinity in coastal waters from in situ data and remotely sensed data using random forest algorithm. *Computers & geosciences*, *75*, 44–56.

Liu, P., et al. (2019). Analysis and prediction of water quality using lstm deep neural networks in iot environment. *Sustainability*, *11*(7), 2058.

Llewellyn, D. W., Shaffer, G. P., Craig, N. J., Creasman, L., Pashley, D., Swan, M., & Brown, C. (1996). A decision-support system for prioritizing restoration sites on the mississippi river alluvial plain. *Conservation Biology*, *10*(5), 1446–1455.

López-Hernández, M., Ramos-Espinosa, M. G., & Carranza-Fraser, J. (2007). Análisis multimétrico para evaluar contaminación en el río lerma y lago de chapala, méxico. *Hidrobiológica*, *17*, 17–30.

Luhtala, H., & Tolvanen, H. (2013). Optimizing the use of secchi depth as a proxy for euphotic depth in coastal waters: an empirical study from the baltic sea. *ISPRS International Journal of Geo-Information*, *2*(4), 1153–1168.

Lumb, A., Sharma, T., & Bibeault, J.-F. (2011). A review of genesis and evolution of water quality index (wqi) and some future directions. *Water Quality, Exposure and Health*, *3*(1), 11–24.

Ma, L., Liu, Y., Zhang, X., Ye, Y., Yin, G., & Johnson, B. A. (2019). Deep learning in remote sensing applications: A meta-analysis and review. *ISPRS journal of photogrammetry and remote sensing*, *152*, 166–177.

MAE. (2005). Ecosystems and human well being: Synthesis. In *Millennium ecosystem assessment.*

Maier, P. M., & Keller, S. (2018). Machine learning regression on hyperspectral data to estimate multiple water parameters. In *2018 9th workshop on hyperspectral image and signal processing: Evolution in remote sensing (whispers)* (pp. 1–5).

Maier, P. M., & Keller, S. (2019). Application of different simulated spectral data and machine learning to estimate the chlorophyll a concentration of several inland waters. In *2019 10th workshop on hyperspectral imaging and signal processing: Evolution in remote sensing (whispers)* (pp. 1–5).

Maimaitijiang, M., Sagan, V., Sidike, P., Hartling, S., Esposito, F., & Fritschi, F. B. (2020). Soybean yield prediction from uav using multimodal data fusion and deep learning. *Remote sensing of environment*, *237*, 111599.

Malago, A., Bouraoui, F., Vigiak, O., Grizzetti, B., & Pastori, M. (2017). Modelling water and nutrient fluxes in the danube river basin with swat. *Science of the Total Environment*, *603*, 196–218.

Malthus, T. J., Hestir, E. L., Dekker, A. G., & Brando, V. E. (2012). The case for a global inland water quality product. In *2012 ieee international geoscience and remote sensing symposium* (pp. 5234–5237).

Mandanici, E., & Bitelli, G. (2016). Preliminary comparison of sentinel-2 and landsat 8 imagery for a combined use. *Remote Sensing*, *8*(12), 1014.

Marren, P. M., Grove, J. R., Webb, J. A., & Stewardson, M. J. (2014). The potential for

dams to impact lowland meandering river floodplain geomorphology. *The Scientific World Journal*, *2014*.

Martin, A., Boutin, J., Hauser, D., Reverdin, G., Pardé, M., Zribi, M., ... others (2012). Remote sensing of sea surface salinity from carols l-band radiometer in the gulf of biscay. *IEEE transactions on geoscience and remote sensing*, *50*(5), 1703–1715.

Matthews, M. W. (2011). A current review of empirical procedures of remote sensing in inland and near-coastal transitional waters. *International Journal of Remote Sensing*, *32*(21), 6855–6899.

Matthews, M. W. (2014). Eutrophication and cyanobacterial blooms in south african inland waters: 10 years of meris observations. *Remote Sensing of Environment*, *155*, 161–177.

Matthews, M. W., Bernard, S., & Winter, K. (2010). Remote sensing of cyanobacteria-dominant algal blooms and water quality parameters in zeekoevlei, a small hypertrophic lake, using meris. *Remote sensing of environment*, *114*(9), 2070–2087.

Medina-Cobo, M., Domínguez, J., Quesada, A., & De Hoyos, C. (2014). Estimation of cyanobacteria biovolume in water reservoirs by meris sensor. *Water research*, *63*, 10–20.

Meisner, D. E. (1983). Use of landsat data to predict the trophic state of minnesota lakes. *Photogramm. Engng Remote Sens*, *49*, 219–229.

Membrillo-Abad, A.-S., Torres-Vera, M.-A., Alcocer, J., Prol-Ledesma, R. M., Oseguera, L. A., & Ruiz-Armenta, J. R. (2016). Trophic state index estimation from remote sensing of lake chapala, méxico. *Revista mexicana de ciencias geológicas*, *33*(2), 183–191.

Mendoza, M., Bocco, G., López-Granados, E., & Bravo Espinoza, M. (2010). Hydrological implications of land use and land cover change: Spatial analytical approach at regional scale in the closed basin of the cuitzeo lake, michoacan, mexico. *Singapore Journal of Tropical Geography*, *31*(2), 197–214.

Mendoza, M. E., Bocco, G., Bravo, M., Granados, E. L., & Osterkamp, W. (2006). Predicting water-surface fluctuation of continental lakes: a rs and gis based approach in central mexico. *Water Resources Management*, *20*(2), 291–311.

Mendoza, M. E., Granados, E. L., Geneletti, D., Pérez-Salicrup, D. R., & Salinas, V. (2011). Analysing land cover and land use change processes at watershed level: a multitemporal study in the lake cuitzeo watershed, mexico (1975–2003). *Applied Geography*, *31*(1), 237–250.

Merino-Ibarra, M., Monroy-Ríos, E., Vilaclara, G., Castillo, F. S., Gallegos, M. E., & Ramírez-Zierold, J. (2008). Physical and chemical limnology of a wind-swept tropical highland reservoir. *Aquatic Ecology*, *42*(3), 335–345.

Mertes, L. A., Smith, M. O., & Adams, J. B. (1993). Estimating suspended sediment concentrations in surface waters of the amazon river wetlands from landsat images. *Remote Sensing of Environment*, *43*(3), 281–301.

Metcalfe, S. E., Davies, S. J., Braisby, J. D., Leng, M. J., Newton, A. J., Terrett, N. L., & O'Hara, S. L. (2007). Long and short-term change in the pátzcuaro basin, central mexico. *Palaeogeography, Palaeoclimatology, Palaeoecology*, *247*(3-4), 272–295.

Meza, F. (2009). Control de calidad de las aguas en chile. *Tierra Adentro*.

Miller, R. L., & McKee, B. A. (2004). Using modis terra 250 m imagery to map concentrations of total suspended matter in coastal waters. *Remote sensing of Environment*, *93*(1-2), 259–266.

Mishra, P., Panda, U. S., Pradhan, U., Kumar, C. S., Naik, S., Begum, M., & Ishwarya, J. (2015). Coastal water quality monitoring and modelling off chennai city. *Procedia Engineering*, *116*, 955–962.

Mishra, S., & Mishra, D. R. (2012). Normalized difference chlorophyll index: A novel model for remote estimation of chlorophyll-a concentration in turbid productive waters. *Remote Sensing of Environment*, *117*, 394–406.

Mobley, C. (1994). Chapter 3: Optical properties of water. *Handbook of Optics*, *1*, 43–3.

Mobley, C. D. (1999). Estimation of the remote-sensing reflectance from above-surface measurements. *Applied optics*, *38*(36), 7442–7455.

Morel, A. Y., & Gordon, H. R. (1980). Report of the working group on water color. *Boundary-Layer Meteorology*, *18*(3), 343–355.

Morris, B. L., Lawrence, A. R., Chilton, P., Adams, B., Calow, R. C., & Klinck, B. A. (2003). Groundwater and its susceptibility to degradation: a global assessment of the problem and options for management.

Moscuzza, C., Volpedo, A. V., Ojeda, C., & Cirelli, A. F. (2007). Water quality index as an tool for river assessment in agricultural areas in the pampean plains of argentina. *Journal of Urban and Environmental Engineering*, *1*(1), 18–25.

Moses, W., Ogashawara, S., Montes, M., De Keukelaere, L., & Knaeps, E. (2017). *Biooptical modeling and remote sensing of inland waters: Atmospheric correction for inland waters; mishra, oi, ed.* Elsevier: Amsterdam, The Netherlands.

Moses, W. J., Gitelson, A. A., Berdnikov, S., & Povazhnyy, V. (2009). Estimation of chlorophyll-a concentration in case ii waters using modis and meris data - successes and challenges. *Environmental research letters*, *4*(4), 045005.

Mountrakis, G., Im, J., & Ogole, C. (2011). Support vector machines in remote sensing: A review. *ISPRS Journal of Photogrammetry and Remote Sensing*, *66*(3), 247–259.

Mouselimis, L., & Gosso, A. (2018). elmnnrcpp: The extreme learning machine algorithm. *R package*, *1*, 1.

Mouw, C. B., Greb, S., Aurin, D., DiGiacomo, P. M., Lee, Z., Twardowski, M., ... others (2015). Aquatic color radiometry remote sensing of coastal and inland waters: Challenges and recommendations for future satellite missions. *Remote sensing of environment*, *160*, 15–30.

Muller-Karger, F. E. (1992). Remote sensing of marine pollution: A challenge for the 1990s. *Marine pollution bulletin*, *25*(1-4), 54–60.

Mundial, B. (2015). Diagnóstico para el manejo integral de las subcuencas tuxpan, el bosque, ixtapan del oro, valle de bravo, colorines-chilesdo y villa victoria pertenecientes al sistema cutzamala. *Comisión Nacional del Agua. México*.

Murphy, S. (2018). *Atmospheric correction of sentinel 2 imagery in google earth engine using py6s.* https://github.com/samsammurphy/gee-atmcorr-S2.

Nandini, S., Merino-Ibarra, M., & Sarma, S. (2008). Seasonal changes in the zooplankton abundances of the reservoir valle de bravo (state of mexico, mexico). *Lake and Reservoir Management*, *24*(4), 321–330.

Nardi, F., Vivoni, E. R., & Grimaldi, S. (2006). Investigating a floodplain scaling relation using a hydrogeomorphic delineation method. *Water Resources Research*, *42*(9).

NASA. (2022). A harmonized surface reflectance product. *https://hls.gsfc.nasa.gov/*.

Natho, M. T. T., S.; Hein. (2022). *Bedeutung der flusseintiefungen fÃ¼r auenreaktivierungen - eine nahrstoffbasierte perspektive. paper presented at the tag der hydrologie, munich, germany.*

Natho, S., Tschikof, M., Bondar-Kunze, E., & Hein, T. (2020). Modeling the effect of enhanced lateral connectivity on nutrient retention capacity in large river floodplains: How much connected floodplain do we need. *Frontiers in Environmental Science*, *8*, 74.

Nelson, J. C., Redmond, A., Sparks, R. E., et al. (1995). *Impacts of settlement on floodplain vegetation at the confluence of the illinois and mississippi rivers.* National Biological Survey, Environmental Management Technical Center.

Nesshöver, C., Assmuth, T., Irvine, K. N., Rusch, G. M., Waylen, K. A., Delbaere, B., ... others (2017). The science, policy and practice of nature-based solutions: An interdisciplinary perspective. *Science of the total environment*, *579*, 1215–1227.

Nguyen, M. D., Baez-Villanueva, O. M., Bui, D. D., Nguyen, P. T., & Ribbe, L. (2020). Harmonization of landsat and sentinel 2 for crop monitoring in drought prone areas: Case studies of ninh thuan (vietnam) and bekaa (lebanon). *Remote Sensing*, *12*(2), 281.

Niroumand-Jadidi, M., Bovolo, F., & Bruzzone, L. (2020). Water quality retrieval from prisma hyperspectral images: first experience in a turbid lake and comparison with sentinel-2. *Remote Sensing*, *12*(23), 3984.

NOM. (1993). *Norma oficial mexicana nom-014-ssa1-1993: Procedimientos sanitarios para el muestreo de agua para uso y consumo humano en sistemas de abastecimiento de agua publicos y privados.* https://agua.org.mx/wp-content/uploads/2010/06/014SSA13.pdf. (Online; accessed on 10 June 2021)

NOM. (2004). *Norma oficial mexicana nmx-aa-038-scfi-2001: Analisis de agua: Determinacion de turbiedad en aguas naturales, residuales y residuales tratadas: Metodo de prueba.* https://www.gob.mx/cms/uploads/attachment/file/166777/NMX-AA-038-SCFI-2001.pdf. (Online; accessed on 10 June 2021)

NOM. (2015a). *Norma oficial mexicana nmx-aa-034-scfi-2015: Analisis de agua - medicion de solidos y sales disueltas en aguas naturales, residuales y residuales tratadas - metodo de prueba.* https://www.gob.mx/cms/uploads/attachment/file/166146/nmx-aa-034-scfi-2015.pdf. (Online; accessed on 10 June 2021)

NOM. (2015b). *Norma oficial mexicana nmx-aa-115-scfi-2015: Analisis de agua - criterios generales para el control de la calidad de resultados analiticos.* https://www.gob.mx/cms/uploads/attachment/file/166150/nmx-aa-115-scfi-2015.pdf. (Online; accessed on 10 June 2021)

Noori, R., Karbassi, A., Moghaddamnia, A., Han, D., Zokaei-Ashtiani, M., Farokhnia, A., & Gousheh, M. G. (2011). Assessment of input variables determination on the svm model performance using pca, gamma test, and forward selection techniques for monthly stream flow prediction. *Journal of hydrology*, *401*(3-4), 177–189.

Odermatt, D., Gitelson, A., Brando, V. E., & Schaepman, M. (2012). Review of constituent retrieval in optically deep and complex waters from satellite imagery. *Remote sensing of environment*, *118*, 116–126.

Odermatt, D., Heege, T., Nieke, J., Kneubühler, M., & Itten, K. (2008). Water quality monitoring for lake constance with a physically based algorithm for meris data. *Sensors*, *8*(8), 4582–4599.

O'Hara, S. L., Street-Perrott, F. A., & Burt, T. P. (1993). Accelerated soil erosion around a mexican highland lake caused by prehispanic agriculture. *Nature*, *362*(6415), 48–51.

Olvera, V. (1990). Estudio de la eutroficación del embalse valle de bravo, méxico. *Master Tesis, UNAM, México*.

Olvera-Viascán, V., Bravo-Inclán, L., & Sánchez-Chávez, J. (1998). Aquatic ecology and management assessment in valle de bravo reservoir and its watershed. *Aquatic Ecosystem Health & Management*, *1*(3-4), 277–290.

Onderka, M. (2008). Remote sensing and identification of places susceptible to sedimentation in the danube river. *Available online: citeseerx. ist. psu. edu/viewdoc/download*.

Osorio-Ocampo, S., Macías, J. L., Pola, A., Cardona-Melchor, S., Sosa-Ceballos, G., Garduño-Monroy, V. H., ... Benowitz, J. (2018). The eruptive history of the pátzcuaro lake area in the michoacán guanajuato volcanic field, central méxico: Field mapping, c-14 and 40ar/39ar geochronology. *Journal of Volcanology and Geothermal Research*, *358*, 307–328.

Otto, P., Vallejo-Rodríguez, R., Keesstra, S., León-Becerril, E., de Anda, J., Hernández-Mena, L., ... Díaz-Torres, J. d. J. (2020). Time delay evaluation on the water-leaving irradiance retrieved from empirical models and satellite imagery. *Remote Sensing*, *12*(1), 87.

Ouillon, S., Douillet, P., & Andréfouët, S. (2004). Coupling satellite data with in situ measurements and numerical modeling to study fine suspended-sediment transport: a study for

the lagoon of new caledonia. *Coral Reefs*, *23*(1), 109–122.

Oyama, Y., Matsushita, B., & Fukushima, T. (2015). Distinguishing surface cyanobacterial blooms and aquatic macrophytes using landsat/tm and etm+ shortwave infrared bands. *Remote Sensing of Environment*, *157*, 35–47.

Pahlevan, N., Smith, B., Schalles, J., Binding, C., Cao, Z., Ma, R., ... others (2020). Seamless retrievals of chlorophyll-a from sentinel-2 (msi) and sentinel-3 (olci) in inland and coastal waters: A machine learning approach. *Remote Sensing of Environment*, *240*, 111604.

Palmer, S. C., Hunter, P. D., Lankester, T., Hubbard, S., Spyrakos, E., Tyler, A. N., ... others (2015). Validation of envisat meris algorithms for chlorophyll retrieval in a large, turbid and optically-complex shallow lake. *Remote Sensing of Environment*, *157*, 158–169.

Panda, S., Garg, V., & Chaubey, I. (2004). Artificial neural networks application in lake water quality estimation using satellite imagery. *Journal of Environmental Informatics*, *4*(2), 65–74.

Papoutsa, C., Retalis, A., Toulios, L., & Hadjimitsis, D. G. (2014). Defining the landsat tm/etm+ and chris/proba spectral regions in which turbidity can be retrieved in inland waterbodies using field spectroscopy. *International journal of remote sensing*, *35*(5), 1674–1692.

Pasolli, L., Melgani, F., & Blanzieri, E. (2010). Gaussian process regression for estimating chlorophyll concentration in subsurface waters from remote sensing data. *IEEE Geoscience and Remote Sensing Letters*, *7*(3), 464–468.

Pattiaratchi, C., Lavery, P., Wyllie, A., & Hick, P. (1994). Estimates of water quality in coastal waters using multi-date landsat thematic mapper data. *International Journal of Remote Sensing*, *15*(8), 1571–1584.

Pedregosa, F., Varoquaux, G., Gramfort, A., Michel, V., Thirion, B., Grisel, O., ... others (2011). Scikit-learn: Machine learning in python. *the Journal of machine Learning research*, *12*, 2825–2830.

Peeters, E. T., Franken, R. J., Jeppesen, E., Moss, B., Bécares, E., Hansson, L.-A., ... others (2009). Assessing ecological quality of shallow lakes: Does knowledge of transparency suffice? *Basic and Applied Ecology*, *10*(1), 89–96.

Pereira, L. S., Andes, L. C., Cox, A. L., & Ghulam, A. (2018). Measuring suspended-sediment concentration and turbidity in the middle mississippi and lower missouri rivers using landsat data. *JAWRA Journal of the American Water Resources Association*, *54*(2), 440–450.

Pérez-Rojas, A., & Torres-Orozco, R. (1992). Geomorfología y batimetría del lago de catemaco, veracruz, méxico. In *Anales del instituto de ciencias del mar y limnología, universidad nacional autónoma de méxico* (Vol. 19, pp. 19–24).

Peterson, K. T., et al. (2020). Deep learning-based water quality estimation and anomaly detection using landsat-8/sentinel-2 virtual constellation and cloud computing. *GIScience & Remote Sensing*, *57*(4), 510–525.

Peterson, K. T., Sagan, V., Sidike, P., Cox, A. L., & Martinez, M. (2018). Suspended sediment concentration estimation from landsat imagery along the lower missouri and middle mississippi rivers using an extreme learning machine. *Remote Sensing*, *10*(10), 1503.

Philippot, L., Hallin, S., & Schloter, M. (2007). Ecology of denitrifying prokaryotes in agricultural soil. *Advances in agronomy*, *96*, 249–305.

Poff, N. L., Allan, J. D., Bain, M. B., Karr, J. R., Prestegaard, K. L., Richter, B. D., ... Stromberg, J. C. (1997). The natural flow regime. *BioScience*, *47*(11), 769–784.

Poortinga, A., Tenneson, K., Shapiro, A., Nquyen, Q., San Aung, K., Chishtie, F., & Saah, D. (2019). Mapping plantations in myanmar by fusing landsat-8, sentinel-2 and sentinel-1 data along with systematic error quantification. *Remote sensing*, *11*(7), 831.

Preisendorfer, R. W. (1986). Secchi disk science: Visual optics of natural waters 1. *Limnology and oceanography*, *31*(5), 909–926.

Pu, F., et al. (2019). Water-quality classification of inland lakes using landsat8 images by convolutional neural networks. *Remote Sensing*, *11*(14), 1674.

Pyo, J., Cho, K. H., Kim, K., Baek, S.-S., Nam, G., & Park, S. (2021). Cyanobacteria cell prediction using interpretable deep learning model with observed, numerical, and sensing data assemblage. *Water Research*, *203*, 117483.

Qin, B., Li, W., Zhu, G., Zhang, Y., Wu, T., & Gao, G. (2015). Cyanobacterial bloom management through integrated monitoring and forecasting in large shallow eutrophic lake taihu (china). *Journal of hazardous materials*, *287*, 356–363.

Ramirez, P., Olvera, V., Pulido, M., & Duran, A. (1998). Presence of vibrio cholerae in a fresh water reservoir of valle de bravo (méxico state, méxico). *INTERNATIONAL REVIEW OF HYDROBIOLOGY*, *83*, 647–650.

Ramírez-Herrejón, J. P., Zambrano, L., Mercado-Silva, N., Torres-Téllez, A., Pineda-García, F., Caraveo-Patiño, J., & Balart, E. F. (2014). Long term changes in the fish fauna of lago de pátzcuaro in central mexico. *Latin American Journal of Aquatic Research*, *42*(1), 137–149.

Ramírez-Zierold, J. A., Merino-Ibarra, M., Monroy-Ríos, E., Olson, M., Castillo, F. S., Gallegos, M. E., & Vilaclara, G. (2010). Changing water, phosphorus and nitrogen budgets for valle de bravo reservoir, water supply for mexico city metropolitan area. *Lake and Reservoir Management*, *26*(1), 23–34.

Ranghetti, L., Boschetti, M., Nutini, F., & Busetto, L. (2020). Sen2r: An r toolbox for automatically downloading and preprocessing sentinel-2 satellite data. *Computers & Geosciences*, *139*, 104473.

Rasmussen, C. E. (2003). Gaussian processes in machine learning. In *Summer school on machine learning* (pp. 63–71).

Reul, N., Tenerelli, J., Chapron, B., Vandemark, D., Quilfen, Y., & Kerr, Y. (2012). Smos satellite l-band radiometer: A new capability for ocean surface remote sensing in hurricanes. *Journal of Geophysical Research: Oceans*, *117*(C2).

RFMA. (2014). *Red de monitoreo ambiental.* https://redfema.ambiente.gob.ar/monitor/agua. (Online; accessed on 15 March 2021)

Ritchie, J. C., Cooper, C. M., & Schiebe, F. R. (1990). The relationship of mss and tm digital data with suspended sediments, chlorophyll, and temperature in moon lake, mississippi. *Remote Sensing of environment*, *33*(2), 137–148.

Ritchie, J. C., Zimba, P. V., & Everitt, J. H. (2003). Remote sensing techniques to assess water quality. *Photogrammetric engineering & remote sensing*, *69*(6), 695–704.

Rodriguez-Galiano, V., Mendes, M. P., Garcia-Soldado, M. J., Chica-Olmo, M., & Ribeiro, L. (2014). Predictive modeling of groundwater nitrate pollution using random forest and multisource variables related to intrinsic and specific vulnerability: A case study in an agricultural setting (southern spain). *Science of the Total Environment*, *476*, 189–206.

Röttgers, R., McKee, D., & Utschig, C. (2014). Temperature and salinity correction coefficients for light absorption by water in the visible to infrared spectral region. *Optics express*, *22*(21), 25093–25108.

Roy, D. P., Li, J., Zhang, H. K., Yan, L., Huang, H., & Li, Z. (2017). Examination of sentinel-2a multi-spectral instrument (msi) reflectance anisotropy and the suitability of a general method to normalize msi reflectance to nadir brdf adjusted reflectance. *Remote Sensing of Environment*, *199*, 25–38.

Roy, D. P., Zhang, H., Ju, J., Gomez-Dans, J. L., Lewis, P. E., Schaaf, C., ... Kovalskyy, V. (2016). A general method to normalize landsat reflectance data to nadir brdf adjusted reflectance. *Remote Sensing of Environment*, *176*, 255–271.

Ruescas, A. B., et al. (2018). Machine learning regression approaches for colored dissolved organic matter (cdom) retrieval with s2-msi and s3-olci simulated data. *Remote Sensing*,

10(5), 786.

Sagan, V., Peterson, K. T., Maimaitijiang, M., Sidike, P., Sloan, J., Greeling, B. A., ... Adams, C. (2020). Monitoring inland water quality using remote sensing: potential and limitations of spectral indices, bio-optical simulations, machine learning, and cloud computing. *Earth-Science Reviews*, *205*, 103187.

Salem, S. I., Strand, M. H., Higa, H., Kim, H., Kazuhiro, K., Oki, K., & Oki, T. (2017). Evaluation of meris chlorophyll-a retrieval processors in a complex turbid lake kasumigaura over a 10-year mission. *Remote Sensing*, *9*(10), 1022.

Samui, P. (2008). Support vector machine applied to settlement of shallow foundations on cohesionless soils. *Computers and Geotechnics*, *35*(3), 419–427.

Sanon, S., Hein, T., Douven, W., & Winkler, P. (2012). Quantifying ecosystem service trade-offs: The case of an urban floodplain in vienna, austria. *Journal of environmental management*, *111*, 159–172.

Santer, R., Zagolski, F., & Gilson, M. (2009). Icol-improve contrast between ocean and land. *BEAM Algorithm Technical Basis Document*.

Santini, F., Alberotanza, L., Cavalli, R. M., & Pignatti, S. (2010). A two-step optimization procedure for assessing water constituent concentrations by hyperspectral remote sensing techniques: An application to the highly turbid venice lagoon waters. *Remote Sensing of Environment*, *114*(4), 887–898.

Sathyendranath, S., et al. (2000). Remote sensing of ocean colour in coastal, and other optically-complex, waters.

Schaeffer, B. A., Schaeffer, K. G., Keith, D., Lunetta, R. S., Conmy, R., & Gould, R. W. (2013). Barriers to adopting satellite remote sensing for water quality management. *International Journal of Remote Sensing*, *34*(21), 7534–7544.

Schiller, H., & Doerffer, R. (1999). Neural network for emulation of an inverse model operational derivation of case ii water properties from meris data. *International journal of remote sensing*, *20*(9), 1735–1746.

Schindler, S., Sebesvari, Z., Damm, C., Euller, K., Mauerhofer, V., Schneidergruber, A., ... others (2014). Multifunctionality of floodplain landscapes: relating management options to ecosystem services. *Landscape Ecology*, *29*(2), 229–244.

Schwarz, U. (2011). Floodplain restoration potential and flood mitigation along the danube. In *Geophysical research abstracts* (Vol. 13).

Senate, U. (2002). Federal water pollution control act. *United State Senate, Washington, DC*.

Sepulveda, R. (2011). Diseño de modelos de calidad del agua mediante el uso de percepción remota. *Master and Doctoral Program in Engineering; National Autonomous University of Mexico: Mexico City, Mexico*.

Seyhan, E., & Dekker, A. (1986). Application of remote sensing techniques for water quality monitoring. *Hydrobiological Bulletin*, *20*(1), 41–50.

Shafique, N. A., Fulk, F., Autrey, B. C., Flotemersch, J., et al. (2003). Hyperspectral remote sensing of water quality parameters for large rivers in the ohio river basin. In *First interagency conference on research in the watershed, benson, az* (pp. 216–221).

Shahzad, M. I., Meraj, M., Nazeer, M., Zia, I., Inam, A., Mehmood, K., & Zafar, H. (2018). Empirical estimation of suspended solids concentration in the indus delta region using landsat-7 etm+ imagery. *Journal of environmental management*, *209*, 254–261.

Sharma, C., Isha, I., & Vashisht, V. (2021). Water quality estimation using computer vision in uav. In *2021 11th international conference on cloud computing, data science & engineering (confluence)* (pp. 448–453).

Shen, M., Duan, H., Cao, Z., Xue, K., Loiselle, S., & Yesou, H. (2017). Determination of the downwelling diffuse attenuation coefficient of lake water with the sentinel-3a olci. *Remote Sensing*, *9*(12), 1246.

Sidike, P., Sagan, V., Maimaitijiang, M., Maimaitiyiming, M., Shakoor, N., Burken, J., ... Fritschi, F. B. (2019). dpen: Deep progressively expanded network for mapping heterogeneous agricultural landscape using worldview-3 satellite imagery. *Remote sensing of environment*, *221*, 756–772.

Silveira Kupssinsku, L., Thomassim Guimaraes, T., Menezes de Souza, E., C Zanotta, D., Roberto Veronez, M., Gonzaga, L., & Mauad, F. F. (2020). A method for chlorophyll-a and suspended solids prediction through remote sensing and machine learning. *Sensors*, *20*(7), 2125.

Soenen, S. A., Peddle, D. R., & Coburn, C. A. (2005). Scs+ c: A modified sun-canopy-sensor topographic correction in forested terrain. *IEEE Transactions on geoscience and remote sensing*, *43*(9), 2148–2159.

Sokoletsky, L. G., Lunetta, R. S., Wetz, M. S., & Paerl, H. W. (2011). Meris retrieval of water quality components in the turbid albemarle-pamlico sound estuary, usa. *Remote Sensing*, *3*(4), 684–707.

Song, K., Li, L., Li, S., Tedesco, L., Hall, B., & Li, L. (2012). Hyperspectral remote sensing of total phosphorus (tp) in three central indiana water supply reservoirs. *Water, Air, & Soil Pollution*, *223*(4), 1481–1502.

Soto-Galera, E., Paulo-Maya, J., López-López, E., Serna-Hernández, J. A., & Lyons, J. (1999). Change in fish fauna as indication of aquatic ecosystem condition in río grande de morelia–lago de cuitzeo basin, mexico. *Environmental Management*, *24*(1), 133–140.

Sparks, R. E. (1995). Need for ecosystem management of large rivers and their floodplains. *BioScience*, *45*(3), 168–182.

Storey, J., Roy, D. P., Masek, J., Gascon, F., Dwyer, J., & Choate, M. (2016). A note on the temporary misregistration of landsat-8 operational land imager (oli) and sentinel-2 multi spectral instrument (msi) imagery. *Remote Sensing of Environment*, *186*, 121–122.

Sudheer, K., Chaubey, I., & Garg, V. (2006). Lake water quality assessment from landsat thematic mapper data using neural network: an approach to optimal band combination selection1. *JAWRA Journal of the American Water Resources Association*, *42*(6), 1683–1695.

Sun, D., Qiu, Z., Li, Y., Shi, K., & Gong, S. (2014). Detection of total phosphorus concentrations of turbid inland waters using a remote sensing method. *Water, Air, & Soil Pollution*, *225*(5), 1–17.

Sun, X., et al. (2022). Monitoring water quality using proximal remote sensing technology. *Science of The Total Environment*, *803*, 149805.

Sutadian, A. D., Muttil, N., Yilmaz, A. G., & Perera, B. (2016). Development of river water quality indices - a review. *Environmental monitoring and assessment*, *188*(1), 1–29.

Svab, E., Tyler, A., Preston, T., Presing, M., & Balogh, K. (2005). Characterizing the spectral reflectance of algae in lake waters with high suspended sediment concentrations. *International Journal of Remote Sensing*, *26*(5), 919–928.

Syariz, M., Jaelani, L., Subehi, L., Pamungkas, A., Koenhardono, E., & Sulisetyono, A. (2015). Retrieval of sea surface temperature over poteran island water of indonesia with landsat 8 tirs image: A preliminary algorithm. *The International Archives of Photogrammetry, Remote Sensing and Spatial Information Sciences*, *40*, 87.

Szegedy, C., Liu, W., Jia, Y., Sermanet, P., Reed, S., Anguelov, D., ... Rabinovich, A. (2015). Going deeper with convolutions. In *Proceedings of the ieee conference on computer vision and pattern recognition* (pp. 1–9).

Tamm, O., & Tamm, T. (2020). Verification of a robust method for sizing and siting the small hydropower run-of-river plant potential by using gis. *Renewable Energy*, *155*, 153–159.

Thorslund, J., & van Vliet, M. T. (2020). A global dataset of surface water and groundwater salinity measurements from 1980–2019. *Scientific Data*, *7*(1), 1–11.

Tilstone, G. H., Lotliker, A. A., Miller, P. I., Ashraf, P. M., Kumar, T. S., Suresh, T., ... Menon, H. B. (2013). Assessment of modis-aqua chlorophyll-a algorithms in coastal and shelf waters of the eastern arabian sea. *Continental Shelf Research*, *65*, 14–26.

Tockner, K., & Stanford, J. A. (2002). Riverine flood plains: present state and future trends. *Environmental conservation*, *29*(3), 308–330.

Todo, K., & Sato, K. (2002). Directive 2000/60/ec of the european parliament and of the council of 23 october 2000 establishing a framework for community action in the field of water policy. *Environmental Research Quarterly*, 66–106.

Toming, K., Kutser, T., Laas, A., Sepp, M., Paavel, B., & Nõges, T. (2016). First experiences in mapping lake water quality parameters with sentinel-2 msi imagery. *Remote Sensing*, *8*(8), 640.

Toming, K., Kutser, T., Uiboupin, R., Arikas, A., Vahter, K., & Paavel, B. (2017). Mapping water quality parameters with sentinel-3 ocean and land colour instrument imagery in the baltic sea. *Remote Sensing*, *9*(10), 1070.

Topp, S. N., Pavelsky, T. M., Jensen, D., Simard, M., & Ross, M. R. (2020). Research trends in the use of remote sensing for inland water quality science: Moving towards multidisciplinary applications. *Water*, *12*(1), 169.

Tundisi, J. G., & Tundisi, T. M. (2016). *Limnologia*. Oficina de textos.

Turner, D. (2010). Remote sensing of chlorophyll a concentrations to support the deschutes basin lake and reservoirs tmdls. *Department of Environmental Quality: Portland, OR, USA*.

Tyler, A., Svab, E., Preston, T., Présing, M., & Kovács, W. (2006). Remote sensing of the water quality of shallow lakes: A mixture modelling approach to quantifying phytoplankton in water characterized by high-suspended sediment. *International Journal of Remote Sensing*, *27*(8), 1521–1537.

UMA. (1998). *An integrated water-monitoring network for wisconsin*. University of Wisconsin-Madison, Water Resources Center and Geological Survey (US). Water Resources Division. Wisconsin District.

UN. (2018,). *United nations world water development report, nature-based solutions for water.*

UNEP. (2016). A snapshot of the world's water quality: Towards a global assessment. *Nairobi, United Nations Environment Programme*.

UNEP. (2021). *Gemsstat: Water programme - water quality data, gemstat and open web services.* https://gemstat.org/data/data-portal/. (Online; accessed on 15 February 2021)

Usali, N., & Ismail, M. H. (2010). Use of remote sensing and gis in monitoring water quality. *Journal of sustainable development*, *3*(3), 228.

Vapnik, V., Golowich, S. E., Smola, A., et al. (1997). Support vector method for function approximation, regression estimation, and signal processing. *Advances in neural information processing systems*, 281–287.

Venohr, M., Hirt, U., Hofmann, J., Opitz, D., Gericke, A., Wetzig, A., ... others (2011). Modelling of nutrient emissions in river systems–moneris–methods and background. *International Review of Hydrobiology*, *96*(5), 435–483.

Vermote, E., Justice, C., Claverie, M., & Franch, B. (2016). Preliminary analysis of the performance of the landsat 8/oli land surface reflectance product. *Remote Sensing of Environment*, *185*, 46–56.

Vermote, E. F., Tanré, D., Deuze, J. L., Herman, M., & Morcette, J.-J. (1997). Second simulation of the satellite signal in the solar spectrum, 6s: An overview. *IEEE transactions on geoscience and remote sensing*, *35*(3), 675–686.

Verpoorter, C., Kutser, T., Seekell, D. A., & Tranvik, L. J. (2014). A global inventory of lakes based on high-resolution satellite imagery. *Geophysical Research Letters*, *41*(18), 6396–6402.

Verrelst, J., Muñoz, J., Alonso, L., Delegido, J., Rivera, J. P., Camps-Valls, G., & Moreno, J. (2012). Machine learning regression algorithms for biophysical parameter retrieval: Opportunities for sentinel-2 and-3. *Remote Sensing of Environment*, *118*, 127–139.

Verrelst, J., Rivera, J. P., Moreno, J., & Camps-Valls, G. (2013). Gaussian processes uncertainty estimates in experimental sentinel-2 lai and leaf chlorophyll content retrieval. *ISPRS journal of photogrammetry and remote sensing*, *86*, 157–167.

Villalobos-Castañeda, B., Alfaro-Cuevas, R., Cortés-Martínez, R., Martínez-Miranda, V., & Márquez-Benavides, L. (2010). Distribution and partitioning of iron, zinc, and arsenic in surface sediments in the grande river mouth to cuitzeo lake, mexico. *Environmental monitoring and assessment*, *166*(1), 331–346.

Vinogradova, N. T., & Ponte, R. M. (2012). Assessing temporal aliasing in satellite-based surface salinity measurements. *Journal of Atmospheric and Oceanic Technology*, *29*(9), 1391–1400.

Vollenweider, R., Kerekes, J., et al. (1982). Eutrophication of waters. monitoring, assessment and control. *Organization for Economic Co-Operation and Development (OECD), Paris*, *156*.

Walling, D., He, Q., Blake, W., et al. (2000). River flood plains as phosphorus sinks. *IAHS Publication(International Association of Hydrological Sciences)*(263), 211–218.

Wang, F., Han, L., Kung, H.-T., & Van Arsdale, R. (2006). Applications of landsat-5 tm imagery in assessing and mapping water quality in reelfoot lake, tennessee. *International Journal of Remote Sensing*, *27*(23), 5269–5283.

Wang, X., Fu, L., & He, C. (2011). Applying support vector regression to water quality modelling by remote sensing data. *International journal of remote sensing*, *32*(23), 8615–8627.

Wang, X., Ma, L., & Wang, X. (2010). Apply semi-supervised support vector regression for remote sensing water quality retrieving. In *2010 ieee international geoscience and remote sensing symposium* (pp. 2757–2760).

Wang, X., et al. (2017). Evaluation of water quality based on a machine learning algorithm and water quality index for the ebinur lake watershed, china. *Scientific reports*, *7*(1), 1–18.

Wang, Y., Xia, H., Fu, J., & Sheng, G. (2004). Water quality change in reservoirs of shenzhen, china: detection using landsat/tm data. *Science of the Total Environment*, *328*(1-3), 195–206.

Watanabe, F. S. Y., Alcântara, E., Rodrigues, T. W. P., Imai, N. N., Barbosa, C. C. F., & Rotta, L. H. d. S. (2015). Estimation of chlorophyll-a concentration and the trophic state of the barra bonita hydroelectric reservoir using oli/landsat-8 images. *International journal of environmental research and public health*, *12*(9), 10391–10417.

Weigelhofer, G., & Hein, T. (2015). Efficiency and detrimental side effects of denitrifying bioreactors for nitrate reduction in drainage water. *Environmental Science and Pollution Research*, *22*(17), 13534–13545.

Whiting, P. J. (2002). Streamflow necessary for environmental maintenance. *Annual Review of Earth and Planetary Sciences*, *30*(1), 181–206.

WHO. (2017). Water quality and health-review of turbidity: information for regulators and water suppliers.

Wilson, R. (2021). *Py6s: A python interface to the 6s radiative transfer.*

Wozniak, M., Bradtke, K. M., & Kreeezel, A. (2014). Comparison of satellite chlorophyll a algorithms for the baltic sea. *Journal of Applied Remote Sensing*, *8*(1), 083605.

WQP. (2021). *Water quality portal.* https://www.waterqualitydata.us. (Online; accessed on 15 November 2021)

Wu, C., Wu, J., Qi, J., Zhang, L., Huang, H., Lou, L., & Chen, Y. (2010). Empirical estimation of total phosphorus concentration in the mainstream of the qiantang river in china using landsat tm data. *International Journal of Remote Sensing*, *31*(9), 2309–2324.

Wu, G. (2003). Seasonal change detection of water quality in texas gulf coast using modis remote sensing data. *UC GIS Summer Assembly*.

Xu, T., Coco, G., & Neale, M. (2020). A predictive model of recreational water quality based on adaptive synthetic sampling algorithms and machine learning. *Water research*, *177*, 115788.

Xue, Y., Kovacic, D. A., David, M. B., Gentry, L. E., Mulvaney, R. L., & Lindau, C. W. (1999). *In situ measurements of denitrification in constructed wetlands* (Tech. Rep.). Wiley Online Library.

Yacobi, Y. Z., Gitelson, A., & Mayo, M. (1995). Remote sensing of chlorophyll in lake kinneret using highspectral-resolution radiometer and landsat tm: spectral features of reflectance and algorithm development. *Journal of Plankton Research*, *17*(11), 2155–2173.

Yang, L., Driscol, J., Sarigai, S., Wu, Q., Lippitt, C. D., & Morgan, M. (2022). Towards synoptic water monitoring systems: A review of ai methods for automating water body detection and water quality monitoring using remote sensing. *Sensors*, *22*(6), 2416.

Yogendra, K., & Puttaiah, E. (2008). Determination of water quality index and suitability of an urban waterbody in shimoga town, karnataka. In *Proceedings of taal2007: The 12th world lake conference* (Vol. 342, p. 346).

Yu, Z., et al. (2020). Spatial-temporal process simulation and prediction of chlorophyll-a concentration in dianchi lake based on wavelet analysis and long-short term memory network. *Journal of Hydrology*, *582*, 124488.

Zessner, S. N. S., M.; Winkler. (2008). *Optimierung von frachterhebungen in gewassern unter berucksichtigung von probenahmehaufigkeit und berechnungsmethodik. in-stream load optimizations under consideration of sampling frequency and algorithm. federal ministry for agriculture, forestry, environment and water management, institut fur wassergute, ressourcenmanagement und abfallwirtschaft, tu wien, vienna, austria.*

Zhang, L., Zhang, L., & Du, B. (2016). Deep learning for remote sensing data: A technical tutorial on the state of the art. *IEEE Geoscience and remote sensing magazine*, *4*(2), 22–40.

Zhang, Y., Ma, R., Duan, H., Loiselle, S., & Xu, J. (2014). A spectral decomposition algorithm for estimating chlorophyll-a concentrations in lake taihu, china. *remote Sensing*, *6*(6), 5090–5106.

Zhang, Y., Wu, L., Deng, L., & Ouyang, B. (2021). Retrieval of water quality parameters from hyperspectral images using a hybrid feedback deep factorization machine model. *Water Research*, *204*, 117618.

Zhang, Y., Wu, L., Ren, H., Deng, L., & Zhang, P. (2020). Retrieval of water quality parameters from hyperspectral images using hybrid bayesian probabilistic neural network. *Remote Sensing*, *12*(10), 1567.

Zhang, Y., Yang, L., Qin, B., Gao, G., Luo, L., Zhu, G., & Liu, M. (2008). Spatial distribution of cod and the correlations with other parameters in the northern region of lake taihu. *Huan Jing ke Xue= Huanjing Kexue*, *29*(6), 1457–1462.

Zheng, Z., Li, Y., Guo, Y., Xu, Y., Liu, G., & Du, C. (2015). Landsat-based long-term monitoring of total suspended matter concentration pattern change in the wet season for dongting lake, china. *Remote Sensing*, *7*(10), 13975–13999.

Zilioli, E., & Brivio, P. (1997). The satellite derived optical information for the comparative assessment of lacustrine water quality. *Science of the Total Environment*, *196*(3), 229–245.

Zingraff-Hamed, A., Noack, M., Greulich, S., Schwarzwälder, K., Pauleit, S., & Wantzen, K. M. (2018). Model-based evaluation of the effects of river discharge modulations on physical fish habitat quality. *Water*, *10*(4), 374.

Zou, Q., et al. (2020). A water quality prediction method based on the multi-time scale bidirec-

tional long short-term memory network. *Environmental Science and Pollution Research*, *27*(14), 16853–16864.

Zweynert, U. (2008). *Moglichkeiten und grenzen bei der modellierung von nahrstoffeintragen auf flussgebietsebene: Untersuchungen am beispiel des modells moneris* (Unpublished doctoral dissertation). Dresden, Techn. Univ., Diss., 2008.